Bulletin
of
The Geological Society of America

VOLUME 67 September 1956 NUMBER 9

CONTENTS

	Pages
Cementation of Triassic arkoses in Connecticut and Massachusetts. By Milton T. Heald	1133–1154
Metamorphism and axial-plane folding in the Poundridge area, New York. By David M. Scotford	1155–1198
Till-pebble isopleth maps of parts of Montana and North Dakota. By Arthur David Howard	1199–1206
Wrench-fault tectonics. By J. D. Moody and M. J. Hill	1207–1246
Composition of organic matter in marine sediments: Preliminary data on hydrocarbon distribution in basins off southern California. By Wilson L. Orr and K. O. Emery	1247–1258
Deformation of Yule marble. Part VII: Development of oriented fabrics at 300°C–500°C. By Francis J. Turner, David T. Griggs, R. H. Clark, and Roberta H. Dixon	1259–1294

Subscription $15.00 per year.

Printing Office: Mt. Royal & Guilford Aves., Baltimore 2, Md.

Communications for publications should be addressed to The Geological Society of America, Dr. H. R. Aldrich, Secretary, 419 West 117 Street, New York, N. Y.

Please give notice of change of address 4 weeks in advance. Claims for non-receipt of the Bulletin of a given month must be sent to the Secretary of the Society before the end of the second succeeding month.

Entered as second-class matter at the Post Office at Baltimore, Md.
under the Act of Congress of July 16, 1894.
Accepted for mailing at special rate of postage provided for in Section 1103
Act of October 3, 1917, authorized on July 8, 1918.

PAPERS IN PRESS FOR FORTHCOMING ISSUES

Precambrian Rocks of Wichita and Arbuckle Mountains, Oklahoma. By Warren B. Hamilton

Stratigraphy, Paleontology, and Paleogeography of the *Elliptocephala asaphoides* Strata in Cambridge and Hoosick Quadrangles, New York. By Christina Lochman

Role of Gravity in Orogenesis. By Walter H. Bucher

Early Precambrian Rocks of the Timiskaming Region, Quebec and Ontario, Canada. By M. E. Wilson

Marine Geology of Johnston Island and its Surrounding Shallows. By K. O. Emery

Igneous and Metamorphic Rocks of the Minnesota River Valley. By E. H. Lund

Reservoir Capacity of Mississippian Limestones in the Hopkinsville Quadrangle, Kentucky. By Eugene H. Walker

Ordovician Shales and Submarine Slide Breccias of Northern Champlain Valley in Vermont. By David Hawley

Stratigraphy of the Onondaga Limestone in Eastern New York. By William A. Oliver, Jr.

BULLETIN OF THE GEOLOGICAL SOCIETY OF AMERICA
VOL. 67, PP. 1133-1154, 4 FIGS., 3 PLS. SEPTEMBER 1956

CEMENTATION OF TRIASSIC ARKOSES IN CONNECTICUT AND MASSACHUSETTS

BY MILTON T. HEALD

ABSTRACT

The normal Triassic arkoses of Connecticut and Massachusetts contain moderate amounts of secondary feldspar and very little secondary quartz. Locally calcite or the zeolite laumontite is important. Secondary albite is more abundant than secondary potash feldspar and forms overgrowths on detrital microcline, orthoclase, and plagioclase. Calcite and laumontite occur as pore fillings and replacements of feldspar. Growths formed after considerable compaction but before pressure solution ceased.

Microcrystalline secondary albite is abundant in the arkoses near intrusives. The albite filled pores and partly replaced mica, garnet, and potash feldspar. Secondary chlorite, epidote, sericite, laumontite, and calcite are common in some contact zones. With increasing distance from the intrusives, the microcrystalline albite becomes coarser and decreases in amount, whereas enlargements on detrital grains become more common.

Large amounts of cryptocrystalline quartz, potash feldspar, and sericite were deposited in the sediments along the border fault in western Connecticut. In some faulted arkoses in the Triassic basin, small to moderate amounts of sericite, chlorite, quartz, barite, albite, and calcite were deposited. Sediments near the eastern border fault have undergone considerable pressure solution, but the amount of cement is not abnormally high.

Most of the cement in the normal arkoses is believed to be of igneous origin because it is chemically similar to the material introduced along igneous contacts. The widespread distribution of cement in areas where exposed igneous bodies are absent suggests that some of the introduced material emanated from the diabase reservoirs at depth. The more siliceous solutions that rose along faults may have been derived from the diabase reservoirs during a different stage of differentiation or they may have emanated from other bodies. The present study indicates that a magmatic source for cement should not be ruled out even though effects of hydrothermal activity may be absent.

CONTENTS

TEXT

	Page
Introduction	1134
Acknowledgments	1134
General nature of the sediments	1134
Detrital minerals	1136
Secondary minerals	1137
Feldspar	1137
Quartz	1138
Calcite	1139
Sericite	1140
Chlorite	1141
Laumontite	1142
Pressure solution	1142
Cementation	1143
General statement	1143
Cementation of the normal arkoses	1143
Cementation near igneous bodies	1144
Lower contact of flows	1144
Intrusive contacts	1144
Origin of cementing material near igneous contacts	1147
Cementation near faults	1148
General statement	1148
Faults at western edge of Triassic basin	1148
Faults within the Triassic basin	1151
Eastern border fault	1151
Origin of cement in the normal arkoses	1152
Conclusions	1153
References cited	1153

ILLUSTRATIONS

Figure	Page
1. Triassic basin in Connecticut and Massachusetts	1135
2. Variation in secondary minerals across contact zone	1144
3. Variation in secondary minerals across contact zone	1145
4. Cemented arkose near fault	1149

Plate — Following page
1. Photomicrographs ... 1146
2. Photomicrographs ... 1146
3. Photomicrographs ... 1146

TABLES

Table — Page
1. Classification of Triassic rocks in Connecticut ... 1136
2. Composition of normal arkoses in Connecticut ... 1137
3. Composition of normal Triassic sedimentary rocks in Massachusetts ... 1138
4. Composition of arkoses near igneous bodies 1139
5. Variation in composition of arkoses across contact zones ... 1140
6. Composition of arkoses and feldspathic sandstones within 1000 feet of large faults 1141

Introduction

This investigation was undertaken to determine the importance of faulting and igneous activity in cementation. The Triassic sediments are well suited for this study because they are faulted and contain igneous bodies; yet relationships have not been complicated by folding and deep burial.

Early detailed studies of the Triassic were made by Davis (1898) in Connecticut and Emerson (1898; 1917) in Massachusetts. More recently the Triassic has been investigated by Longwell (1922; 1928), Bain (1932; 1941), and Willard (1951; 1952). Krynine (1950) made an extensive study of the petrology of the sedimentary rocks and noted that some of the rocks near faults and igneous bodies were unusually well cemented.

Most sampling in this investigation was done in Connecticut because igneous bodies and faults are common (Fig. 1) and the geology has been recently studied (Krynine, 1950). Approximately 300 specimens were collected; 125 were studied in thin section. Mainly arenites were investigated because they were sufficiently permeable for cementation and could be readily studied in thin section. Most of the conglomerates have a sandy matrix in which the cementation is similar to that in the associated arenites.

Acknowledgments

This paper represents part of an investigation conducted under project grant G-98 from the National Science Foundation, to which the writer wishes to express his gratitude. The writer is indebted to Joe W. Peoples for the loan of specimens and for helpful discussions of the problem. The loan of several thin sections and the critical reading of the manuscript by James H. C. Martens are gratefully acknowledged. Appreciation is expressed to John C. Ludlum for suggesting improvements in the manuscript.

General Nature of the Sediments

The present classification of Triassic rocks in Connecticut (John Rodgers, 1955, Personal communication) is based on Krynine's terminology (1950) for the main formations and Emerson's terminology (1917) for the lava flows. The older classification of Davis (1898), which has been widely used, is compared with the present classification in Table 1.

The New Haven arkose is a fluvial deposit consisting of coarse arkoses and conglomerates with some siltstones and shales. The Meriden formation is composed mainly of fine-grained deposits of lacustrine or swamp origin and three lava flows. The characteristic sediments are siltstones, shales, and fine-grained arkoses. The Portland formation is a fluvial deposit composed of coarse arkoses and conglomerates. The formations grade into fanglomerates near the eastern border fault.

In Massachusetts the Triassic has been subdivided into the Sugarloaf formation, the Turners Falls sandstone, the Longmeadow sandstone, the Chicopee shale, and the Mount Toby conglomerate (Emerson, 1917; Willard, 1951). The Sugarloaf formation is composed of coarse arkoses and arkosic conglomerates. The Mount Toby conglomerate consists mainly of coarse detritus from metamorphic rocks. The Longmeadow sandstone and Turners Falls sandstone are medium-grained micaceous sandstones with moderate amounts of feldspar.

Igneous rocks are not as common in the Triassic of Massachusetts although the Hol-

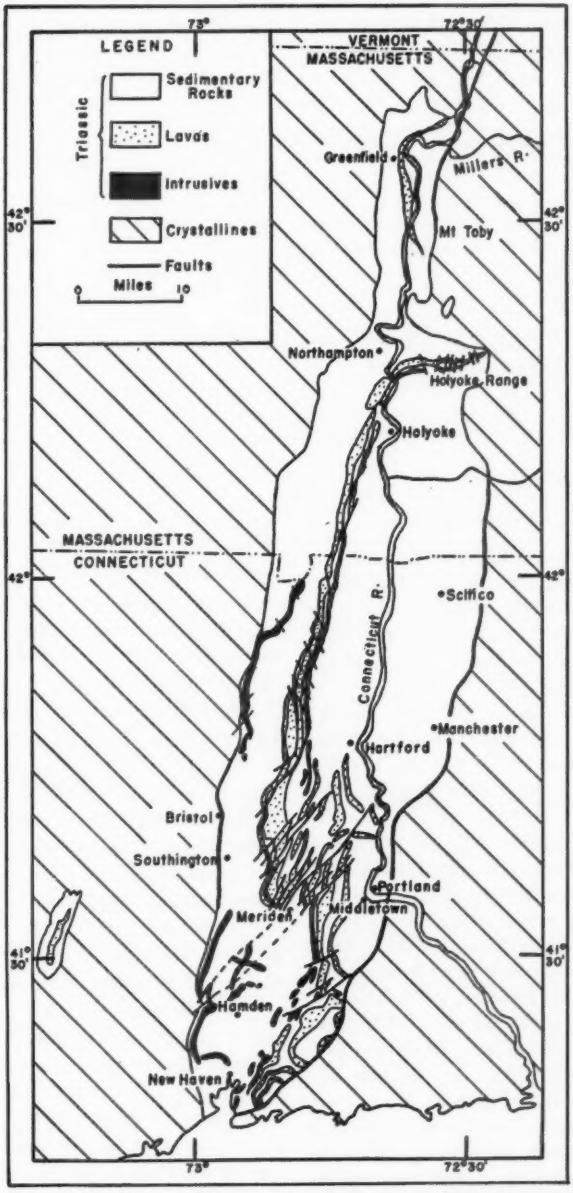

FIGURE 1.—TRIASSIC BASIN IN CONNECTICUT AND MASSACHUSETTS
After Longwell, 1933

yoke (main) lava flow is fairly continuous. Dikes are uncommon, and thick sills are absent. Faults are also less numerous in Massachusetts.

and orthoclase. The plagioclase is considerably more altered than the potash feldspar although some albite grains are fresh. In the perthitic grains of potash feldspar, the albite lamellae

TABLE 1.—CLASSIFICATION OF TRIASSIC ROCKS IN CONNECTICUT

Davis	Krynine and Emerson		Maximum thickness in feet
Upper sandstones	Portland arkose		4000
Posterior trap sheet	Meriden formation	Hampden basalt member	150
Posterior shales		Upper sedimentary division	1075
Main trap sheet		Holyoke basalt member	500
Anterior sandstones and shale		Lower sedimentary division	1000
Anterior trap sheet		Talcott basalt member	250
Under sandstones	New Haven arkose		8500

DETRITAL MINERALS

Detrital minerals in the Triassic sediments of Connecticut have been studied in detail by Krynine (1950). The composition and grain size of the detrital constituents were studied in this investigation because of their possible effect on cementation.

The percentages of the principal detrital minerals and the secondary constituents are given in Tables 2–6. In determining the percentages by the point-counter method, 500–1000 points were counted depending on the uniformity of the sample. With this number of points the results could generally be duplicated within 1 or 2 per cent for the cement and within 4 per cent for the major detrital constituents. Greater precision in the measurement of individual thin sections would be of little significance because of the considerable variation in lithology within single outcrops. The percentages given include pore space so that specimens with different amounts of pore filling can be more easily compared.

The detritus in the fine- to coarse-grained arkoses is composed mainly of individual mineral grains, whereas in the very coarse sediments rock fragments predominate. Most of the specimens studied contain more than 25 per cent feldspar and are therefore classified as arkoses. The feldspars, in order of abundance, are microcline, sodic plagioclase, are generally turbid because of specks of clay and hematite. The pink color of grains of potash feldspar, as seen in the hand specimen, is commonly due to the hematite which is concentrated in the lamellae. In thin section the lamellae with hematite are light red under reflected light.

Grains of microcrystalline albite are present in the arkoses of the upper sediment division of the Meriden formation and in the New Haven arkose in Fair Haven. Emerson (1898, p. 366) reported large fragments of "white diabase" composed of microcrystalline albite in the sediments above the main flow in Holyoke, Massachusetts, and concluded that they represented pyroclastic material. Although the grains in the Connecticut arkoses are much smaller, many of them may also be of volcanic origin. Where secondary albite has been introduced near dikes, it is difficult to distinguish between the fine-grained secondary albite and the primary microcrystalline albite.

In most of the arkoses studied, hematite coats detrital grains and occurs with argillaceous material which fills pore spaces to a small extent. Krynine (1950, p. 21) found that the red argillaceous material was a mixture of clay minerals, gibbsite, and hematite. In Tables 2–6, the red material is referred to as hematitic clay.

TABLE 2.—COMPOSITION OF NORMAL ARKOSES IN CONNECTICUT

In per cent by volume including pore space

Specimen no.	1	2	3	4	5	6	7	8	9	10	11	12A	12B	13	14	15	16	17	18	19	20
Detrital quartz	46	48	41	47	50	45	47	39	41	39	39	43	36	42	41	44	43	40	37	40	37
Secondary quartz	tr	tr	1	4	1	tr	1	tr	4	tr	tr	tr	tr	tr	tr	1	tr	1	tr	tr	tr
Detrital feldspar	36	29	38	31	23	16	11	43	38	27	30	28	34	36	35	28	24	34	30	29	38
Secondary feldspar	9	10	12	6	tr	tr	tr	tr	4	10	5	5	6	tr	3	tr	tr	8	7	8	7
Detrital mica and chlorite	tr	tr	tr	2	8	tr	3	4	5	10	12	4	5	10	8	11	15	3	6	8	4
Miscellaneous detrital		1			2	2	1	1	tr	1	5	5	3	5	2	8	4	4	5	3	tr
Hematitic clay	3	5	2	tr	3	5	7	5		3	3	5	9	5	7	3	7	8	7	7	3
Calcite				5						3	1	tr	tr								
Laumontite					6	32	30									tr	tr				
Secondary sericite					6			7	3												
Porosity*	6	7	6	5	1	<1	<1	1	5	7	4	9	7	1	4	5	6	2	7	5	10
Grain size†	C	C	C	C	C	C	C	M	M	M	M	C	F	M	M	VC	M	M	M	C	VC

* Porosity determined in thin section

† Estimated median weight size of the detrital grains. F = fine sand; M = medium sand; C = coarse sand; VC = very coarse sand (limits after Wentworth, 1922)

New Haven arkose

1–3. Abandoned sandstone quarry in Fair Haven East. 41°17′57″ N.; 72°53′16″ W. New Haven quadrangle

4. East end of Russo Street, East Haven. 41°18′52″ N.; 72°51′27″ W. Branford quadrangle

5. Entrance to Wilbur Cross Parkway at Dixwell Avenue, Hamden. 41°21′58″ N.; 72°55′19″ W. New Haven quadrangle

6. One mile west of Cherry Hill, Hamden. 41°22′15″ N.; 72°57′3″ W. New Haven quadrangle

7. Route 10A, 0.3 mile north of Whitney Lake, Hamden. 41°21′31″ N.; 72°54′36″ W. New Haven quadrangle

8 and 9. Road cut on Route 72 in Forestville. 41°40′22″ N.; 72°54′4″ W. Bristol quadrangle

Portland formation

10–12. Abandoned sandstone quarry in Portland. 12A, coarse-grained portion of specimen; 12B, fine-grained portion

13. Route 6A, quarter of a mile west of junction with Route 17, Portland. 41°34′28″ N.; 72°36′46″ W. Middle Haddam quadrangle

14. Quarter of a mile south of Crystal Lake, Middletown. 41°30′45″ N.; 72°38′45″ W. Middletown quadrangle

15. Half a mile southeast of Dooley Pond, Middletown. 41°30′20″ N.; 72°39′48″ W. Middletown quadrangle

16. Route 17, 2¾ miles north of Durham. 41°30′14″ N.; 72°40′23″ W. Middletown quadrangle.

17. Scantic River, Scitico. 41°58′00″ N.; 72°31′10″ W. Broad Brook quadrangle

18–20. Road cuts on Wilbur Cross Parkway, northeast of junction with Route 44A, Manchester. 17, 2 miles from junction; 18, 3 miles from junction; 19, 3¼ miles from junction

SECONDARY MINERALS

Feldspar

Secondary feldspar is the chief authigenic mineral in most of the arkoses. Albite predominates over potash feldspar except along some of the faults. The secondary feldspar may occur as a rim on detrital grains, as a filling of fractures in feldspar grains, as a microcrystalline aggregate in the interstices, or as a replacement of other minerals.

The rims on detrital plagioclase are consistently albite, but the rims on potash feldspar may be potash feldspar or albite. In the arkoses on Long Mountain, Amherst, Massachusetts, the detrital grains of potash feldspar have rims

of secondary potash feldspar surrounded by rims of albite. In other areas the rims are composed of only one feldspar. Most of the rims are not in exact optical continuity with the detrital cores because of the difference in composition between the rims and core. The albite rims on microperthite are essentially in optical continuity with the albite lamellae.

Commonly the secondary albite next to the detrital cores is polysynthetically twinned, but the sharpness of the twinning decreases away from the core. The outer portions of the larger growths are untwinned. The extinction in secondary potash feldspar is slightly undulatory, but sharp microcline twinning is absent.

The feldspar growths are euhedral except where enlargement has been impeded by other grains. The early formed feldspar is characteristically turbid owing to tiny inclusions. At least part of the inclusions are hematite for much of the turbid feldspar is pink. Liquid inclusions are uncommon inasmuch as the average index of the turbid feldspar is not abnormally low. The inclusions do not represent foreign matter which has remained essentially in place on the surfaces of the detrital grains because the early crack fillings within the grains are as turbid as the rims. Although some loose particles were redistributed, they were engulfed in the early formed feldspar; hence most of the later feldspar crystallized free of inclusions (Pl. 1, fig. 1).

Near igneous bodies and some faults, the secondary feldspar occurs as a fine-grained crystalline aggregate. Except for these occurrences there is little secondary feldspar without detrital cores.

Secondary feldspar replaced part of the hematite coating on detrital grains. Although normally the core boundaries are well marked, the coating is thinner under the secondary outgrowths than it is on the free surfaces of the detrital grains. The surfaces of the secondary growths are free of hematite or clay. Quartz near feldspar grains that were enlarged is commonly slightly replaced by the feldspar outgrowths (Pl. 1, fig. 2). Much of the original hematite coating on quartz is clearly visible within the replacing feldspar. Because two dust rings are present, these growths might be mistaken for worn overgrowths. Some of the replacing feldspar is prismatic and therefore resembles columns of microstylolites.

Fedlspar normally does not occur as a vein filling in arkoses, but albite was deposited along with calcite in fractures which cut shale near New Britain, Connecticut.

Quartz

Secondary quartz is much less common than secondary feldspar except near faults. The growths are small and less turbid than those of feldspar. Normally the quartz occurs as rims on detrital grains and as a filling where grains have been fractured. The healed fractures are not easily detected because the secondary quartz is commonly clear and in optical con-

TABLE 3.—COMPOSITION OF NORMAL TRIASSIC SEDIMENTARY ROCKS IN MASSACHUSETTS

In per cent by volume including pore space

Specimen no.	21	22	23	24	25	26
Detrital quartz	42	45	45	39	47	34
Secondary quartz	tr	1	tr	2	tr	tr
Detrital feldspar	34	43	43	17	10	10
Secondary feldspar	7	6	3	2	tr	tr
Mica and chlorite	6	1	1	25	27	55
Miscellaneous detrital	1		1	4	2	1
Hematitic clay	tr	tr	4	tr	tr	tr
Calcite	9	4		6	14	
Porosity	1	<1	3	5	<1	<1
Grain size*	C	G	G	M	G	F

* F = fine sand; M = medium sand; C = coarse sand; G = granules

Sugarloaf formation

21 and 22. Route 5 at Hampshire-Hampden county line. 42°17′5″ N.; 72°36′57″ W. Mt. Holyoke quadrangle

23. In Holyoke Range, 1000 feet north of summit of Long Mountain 42°18′28″ N., 72°29′4″ W. Belchertown quadrangle

Turners Falls sandstone

24. Route 47, 2½ miles north of Sunderland. 42°29′55″ N.; 72°33′44″ W. Mount Toby quadrangle

Mount Toby conglomerate

25 and 26. Route 2, ¾ mile west of the Connecticut River. 42°36′27″ N.; 72°30′21″ W. Greenfield quadrangle

TABLE 4.—COMPOSITION OF ARKOSES NEAR IGNEOUS BODIES

In per cent by volume including pore space

Specimen no.	27	28	29	30	31	32	33	34	35	36	37
Distance from contacts in feet	25	100	4	55	0.4	0.2	0.1	12	4	140	170
Detrital quartz	51	54	31	49	53	59	35	42	50	27	32
Secondary quartz	1	1			1				6	1	tr
Detrital feldspar	26	28	46	30	23	20	34	33	24	37	35
Secondary albite rims		1	6	5	1			4	4	11	12
Secondary microcrystalline albite		11	8	6	15	13	27	20			
Detrital mica and chlorite	1	2	1	1				tr	13	1	2
Hematitic clay	2	3	4	3	3						
Calcite			1							23	16
Laumontite	19										
Secondary chlorite						8			2		
Miscellaneous			1		1		3	1	1		2
Porosity	<1	<1	2	6	3	<1	<1	<1	<1	<1	1
Grain size*	C	G	M	C	VC	C	C	C	M	M	M

*M = medium sand; C = coarse sand; VC = very coarse sand; G = granules

New Haven arkose

27. West end of dike at Pine Rock, Hamden, Connecticut. 41°20′12″ N.; 72°57′18″ W. New Haven quadrangle
28. Southeast of intrusive at Snake Rock, New Haven, Connecticut. 41°19′22″ N.; 72°53′48″ W. New Haven quadrangle

29 and 30. East side of small dike in eastern sandstone quarry in Fair Haven East, Connecticut. 41°17′57″ N.; 72°53′2″ W. New Haven quadrangle

31. Near small dike in road cut on Route 1, 1 mile west of East Haven, Connecticut. 41°17′20″ N. 72°53′48″ W. New Haven quadrangle
32. Below West Rock sill at Clark-Barone quarry, New Haven, Connecticut. 41°21′3″ N.; 72°58′32″ W. New Haven quadrangle
33. At contact of small dike on west side of railroad cut south of tunnel in Fair Haven East, Connecticut. 41°18′2″ N.; 72°52′49″ S. New Haven quadrangle
34. Midway between two small dikes at the railroad cut in Fair Haven East

Sugarloaf formation

35. Below Holyoke flow on Long Mountain, Holyoke Range, Massachusetts. 42°18′17″ N.; 72°29′8″ W. Belchertown quadrangle

Meriden formation

36 and 37. Below Hampden flow, Route 72 quarter of a mile east of Route 5, Berlin, Connecticut. 41°37′28″ N.; 72°44′17″ W. Middletown quadrangle

tinuity with the detrital grain. Much of the quartz introduced along faults and dikes is cryptocrystalline and is intergrown with feldspar. Small veins of coarse-grained quartz are also common near faults.

Calcite

Calcite occurs as an interstitial filling, as a replacement of other minerals, and as a vein filling. The calcite is undeformed; yet surrounds bent mica and fractured feldspar. It probably was introduced after compaction, although late recrystallization would have obliterated evidence of deformation.

Most of the calcite is present as a replacement of other minerals. Feldspars were particularly susceptible to replacement. Completely replaced grains are commonly indicated by a ring of hematite within the calcite (Pl. 1, fig. 3). In some specimens a few grains are completely replaced and the remaining grains

are unaltered. The more calcic plagioclases apparently altered first. Although overgrowths were seldom replaced, replacement occurred after growth because some completely altered feldspar cores have secondary rims. If replacement had preceded growth, a rim could not have formed because of the lack of a suitable nucleus. In some of the arkoses bordering dikes, the microcrystalline matrix of secondary albite was partly replaced by calcite. Quartz is slightly replaced by calcite in some of the calcareous arkoses of the Meriden formation. Near the fault at Roaring Brook, Connecticut, calcite occurs in one-inch crystals which poikilitically enclose many detrital grains. This calcite appears to have replaced an interstitial filling of sericite.

Small veins of calcite cut the sediments locally. Although the veins are more common near faults and igneous bodies, they also occur in some of the normal sediments. Calcite may be the chief vein filling or it may be subordinate to quartz. Commonly the calcite is later than quartz, for it occupies the central portion of the veins.

TABLE 5.—VARIATION IN COMPOSITION OF ARKOSES ACROSS CONTACT ZONES

In per cent by volume including pore space

Specimen no.	38	39	40	41	42	43	44	45	46	47	48	49	50	51	52	53	54
Distance from contact in feet	5	25	40	60	35	100	150	1	9	17	17	35	0.1	9	45	45	60
Detrital quartz	40	48	57	49	43	40	42	54	40	42	51	51	45	42	37	30	43
Secondary quartz rims		tr	1	2	1	1	8	1	3	3	3	3		1	3	1	1
Detrital potash feldspar	12	15	14	17	5	16	7	17	11	10	14	13	2	21	13	15	15
Detrital plagioclase	10	8	9	8	23†	14	7	13	7	15	16	20	29†	15	28	20	18
Secondary albite rims	tr	1	1	3	1	6	1	tr			tr	2		7	8	7	6
Secondary microcrystalline albite	30*	21	11	10	22	18		7		8	6	2	13*	6	2		
Detrital mica and chlorite			2	2	tr	2	2	3	3	2	3	4	tr	2	1	6	2
Miscellaneous detrital	1	3	1	1	1	1			1	1	1				1		
Hematitic clay				tr		tr					tr	tr			tr	5	9
Calcite													8		2		3
Secondary sericite	tr			1						1	2	3				5	
Secondary chlorite	7	2	2	3			3	4	12	tr			tr				
Secondary epidote							28		21	14							
Porosity	<1	1	2	4	3	2	2	<1	1	4	3	2	2	6	4	10	3
Grain size**	C	C	VC	C	C	C	C	VC	VC	C	VC	VC	C	C	C	M	C

* Includes small amounts of fine sericite and quartz

† Probably includes some secondary albite which is pseudomorphous after detrital potash feldspar

** M = medium sand; C = coarse sand; VC = very coarse sand

New Haven arkose

38–41. South contact zone at west end of dike at Mill Rock, Hamden, Connecticut

42–44. South contact zone at Mill Rock opposite Winchester Street

45–49. North contact zone at east end of Mill Rock on Whitney Avenue. Specimens 44 and 45 are from green patches in the arkose; other specimens are typical red arkoses

50–54. Contact zone at dike on Russo Street, East Haven, Connecticut

Calcite is easily leached during weathering particularly in the porous rocks. Inasmuch as feldspar is commonly replaced by calcite, leaching of calcite is indicated where voids occur within feldspar. The outer margins of the grains are not significantly corroded because the secondary feldspar was not easily replaced by calcite. In most specimens where there is evidence of the removal of calcite, the present porosity is so small that the original amount of calcite could not have been high.

Sericite

Secondary sericite occurs in some arkoses near igneous bodies and mineralized fault zones. It may constitute the entire pore filling

TABLE 6.—COMPOSITION OF ARKOSES AND FELDSPATHIC SANDSTONES WITHIN 1000 FEET OF LARGE FAULTS

In per cent by volume including pore space

Specimen no.	55	56	57	58	59	60	61	62	63	64	65	66	67	68	69	70	71
Approximate distance from fault in feet	500	500	80	100	350	120	120	420	250	10	150	400	700	700	500	15	100
Detrital quartz	50	48	65	55	61	43	59	61	37	35	41	46	52	48	43		
Secondary quartz rims	11	6	4	1	4		2	3	tr	tr	4	tr	tr	tr	1	23	44
Detrital feldspar	16	16	19	21	10	17	13	25	33	36	24	34	31	35	31		
Secondary feldspar rims	2	1							8	9	5	tr	tr	tr	tr		
Cryptocrystalline quartz, feldspar, and sericite	17	26															
Detrital mica and chlorite	2	2	tr	2	1	4	tr	tr	14	6	14	6	6	9	5	44	34
Hematitic clay									7		1	5	tr	3	10	8	4
Calcite						34				11	9	8	4		4	24	14
Laumontite														tr			
Secondary sericite	2	1	12	18	18	1	19	10									
Barite					tr												
Miscellaneous				2			3			2	2	1	4	3		1	4
Porosity	<1	<1	<1	1	6	<1	4	1	1	<1	<1	<1	2	2	5	<1	<1
Grain size*	VC	VC	VC	C	VC	C	C	VC	M	F	M	M	C	C	M	G	G

* F = fine sand; M = medium sand; C = coarse sand; VC = very coarse sand; G = granules

Near faults at western border of basin

55 and 56. New Haven Arkose. King Street, half of a mile south of Farmington Avenue, Bristol, Connecticut. 41°40′54″ N.; 72°55′26″ W. Bristol quadrangle

57–59. New Haven Arkose. North Branch of Roaring Brook, Southington, Connecticut

61–62. New Haven Arkose. South Branch of Roaring Brook

Near faults within the basin

63. Sugarloaf formation. Near fault west of Long Mountain in Holyoke Range, Massachusetts. 42°18′18″ N.; 72°29′10″ W. Belchertown quadrangle

64. Longmeadow sandstone. Near fault south of Kennedy Pond, Holyoke, Massachusetts. 42°16′20″ N.; 72°36′31″ W. Mt. Holyoke quadrangle

65. Mount Toby conglomerate. West of fault at Whitmore Pond, 3 miles north of Sunderland, Massachusetts. 42°30′21″ N.; 72°33′25″ W. Mount Toby quadrangle

Near east border fault

66. Portland formation. Route 6A, 600 feet west of junction with route 17, Portland, Connecticut. 41°34′29″ N.; 72°36′31″ W. Middle Haddam quadrangle

67 and 68. Portland formation. Route 17, 1 mile north of junction with Route 6A, Portland Connecticut. 41°35′14″ N.; 72°36′45″ W. Middle Haddam quadrangle

69. Portland formation. West side of Lake Quonnipaug, Connecticut. 41°23′35″ N.; 72°41′58″ W. Durham quadrangle

70 and 71. Mount Toby conglomerate. South bank of the Connecticut River just west of the mouth of Millers River, Massachusetts. 42°35′46″ N.; 72°30′2″ W. Greenfield quadrangle

but generally is intergown with microcrystalline secondary quartz and feldspar. In fractured rocks it occurs in veinlets with quartz. A small amount of secondary sericite is also present in some arkoses far removed from igneous bodies or faults. The turbidity of feldspar is probably due partly to sericitization although some of the arkoses with abundant secondary sericite have fresh feldspar.

Chlorite

Light-green pleochroic chlorite occurs in many arkoses near igneous contacts and in a few faulted arkoses. The chlorite generally occurs in small irregular clumps or in spherulitic masses within the microcrystalline albite matrix. Chlorite is particularly abundant in specimens that contain secondary epidote and fills many of the voids and replaces detrital grains.

Laumontite

Many of the arkoses in Hamden and northern New Haven, Connecticut, contain considerable laumontite. Traces of laumontite also occur in arkoses in Middletown and Portland. In some specimens the zeolite fills pore spaces and partly replaces the feldspar, especially potash feldspar (Pl. 1, fig. 4). In replaced perthite, the albite lamellae are left as relics within the laumontite.

The optical properties of the laumontite are:

$N_x = 1.505$ 2V small (−)
$N_y = 1.510$
$N_z = 1.514$

The indices are slightly lower than those reported by Winchell (1951, p. 342); hence the water and calcium content may be low. X-ray diffraction data agree with those given for laumontite from Transylvania (A.S.T.M. X-ray diffraction data cards, 1950). Dana (1891) reported occurrences of laumontite in veins cutting diabase at Mill Rock and Whitney Peak in Hamden, Connecticut. Laumontite has also been found in the Triassic diabases of New Jersey (Fenner, 1910) and Virginia (Shannon, 1924), but no zeolites were reported in the associated sediments.

The fact that laumontite occupies cracks in fractured detrital grains and surrounds deformed mica indicates that it formed after at least initial compaction of the sediments. Although laumontite may result from alteration of original feldspar in sediments (Williams, Turner, and Gilbert, 1954, p. 301), part of the material for the laumontite in the Triassic must have been introduced because much of it occurs as interstitial filling. The introduced material may be of igneous origin, for laumontite is present in some of the diabases and in the contact zone at Pine Rock in Hamden, Connecticut.

Pressure Solution

Although no large stylolite seams were observed, closely spaced microstylolite seams are locally common. A small to moderate amount of solution also occurred where grains were under stress at points of contact.

The importance of pressure solution in pore reduction in the Triassic sediments is difficult to determine because of the numerous variables involved. In well-sorted quartz sandstones considerable pressure solution is commonly indicated where porosity before cementation was low. However, in the arkoses studied, sorting varied considerably, and porosity was reduced by deformation of mica as well as by pressure solution.

Considerable pressure solution occurred in sediments along the eastern border fault for a distance of at least 1000 feet from the fault. Although some porosity was lost through deformation of grains and cementation, a large part of the reduction resulted from pressure solution. Practically all grain contacts are conspicuously sutured (Pl. 1, fig. 5), and closely spaced microstylolite seams are prevalent. The rocks in this area were apparently subjected to greater stress because of the border faulting. Deformation is further indicated by slickensided surfaces.

Pressure solution is not as widespread along other faults studied. Near the fault on Long Mountain, Massachusetts, brecciation commonly attended pressure solution. However, some specimens show evidence of brecciation with little pressure solution apparently because deformation was relatively rapid. A moderate amount of pressure solution occurred along the fault at the western edge of the Triassic basin in Bristol and Southington, Connecticut. Replacement by introduced minerals in this area probably obliterated some evidence of pressure solution.

The amount of pressure solution in arkoses near igneous contacts varies considerably even along the same body. These differences seemed to be related to differences in deformation rather than composition of the pervading solutions because the more highly pressolved[1] specimens were also more fractured.

The greater solubility of quartz under stress compared to feldspar is striking in the moderately pressolved specimens. Quartz tends to be penetrated by other minerals, and mutual contacts between quartz grains are sutured,

[1] Pressolved specimens are specimens which have undergone pressure solution.

whereas the borders of feldspar grains are little affected. Much of the feldspar was under considerable stress for it is commonly fractured. In highly pressolved specimens, grains of both quartz and feldspar are sutured; hence differences in solubility are not apparent. Presumably the solution of quartz was also greater than that of feldspar in these specimens. In many sandstones quartz is more easily pressolved than feldspar (Heald, 1955, p. 109).

The fact that muscovite is resistant to pressure solution is evident in the micaceous arkoses. Many quartz grains that apparently had fairly high sphericity originally have flat contacts against muscovite because the quartz dissolved without affecting the muscovite. Where compaction or deformation was great, muscovite was penetrated by other grains. However, most of this penetration appears to have been accomplished by mechanical deformation rather than by solution. Biotite and chlorite are more easily pressolved than muscovite, for their contacts are more highly sutured (Pl. 1, fig. 6). Garnet is generally resistant to pressure solution, but some grains are sutured (Pl. 2, fig. 1).

The relationship between pressure solution and clay content in the Triassic sediments is not so apparent as in the St. Peter sandstone (Heald, 1956). Nevertheless, clay may have promoted solution, for the coarse detritus in some of the shaly beds is more highly sutured than the grains in the associated arkoses.

The time of pressure solution relative to cementation could not be determined with certainty. Although some secondary growths are sutured, most of the growths show no evidence of pressure solution. Apparently solution occurred mainly before authigenesis but continued to a limited extent after the growth of secondary rims. Inasmuch as many grains were fractured before secondary growths formed, stress conditions must have been particularly favorable for pressure solution before cementation. Pressure solution accompanying late faulting probably occurred after the onset of cementation; however, the evidence is not clear because of brecciation and mineral alteration in the faulted zones.

Cementation

General Statement

To evaluate the importance of igneous activity and faulting in cementation, specimens of arkoses were collected near igneous bodies and faults, and these were compared with normal[2] arkoses which were outside contact zones. In sampling the normal arkoses the effect of concealed igneous bodies that might be near by could not be determined; however, the degree of cementation, on the average, should be normal because the specimens were collected from widely scattered areas.

Cementation of the Normal Arkoses

In addition to the original hematite and clay, which act as binding materials, a moderate amount of precipitated cement is commonly present in the normal arkoses of the New Haven and Portland formations of Connecticut and the Sugarloaf formation of Massachusetts. In the Triassic sediments of Connecticut, cementation was thought to be unimportant except in the vicinity of major faults and igneous bodies (Krynine, 1950, p. 85). However, the present study indicates that in most arkoses more than half the porosity that remained after compaction was lost by cementation.

Although detrital quartz exceeds feldspar in most of the arkoses, secondary quartz is much less abundant than secondary feldspar. Except for a few specimens, the secondary feldspar is albite. A moderate amount of calcite is present in nearly half the arkoses studied, but most of it occurs as a replacement of detrital grains rather than as an interstitial cement. Only a few specimens of the normal arkoses contained secondary sericite or secondary chlorite. Considerable zeolite occurs in the arkoses in Hamden and northern New Haven but is uncommon in other areas.

Although variations in cementation within the normal arkoses can not be given in great detail because of limited sampling, the general distribution of the cement may be outlined. A

[2] Following Krynine (1950, p. 87) "normal arkose" is used to designate the arkoses of fluvial origin, which are not near igneous bodies or major faults.

comparison of lithologically similar specimens indicates that the distribution of cement is probably unrelated to stratigraphic position. It might be expected that the youngest and stratigraphically highest units would be least cemented. However, samples of the Portland formation from Scitico and Portland, Connecticut, contain an average amount of cement. Some of the specimens of the Portland formation from Middletown (Table 2, specimen 15) are poorly cemented, but some of the arkoses from the lower part of the New Haven formation also have little cement (Table 2, specimen 8). The Meriden formation appears to be better indurated than the other units, but is finer-grained and more micaceous than most of the other arkoses and was deposited in a different environment (Krynine, 1950, p. 31).

The matrix of the arkosic conglomerates is generally sandy; therefore, their cementation is similar to that of the arkoses in the arenite size range. No appreciable difference in the amount of precipitated cement was observed in the coarse- and fine-grained arenites, although with more samples some significant differences might have been detected. The highly argillaceous arkoses contained little precipitated cement apparently because they were impervious to circulating solutions. The hematite and clay coatings do not appear to have retarded the enlargement of grains because secondary growths are common in some of the arkoses in which detrital grains are fairly heavily coated.

Cementation Near Igneous Bodies

Lower contacts of flows.—The sediments most closely associated with the lava flows are in the Meriden formation. Inasmuch as the sediments in this formation are largely composed of fine-grained lacustrine deposits (Krynine, 1950, p. 31), they could not be compared directly with the coarser sediments of fluival origin. The arkoses in the Meriden formation appear to be uniformly well cemented regardless of distance from the flows; therefore, the flows probably had little direct effect on the cementation of these sediments. On Long Mountain, in the Holyoke Range in Massachusetts, a flow rests on typical coarse-grained arkoses. The one sample examined near the base of this flow contained somewhat more cement than the average arkose; hence cement may have been introduced from the flow.

Intrusive contacts.—Specimens of arkose were examined at 10 localities where dikes or sills cut the New Haven arkose in southern Connecticut

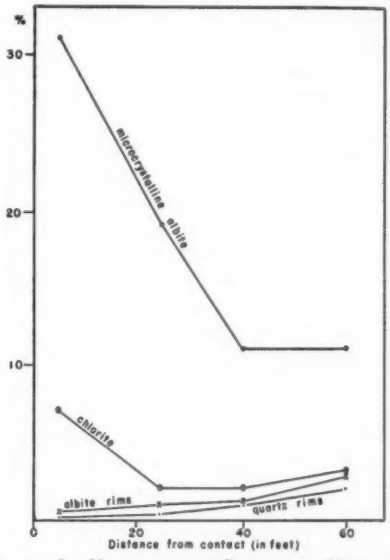

FIGURE 2.—VARIATIONS IN SECONDARY MINERALS ACROSS CONTACT ZONE
West end of dike at Mill Rock, Hamden, Connecticut

(Tables 4, 5). Except at Pine Rock, a large amount of secondary albite occurs in the contact zones with minor amounts of secondary quartz, chlorite, and sericite. At Pine Rock the secondary minerals are mainly zeolite and sericite. At 4 localities the arkoses were sampled along traverses perpendicular to the contacts. Specimens were collected out to a distance of 60–150 feet, depending on the size of the exposures. Three of the zones sampled were at different points along Mill Rock in Hamden, and one was at the dike on Russo Street in East Haven. At these localities the intrusives cut bedding approximately at right angles; hence, specimens of originally similar lithology could be compared at different distances from the dikes (Table 5).

The variations in mineralogy across the contact zone at two of the intrusives are given in Figures 2 and 3.

At the contacts studied, the changes in mineralogy and texture which occur with increasing distance from the intrusives are generally the same although the widths of the affected zones differ. The interstices of the arkoses at the

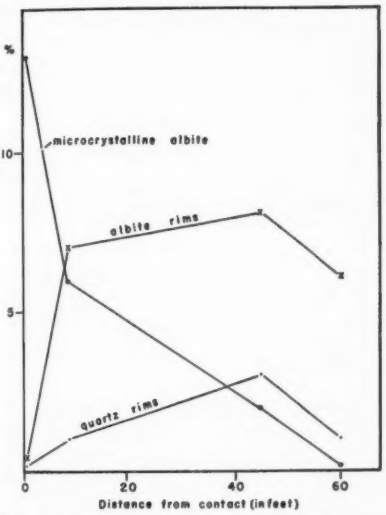

FIGURE 3.—VARIATION IN SECONDARY MINERALS ACROSS CONTACT ZONE

Coarse arkose at dike on Russo Street, East Haven, Connecticut

contacts are typically filled with very fine-grained albite (Pl. 2, fig. 3) and a small amount of chlorite and sericite. Overgrowths on detrital grains are scarce. The most extensive corrosion and replacement also occurs at the contacts. With increasing distance from the intrusives, the interstitial albite filling becomes coarser-grained (Pl. 2, fig. 4) and decreases in amount, whereas enlargements on both feldspar and quartz increase. Where the amount of interstitial albite becomes negligible, the number and size of the secondary enlargements are approximately the same as in the normal arkoses.

Overgrowths apparently could not form at the contacts because of the high rate of nucleation in the more highly concentrated solutions near the contacts; therefore, the albite crystallized as a microcrystalline mosaic. At intermediate distances from the contacts, where solutions were less concentrated, a coarser interstitial filling formed and some enlargements developed. At the outermost zone, where solutions were relatively weak, most of the albite could form as enlargements. The interstitial albite and secondary enlargements appear to have formed simultaneously in a given specimen because the cores of the interstitial albite crystals and the inner portion of the secondary enlargements are very turbid, whereas the margins of the interstitial crystals and enlargements are generally clear. The turbidity is due to a fine dust of clay and in some places hematite.

There are some variations in the texture of the secondary minerals within single thin sections, particularly in the specimens at intermediate distances from the contacts. The interstitial filling of albite in some pores is noticeably coarser than the filling in the rest of the specimen. Apparently the influx of mineral matter into these pores was slower than average; hence, larger crystals formed. In the pores with the least filling, the albite tends to be coarsest. It seems that variations in the relative amount of interstitial albite and albite enlargement in different pores depended on the number of detrital feldspar grains suitable for enlargement at the margin of a given pore as well as the rate of movement of solute into the pore. Nearly all the secondary quartz was deposited as enlargements on quartz grains rather than as separate crystals in the interstices apparently because the concentration of silica in the solutions was relatively low and a large number of detrital quartz grains were available for enlargement.

In addition to the filling of open spaces, considerable replacement of detrital grains occurred within a few feet of the intrusives. Most of the quartz grains have irregular borders because of corrosion; most mica and garnet were albitized. Replaced mica is easily recognized because of traces of dark matter along the former cleavage planes (Pl. 2, fig. 5). Pseudomorphs containing disseminated iron oxide and sphene presumably represent altered biotite or chlorite. Muscovite was apparently more resistant to replacement than biotite and chlorite, for muscovite is present in many of the contact rocks where other micaceous minerals are absent. Completely replaced garnet would be difficult to recognize, but in many of the pseudomorphs remnants of garnet are preserved at the core

(Pl. 2, fig. 2). The albite in the pseudomorphs forms a relatively coarse mosaic of interlocking crystals (Pl. 2, fig. 6), which average 0.05 mm in diameter even where the albite filling in the pores is nearly submicroscopic. Hematite is generally absent near the igneous contacts, but magnetite and chlorite and, in some specimens, epidote occur instead.

In most specimens, grains of potash feldspar are slightly albitized at the margins (Pl. 3, fig. 1) and along fractures. The replacing albite forms a single unit that has approximately the same orientation as the potash feldspar and is in optical continuity with albite lamellae in the grains that are perthitic. Unreplaced portions of the potash feldspar are commonly free of sericite and are fresh. The fact that only small remnants of some potash feldspar grains are left suggests that other grains of potash feldspar may have been completely replaced by albite. These grains could not be distinguished from original detrital albite. The albitization of potash feldspar occurs in some specimens as far as 100 feet from the intrusives.

Nearly all the detrital plagioclase near the contacts is very turbid, apparently from partial sericitization and kaolinization. Potash feldspar is rarely altered, but the albite lamellae within the perthitic grains are very turbid.

Secondary epidote is important in a few of the samples from the contact zone at Mill Rock (Pl. 3, fig. 2). Its distribution in the contact zone does not seem to bear any relationship to distance from the contacts. Small epidote-rich patches of arkoses may occur fairly near the intrusive and up to 150 feet away. Secondary

---

PLATE 1.—PHOTOMICROGRAPHS

FIGURE 1.—Two stages of fracturing in orthoclase. Early fractures (1) are filled with turbid albite, whereas late fractures (2) are filled with clear albite. Sugarloaf formation, Route 5 at Hampshire-Hampden county line. Crossed nicols. × 195

FIGURE 2.—Margin of large quartz grain (Q) replaced by secondary albite outgrowths (arrows) from feldspar grains (F). The dark hematite coating on the quartz grain was not replaced. New Haven arkose (Table 2, specimen 20). Crossed nicols. × 80

FIGURE 3.—Calcite pseudomorph (P) with ring of hematite which represents the original coating on the replaced grain. Calcite in the pseudomorph is in optical continuity with the calcite (C) which fills pores. Replaced grain may have been a somewhat calcic plagioclase. Albite (A) in contact with calcite is unreplaced and has a large twinned outgrowth (arrow). Portland formation (Table 2, specimen 10). Crossed nicols. × 75

FIGURE 4.—Laumontite (L) as a pore filling and replacement (arrows) of feldspar (F). New Haven arkose, 25 feet from dike at Pine Rock, Hamden, Connecticut (Table 4, specimen 27). Crossed nicols. × 40

FIGURE 5.—Sutured contacts between detrital grains due to pressure solution. Portland formation (Table 2, specimen 13). Crossed nicols. × 80

FIGURE 6.—Sutured contacts between quartz grains (Q) and biotite (black) resulting from pressure solution. Biotite is only slightly deformed in spite of deep penetrations. New Haven arkose (Table 2, specimen 8). Crossed nicols. × 55

PLATE 2.—PHOTOMICROGRAPHS

FIGURE 1.—Sutured garnet contact (arrow) due to pressure solution. Portland formation, approximately 700 feet from east border fault (Table 6, specimen 67). Plain light. × 120

FIGURE 2.—Garnet partly replaced by albite (A). Dashed line indicates original outline of the garnet. New Haven arkose, 25 feet from dike at Mill Rock (Table 5, specimen 39). Plain light. × 80

FIGURE 3.—Introduced cryptocrystalline albite, 5 feet from dike at Mill Rock. Raggedness of detrital grains is due to corrosion. New Haven arkose (Table 5, specimen 38). Crossed nicols. × 85

FIGURE 4.—Shows coarser introduced albite. Specimen is 35 feet farther from dike than the specimen shown in Figure 3. The cores of the small albite crystals are characteristically turbid, whereas the outer margins are clear. New Haven arkose (Table 5, specimen 40). Crossed nicols. × 85

FIGURES 5, 6.—Microcrystalline albite pseudomorphous after mica. Former cleavage planes are marked by streaks of opaque matter. Albite is uniformly turbid. New Haven arkose, 25 feet from dike at Mill Rock (Table 5, specimen 39). Figure 5, plain light. Figure 6, crossed nicols. × 90

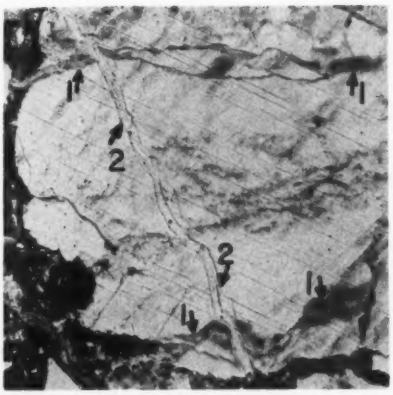

FIGURE 1

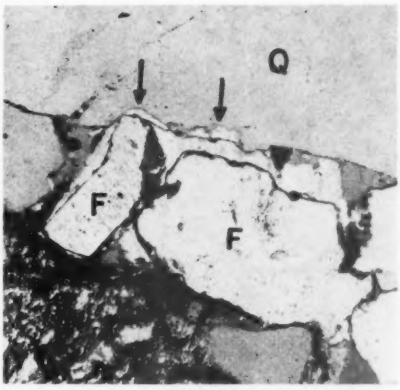

FIGURE 2

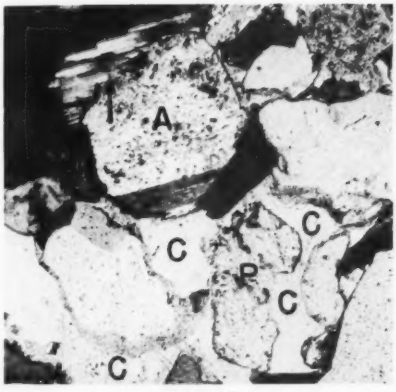

FIGURE 3

FIGURE 4

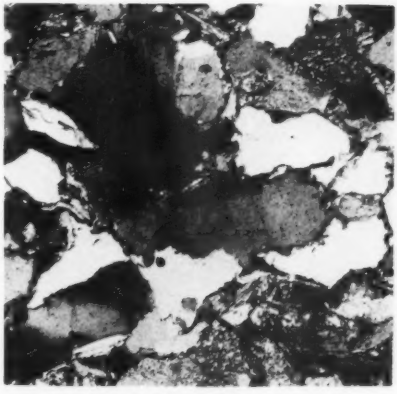

FIGURE 5

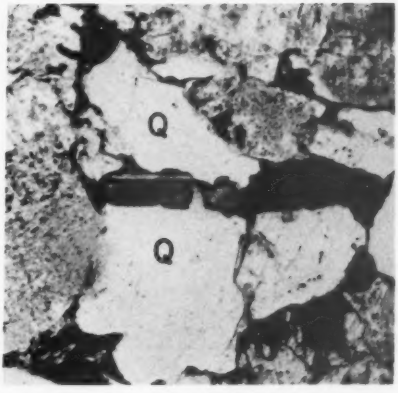

FIGURE 6

PHOTOMICROGRAPHS

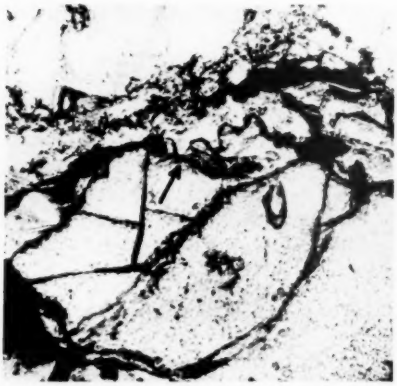

FIGURE 1

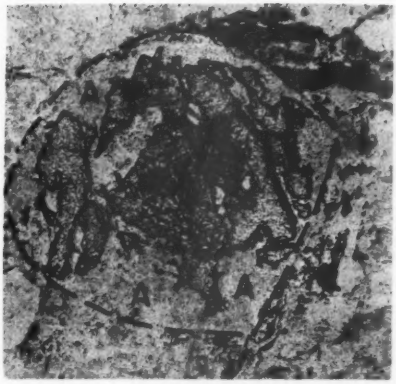

FIGURE 2

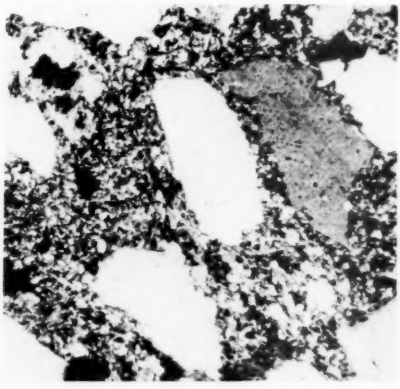

FIGURE 3

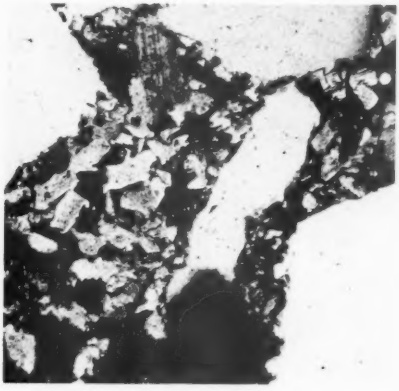

FIGURE 4

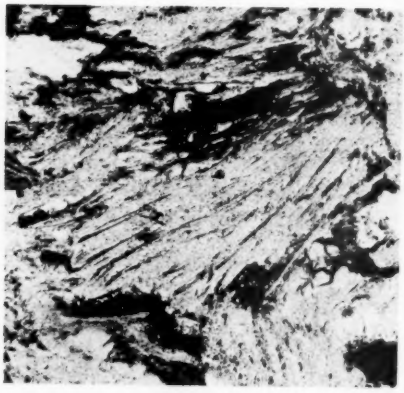

FIGURE 5

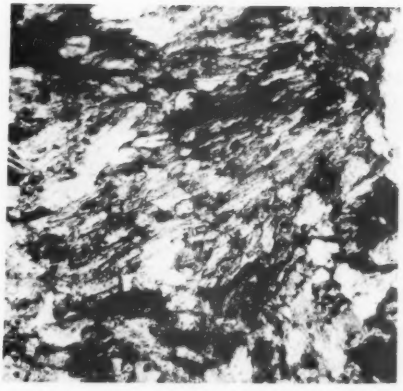

FIGURE 6

PHOTOMICROGRAPHS

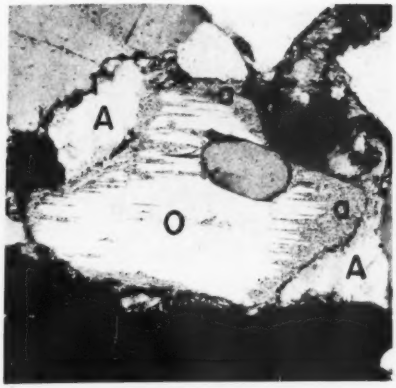

FIGURE 1

FIGURE 2

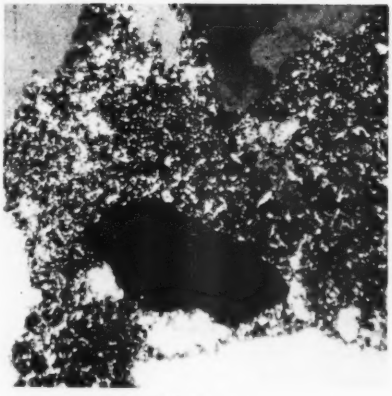

FIGURE 3

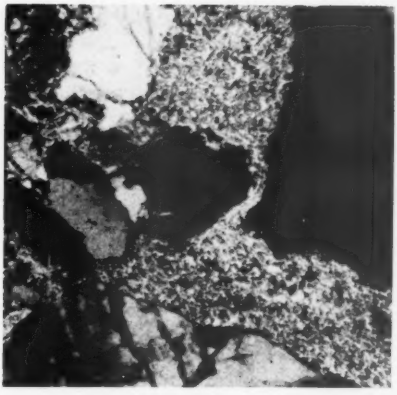

FIGURE 4

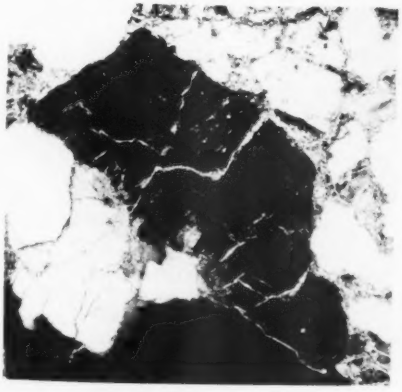

FIGURE 5

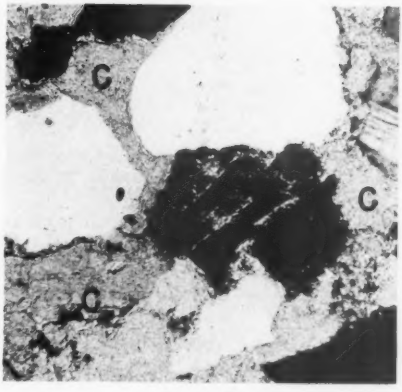

FIGURE 6

PHOTOMICROGRAPHS

albite is less common in specimens with epidote, but secondary quartz and chlorite are moderately abundant. Many of the detrital grains are deeply corroded. The abnormally low proportion of detrital feldspar in the epidote-bearing rocks indicates that feldspar was more easily destroyed than quartz.

Although calcite is present in the contact zone along the dike at Russo Street, it is not necessarily genetically related to the dike. The amount of calcite at the contact is no greater than that in some of the normal arkoses. The decrease in calcite away from the dike is due partly to the removal of calcite through weathering. Calcite crystallized after secondary feldspar, for it replaces feldspar enlargements as well as the detrital grains. At the contact the calcite in the matrix appears to have replaced interstitial secondary albite because the inclusions in the calcite resemble those in the albite.

Origin of the cementing material near igneous contacts.—Two theories are considered for the origin of cement near igneous bodies. (1) The cement may be the result of the recrystallization of pre-existing sedimentary material or (2) it may have been introduced from a magmatic source.

If simple recrystallization had occurred, one would expect a cement of quartz, potash feldspar, and albite instead of one composed almost exclusively of albite, because potassium and silicon as well as sodium are considered to be mobile (Ramberg, 1952, p. 243). If selective recrystallization of plagioclase had occurred, the amount of detrital plagioclase should decrease as secondary albite increases. However, the amount of secondary albite and detrital plagioclase appear to vary independently (Table 5). Although the detrital plagioclase has undergone some sericitization and kaolinization, the original grains are little modified. For these reasons, it appears unlikely that the cement was chiefly the result of recrystallization of original sedimentary material.

A magmatic source for most of the albite cement near igneous bodies seems more probable inasmuch as the residual solutions from basic magmas are commonly sodic. The veinlets and interstitial fillings of albite and quartz in many basic intrusives are believed to have formed from residual liquids (Bowen, 1910, p. 662; Walker, 1940, p. 1097; Von Eckermann, 1938, p. 412). Some of the veinlets in the Triassic diabases in Virginia (Shannon, 1924, p. 27) and in Massachusetts (Emerson, 1917, p. 263) are mainly albite. The late pegmatitic phase in the Holyoke sheet at Tariffville, Connecticut, is more sodic than the normal basalt (Peoples, 1955, Personal communication). A feldspathic dike high in soda has been reported in New Haven, Connecticut (Hovey, 1897).

The mineralogical and textural changes in the contact zones strongly suggest that the introduced material emanated from the adjacent intrusives rather than from bodies at depth. The largest amount of material was consistently deposited at the contacts. The fine-grain size of the introduced material at the contacts suggests rapid deposition from relatively concentrated solutions. Had the solutions originated at depth,

---

PLATE 3.—PHOTOMICROGRAPHS

FIGURE 1.—Margin of orthoclase (O) grain replaced by turbid albite (a). Albite overgrowths (A) on the orthoclase are clear except near the core boundary. New Haven arkose, 25 feet from dike at Mill Rock (Table 5, specimen 39). Crossed nicols. × 110

FIGURE 2.—Epidote (E) filling pores and replacing detrital grains. New Haven arkose, 150 feet from dike at Mill Rock (Table 5, specimen 44). Plain light. × 85

FIGURE 3.—Cryptocrystalline filling of quartz and feldspar with a small amount of sericite. Detrital grains corroded. New Haven arkose, approximately 500 feet from fault at Bristol, Connecticut (Table 6, specimen 55). Crossed nicols. × 45

FIGURE 4.—Pore filling of secondary sericite. New Haven arkose, 420 feet from fault at Roaring Brook, Connecticut (Table 6, specimen 60). Crossed nicols. × 85

FIGURE 5.—Sericite filling cracks in fractured grain of orthoclase (black). New Haven arkose, 100 feet from fault at Roaring Brook (Table 6, specimen 58). Crossed nicols. × 40

FIGURE 6.—Replacement of sericite matrix by calcite (C). Remnant sericite in cracks of feldspar grain (black). Three feet above base of the Triassic, 120 feet from fault at Roaring Brook (Table 6, specimen 60). Crossed nicols. × 100

it is unlikely that they would have been so well channeled along the intrusives. Channeling of solutions along the upper contact of the West Rock sill would have been particularly difficult where the contact has a slight dip. The prevalent influx of material is easily accounted for on the assumption that it originated in the nearby intrusive.

Some alumina and silica were probably introduced along with soda in the specimens that have large amounts of secondary albite. Although alumina was released in the replacement of mica and garnet, aluminous minerals in the normal arkoses apparently were not adequate to supply all the necessary alumina for albite. The corrosion of quartz yielded some silica for albite but was not sufficient to account for all the silica in the secondary albite. The fact that small quartz enlargements are present except near contacts suggests that additional silica was introduced after the early influx of albite. Some sericite may have been introduced, but it is possible that all the sericite resulted from the albitization of potash feldspar and mica. Chlorite probably formed as a consequence of the alteration of hematite, biotite, and garnet. In a few thin sections secondary chlorite occurs in some pores, and hematite in others; however, the two minerals never occur together. Some of the constituents for epidote may have been introduced, but its distribution is so erratic that its origin is difficult to ascertain. Calcium, aluminum, and iron were made available for epidote as a result of the replacement of plagioclase and iron-bearing silicates. However, in the specimens that have a large amount of epidote, it is doubtful whether replacement within the specimen would have yielded sufficient material for the formation of epidote. Constituents released in other parts of the contact zone may have migrated to the epidote-rich areas, so an outside source was not necessary. At the contacts studied, there is little evidence that calcite was introduced from the adjacent intrusives. If calcite was added, it came in after the other minerals had formed. Thus, in spite of the fact that several secondary minerals occur in the contact zones, the introduced material seems to have been largely limited to albite and a small amount of excess silica and possibly some late calcite. The other secondary minerals could have formed mainly through a recombination of constituents already present.

Cementation Near Faults

General statement.—The relationship between cementation and faulting in the Triassic sediments is difficult to determine because most faults are poorly exposed and the sediments in faulted zones are commonly brecciated. Nevertheless, the present study indicates that although sediments are well cemented along some faults the introduction of material was not as consistent as along intrusives. For purposes of description, the faulted zones investigated are grouped as follows: (1) faults at the western edge of the Triassic basin, (2) faults within the basin, and (3) eastern border faults. Movement along the eastern border faults was recurrent during the entire period of deposition (Krynine, 1950, p. 119). Faults at the western edge of the basin developed after the lower sediments formed, possibly near the end of Triassic deposition (Wheeler, 1937, p. 61). Although some of the faulting within the basin may have taken place before sedimentation ceased, most of the movement occurred after the period of deposition.

Faults at western edge of Triassic basin.—Arkoses are well exposed near the fault on the east side of Hurley Hill in Bristol, Connecticut, where the Triassic sediments are faulted against the Hartland schist. The arkoses have been bleached light gray and are uniformly well cemented.

Although some secondary outgrowths occur on the detrital grains, the chief cement is a cryptocrystalline intergrowth of quartz and feldspar with a small amount of sericite (Pl. 3, fig. 3). Where the amount of feldspar is small, the cryptocrystalline material approaches a chert cement, but normally a third to a half of the cement is feldspar. The introduced feldspar appears to be entirely potash feldspar, although the cement is so fine-grained in places that a positive identification could not be made.

The fact that outgrowths occur on many of the detrital grains suggests that normal secondary enlargement preceded the deposition of the cryptocrystalline cement. However, although the relationships are obscure in some places, there is evidence that the secondary enlarge-

ments formed after the deposition of the cryptocrystalline cement. At most of the contacts between the secondary enlargements and the cryptocrystalline cement, prismatic crystals of quartz or feldspar extend into the secondary enlargements (Fig. 4). The good crystal terminations on many of the prismatic growths suggest that they grew freely into open spaces. It therefore appears that some openings were present after the period of deposition of the cryptocrystalline cement. Many of the openings were partly bordered by detrital grains, for prismatic crystals project from some of the detrital surfaces. Many of these openings were later filled by secondary enlargements from the grains bordering the openings. The size of the secondary enlargements seems to have been governed by the size of the available openings. The fact that a few of the original pores in the arkose were completely filled by secondary outgrowths suggests that certain pores tended to be isolated and escaped filling by the cryptocrystalline cement. The pores with better connections with the early channelways were more completely filled by the cryptocrystalline cement.

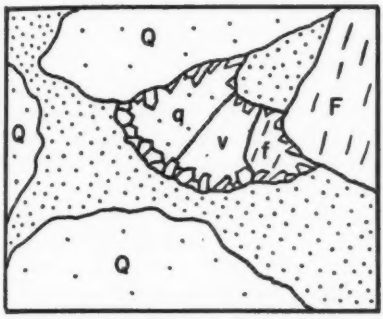

FIGURE 4.—CEMENTATION OF ARKOSE NEAR FAULT

Hurley Hill, Bristol, Connecticut

Void (v) left after deposition of cryptocrystalline quartz and feldspar (heavily stippled) was lined with stubby prismatic crystals of quartz and feldspar and later partially filled with secondary quartz (q) and feldspar (f). Q—detrital quartz. F—detrital feldspar. ×60

At least four periods of fracturing occurred in this area. Openings along the early fractures are filled with cryptocrystalline quartz and feldspar. In the fractures that formed during the second period of deformation, the quartz and feldspar filling is coarse and tends to be in optical continuity with grains along fractures. Quartz deposition was more rapid than feldspar deposition because the fractures in quartz are completely healed, whereas those in feldspar are commonly partly filled. Optically continuous lobes of quartz also extend into fractured feldspar where the two minerals are in contact. Openings that formed during the third period of fracturing are filled with quartz or sericite. The fractured quartz grains continued to be healed with quartz, but the fractures in feldspar were filled with sericite. Fractures in the cryptocrystalline matrix were filled with quartz and sericite. The last period of fracturing was followed by the deposition of nearly pure quartz. The fracture fillings thus indicate that potash feldspar formation gave way to sericite deposition, whereas quartz crystallized continuously and outlasted the other minerals.

The quantity of secondary minerals in these arkoses is greater than would be expected from simple filling of original pores. In some specimens space for introduced material was made available by fracturing. Appreciable detrital material was probably lost through leaching and replacement. Both quartz and feldspar were corroded as shown by embayments in the grains. Although coarse grains of quartz, feldspar, muscovite, and mica schist are present, fine-grained detritus that constitutes at least a small part of most of the coarse arkoses is absent. Clay- and silt-size material as well as coarse grains of unstable minerals were apparently leached or replaced. Solution occurred early, for embayments in the corroded detrital grains are commonly filled with the cement which was first introduced. As the arkoses were apparently little cemented before faulting additional space may have been made available by general opening up of original pores during the early period of deformation and influx of solutions.

The sequence of events in the faulted sediments at Hurley Hill may be summarized as follows: (1) corrosion of coarse grains and complete solution of the fine detritus; (2) partial filling of voids with very fine-grained quartz and feldspar; (3) growth of stubby prisms of quartz and laths of feldspar around the remain-

ing voids; (4) complete filling of voids with quartz and feldspar as growths in optical continuity with detrital grains; (5) deposition of optically continuous quartz in fractured quartz grains and filling of fractured feldspar with sericite; and (6) growth of prismatic quartz crystals along late fractures.

Arkoses and feldspathic sandstones are well exposed along both branches of Roaring Brook in Southington, Connecticut, near the fault which is believed to border the basin in this area (Wheeler, 1937, p. 23; Krynine, 1950, p. 53). In specimens collected 80–450 feet from the fault, detrital feldspar was highly fractured and a large amount of sericite was introduced (Pl. 3, fig. 4). Considerable pressure solution also occurred in these sediments.

The sericite is clearly secondary because it fills fractures as well as original pores. Some feldspar has been partly replaced by sericite, but most of the sericite within feldspar is simply a fracture filling (Pl. 3, fig. 5). In spite of the abundance of sericite many grains of both potash feldspar and plagioclase are amazingly fresh.

Small secondary quartz enlargements are common in many of the specimens, although outgrowths on feldspar are absent. The quartz apparently formed after sericite and grew in the pores which were not completely filled with sericite. Traces of sericite generally occur at the boundary between the detrital cores and the outgrowths, but the surfaces of the growths are free of sericite except where they grew into a mass of sericite. Growths into sericite have frayed borders and contain inclusions of sericite.

Some of the arkoses near the fault are cemented with calcite (Pl. 3, fig. 6). The calcite is commonly in 1-inch crystals and poikilitically encloses many of the detrital grains. Although the calcite has the general appearance of a simple filling, there is evidence that it replaced a pre-existing sericite cement. Small cracks in feldspar are filled with sericite, whereas the more open fractures are filled with calcite. In the noncalcareous arkoses in this area, all fractures in feldspar are filled with sericite. This suggests that calcite replaced sericite except in the narrow cracks. Where a fracture tapers, sericite generally occurs only near the narrow end of the fracture. It seems unlikely that sericite was deposited in the small fractures within grains after calcite was introduced because the grains would have been completely sealed by calcite.

A small amount of pyrite is present in the arkoses along Roaring Brook. The pyrite occurs in small masses in the pores and tends to replace the margins of bordering detrital grains. Sericite deposition outlasted the formation of pyrite, for a layer of sericite rims pyrite in the open pores. The iron for the pyrite may have been derived from iron-bearing detrital constituents, which were apparently destroyed during the influx of sericite.

Mineralization at the old copper mine 2 miles north of Bristol is believed to be related to a fault along the western margin of the basin (Bateman, 1923). Arkose from this mine shows evidence of crushing, but contains less cement than the arkose at Hurley Hill and Roaring Brook. The cement is largely quartz with minor sericite, feldspar, calcite, and sulphides. Small veins are also chiefly quartz with minor calcite and sulphides.

The deposition of quartz, sericite, and potash feldspar along the western border faults indicates that the main constituents in the solutions were silica, alumina, and potash. Differences in the relative amounts of these constituents caused differences in mineralogy along the faults. The deposition of sericite after feldspar indicates that the ratio of potash to alumina was probably decreasing although falling temperature may also have been a factor. The late deposition of quartz suggests that there was an increase in silica relative to the other constituents.

The solutions which rose along the fault at the Bristol Copper Mine were considered to be related to igneous activity that occurred before the end of Triassic sedimentation (Bateman, 1923, p. 130). The present study supports the idea that the mineralization was relatively early because the solutions were introduced before the arkoses were cemented. However, these solutions were not similar to the soda-rich solutions that emanated from the diabases now exposed. The low-soda solutions that rose along the faults may have been derived from a diabasic magma that had undergone a change in composition, perhaps through greater differentiation at depth. Another possibility is that the solutions were originally sodic but became en-

riched in potash through replacement of potash minerals along the channel-ways (Fenner, 1936, p. 301). Potash minerals are partly replaced by albite along some of the exposed dikes, but apparently the albitization was not intense enough to yield large amounts of potash. However, the process may have been more effective at depth.

Faults within the Triassic basin.—Arkoses were examined in four areas where known faults occur within the Triassic basin. In general, faults in the sediments are concealed.

Arkoses are well exposed near the fault which is located 1000 feet west of Long Mountain in the Holyoke Range, Massachusetts (Bain, 1941). The arkoses 30–60 feet from the fault are considerably brecciated and most grain contacts are highly sutured as a result of pressure solution. Secondary rims are uncommon; many rims have been destroyed by granulation and pressure solution, for some growths are fractured or have undergone some pressure solution. Sericite, chlorite, and a little barite and quartz were deposited around the breccia fragments. A small amount of barite and quartz also occur in veinlets. In addition to filling open spaces, barite replaced some of the mica and a little feldspar. A small part of the barite was replaced, for it is cut by quartz euhedra containing inclusions of barite.

Arkoses 250–500 feet from the fault apparently were unaffected by the faulting because they are not abnormally pressolved or brecciated, and barite, secondary sericite, and chlorite are absent. The amount of secondary feldspar and quartz is about the same as in the normal arkoses.

In the vicinity of the fault at Hanover Pond in Cheshire, Connecticut (Krynine, 1950, p. 122), the arkoses are cut by small veins of quartz, calcite, and barite. Thin sections of two specimens show an interstitial filling of quartz with a small amount of sericite, feldspar, and calcite. Quartz occurs as outgrowths and as a coarse mosaic of interlocking crystals. The secondary feldspar is mainly albite and is present as an optically continuous filling in fractured feldspar and as a fine-grained mosaic between detrital grains. Locally the specimens are brecciated and highly pressolved. Except for the small amounts of feldspar and calcite, the material introduced is similar to that at Long Mountain.

At the fault near Kennedy Pond in Holyoke, Massachusetts (Emerson, 1898, p. 470), no mineralization was observed. Although the arkose along the fault is well indurated, the amount and type of cement is similar to that in the unfaulted arkoses in this area. Sandstone 150 feet from the fault at Whitmore Pond in Massachusetts also shows no evidence of abnormal cementation (Table 6, specimen 63).

Eastern border fault.—At the three localities studied near the eastern border fault, the cementation appears to be unrelated to faulting. One of the few areas where the border fault is exposed is near Millers Falls, Massachusetts, where the Millers River enters the Connecticut River (Keeler and Brainard, 1940). In the sediments near the fault there is little secondary quartz or secondary feldspar, but considerable calcite is present (Table 6). The calcite was not necessarily introduced along the fault because some of the sediments three-fourths of a mile from the fault are moderately calcareous (Table 3, specimen 25).

Several exposures of conglomerate with interbedded arkosic sandstones occur 400–1500 feet from the border fault in Portland, Connecticut. Slickensided fracture surfaces are common, and thin sections indicate considerable pressure solution; yet most specimens are little cemented (Table 6). Some calcite was probably removed by weathering, but voids are scarce; hence calcite was never abundant. The abnormally low porosity is due to greater pressure solution and deformation of the grains.

The sediments that crop out about 500 feet from the border fault at Lake Quonnipaug, Connecticut, are also little cemented. A small amount of calcite and secondary quartz is present, but the porosity is fairly high (Table 6, specimen 67).

It is possible that the concealed sediments nearer the fault are better cemented; however, if solutions rising along the fault were a major factor in cementation, more introduced material should be present in the vicinity of the fault. Arkoses exposed in the quarries at Portland, 2 miles from the border fault, are actually better cemented than the sediments within a few hundred feet of the fault.

Origin of Cement in the Normal Arkoses

The normal arkoses which are far removed from faults and igneous bodies contain a moderate amount of secondary albite and very little secondary quartz. Locally calcite or zeolite is present. On the basis of previous investigations, One would not expect feldspar to be the chief cement in these fluvial deposits. According to Pettijohn (1949, p. 502) no occurrences of authigenic feldspar in fresh-water sandstones have been reported. Crowley (1939) considered that the presence of secondary feldspar could be used as a criterion of marine origin.

To account for the abundant albite cement in the arkoses studied, the following sources are considered: (1) meteoric water, (2) interbedded shales, (3) original sediments, and (4) magmatic solutions.

Meteoric water apparently was not important in the silicate cementation because the amount of silicate cement in highly weathered samples is not significantly different from that in relatively fresh samples from deep road cuts or quarries. If meteoric waters were the main source of the cementing material, a siliceous cement rather than one rich in albite would be expected. It is possible that meteoric water redistributed some of the carbonate cement.

The cementing material apparently was not derived from shales, because the arkoses are rarely interbedded with shale. Furthermore shale would normally yield silica (Pettijohn, 1949, p. 482) rather than soda-rich material.

Although secondary albite could have been derived from original constituents within the sediments, there is no supporting evidence for this hypothesis. Halite and glauberite are possible sources of sodium, but apparently these minerals were never abundant in the Triassic of Connecticut (Krynine, 1950, p. 168). Laumontite is another possible source of sodium; however, if laumontite had been widely distributed, feldspar should show more evidence of alteration, because in all the laumontite-bearing specimens feldspar is partly replaced by laumontite. Finely divided detrital albite is not a probable source of the secondary albite because complementary fine-grained quartz and potash feldspar are scarce in the normal arkoses. If fine-grained quartz and potash feldspar had also recrystallized, secondary growths of quartz and potash feldspar would be more common. Apparently there was no significant redistribution of material by pressure solution because the composition of the cement is not similar to the material that pressolved. Detrital quartz is more abundant than feldspar and is more highly pressolved; therefore, the material which dissolved under stress was rich in silica rather than soda. It is possible that some of the quartz cement resulted from pressure solution; however, simple recrystallization did not occur because the more highly pressolved specimens are not necessarily well cemented.

Evidence indicates that the cementing material could have been of igneous origin. The cement in the normal arkoses is chemically similar to the material introduced along igneous contacts. Both are generally rich in albite and low in quartz. At the contacts, the introduced albite forms a microcrystalline matrix, but with increasing distance from the contacts the amount of albite in the matrix decreases and overgrowths on detrital grains become more common. As pointed out in a previous section, the albite overgrowths in the contact zone formed at the same time as the microcrystalline albite. Although the exact time of cementation outside the contact zones could not be determined, it appears that the cement was precipitated after initial compaction. It is therefore possible that the cement was introduced during the period of igneous activity.

The fact that outside of actual contact zones the amount of cement in the arkoses does not appear to be closely related to the distance from igneous bodies might be advanced as evidence against a magmatic source for the cement. However, once the solutions were emitted, their distribution would have been governed by the permeability of the sediments and attitude of the beds.

On the basis of the amount of igneous rock exposed, it might be argued that magmatic solutions would have been inadequate to account for the large quantity of albite cement. If it is assumed that the total thickness of Triassic arkoses averages 7000 feet (Krynine, 1950) and that they contain 5 per cent secondary albite, the total amount of introduced albite would be equivalent to a sheet 350 feet thick. The total thickness of flows and sills average about 1000 feet. Volumetrically dikes

and other intrusives are relatively unimportant. Therefore, the amount of igneous rock within the Triassic sediments does not appear sufficient to yield all the albite that occurs as a cement in the sediments. However, additional solutions from parent diabase reservoirs at depth would satisfactorily account for the observed amount of cement. The solutions that promoted albitization in many areas are thought to have originated from deep-seated basic magmas (Agrell, 1939, p. 336; Larsen, 1928, p. 429).

Albite-rich solutions from depth apparently were not channeled along the major faults because secondary quartz rather than albite predominates in the fault zones studied. If albite solutions were introduced before the period of major faulting within the basin, they may have followed minor fractures and permeated the sediments generally. Solutions could have circulated freely in the arkoses because of their relatively high permeability. Shales must have restricted the flow of solutions; yet the albite veinlets that cut shales in the New Britain area indicate that some solutions passed through shales along fractures. However, it is not known whether fractures in shale were common during the main period of cementation.

Conclusions

This study indicates that sediments outside of contact zones may be largely cemented by material of magmatic origin even though there is no normal evidence of hydrothermal activity. In many studies, an igneous source for cementing material is ruled out where direct effects of hydrothermal activity are not apparent. This reasoning is not necessarily valid because, except for local epidotization and greater replacement in close proximity to the intrusives, normal evidence of hydrothermal activity is absent in the arkoses in the contact zones where considerable albite has been introduced. Inasmuch as dikes and telethermal ore deposits do occur in many sedimentary areas, the possibility of a magmatic source for cement should be considered even if other evidence of hydrothermal activity is absent.

References Cited

Agrell, S. O., 1939, The adinoles of Dinas Head, Cornwall: Min. Mag., v. 25, p. 305–337

Bain, G. W., 1932, Northern area of Connecticut Valley Triassic: Am. Jour. Sci., v. 23, p. 57–77

——1941, The Holyoke Range and Connecticut Valley structure: Am. Jour. Sci., v. 239, p. 261–275

Bateman, A. N., 1923, Primary chalcocite, Bristol Copper Mine, Connecticut: Econ. Geology, v. 18, p. 122–166

Bowen, N. L., 1910, Diabase and granophyre of the Gowganda Lake district, Ontario: Jour. Geology, v. 18, p. 658–674

Crowley, A. J., 1939, Possible criterion for distinguishing marine and non-marine sediments: Am. Assoc. Petroleum Geologists Bull. 23, p. 1716–1720

Dana, J. D., 1891, The four "Rocks" of the New Haven region: Am. Jour. Sci., v. 42, p. 79–110

Davis, W. M., 1898, The Triassic formation of Connecticut: U. S. Geol. Survey Ann. Rept. 18, pt. 2, p. 1–192

Emerson, B. K., 1898, Geology of Old Hampshire County, Massachusetts: U. S. Geol. Survey Mon. 29, 790 p.

——1917, Geology of Rhode Island and Massachusetts: U. S. Geol. Survey Bull. 597, 289 p.

Fenner, C. N., 1910, The Watchung basalt and the paragenesis of its zeolites and other secondary minerals: N. Y. Acad. Sci. Annals, v. 20, pt. 2, p. 93–187

——1936, Bore hole investigations in Yellowstone National Park: Jour. Geology, v. 44, p. 225–315

Heald, M. T., 1955, Stylolites in sandstones: Jour. Geology, v. 63, p. 101–114

——1956, Cementation of Simpson and St. Peter sandstones in parts of Oklahoma, Arkansas, and Missouri: Jour. Geology, v. 64, p. 16–30

Hovey, E. O., 1897, A relatively acid dike in the Connecticut Triassic area: Am. Jour. Sci., v. 3, p. 287–292

Keeler, J., and Brainard, C., 1940, Faulted phyllite east of Greenfield, Massachusetts: Am. Jour. Sci., v. 238, p. 354–365

Krynine, P. D., 1950, Petrology, stratigraphy, and origin of the Triassic sedimentary rocks of Connecticut: Conn. State Geol. and Nat. Hist. Survey Bull. 73, 247 p.

Larsen, E. S., Jr., 1928, A hydrothermal origin of corundum and albitite bodies: Econ. Geology, v. 23, p. 398–433

Longwell, C. R., 1922, Notes on the structure of the Triassic rocks in southern Connecticut: Am. Jour. Sci., v. 4, p. 223–226

——1928, The Triassic of Connecticut: Am. Jour. Sci., v. 16, p. 259–263

——1933, The Triassic belt of Massachusetts and Connecticut: 16th Internat. Geol. Cong. Guidebook 1, p. 93–101

Pettijohn, F. J., 1949, Sedimentary Rocks: N. Y., Harper and Brothers, 526 p.

Ramberg, H., 1952, The origin of metamorphic and metasomatic rocks: Chicago, Univ. of Chicago Press, 317 p.

Shannon, E. U., 1924, The mineralogy and petrology of intrusive diabase at Goose Creek, Loudoun County, Virginia: U. S. Natl. Mus. Proc., v. 66, 86 p.

Von Eckermann, H., 1938, A contribution to the knowledge of the late sodic differentiates of basic eruptives: Jour. Geology, v. 46, p. 412–437

Walker, F., 1940, Differentiation of the Palisade diabase, New Jersey: Geol. Soc. America Bull. 51, p. 1059–1106

Wentworth, C. K., 1922, A scale of grade and class terms for clastic sediments: Jour. Geology, v. 30, p. 377–392

Wheeler, G., 1937, The west wall of the New England Triassic lowland: Conn. State Geol. and Nat. Hist. Survey Bull. 58, 73 p.

Willard, M. E., 1951, Bedrock geology of the Mount Toby quadrangle, Massachusetts: U. S. Geol. Survey Geol. Quadrangle Map.

—— 1952, Bedrock geology of the Greenfield quadrangle, Massachusetts: U. S. Geol. Survey Geol. Quadrangle Map.

Williams, H., Turner, F. J., and Gilbert, C. M., 1954, Petrography: San Francisco, W. H. Freeman and Co., 406 p.

Winchell, A. N., 1951, Elements of optical mineralogy: 4th ed., N. Y., John Wiley and Sons, 551 p.

West Virginia University, Morgantown, West Virginia

Manuscript Received by the Secretary of the Society, August 1, 1955

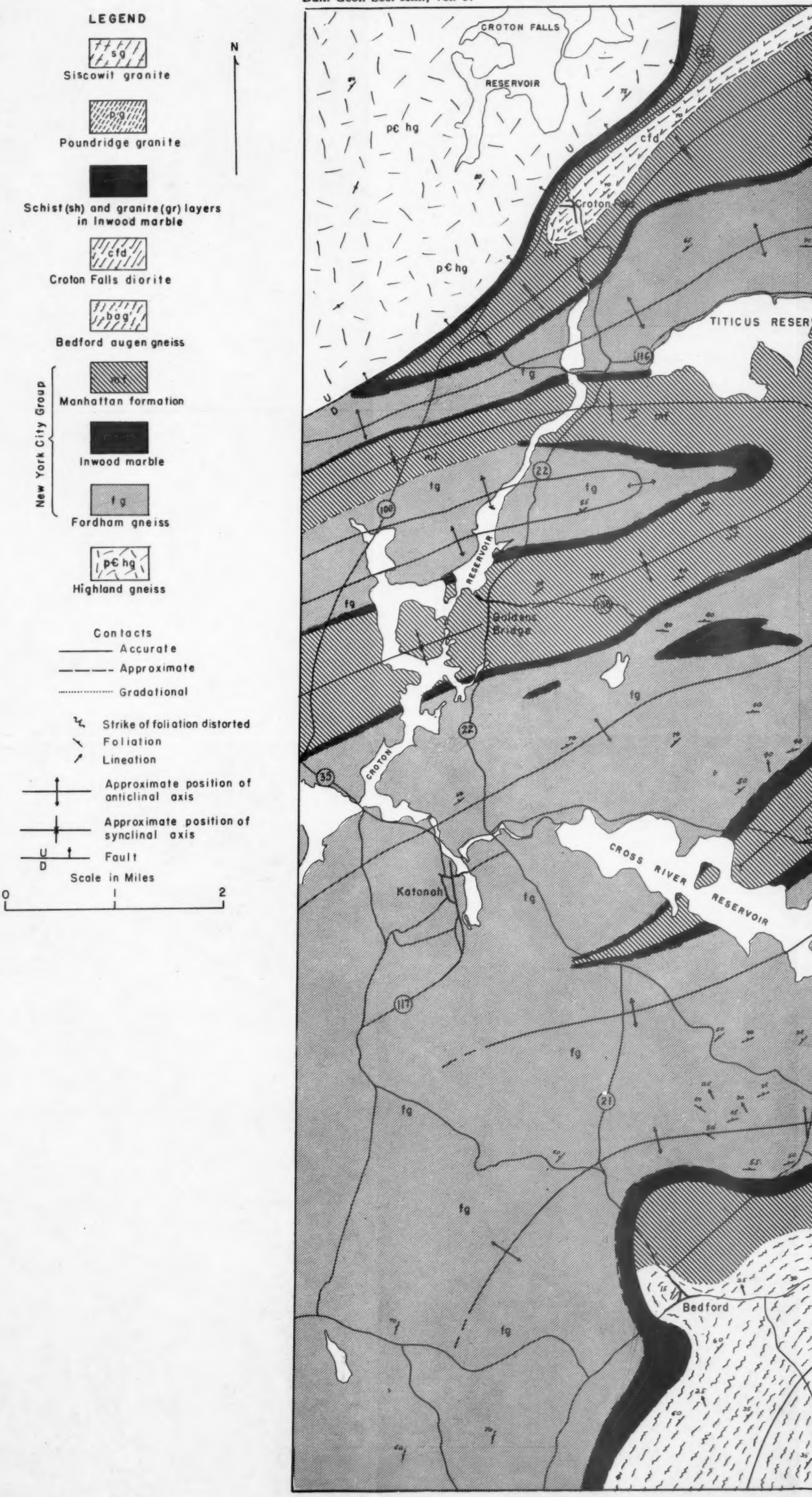

GEOLOGIC MAP OF NORTHEASTERN WESTCH

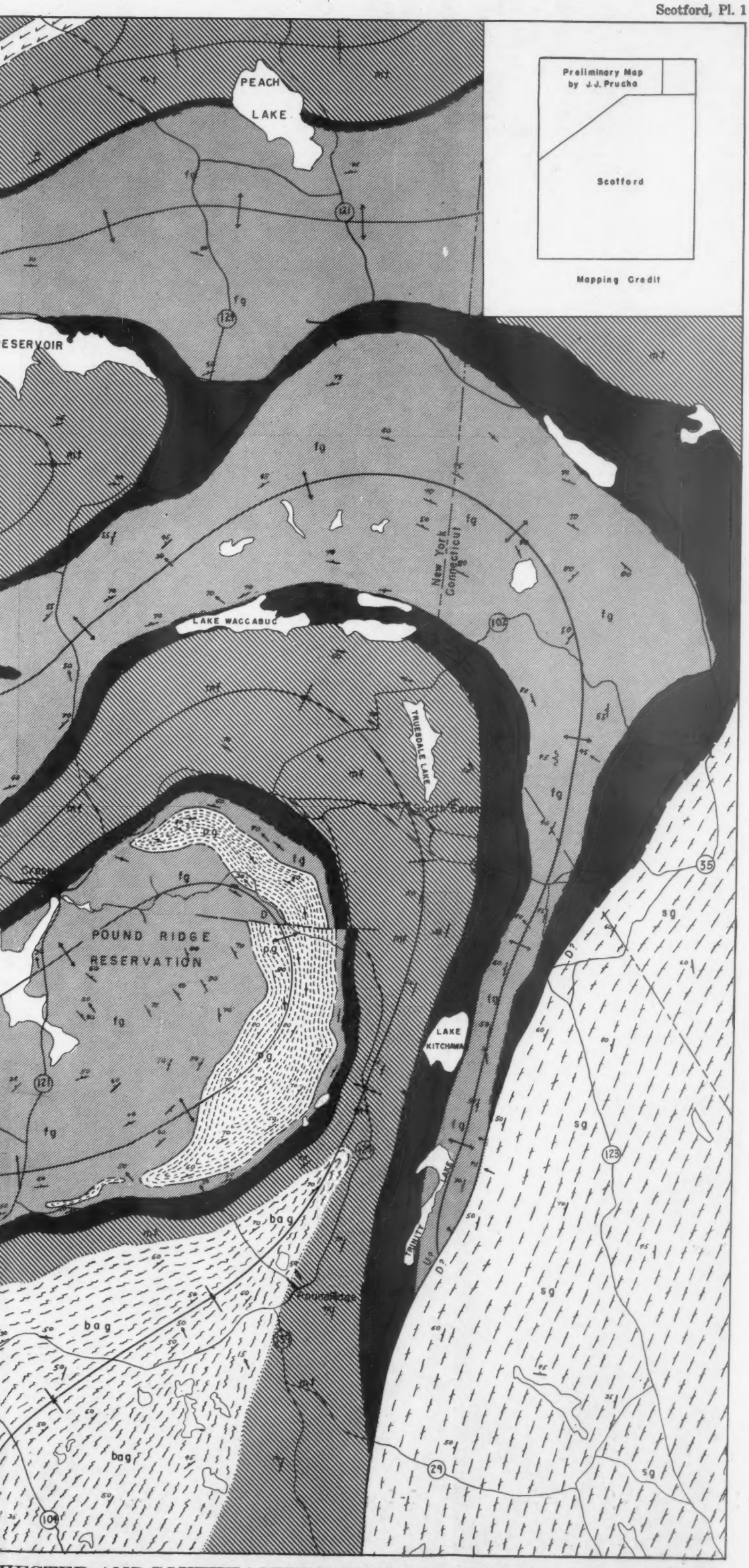

HESTER AND SOUTHEASTERN PUTNAM COUNTIES, NEW YORK

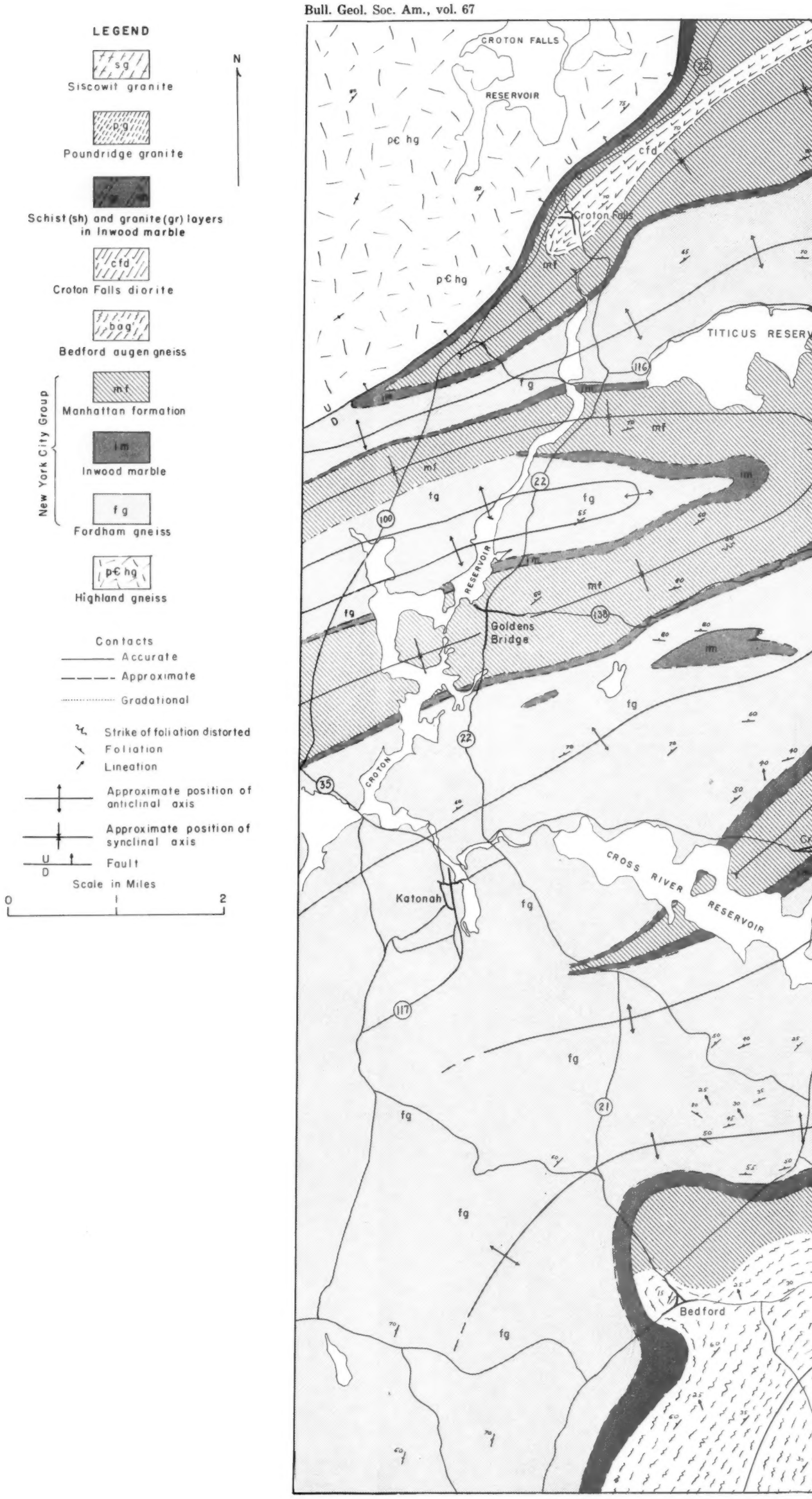

GEOLOGIC MAP OF NORTHEASTERN WESTCHE

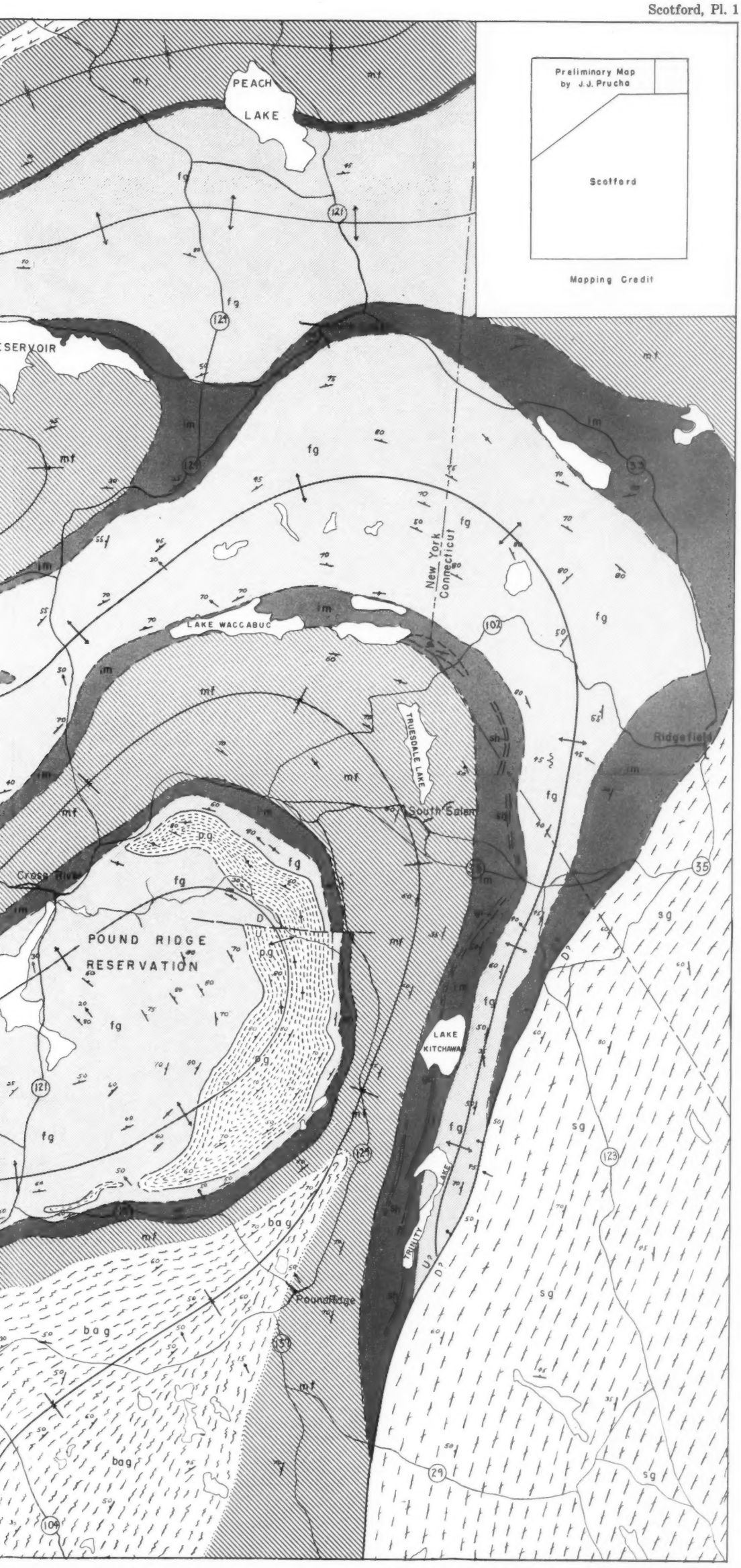

HESTER AND SOUTHEASTERN PUTNAM COUNTIES, NEW YORK

Introdu
Loca
Prev
Prob
Acknow
Stratig

BULLETIN OF THE GEOLOGICAL SOCIETY OF AMERICA
VOL. 67, PP. 1155-1198, 9 FIGS., 4 PLS. SEPTEMBER 1956

METAMORPHISM AND AXIAL-PLANE FOLDING IN THE POUNDRIDGE AREA, NEW YORK

BY DAVID M. SCOTFORD

ABSTRACT

The Poundridge area in northeastern Westchester County, New York, is underlain by the Poundridge and Siscowit granites, the Fordham gneiss, Inwood marble, and the Manhattan formation, comprising the New York City group. Field evidence, including the fact that the Lowerre quartzite does not seem to exist, leads to the conclusion that the New York City group is a conformable sequence either of entirely Precambrian or Paleozoic (pre-upper Ordovician) age. It thus cannot be correlated with the Precambrian Highland gneiss and lower Paleozoic Poughquag quartzite-Wappinger limestone-Hudson River shale sequeuce of Dutchess County to the north.

The area has been subjected to regional metamorphism of the sillimanite-almandite subfacies of the amphibolite facies and lies within the sillimanite zone. The sedimentary antecedent of the Fordham gneiss was probably a graywacke; the Inwood marble, a cherty limestone; and the Manhattan formation, a siliceous and argillaceous shale.

Alkaline metasomatism has altered the Manhattan formation and an associated basic igneous body to the Bedford augen gneiss. It has also extensively affected the Inwood marble and has granitized an interlayered argillaceous bed. A migmatite phase of the Fordham gneiss, intermediate in composition between the Poundridge granite and the normal Fordham gneiss, appears to be a result of metasomatism. The Poundridge granite may be a product of the same metasomatic process in a more intense form or may be magmatic. In which case the migmatite could have resulted from a partial conversion of the gneiss necessitated by the equilibrium requirements of the PT environment induced by the granitic intrusion. Although not necessarily magmatic, the Poundridge granite is a synkinematic body contemporaneous with the last major deformation of the area.

Metamorphism has obliterated intraformational bedding planes. Foliation is the most prominent structural feature in all rock units. Its strike swings in a large arc around the central Poundridge mass. Lineation, consisting of alignment of inequate minerals and the axes of folds of differing amplitudes, shows a strong preferred orientation in its consistently northwestward plunge.

The Manhattan formation crops out in a belt which also forms a large arc through the area flanked on either side by successive belts of Inwood marble and Fordham gneiss. The conformable nature of the Fordham-Inwood-Manhattan sequence allows this map pattern to be interpreted as a secondarily folded syncline herein called an axial-plane fold. This interpretation is supported by additional structural evidence.

This structural complex resulted from the broad folding of pre-existing isoclinal folds which lay between the present Highland gneiss fault and the Siscowit granite fault. These folds were squeezed into axial-plane folds when the Highland gneiss block was thrust southeastward toward the Siscowit granite, which acted as a buttress but which may have been displaced to the southeast.

CONTENTS

TEXT

	Page
Introduction	1156
Location and geologic setting	1156
Previous work	1157
Problem investigated	1157
Acknowledgments	1158
Stratigraphic relationships	1158
Mineralogy	1160
General statement	1160
Determinative methods	1160
Petrography	1167
Introduction	1167
Manhattan formation	1168
Fordham gneiss	1170

	Page
Amphibolite	1173
Inwood marble	1174
Poundridge granite	1176
Siscowit granite	1177
Bedford augen gneiss	1177
Bedford pegmatites	1179
Summary of criteria for distinguishing Fordham gneiss and Manhattan schist	1179
Metamorphism	1180
General statement	1180
Facies and zone	1180
Origin of metasediments	1181
Metasomatism	1184
Structural elements	1190
Introduction	1190
Regional setting	1191
Bedding	1191
Foliation	1191
Lineation	1192
Fold axes	1192
Drag folds	1193
Faults	1193
Interpretation	1194
References cited	1197

ILLUSTRATIONS

Figure	Page
1. Index map	1157
2. Sillimanite-almandite subfacies of amphibolite facies	1180
3. Cation variation	1188
4. Stereographic projection of poles of foliation	1191
5. Stereographic projection of lineation	1192
6. Stereographic projection of fold axes	1192
7. Plane table map of Poundridge granite-Fordham gneiss contact at the northeastern margin of Poundridge mass	1195
8. Diagramatic representation of axial-plane folding principle	1196
9. Block diagram of a portion of the Poundridge area showing axial-plane fold interpretation	1196

Plate	Facing page
1. Geologic map of northeastern Westchester and southeastern Putnam counties, New York	1155
2. Photomicrographs	1168
3. Photographs of Fordham gneiss and Bedford augen gneiss	1169
4. Structural map of Poundridge area, New York	1198

TABLES

Table	Page
1. Comparative stratigraphic interpretation of southern New York	1159
2. Plagioclase paragenesis	1162
3. Variations of biotite	1164
4. Optical data and compositions of clinopyroxenes	1165
5. Optical data and partial composition of hornblende	1166
6. Optical properties of sillimanite	1167
7. Measured modes of the Manhattan schist	1169
8. Measured modes of the Fordham gneiss	1171
9. Measured modes of the Fordham migmatite gneiss	1172
10. Measured modes of the amphibolite	1174
11. Estimated modes of the Inwood marble	1175
12. Estimated modes in the granite layer in Inwood marble	1176
13. Measured modes in the Poundridge granite	1177
14. Estimated modes in the Bedford augen gneiss	1178
15. Comparison of the chemical composition of the Fordham gneiss and Manhattan schist with average graywacke and shale	1182
16. Calculated and determined rock analyses	1184
17. Ions added and subtracted to form the Bedford augen gneiss	1186
18. Cation replacement in the migmatite phase of the Fordham gneiss based on 160 oxygen ions	1187
19. Substitutions necessary to alter the migmatite to the Poundridge granite	1189

Introduction

Location and Geologic Setting

The investigation which forms the basis of this paper concerns the northeastern corner of Westchester County, New York, 35 miles north of New York City and 20 miles east of the Hudson River (fig. 1). An area of about 50 square miles centered in the Ward-Poundridge Reservation, was mapped in detail. The adjacent country was examined in a reconnaissance fashion.

This area lies within a high-grade metamorphic terrain near the southeastern extremity of the New England petrographic province. The degree of metamorphism decreases to the northwest. Unmetamorphosed Cambro-Ordovician sediments are exposed within 25 miles although the crystalline rocks of the Hudson Highlands intervene.

The maximum relief within the mapped area is 560 feet. Heights are underlain by gneiss and granite, lower elevations by schist, and valleys by marble. Glacial drift conceals most of the bedrock in the topographic lows, but exposures at higher levels are excellent. The topography is marked by two opposing arcuate escarpments, separated by a belt of schist and marble 2 miles

wide. The southern escarpment, facing successively north, east, and south, marks the border of the unit herein called the Poundridge mass. This prominent topographic and structural feature consists of a large crescent-shaped exposure

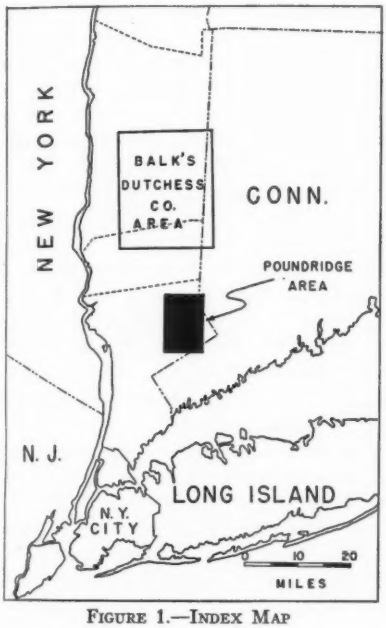

FIGURE 1.—INDEX MAP

of Poundridge granite surrounded by Fordham gneiss. The northern escarpment, which faces east, south, and west, defines the edge of a Fordham gneiss belt.

Previous Work

The earliest published reference to the Poundridge area is by J. G. Percival (1842) who accurately described the general trends of the major rock units in his reconnaissance study of the geology of Connecticut. Berkey (1907; 1911) and Berkey and Rice (1919) described the same lithologic units in other parts of Westchester and Putnam counties. Luquer and Ries (1896) and Barbour (1930) studied the Bedford augen gneiss and the Bedford pegmatite district. Bell (1936) investigated the petrography of the Poundridge granite and published in abstract. The detailed investigation by Balk (1936) and Barth (1936) of the structure and petrology of Dutchess County, New York, has much bearing on the present study. Fluhr (1950) studied the structure and petrology of a large portion of Westchester and Putnam counties in connection with construction of the Delaware aqueduct and published a generalized geologic map of that area.

Problem Investigated

The writer's interest in the Poundridge area was first aroused by the fascinating map pattern of the northern portion of that area shown on Balk's (1936) small-scale geologic map of Dutchess County and vicinity. The Poundridge area is not discussed in the paper accompanying that map, but Balk (1932), as well as Fluhr (1950), has alluded to the great structural complexity of that part of Westchester County, and to the many unsolved problems. It was in the hope that the structure of this highly deformed area could be elucidated by large-scale detailed mapping that the writer undertook the present study. In addition, the variety of high-grade metamorphic and metasomatized rock types seemed to offer an excellent opportunity to investigate petrographically some aspects of the problems of regional metamorphism and granitization.

The area studied is a structurally anomalous one. From New York City northward to the Poundridge area the Fordham gneiss-Inwood marble-Manhattan schist sequence is involved in uniform northeastward-striking isoclinal folds. In the region to the south of the Pre-Cambrian gneiss mass, these formational belts are thrown into a remarkably circuitous pattern characterized by large arcs of several miles radius (Pl. 1). Two explanations appear possible: that a thrust fault which has been postulated as separating the Fordham and Inwood (Balk, 1932) has been complexly folded, or that these three formations are conformable and have undergone secondary folding on a large scale. On the basis of the investigation here presented, the second thesis is adopted and termed axial-plane folding.

In addition to the structural complex, there is also the problem of the origin of the Poundridge granite and associated migmatite as well as the premetamorphic character of the three

principal formations. These questions were attacked by detailed petrographic and mineralogic analysis leading to the conclusions discussed in the section on metamorphism and metasomatism.

Acknowledgments

The writer wishes to thank the Society of Sigma Xi whose grant-in-aid from the Sigma Xi-Resa Research Fund helped support the field work. The salaries of two laboratory assistants, who did drafting, integrating stage analyses, and mineral separations, were paid by Miami University, Oxford, Ohio. The cost of photostats and some of the drafting was borne by the Miami University Research Fund. William Kneller did additional integrating stage work.

Gordon Bell introduced the writer to the area and allowed him to read an unpublished manuscript on the Poundridge granite. John J. Prucha, then New York State Senior Geologist, spent several days in the field with the writer in the Poundridge area and in that area to the northeast which Prucha is mapping. Ideas derived from these excursions were most helpful in unravelling the structural problem.

As the mapping progressed, it became apparent that the area mapped in detail by the writer (Pl. 4) was part of a somewhat larger structural province. In order to present a more coherent description, the entire area is included on Plate 1 by the addition of a part of a preliminary map by Dr. Prucha.

Stratigraphic Relationships

Structural interpretations in the southeastern New York and southern New England areas are seriously hampered by the lack of a known detailed stratigraphic section. The excellent stratigraphic work being done in northern New England cannot be adapted to the high-grade metamorphic terrane lying to the south until the intervening mapping has been completed and recognizable units traced southward. Regional metamorphism and extreme deformation may have obliterated these units, but hope of their recognition and use lies solely in their first being defined in areas of less severe tectonic and metamorphic change.

For these reasons, the writer has shown on his map only the rock types and the attitude of structural elements which can be observed in the field. Structural interpretation is kept at a minimum.

The stratigraphic units adopted are the Fordham gneiss, the Inwood marble, and the Manhattan formation, comprising the New York City group. The names Inwood marble rather than Inwood limestone, Manhattan formation rather than Manhattan schist, and the New York City group are adopted as suggested by John J. Prucha (In preparation). The term Manhattan schist is employed, however, wherever reference is made to the schistose or gneissic phase of that formation. The Lowerre quartzite, which has been considered to lie between the Inwood marble and Fordham gneiss was not observed in the Poundridge area. Other recent workers in southern New York (Fluhr, 1950; Prucha, 1955) also failed to find the Lowerre quartzite and concluded that it does not exist.

This group of highly metamorphosed rocks was first studied in detail by Merrill (1902). He concluded that the Fordham gneiss could be correlated with the Precambrian Highlands gneiss of Putnam and Dutchess counties, and that the Lowerre quartzite, Inwood marble, and Manhattan schist were correlative with the lower Paleozoic Poughquag quartzite, Wappinger limestone, and Hudson River shale which overlie the Highlands gneiss. This interpretation was discarded by Berkey (1907), Clarke (1908), and others who considered the Lowerre, Inwood, and Manhattan, as well as the Fordham gneiss, as Precambrian and not to be correlated with the lower Paleozoics above the Highland gneiss.

A return to the earlier conclusions of Merrill resulted from Balk's (1936) detailed mapping in Dutchess County. Here increasing grade of metamorphism can be traced from west to east, resulting in the conversion of the Hudson River shale into high-grade schist and of the Wappinger limestone into a marble. Balk believed the schist to be the Manhattan schist and the marble the Inwood marble, thus, lower Paleozoic. Balk assumed (1936, p. 689) that no structural or stratigraphic discontinuity which would destroy this correlation existed

TABLE 1.—COMPARATIVE STRATIGRAPHIC INTERPRETATIONS OF SOUTHERN NEW YORK

Merrill (1902)	Berkey and Rice (1919)	Balk (1936)	Present Interpretation	
			North of Hudson Highlands	South of Hudson Highlands
	Cambro-Ordovician: Hudson River shale			
	Cambro-Ordovician: Wappinger limestone			Manhattan formation
	Cambrian: Poughquag quartzite			Inwood marble
Silurian: Hudson schist (= Manhattan)	Manhattan schist	Cambro-Ordovician: Manhattan schist = Hudson River pelite	Cambro-Ordovician: Hudson River shale	New York City Group pre-Upper Ordovician
Silurian: Stockbridge dolomite (= Inwood)	Inwood limestone	Cambro-Ordovician: Inwood limestone = Wappinger limestone	Cambro-Ordovician: Wappinger limestone	
Cambrian: Poughquag quartzite (= Lowerre)	Precambrian: Lowerre quartzite	Cambrian: Lowerre quartzite = Poughquag quartzite	Cambrian: Poughquag quartzite	Fordham gneiss
Precambrian: Fordham gneiss	Fordham gneiss = Highland gneiss	Precambrian: Fordham gneiss = Highland gneiss	Precambrian: Highland gneiss	

between the area he mapped in detail and the New York City area.

This investigation in the Poundridge area and recent work done in the surrounding district brings to light just such a break. The area studied by Balk (1936) and Barth (1936) lies north of the southern belt of Highland gneiss. The marble and schist there may well be the metamorphic equivalents of the lower Paleozoic rocks to the west, but they are not necessarily equivalent to the Inwood marble and Manhattan formation which lie south of the gneiss belt. For the reasons enumerated below the writer believes that the New York City group, whether Paleozoic or Precambrian, is a conformable sequence and cannot be correlated with the lower Paleozoic rocks or their metamorphic equivalents north of the Highland gneiss (Table 1).

(1) The Fordham gneiss cannot be correlated with the Precambrian Highland gneiss; they are petrographically quite dissimilar. The two rocks are easily distinguished in the field; they differ in mineral composition; and the Fordham shows a lower grade of metamorphism than the Highland gneiss. The fewer granitic intrusions in the Fordham are more acidic than those in the Highland gneiss. Faults involving the Highland gneiss are not accompanied by crushed or sheared zones as is commonly true in the Fordham gneiss (Fluhr, 1950). John Prucha (Personal communication) is undertaking differentiation of the Highland gniess and finds no units similar to the Fordham gneiss.

(2) There are interbedded marbles in the Fordham gneiss and gneissic layers in the Inwood marble near the contact between these formations. Further, there is no evidence of unconformity or major faulting along the contact. This lends strength to the contention that the Fordham gneiss is the conformable lower unit of the New York City group.

(3) No Lowerre quartzite has been found separating the Fordham from the Inwood. Thus a correlation of that unit with the Poughquag quartzite is improbable. As a result the New York City group, consisting of a gneiss, a marble, and a schist, is lithologically different from the gneiss-sandstone-limestone-shale sequence of the lower Paleozoic rocks to the north.

Mineralogy

General Statement

The collective mineralogy of the Poundridge rocks is here presented. Reference is made to these data in the following sections on petrography and petrology.

Quartz and plagioclase are the most abundant of the 30 recognized mineral species. Orthoclase, perthite, microcline, biotite, hornblende, clinopyroxene, muscovite, and sillimanite are also common; tremolite, sericite, apatite, zircon, sphene, tourmaline, kaolinite, clinozoisite, limonite, hematite, magnetite, olivine, phlogopite, chlorite, serpentine, antigorite, epidote, scapolite, garnet, and cordierite occur in small amounts.

Determinative Methods

Refractive indices were determined by immersion methods with oils calibrated to 0.002 except those oils above 1.70 for which the steps were 0.01. The oil temperature was controlled, and calibration checked with the Abbe and Joly refractometers.

As a check against the universal-stage determination, the $N_{z'}$ and $N_{z'}$ values for the plagioclase were found on cleavage plates after the method of Tsuboi (1923). A few plagioclase determinations were made by the Tsuboi (1934) dispersion method employing a quartz monochromator. The anorthite content as determined by the two methods commonly differed about 4 per cent. The dispersion method was unsatisfactory for many samples because corrosion on the cleavage flakes made the match signal difficult to see.

The discrepancy in results in determination of plagioclase composition by the universal-stage and immersion methods has been noted by several workers (Emmons *et al.*, 1953, p. 11). Because of the low concentration of plagioclase in many sections and the necessity of making determinations at a specific point in the slide, the universal-stage method was used throughout this study. Therefore, in the data presented, the error is systematic.

The indices of clinopyroxene, amphibole, garnet, and sillimanite were determined from specimens separated by heavy liquids. The N_{γ}

values for the clinopyroxenes were determined on {110} parting tablets which yield off-centered optic axis figures. The amphibole {100} cleavage was used to measure N_y.

The four-axis universal-stage plagioclase-determination method was used (Turner, 1947). This method involves the plotting stereographically of the X, Y, and Z directions of adjacent twin individuals and the pole of the composition face. Although accuracy is increased if more than one type of twin can be plotted in the same crystal, commonly these rocks contain small crystals with only one type twin.

Optic-angle measurements were made with the Leitz four-axis universal stage; the direct-measurement method in which both axes are brought into parallelism with the microscope axis was used. This is far more accurate than the single-axis method and a high degree of precision can be expected (Fairbairn and Podolsky, 1951). The axial angle was measured four times in each sample; each measurement was made at a different position of rotation on the A_s axis 90° from the previous one and with the axial plane in the 45-degree position. Readings were averaged, and the difference between the average and the greatest deviation was considered the limit of error. This was usually not more than 1°. Strong absorption in the amphiboles made the vertical alignment of the axial plane difficult. Nonuniform extinction of the pyroxene crystals was the principal cause of error.

The $C \wedge Z$ value for the amphiboles and pyroxenes was determined on the universal stage using the method of Buni (Haff, 1941). Although other methods are more accurate, they require twinned crystals which were lacking in the slides examined. As a result, accuracy was low. More than one determination was made on each slide; results varied as much as 5°.

Biotite birefringence was measured on the universal stage with the aid of a Berek compensator. The mineral thickness was determined from the known birefringence of an adjacent quartz grain which had been rotated so that its optic axis lay parallel to the microscope stage. At least two biotite crystals in each slide were so examined always using an adjacent quartz grain for thickness determination, yet in some the results differed as much as 0.01. The greatest error always occurred with grains showing strong absorption. The average error was 0.0038.

Sections thought to contain orthoclase were stained with a strong solution of sodium cobaltinitrite after the slide was etched with hydrofluoric acid fumes (Chayes, 1952). The potash feldspar takes a bright yellow stain, the other minerals being unaffected. This method was adopted because it is difficult to distinguish between untwinned plagioclase and orthoclase.

Quartz, the most abundant mineral in the Poundridge rocks, amounts to 30–40 per cent in the schists, gneisses, and granites, somewhat less in the amphibolite, and little in the marble. Quartz anhedra are commonly elongated (*e.g.*, .045 x .15 mm) parallel to the trace of the foliation. Smaller, more nearly equate crystals are associated with small feldspar grains or are included in the larger feldspar crystals.

Although undulatory extinction is common, quartz more characteristically shows faint strain shadows. Chayes (1952) recorded perthitic microcline associated with highly undulant quartz in some calc-alkaline granite from New England. The Poundridge granite contains a large amount of perthitic microcline, but the quartz shows only incipient undulatory extinction or none.

Plagioclase, the most abundant and widely distributed feldspar, is present in all rock types except a few marbles. The anorthite content ranges from 7 per cent in the Poundridge granite to 81 per cent in one amphibolite, with most plagioclase averaging 32–36 per cent. The anhedral crystals are commonly corroded with sericite although some fresh plagioclase veinlets occur in the gneisses. Small rounded quartz inclusions are present in many crystals, and a few show myrmekitic intergrowth, particularly in the granite.

Undulatory extinction of plagioclase crystals in many rock types is associated with the less common occurrence of bent twin lamellae. Although twinning is common in the plagioclase, it is not universal. The untwinned appearance

of many crystals may be a function of orientation rather than a lack of twinning; the plane of the section is parallel to (010), making albite twinning invisible. A determination of twin laws with the universal stage indicates that the albite, pericline, and carlsbad twins are present. Albite twinning is common and in some gneisses is associated with pericline twinning. Carlsbad twinning is relatively rare. According to Turner (1951) this group of twins, and the absence of complex twins, is characteristic of metamorphic rather than igneous rocks. Even though the albite in the Poundridge granite exhibits this same simple twinning, the fact cannot be regarded as evidence of a nonigneous origin since the amount of plagioclase is minor. Of more significance is the lack of complex igneous-type twinning in the adjacent migmatitic gneisses. This would indicate that these rocks have not undergone injection of igneous material, but may be attributed to metasomatism and metamorphic differentiation. The same may be said regarding the amphibolites whose plagioclase shows only simple twinning. This indicates that these rocks are either nonigneous or recrystallized during metamorphism.

TABLE 2.—PLAGIOCLASE PARAGENESIS

% An	Quartz	Perthite	Microcline	Orthoclase	Biotite	Garnet	Muscovite	Hornblende	Sillimanite	Pyroxene	Sphene	Scapolite	Calcite
7	×		×		×								
8	×	×	×		×								
10	×	×	×		×								
11	×	×	×		×		×						
12	×		×			×							
13	×	×	×		×		×						
14	×		×	×	×								
15	×	×	×		×								
16	×		×		×			×					
19	×				×			×					
20	×			×	×								
25	×		×	×			×						
26	×		×		×	×							
27	×			×	×	×	×						
28	×		×		×								
29	×		×		×	×	×						
30	×			×	×								
31	×		×		×			×					
32	×		×	×	×		×			×	×		
33	×		×	×				×			×		
34	×			×	×	×		×		×			
35	×				×			×					
36	×			×	×	×			×				
37					×			×		×			
38	×				×			×					
39	×				×	×		×	×	×			
40	×				×			×		×	×		
42	×			×		×				×			
44	×				×						×	×	×
48	×			×	×	×			×				
81	×				×	×		×					

Some specimens of gneiss bordering the Poundridge granite and one amphibolite contain plagioclase which exhibits a zonelike change in composition at the outer fringe of the mineral from An_{22} to An_{11}. This is attributed to a metasomatic atleration and not to a liquid-crystal disequilibrium.

A granitic layer in marble contains plagio-

clase with untwinned interiors and well-twinned borders. The interiors are not a potassium feldspar since they did not take the sodium cobaltinitrite stain. Whether there is a difference in composition between the interior and exterior of these crystals could not be determined, and the writer knows of no explanation of this condition.

Table 2 is a summary of plagioclase paragenesis with increasing anorthite content. Plagioclase from all rock types is included, and, where more than one specimen contained the same plagioclase, the associated minerals in all specimens are considered paragenetic. Although quartz and biotite occur throughout the range of plagioclase composition, the other minerals are more restricted in their association. Perthite, found only in the granite, is associated with sodic plagioclase (An_5–An_{18}). Microcline, occurring in the granite and bordering gneisses, is found with more calcic plagioclase (7 to 33 per cent An). Orthoclase in the schist and gneisses is associated with plagioclase that is from 14 to 81 per cent An. Garnet occurs in a wide variety of rocks and is found with plagioclase ranging from 12 to 81 per cent An. Muscovite occurs with sodic and intermediate plagioclase (12–31 per cent An).

Hornblende and pyroxene are found principally in amphibolite, but the pyroxene is not present unless the plagioclase contains at least 32 per cent An, while the hornblende may be associated with plagioclase as sodic as 16 per cent An. Sillimanite, although found in many schist specimens, is present only where the plagioclase is relatively calcic (36–44 per cent An).

One or more of the *alkaline feldspars* (microcline, orthoclase, or perthite) occurs widely in all the rock types except the amphibolite. Perthite is confined to the Poundridge granite and pegmatite dikes, while microcline is present in the gneisses and schists as a result of potash metasomatism where it has apparently replaced the earlier feldspar and quartz. Orthoclase, fairly common in the Fordham gneiss and Manhattan formation, appears to be a primary metamorphic constituent and not the result of later metasomatism. Microcline is also present as a skarn mineral in the marble, and, with plagioclase, forms the augen in the Bedford augen gneiss as well as occurring in the groundmass.

Biotite is present in all of the rock types. The content ranges from less than 1 per cent in granite and marble to 75 per cent in some schists.

Three types are recognized:

(1) Green: X = tan
$Y = Z$, dark green or olive green

(2) Red-brown: X = light tan
$Y = Z$ bright red or reddish brown

(3) Brown: X = tan
$Y = Z$, brown to dark brown

The pleochroism of 73 specimens was noted; the refractive index (N_z) of 43 and the birefringence of 19 were determined (Table 3).

There is considerable overlapping of the three varieties in the range of refractive indices from 1.623 to 1.682, but the green biotite shows the highest average, N_z, 1.666, the red-brown shows 1.654, and the brown, 1.653.

Plotting the average index and birefringence of each type on Winchell's chart (1951, p. 347) the following compositions are obtained:

(1) Green biotite: 70 per cent annite
30 per cent phlogopite

(2) Red-brown: 35 per cent annite
35 per cent siderophyllite
15 per cent phlogopite
15 per cent eastonite

(3) Brown: essentially the same composition as the red-brown variety

This seems to indicate that all three varieties have a high ratio of iron to magnesium with the green type containing somewhat less alumina. However, Hall's work (1941) indicates that there is no satisfactory correlation between index and composition in the biotites. He finds that in most instances, greenish-brown biotites are either high in FeO and low in TiO_2 and MgO, or low in FeO and TiO_2 and high in MgO.

Engel and Engel (1953) report the association of reddish-brown biotite in the granitized

TABLE 3.—VARIATIONS OF BIOTITE

Rock Type	Green biotite		Red-brown biotite		Brown biotite	
	N_z	$(N_z - N_x)$	N_z	$(N_z - N_x)$	N_z	$(N_z - N_x)$
Poundridge granite	1.654					
Border gneiss	1.659				1.623	.057
	1.662				1.658	.054
	1.676				1.672	.053
	1.682	.062				
Fordham gneiss			1.637	.048	1.634	
			1.646	.054	1.643	
			1.649	.050	1.649	.058
			1.651		1.653	
			1.654	.059	1.665	
			1.660		1.666	.056
			1.661			
Granite layer in Fordham gneiss			1.650			
Manhattan schist			1.642		1.656	
			1.652	.054		
			1.653			
			1.658			
			1.659			
Augen gneiss			1.649			
			1.649	.055		
			1.653			
			1.655			
			1.655	.052		
Amphibolite			1.639	.054	1.642	.048
			1.647	.053	1.670	.062
			1.654	.055		
			1.658	.054		
			1.661			
			1.661			
			1.668			
			1.681			
Marble			1.640	.045		
Siscowit granite			1.662	.063		
Average	1.666	.062	1.654	.053	1.653	.054

and migmatized orthogneisses and greenish biotite in those least injected and altered orthogneisses of the Adirondacks. To some extent the opposite appears true of the gneisses in the Poundridge area. Green biotite is most abundant in the Poundridge granite and the bordering injected and metasomatized gneisses (Table 3). Red-brown biotite occurs most commonly in the amphibolite layers in the Fordham gneiss and in the Manhattan schist; both of these are among the least metasomatized rocks in the area. Yet, it is true that red-brown biotite is also found in the highly metasomatized Bedford augen gneiss. Thus it seems possible that the green biotite is a result of autometamorphism of the Poundridge granite and bordering gneiss which has resulted in a retrogression of the red to the green variety in response to a lower temperature environment.

Clinopyroxene, sparse (never more than 10 per cent) in the amphibolites and more abundant (up to 23 per cent) in the metasomatized marble, is colorless, or faintly greenish, and strongly anhedral, being embayed and replaced in the amphibolites by hornblende and biotite (Pl. 2, fig. 4). It is closely associated with phlogopite or scapolite in the marble. In some amphibolite specimens replacement has progressed to a point where the clinopyroxene occurs as small anhedral fragments in the interstices. Yet the fragments retain opitcal continuity, indicating the former existence of much larger crystals up to 3 mm in length.

The optic angle, N_y and $C \wedge Z$, were determined for each. The approximate compositions (Table 4) are inferred from Hess' diagram (1949) as presented by Tröger (1952, p. 62). These data indicate two types of clinopyroxene with only small variation within each type. Using the names as defined by Hess (1941), these are salite (Wo_{46} to Wo_{48}, En_{30} to En_{33}, Fs_{20} to Fs_{23}) found in the amphibolites, augen gneiss, and two marble specimens, and diopside (Wo_{48} to Wo_{50}, En_{42} to En_{47}, Fs_9 to Fs_{10}) which occurs in the marble and in a quartz-feldspathic layer within the marble. The two marble specimens containing salite are the only ones with amphibole.

Horneblende is abundant in the amphibolite and is present in the Fordham gneiss, Bedford

augen gneiss, and Inwood marble. Random sections of the amphibolite taken perpendicular to the foliation contain either predominantly basal or predominantly prismatic sections of

TABLE 4.—OPTICAL DATA AND COMPOSITION OF CLINOPYROXENES

Specimen	2V	$C \wedge Z$	N_y	Composition		
				Wo	En	Fs
In amphibolite						
14	57.7 ± .7°	42°	1.702	47	30	23
	58.1 ± .9°	44°				
13	57.6 ± .3°	40–43°	1.701	47	32	21
	58.2 ± .8°					
80	61.5 ± .9°	40–46°	1.698	47	32	21
	57.4 ± 1.0°					
	54.0 ± 1.0°					
53	57.8 ± .5°	48–51°	1.700	46	32	22
21	59.1 ± .2°	43–44°	1.700	48	30	22
49	58.1 ± 2.0°	44°	1.705	47	33	20
In marble						
88	57.9 ± 1.4°	42°	1.685	48	42	10
	57.4 ± 1.1°					
75	58.4 ± .3°	40°	1.682	50	42	8
	57.9 ± .8°	42°				
61	56.5 ± .8°	38°	1.675	50	47	3
	58.6 ± .7°	40°				
85	57.9 ± .9°	45°	1.699	47	32	21
	58.0 ± 1.3°	46°				
96	59.8 ± .8°	36°	1.698	48	32	22
In quartz-feldspathic layer in marble						
71	58.8 ± .8°	40°	1.676	50	47	3
	57.2 ± .7°	44°				
In augen gneiss						
40	57.6 ± 1.6°	40°	1.699	47	32	21
	57.9 ± .8°	43°				

hornblende, indicating a rough preferred orientation of the *c* axes in the plane of foliation. If clinopyroxene is present, the hornblende exhibits a reaction relationship to it and is commonly replaced by biotite, particularly near granite contacts.

The optical properties of hornblende from 29 rock specimens are summarized on Table 5. Because of the complexity of the chemical composition of hornblende, involving extensive isomorphous substitution, approximating composition from optical data presents serious problems. As many as five or six factors may combine to control a particular property. Although much careful work has been done on this problem, the best that can be presented is a rough correlation of optical properties with a few selected chemical variables. It has long been known that the ratio Fe:Mg has an influence on the optic angle and refractive index. This value was calculated from the data given by Sundius (1946) by the method suggested by Herz (1950, Ph.D. dissertation, The Johns Hopkins Univ.). In addition, the value of the ratio $MgAl_y/Y$ for each specimen was obtained by reference to the chart prepared by Rosenzweig and Watson (1954, Fig. 1). The *Y* group is Mg (Mg, Al)$_4$, in which Fe$''$ and Mn$''$ may replace Mg and Fe$'''$ and Ti may replace the Al. Thus an increase in the above ratio would indicate a decrease in the heavy metal substitution in the *Y* group.

The Mg:Fe ratio was plotted against the composition of the associated plagioclase and the modal percentage of the associated quartz and biotite, but no systematic variation emerged. Evidently the substitution of these metals was not a function of total rock composition except for the hornblende found in the marble. There the Mg:Fe ratio (Specimens 85, 96) is understandably high.

No compositional significance could be ascertained from the pleochroism.

Garnet is a common minor constituent of the schist and gneiss and occurs less frequently in the augen gneiss and amphibolites. In thin section, it is colorless or pink and is strongly embayed with inclusions of magnetite. In some schist specimens, it appears to be partially replaced by biotite and sillimanite. The indices of refraction of 20 crystals range from 1.779 to 1.815, with an average of 1.800, which suggests a dominantly almanditic garnet.

Sillimanite occurs in small amounts in half of the Manhattan formation specimens and in one specimen of Fordham migmatite gneiss and augen gneiss. It is the only member of the (Al_2SiO_5) polymorphic group present and occurs as stubby prisms or basal sections in the schists, but is fibrous in the migmatite gneiss. The association of the fibrous variety with

TABLE 5.—OPTICAL DATA AND PARTIAL COMPOSITION OF HORNBLENDE

Specimen	Pleochroism	N_y	$-2V$	$C \wedge Z$	Mg/Mg + Fe	Mg + Al$_y$/Y
			In amphibolite			
5	tan-green-drk. green	1.670	72.4 ± .4° 74.8 ± .4°	18°	50	.58
11	tan-green-drk. green	1.682	69.5 ± .3° 69.9 ± .6°	19°	38	.53
13	tan-brown-green	1.672	72.4 ± .6° 73.2 ± .2°	13°	48	.57
14	tan-brown-green	1.683	68.5 ± .7° 69.7 ± .4°	13–16°	36	.50
9	tan-olive green-drk. green	1.671	75.1 ± 2.6° 76.4 ± .2°	14°	49	.58
10	tan-olive green-drk. green	1.680	67.4 ± .3° 67.4 ± .5°	20°	40	.52
21	tan-green-drk. green	1.681	73.8 ± .5°	12°	39	.55
22	tan-green-brown	1.679	69.1 ± 2.1° 71.3 ± 1.6°	20–23°	41	.53
28	tan-blue-green	1.678	70.2 ± 1.2° 71.3 ± .2°	18°	42	.53
35	tan-green-drk. green	1.689	57.1 ± .2° 59.3 ± 1.3°	13°	31	.40?
43	tan-blue-green	1.671	76.1 ± .6° 77.2 ± 1.0°	17°	49	.60
44	tan-green-drk. green	1.684	63.3 ± .5° 65.2 ± 1.5°	15–20°	35	.45?
49	tan-green-drk. green	1.687	68.4 ± 1.5° 68.9 ± .6°	11°	33	.50
50	tan-green-drk. green	1.681	65.3 ± 1.0°	15–17°	39	.50
52	tan-green-drk. green	1.689	60.9 ± .9° 61.0 ± .5°	9–12°	21	.40?
53	tan-green-drk. green	1.689	64.0 ± .8° 64.5 ± .6°	18°	31	.40?
73	tan-green-drk. green	1.671	68.8 ± .4° 71.4 ± .5°	13°	49	.57
80	tan-green-drk. green	1.672	73.7 ± 1.0°	13°	48	.57
			In Inwood marble			
85	colorless-gray-blue	1.655	73.9 ± .9° 74.3 ± 1.3°	16–19°	65	.65
96	tan-green-blue	1.659	74.7 ± 1.0°	16°	61	.65
			In Bedford augen gneiss			
55	tan-green-drk. green		66.5 ± 1.2° 67.0 ± 1.4°	10°		.50
39A	tan-green-drk. green	1.670	75.6 ± .7° 76.9 ± .7°	14°	50	.68
91	tan-green-drk. green	1.677	68.2 ± .6°	12°	57	.57
92	tan-green-drk. green	1.684	55.0 ± 1.8°	13°	36	.45?
			In Fordham gneiss			
3	tan-green-drk. green	1.660	80.0 ± .5°	20°	60	.68
7	green-blue-yellow	1.674	71.2 ± .5° 71.5 ± 1.2°	13–18°	46	.57
54	tan-green-drk. green	1.682	65.2 ± 1.1°	14–16°	38	.48?
74	tan-green-drk. green	1.666	68.1 ± 1.5° 69.0 ± .6°	16–19°	54	.52
98	tan-green-drk. green	1.660	76.7 ± 2.1°	small	60	.66

migmatite gneisses and the prismatic variety with the less metasomatized rock was noted by Sanders (1954) in the Kenya basement system. There the prismatic sillimanite was converted to fibrolite as alkali metasomatism became significant. This parallelism appears to hold in the Poundridge area although the reason for it remains obscure in both areas. Where the rock foliation is crinkled, the sillimanite imitates the contorted shape of the biotite laths with which it is closely associated. In places, both minerals form pod-shaped elongated patches in the foliation.

TABLE 6.—OPTICAL PROPERTIES OF SILLIMANITE

Specimen	2V	N_g	N_z
15A	27.7 ± .4°	1.659	1.676
57	30.3 ± 1.4°	n.d.	n.d.
59	28.0 ± .6°	1.658	1.677
60	23.5 ± .7°	1.658	1.677
79	29.2 ± .8°	n.d.	n.d.
97	33.1 ± 2.1°	n.d.	n.d.
38	30.2 ± .9°	1.660	1.676

The optical properties of seven specimens shown on Table 6 indicate uniformity of refractive indices but rather wide variation in optic angle. Since there is fair confidence in the accuracy of the 2V determination, the cause of the variation is not known.

Olivine constitutes 3 per cent of one marble specimen and has the following optical properties: $2V = 85.2° \pm 2.3°$, $N_x = 1.640$ $N_y = 1.654$, $N_z = 1.673$. This indicates substantially pure forsterite (Kennedy, 1947). The large, scattered crystals are surrounded by antigorite.

Scapolite is present in about half of the marble specimens, ranging from a trace to 40 per cent of the rock. Its indices are $N_o = 1.590 \pm .001$, $N_E = 1.554 \pm .001$. This represents a composition of 80 per cent $Ca_4Al_6Si_6O_{24}Co_3$, 20 per cent $Na_4Al_3Si_9O_{24}Cl$ (Winchell, 1951, p. 353). It is associated with pyroxene or olivine and phlogopite.

Cordierite makes up 38 per cent of one specimen of Fordham gneiss. It has an optic angle of $52.4 \pm 2°$ and the following indices: $N_x = 1.543$, $N_y = 1.551$, and $N_z = 1.552$. According to Tröger (1952, p. 51) this indicates an approximate composition of 68 per cent $Mg_2Al_4SiO_{18}$, 32 per cent $Fe_2Al_4Si_5O_{18}$. There is also the possibility that small amounts of alkalies and water are present. In thin section medium-sized cordierite anhedra are closely associated with biotite and sillimanite (Pl. 2, fig. 2). Garnet is also prominent in this specimen. It has been pointed out by Folinsbee (1941) that the association of garnet, biotite, and cordierite requires a restricted garnet composition of 71–78 per cent almandite, 15–20 per cent pyrope, 2 per cent spessartite, and less than 5 per cent grossularite. An increase in calcium would increase the grossularite content of the garnet, but would prevent the appearance of cordierite as it can not accommodate calcium in its structure. Thus garnets associated with cordierite are predominantly of the iron-magnesium type. This is in accord with the 1.797 index of the garnet in this specimen. Also, this association seems to indicate an original sediment richer in iron and magnesium than in calcium. The presence of sillimanite and the lack of feldspar in this particular specimen further distinguishes it from the more typical Fordham gneiss and indicates a predominance of alumina over the alkalies.

PETROGRAPHY

Introduction

To provide a more coherent presentation, the stratigraphic relationships of the metasediments are described in a previous section. The petrographic descriptions of these rocks and the igneous intrusives follow. It was found convenient during the field mapping to group the gneisses, schists, and marbles into the Fordham gneiss, Manhattan formation, and Inwood marble. No differentiation within these units could be made, and stratigraphic work in southeastern New York and western Connecticut may necessitate redefinition or discontinuance of these terms. The writer believes that the units are applicable to the Poundridge area and hopes that the following descriptions of the Fordham gneiss and Manhattan formation will help remove some of the confusion which has arisen in other areas where attempts have been made to assign these names. The

many similarities between the two rocks makes it impossible to classify a few outcrops, but the distinctions do serve in most places.

Manhattan Formation

The Manhattan formation is principally a fairly coarse, high-grade gneissic schist. It is well foliated and commonly slabby in vertical exposures. A thin, alternately black and light-gray banding, a fraction of an inch wide, emphasizes the foliation. In a few places, this foliation is crinkled into small-amplitude folds.

The schist is light gray on a fresh surface but weathers to rusty brown or dark brown to black. The exposed foliation surface is light gray, speckled with small grains of black biotite and where sillimanite is present has a faint purplish hue. Small garnet porphyroblasts are common in many places on the weathered foliation surface. One prominent layer of augen schist just east of Boutonville is associated with numerous granitic layers. It is far removed from and not considered a part of the Bedford augen gneiss.

Granite layers, ranging in width from 5 to 20 feet, parallel the foliation of the schist generally for a few tens of feet before pinching out. Although mostly conformable, in some places the granites cut the foliation for short distances. They are moderately coarse, but in some exposures pink and white feldspar crystals up to an inch in size protrude on the weathered surface. In a few places, elongated knots of garnet, aligned in fairly definite rows paralleling the granite foliation, suggest a relict structure derived from the granitization of a garnet-bearing metasediment.

Elliptical garnetiferous granite pods, with their long axes averaging a foot in length, and smaller quartz pods of similar shape parallel the trace of the schist foliation. Amphibolite layers are less abundant and, unlike the granite bands, are strictly conformable. Small conformable and cross-cutting pegmatites are common and in a few places have caused small drag folds in the adjacent schist, indicating an upward intrusive direction.

A partial section of the Manhattan formation was measured along the road a quarter of a mile east of Boutonville. It is presented as a typical sequence and shows the relative proportion of the components, although the granite is somewhat more abundant in this locality than elsewhere.

Section of Manhattan Formation a Quarter of a Mile East of Boutonville, New York

	Feet
Granite	10
Augen schist	5
Covered	50
Garnetiferous mica schist	5
Covered	150
Granite with narrow layers of schist	50
Covered	40
Coarse granite	12
Garnetiferous mica schist	5
Discordant garnetiferous granite with many thin schist layers	10
Garnetiferous mica schist	5
Garnetiferous granite	5
Amphibolite	5
Total	387

The measured modal analysis of the Manhattan schist (Table 7) shows the rock to be a quartz-plagioclase-biotite-garnet schist with sillimanite present in the majority of specimens and potassium feldspar commonly present. The microscopic texture is typically lepidoblastic. Small to medium aligned laths of red-brown biotite are segregated into bands but range widely in the perfection of orientation. In many slides the biotite shows optical

---

PLATE 2.—PHOTOMICROGRAPHS

FIGURE 1.—Microaugen of microcline in groundmass of displaced bands of quartz, biotite, and feldspar
FIGURE 2.—Sillimanite (Si) and biotite (Bi) included in large crystals of cordierite (Co)
FIGURE 3.—Plagioclase crystal partially replaced by microcline in migmatite
FIGURE 4.—Hornblende and biotite partially replacing large pyroxene crystal
FIGURE 5.—Crinkled foliation band consisting of closely associated biotite and sillimanite
FIGURE 6.—Unusual association of pyroxene (Py), quartz (Qu), and microcline (Mi) in schistose layer

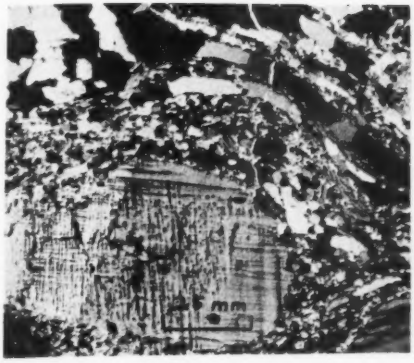

FIGURE 1

FIGURE 2

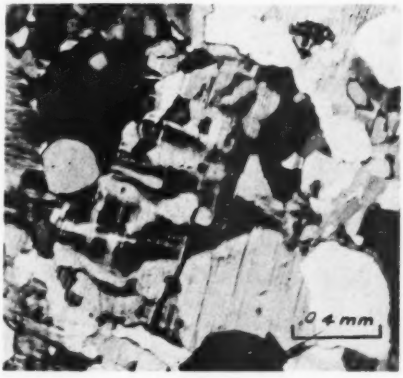

FIGURE 3

FIGURE 4

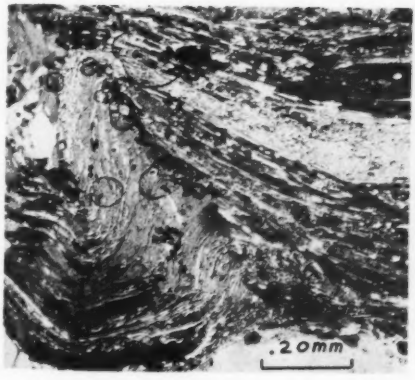

FIGURE 5

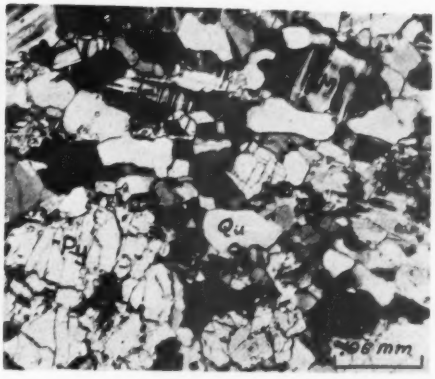

FIGURE 6

PHOTOMICROGRAPHS

FIGURE 1

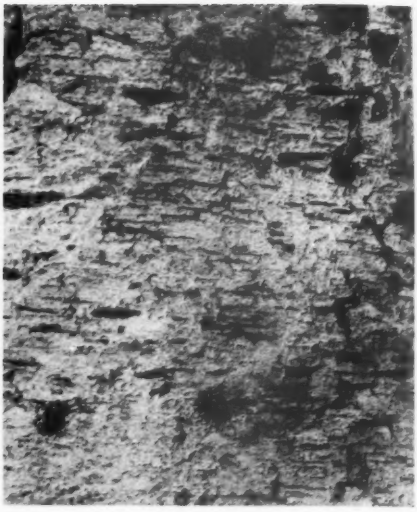

FIGURE 2

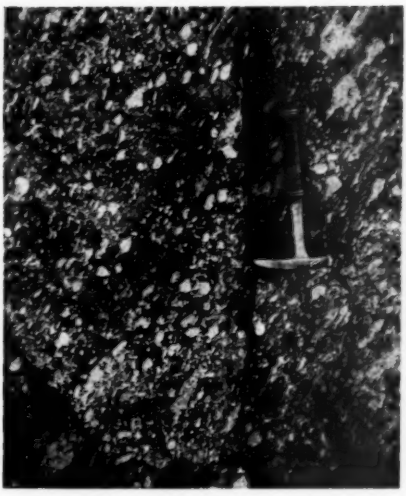

FIGURE 3

FIGURE 4

PHOTOGRAPHS OF FORDHAM GNEISS AND BEDFORD AUGEN GNEISS

continuity. The darker bands of the schist also commonly contain patches or lenticles of sillimanite closely associated with the biotite (Pl. 2, fig. 5). Most of the sillimanite grains are small and prismatic and are oriented with the basal section nearly parallel to the slide. In many specimens the biotite laths bend around the larger porphyroblasts of garnet that occur in the darker bands; the larger garnet crystals are roughly elliptical with the long axis parallel to the trace of the foliation.

The light bands, as wide or wider than the dark ones, commonly contain quartz anhedra with sutured boundaries and elongated parallel to the trace of the foliation. In places the larger quartz crystals contain well-oriented planes of liquid inclusions, the traces of which mal large angles with the foliation. No special stu of these planes was made, but the uniform orientation of such planes has been noted by the author elsewhere (Scotford, 1951).

In some specimens the light bands are composed entirely of elongated quartz. Although the light bands resemble injected quartz veinlets, the writer considers them products of metamorphic differentiation. In the rocks containing less siliceous light bands, the elongated quartz grains are accompanied by masses of fine-grained quartz showing mortar structure and commonly accompanied by equally small feldspar grains. However, in most slides, the feldspar occurs more abundantly as medium-sized, somewhat elongated anhedra only slightly more concentrated in the light bands. Plagioclase ranging in composition from An_{28} to An_{49} is the most common feldspar. It is estimated that more than half the plagioclase shows twinning. The abundance of untwinned plagioclase or plagioclase oriented with the twin composition plane parallel to the slide was demonstrated when the slides were stained to allow recognition of orthoclase. In a few places the

TABLE 7.—MEASURED MODES OF THE MANHATTAN SCHIST

Minerals	56	57	58	59*	60	68†	78	79	81	97	105†	Average
Quartz	38.1	42.7	31.5	30.0	25.0	40.5	30.9	35.2	46.0	40.9	37.1	36.9
Plagioclase, An_{26-49}	29.4	24.9	29.2	2.0	2.0	45.0	33.3	16.0	35.6	21.4	27.8	26.5
Orthoclase		11.5	10.3	25.0	21.2			tr			12.5	5.6
Microcline				5.0	4.0							0.4
Biotite	20.4	13.1	26.0	20.0	38.8	14.7	31.8	24.7	18.5	28.3	22.5	23.6
Sillimanite		4.7		8.0	4.7		tr	2.1		5.5		1.7
Garnet	12.0	2.8	2.8	10.0	1.0		4.1	22.0	tr	tr	tr	3.5
Muscovite				tr					tr	3.7		0.4
Sericite	tr	tr	tr	tr		tr			tr		tr	tr
Zircon	tr	tr	tr			tr	tr	tr			tr	tr
Hematite						tr						tr
Magnetite	tr	tr	tr	tr	3.2	tr	tr	tr	tr	tr	tr	0.4
Apatite	tr								tr			tr
Clinozoisite						tr						tr
Tourmaline											tr	tr

* Estimated modes, not included in average
† Schist layer in Inwood marble

PLATE 3.—PHOTOGRAPHS OF FORDHAM GNEISS AND BEDFORD AUGEN GNEISS

FIGURE 1.—Exposed anticlinal crest in Fordham gneiss east of Lake Kitchawan
FIGURE 2.—Mineral lineation on foliation plane of Fordham gneiss
FIGURE 3.—Exposure of diorite phase of Bedford augen gneiss
FIGURE 4.—Dark and light bands of Fordham gneiss distorted by pegmatitic intrusions

twin lamellae are bent. Orthoclase, present in half the specimens, reaches a maximum abundance of 25 per cent. The grains are medium to large and anhedral, and, in one slide, show slight myrmekitic intergrowth. Microcline, found in two specimens, is either large grains associated with the orthoclase, or small grains concentrated in the fine-grained quartz masses.

In the less common exposures where incipient fracture cleavage has contorted the foliation into small crinkles (Pl. 2, fig. 5) the texture is somewhat different. The banding is blurred by the small-amplitude folding of the biotite laths. The intimately associated sillimanite closely follows these crinkles; the quartz-segregation banding is obliterated. The quartz anhedra are more equidimentional and are associated with the large feldspar anhedra.

In one slide the biotite and sillimanite replaced a large embayed crystal of garnet, but much of the garnet has become disassociated from the biotite-sillimanite bands and is isolated in quartz-feldspathic masses.

Fordham Gneiss

The Fordham gneiss is differentiated into normal and migmatite gneisses. The fundamental distinction is the presence of microcline of metasomatic origin in the migmatite gneiss and its absence in the normal phase. In addition migmatite gneiss occurs principally near contacts with the Poundridge granite. It is also associated with lesser granitic intrusions and in places displays a coarse *lit-par-lit* relationship with the granitic layers. Amphibolites, granitic rocks, and a few marble layers are ubiquitous within both types of Fordham gneiss and are described separately.

The normal phase of the Fordham gneiss is the most extensive rock unit in the Poundridge area. It forms the major portion of the central Poundridge mass as well as the large arcuate belt which girdles the area on the north and east. It is typically a coarsely banded, gray gneiss. In much of the material, the alternately light-gray and dark-gray to black bands are 2–3 inches wide. Thin dark lines in the light bands and a light lines in the dark bands is common. In many localities the gneiss appears to be composed of varying proportions of two end members—a black amphibolite and a light-gray conformable granite. Though probably not genetically valid, this description serves as an aid in visualizing the variable abundance of light or dark bands which characterizes this gneiss. Less commonly the bands are thin and the foliation becomes coarsely schistose. Outcrops of Fordham gneiss are more commonly rounded than slabby or angular. The fresh rock light gray to balck and the weathered surface is dark gray to black.

One of the most characteristic features of the Fordham gneiss is the frequency of folding and the distortion of the foliation planes. The fold axes of small folds are measurable in most outcrops. Folds ranging up to 100 feet in amplitude are present at several localities (Pl. 3, fig. 1). In many places these folds, although hidden cause radical changes in the strike of the foliation for short distances and make the determination of the foliation trend difficult. This type of folding is a criterion for distinguishing the Fordham and the Manhattan in the Poundridge area.

The measured modal analysis of the normal phase of the Fordham gneiss (Table 8) indicates a plagioclase-quartz-biotite rock with less abundant hornblende, potassium feldspar, and garnet. The dominant mineral, plagioclase, ranges in composition from An_{24} to An_{40}, but most commonly an andesine containing about 32 per cent of the anorthite molecule. All three varieties of biotite are present with brown and red-brown predominant over green. Dark-green to blue-green hornblende, although averaging only 4.6 per cent of the rock, is a characteristic mineral of the Fordham gneiss; it is present in most specimens and serves to distinguish the Fordham gneiss from the Manhattan schist in thin section.

The texture is characteristically granoblastic and roughly banded. The light bands are composed either of elongated and aligned quartz anhedra or of a mixture of quartz and feldspar, and the dark bands contain concentrations of roughly oriented biotite, hornblende, and garnet with abundant plagioclase. In the absent of recognizable banding, foliation is expressed by the poorly oriented biotite laths. This contrasts with the texture of the Manhattan formation which is characterized by well-oriented mica. Where the banding is most distinct in the gneiss, it is caused by pure quartz

veinlets up to 1 mm wide. Less typically, hornblende, concentrated in bands, is oriented with its longest direction parallel to the foliation. In places there is no noticeable banding. Biotite gives the rock a strongly foliated lepidoblastic texture. In a few specimens foliation is marked by narrow bands of fine-shredded, poorly oriented biotite and small crushed quartz grains that bend around the larger feldspar crystals. In a few samples biotite appears to have partially replaced the hornblende and scattered chlorite has replaced biotite.

Table 8.—Measured Modes of the Fordham Gneiss (Normal Phase)

Minerals	3	7	12*	11[2]	29	27	31	37	51	54	74	76	99	98	Average
Quartz	15.1	22.9	50.0	29.3	31.9	38.8	29.6	33.6	28.4	31.2	13.9	21.0	56.3	37.4	29.9
Plagioclase, An_{24-40}	57.5	24.6	35.0	60.0	41.5	39.4	54.5	32.3	63.0	52.5	42.0	49.5	35.2	50.3	46.3
Orthoclase					2.4			13.1			2.6	5.6			2.6
Microcline									tr						tr
Biotite	15.5	23.4	15.0	10.7	19.9	15.7	12.8	21.0	4.4	10.2	10.0	7.3	6.2	9.4	12.8
Muscovite				tr	4.3			tr					tr		tr
Hornblende	12.1	9.3				4.7	2.3			6.1	32.2		tr	tr	4.6
Garnet	tr	13.6			tr	1.0	0.9	1.0		tr			tr	tr	1.3
Sericite								tr	2.0	tr		5.0	2.0		0.6
Kaolinite	tr		tr	tr	tr	tr	tr		2.0						tr
Zircon	tr		tr		tr		tr	tr		tr				tr	tr
Hematite						tr							tr		tr
Magnetite		6.0	tr	tr	tr	tr		tr	tr	tr			tr		tr
Apatite					tr		tr	tr	tr	tr		tr		tr	tr
Actinolite										tr				2.9	tr
Clinozoisite										tr	tr	tr			tr
Chlorite												11.4			0.9
Epidote												tr			tr

* Estimated mode, not included in average

The migmatite phase of the Fordham gneiss is transitional between the perthite-rich Poundham some distance from the Poundridge granite.

Modal analysis indicates a quartzose microcline- and perthite-rich granite with subordinate plagioclase, biotite, and muscovite. A distinctive texture characterizes the rock. Large elliptic porphyroblasts of microcline or perthite are set in a fine-grained groundmass of quartz, feldspar, and biotite. Narrow continuous veinlets of elongated quartz grains alternate with bands composed of microcline and biotite. These laminations, which average 0.075 mm in thickness, express the foliation and are notably deflected and wrapped around the feldspar anhedra (Pl. 2, fig. 1).

Perthitic pegmatite veins are the third type of granitic rock associated with the gneiss. These range in thickness from a few inches to several feet, and cut the gneiss foliation. Drag of the adjacent gneiss foliation, indicating a generally upward movement of the pegmatite, was noted in a few places.

Three types of granitic rock are associated with the Fordham gneiss. A moderately coarse light-gray to pink granite occurs as conformable layers averaging about 5 feet in width. These layers do not appear to be intrusive, and since their composition is similar to that of the lighter gneiss bands it is probable that they are the more prominent light bands of the gneiss. A coarse pink granite occurs in layers up to 30 feet thick which are generally conformable but in places cut the gneissic foliation. This is a foliated perthite microcline granite. The foliation wraps megascopic and microscopic feldspar porphyroblasts.

These layers extend for 50 to 100 feet, generally parallel to the foliation of the gneiss,

ridge granite and the microcline- and perthite-deficient normal phase of the Fordham gneiss. Its composition is similar to that of the normal phase, but it is characterized by the presence and contorted foliation planes. A mineral lineation is common, and almost every exposure contains small-amplitude folds with measurable fold axes.

TABLE 9.—MEASURED MODES OF THE FORDHAM MIGMATITE GNEISS

Minerals	1	4	6	8	15A*	18	19	23*	26	36	39	45	46	47	48	Average
Quartz	40.5	32.0	41.0	21.4	7.4	44.2	51.2	19.2	49.0	27.0	40.0	28.6	39.0	34.9	38.2	35.8
Plagioclase, An_{6-40}	50.9	50.0	19.4	37.9			21.8	40.9	24.8	37.9	37.1	37.3	19.0	13.4	11.1	28.3
Orthoclase								27.2		7.9		5.3				2.5
Microcline	tr	13.3	32.7	2.0		27.0	24.0	3.9	18.7	8.3	2.0	15.7	12.7	tr	8.9	14.3
Perthite			5.0			10.4	2.0						22.0	48.5	40.8	9.0
Biotite	6.7	4.3	1.8	38.9	19.9	8.2	1.1	3.9	7.4	19.2	21.0	12.4	7.3	3.3	1.1	9.7
Muscovite			tr			tr	tr			tr		tr				tr
Hornblende	2.2							4.9			tr					0.3
Sericite									tr							tr
Kaolinite			tr	tr		10.2		tr		tr		tr	tr			tr
Zircon		tr		tr	tr	tr		tr	tr	tr	tr	tr	tr		tr	tr
Hematite				tr					tr	tr	tr	tr	tr	tr	tr	tr
Magnetite	tr			tr	tr			tr		tr		tr				tr
Apatite	tr					tr		tr		tr	tr					tr
Garnet				tr	25.9						tr	tr		tr		tr
Myrmekite				tr							tr		tr			tr
Cordierite					34.0											
Sillimanite					12.7											
Sphene											tr	tr				tr
Piedmontite										tr						tr
Chlorite												0.9				tr

* Cordierite-sillimanite gneiss not included in average

of microcline and perthite. It is found most abundantly near the borders of the Poundridge granite, but is widely distributed throughout the exposed area of the Fordham gneiss and is generally associated with granitic layers and small pegmatites.

The migmatite phase ranges from a massive fairly coarse granitic rock with indistinct foliation, different from the Poundridge granite only in the presence of plagioclase and microcline and more abundant biotite, to a well-foliated finely banded gneiss which contains pink microcline in small grains or larger porphyroblasts that cause deflection of the foliation. The porphyroblasts reach a maximum length of 3 inches. In a few places, the rock appears to have been highly mobilized and contains distorted gneissic layers as well as amphibolite, granite, and pegmatite units (Pl. 3, fig. 4), constituting a typical mixed rock. Elsewhere the rock is schistose with crinkled

Measured modal analyses (Table 9) shows quartz to be the most abundant mineral, plagioclase and microcline common, and perthite and biotite less abundant. This contrasts with the composition of the normal phase (Table 8) in which plagioclase is the most abundant mineral and in which there is no perthite, very little microcline, and a larger percentage of biotite, hornblende, and garnet. The plagioclase of the migmatite phase ranges in composition from An_6 to An_{40}, but is commonly an oligoclase with about 26 per cent anorthite which is somewhat more sodic than that found in the normal phase. Most of the biotite is the green variety, but there is some brown and a little of the red. Myrmekite, present in a few specimens of the migmatite phase, is absent from the normal phase.

Microscopically the foliation is commonly expressed by the small elongated quartz grains (*e.g.*, 0.045 x 0.15 mm) which are concentrated

in veinlets with small crystals of microcline. The veinlets are deflected by large, roughly elliptical crystals of microcline, perthite, or plagioclase. Small sparse biotite laths parallel the foliation in some slides. The texture strongly suggests that much of the quartz, microcline, and perthite is of replacement origin. The minerals are fresh and commonly occur in veinlets or broad bands which separate zones or patches of the dark minerals, biotite and hornblende, as well as corroded plagioclase. Several slides contain crystals of plagioclase which are embayed and apparently partially replaced by perthite or microcline (Pl. 2, fig. 3).

The optical continuity of the isolated fragments of plagioclase occurring within larger microcline crystals indicates the former existence of larger plagioclase anhedra. Small rounded quartz grains are commonly included in the perthite and microcline, indicating the possibility that the quartz was also replaced by feldspar.

In some specimens narrow fresh borders surround twinned plagioclase crystals. The twin lamellae extend from the main crystal to the border, but a different extinction position in the border indicates a change in composition, determined to be An_{22} in the main crystal and An_{11} in the band. These do not have the appearance of typical zoned plagioclase and, because they are found in a nonmagmatic rock, they are considered to be products of alkali metasomatism.

Several layers of marble ranging from 3 to 15 feet in thickness occur in the Fordham gneiss. Similar carbonate beds have been noted by others and have been considered lithologic units within the Fordham rather than Inwood marble, although some occur near the Inwood-Fordham contact. The marble is medium-grained gray to light green where fresh and light brown on the weathered surface. The rock is faintly foliated. The specimen examined microscopically (Table 11, specimen 96) was about half dolomite with plagioclase, microcline, tremolite, diopside, and sphene. These metasomatized marble layers may be the host rock of the ubiquitous amphibolites.

One exposure of cordierite-sillimanite Fordham gneiss was observed within 100 feet of the contact with the Poundridge granite. This is the only place where these two minerals have been found in the Fordham gneiss. The rock is a well-foliated, finely banded gneiss which weathers to a reddish brown. Microscopically (Table 8, specimen 15A) the texture is lepidoblastic with generally oriented biotite laths bending around large garnet porphyroblasts. The cordierite crystals are large and contain small biotite and sillimanite grains (Pl. 2, fig. 2). Most of the sillimanite is fibrous and also bends around the garnet. The best explanation of the association of sillimanite and cordierite appears to be the contact metamorphism of a sillimanite-bearing gneiss resulting in the formation of cordierite. The proximity of the Poundridge granite lends some force to this idea.

Amphibolite

Amphibolite layers ranging from a fraction of a foot to 15 feet in width are present everywhere in the Fordham gneiss and are common in the Manhattan formation. They lie between the foliation planes and are concordant; in places they are cut by pegmatites and younger granites. They tend to be continuous for long distances down the strike, but pinch out or form boudinage structure, particularly near the contact with the Poundridge granite. They also occur as conformable xenoliths within the granite. They are massive but possess a foliation marked by narrow, widely spaced light bands and in many places show a mineral lineation. Near the contacts with the younger granites they tend to become more micaceous and schistose.

The rock contains a large proportion of green hornblende with abundant andesine and red-brown biotite and less quartz (Table 10). Many specimens have a small amount of clinopyroxene (Wo_{47}, En_{32}, Fs_{21}) and garnet (Table 4); a trace of calcite was observed in one.

The texture is intermediate between granoblastic and lepidoblastic. Typically the foliation is caused by alignment of the slightly elongated hornblende anhedra which commonly measure 0.3 mm in the longest direction. The plagioclase, quartz, and biotite grains are equal in size or smaller than the hornblende. In some slides the biotite laths are also aligned. In many samples there is a discernible banding of hornblende, biotite, clinopyroxene, and

strongly embayed garnet, all slightly concentrated in narrow zones which parallel the foliation. In any one slide the hornblende crystals are either predominantly basal or predominantly prismatic sections, indicating a tendency toward preferred orientation which the appearance of zones and are regarded as metasomatic in origin.

Inwood Marble

The Inwood marble is exposed principally in two arcuate belts on both sides of the Man-

TABLE 10.—MEASURED MODES OF THE AMPHIBOLITE

Minerals	5	9	10	11	13	14	21	22	35	43*	44*	49	50	52	53	80*	107†	109†
Quartz	21.5	14.8	17.7	16.7	4.7	4.4	2.6	3.2	23.1	15.5	11.1	8.3	15.6	28.3	31.4	26.9	13.3	10.7
Plagioclase, An_{28-42}	15.9	13.2	14.6	26.4	25.6	27.7	20.8	33.6	24.9	24.0	29.4	35.2	20.0	22.8	14.3	40.4	15.9	26.4
Biotite	2.0	0.2	8.4	0.1	0.13		1.8		9.0	tr	0.4	2.3		7.1	5.6	19.4	tr	1.9
Hornblende	55.8	69.9	57.5	55.8	61.5	61.9	62.8	58.4	34.8	52.5	56.4	29.0	57.2	39.8	45.2	5.7	57.0	58.4
Pyroxene					8.2	3.5	11.8	3.2				8.0			1.7	7.5		
Garnet	tr		1.9			tr				8.6		17.3					2.2	
Zircon	2.0	0.4		0.8	tr				tr		tr			tr	tr	tr		
Apatite	tr		tr		tr				tr	tr			tr	tr				
Magnetite	3.1	1.4	0.6	tr	tr	2.7	tr	1.7	8.1	tr	2.6	1.0	7.2	2.1	2.0	tr	6.7	2.5
Hematite			tr													tr	tr	
Kaolinite				tr			tr				tr		tr					
Sphene							tr											
Muscovite										tr								
Clinozoisite												tr						
Sericite												tr						
Calcite												tr						

* Amphibolite in Manhattan formation

† Harrison (?) diorite

is observed megascopically in the mineral lineation.

Wherever observed the clinopyroxene crystals (as large as 0.6 mm) are strongly embayed and have been partially replaced by hornblende and biotite (Pl. 2, fig. 4). Whever amphibolite is cut by granite, particularly near the contact, there is a decrease in the amount of hornblende and clinopyroxene and an increase in biotite. These facts indicate that a reaction relationship existed between the amphibolite and granite in which the original dark minerals of the amphibolite were altered to bring them more nearly into equilibrium with those in the granite at the time of intrusion.

A few plagioclase crystals have fresh more sodic rims similar to the plagioclase in the migmatite phase of the Fordham gneiss. Because these are single borders, are fresher than the interior, and are narrow, they do not have

hattan formation. These rock belts curve around the Poundridge mass and separate it from the northern and eastern zone of Fordham gneiss. The outer belt is wider and contains more granitic and schistose layers than the inner. No accurate thickness could be determined, but the mapped pattern of the eastern belt suggests that the total thickness is 1240 feet.

In addition to marble, there are several narrow schistose (Pl. 2, fig. 6) layers (Table 7, specimens 59, 68, 105), a few amphibolite units, and a prominent granitic belt which is described separately. The marble is sugary, medium-grained, white to blue-gray on the fresh surface and rusty brown where weathered. It is commonly micaceous or contains thin dark discontinuous lines indicating the presence of dark silicate minerals. This gives the rock a darker color. Bedding is not readily recognizable, but faint color banding and

broad shallow grooving on the exposed surface, probably caused by compositional differences, may express this structure which appears to parallel the foliation. Further indication of this is the parallelism of schistose layers and

and the diopside is strongly embayed. Where abundant the scapolite occurs as large masses of anhedral crystals.

A layer of granitic rock about 50 feet thick lies within the outer marble belt and forms a

TABLE 11.—ESTIMATED MODES OF THE INWOOD MARBLE

Minerals	33	61	64	66	75	85	88	96*	103	104
Carbonate	95	40	85	85	70	40	20	50	92	60
Quartz		25				4	tr	tr	2	
Microcline		15				30		10		
Orthoclase	tr				10					
Plagioclase, An_{32-46}						1	12	10	1	
Forsterite	3		5							
Tremolite								17		
Diopside	tr	15			15	15	23	10		
Antigorite	1									
Phlogopite	2		5	15	5				4	5
Magnetite	tr	tr			tr		tr	tr		
Serpentine		3	8	tr						35
Scapolite			2	tr			40	3		
Sphene					tr		3		tr	
Hornblende						7				
Biotite							2			

* Marble layer in Fordham gneiss

foliation. Quartz and feldspar stringers a few inches thick are common in the marble and parallel the foliation.

Estimated modal analyses (Table 11) indicate a highly impure somewhat dolomitic marble. Only the carbonates which compose 20–95 per cent of the rock are common to all specimens. Diopside (Wo_{50}, En_{42}, Fe_8) is the most abundant silicate. Quartz, microcline, orthoclase, andesine, phlogopite, serpentine, and forsterite are common, although irregularly distributed. One specimen (Table 11, 85) is of special interest because of its unusual mineral association of dolomite, quartz, microcline, plagioclase, diopside, and hornblende.

The microscopic texture of the marble is moderately coarse and granoblastic, although in some specimens the foliation is revealed by the alignment of somewhat elongated dolomite anhedra. In some slides there is poor orientation of phlogopite laths, while in others a banding caused by the concentration of feldspar and diopside is discernible. Commonly the forsterite is partially replaced by serpentine,

ridge stretching for several miles in an otherwise low-lying area. The rock is light gray to white and medium-textured, except where moderately large feldspar augen are visible. The foliation is fine and a slight lineation is common on the foliation surface. On some exposures, a fresh wet surface shows a distinctive bird's-eye-maple texture. One of the best exposures is on Kitchawan road half a mile east of Highway 124 on the top of a hill opposite a small cemetery.

Mineralogically (Table 12) the rock is a microcline granite averaging about 55 per cent microcline and 35 per cent quartz with smaller amounts of biotite and minor oligoclase. The microscopic texture, however, is not that of a typical magmatic granite. A distinct foliation is revealed by a series of parallel quartz veinlets which are commonly continuous and bend around large microcline anhedra. There is fine-grained microcline in the groundmass as well as minor quantities of aligned biotite and muscovite. Some modification occurs where large microcline crystals are lacking, or where

the quartz veinlets are not continuous and the mica is not oriented.

The rock is considered the product of metasomatic replacement of an originally argillaceous bed within the marble. Other narrower feldspathic layers (one containing diopside) are common throughout the marble belt.

TABLE 12.—ESTIMATED MODES IN GRANITIC LAYER IN INWOOD MARBLE

Minerals	62	63	63A	69	70	72	83	84	86	89
Quartz	30	30	30	40	25	55	35	25	40	45
Microcline	60	70	60	45	60	42	50	60	53	40
Oligoclase (An_{12})				5	tr	tr		5	5	
Biotite	10			13	15	3	15	8		15
Chlorite	1	1	tr	2				1		
Muscovite	tr	tr	10	5		tr	1		tr	
Clinozoisite	tr				tr					
Magnetite	tr	tr			tr	tr			tr	tr
Kaolinite		tr	tr							
Sericite					tr	tr		tr		
Sphene					tr					
Garnet				tr		tr		tr	tr	tr
Apatite							tr			
Zircon							tr			tr
Tourmaline								tr	tr	

Poundridge Granite

The Poundridge granite, so named by Gordon Bell (1936), forms a large crescent-shaped exposure in the center of the area mapped. It and a large mass of Fordham gneiss which it partially encircles constitute the Poundridge mass, a prominent topographic high (Pl. 1). The outer contact is with a narrow band of Fordham gneiss, which in turn is in contact with Inwood marble and is marked by a precipitous cliff, particularly on the southern and eastern sides.

The granite is of medium coarseness, pink to buff where fresh and light reddish brown to dark brown on the weathered surface. The most prominent foliation occurs where biotite flakes are aligned. In many places books of biotite 1–2 inches long and about a quarter of an inch thick are distributed through the rock with a uniform orientation that imparts an obvious flow foliation parallel to the contact. In many exposures the rock appears massive, but careful examination reveals a parallelism of slightly elongated quartz and feldspar crystals. The foliation is further expressed where inclusions are aligned with their longest dimensions in a preferred orientation. On the weathered surface a closely spaced fracturing commonly parallels the foliation.

In the precipitous exposure on the southeast-facing cliff of the Poundridge mass, six layers of gneiss, ranging in thickness from 3 to 25 feet, alternate with narrow belts of granite over a stratigraphic distance of 300 feet. The contacts between the gneiss septa and granite are sharp and largely concordant (Fig. 7). The gneiss is curved and bent near the contact, and in places the granite invades the gneiss for short distances across the foliation. A few of the gneiss layers are completely isolated within the granite. Small pegmatites and amphibolite layers are common in the contact zone, occurring in the granite and the gneiss. Tabular amphibolite xenoliths are the most common type and are somewhat concentrated near the contact. The main mass of granite is slightly finer-grained than that interlayered with the gneiss and contains less microcline and biotite. The significance of this *lit-par-lit* contact is discussed in the section on petrology.

Measured modal analysis (Table 13) indicates alaskite (116) according to Johannsen's classification. The rock contains a small percentage of biotite, is rich in quartz and microperthite, and has an average of 10 per cent microcline. A

small proportion of the microperthite is the microcline perthite variety. Albite (An_5–An_{10}), garnet, zircon, and magnetite are persistent secondary minerals. Fibrous sillimanite, making up 2.6 per cent of one specimen is concentrated

TABLE 13.—MEASURED MODES IN THE POUNDRIDGE GRANITE

Minerals	15	94	95	100	Average
Quartz	30.0	54.3	46.0	46.7	44.2
Microperthite	68.2	30.2	35.7	29.8	42.0
Microcline		13.6	18.4	18.8	10.3
Albite		tr	tr	tr	tr
Biotite	1.95	1.7		0.49	1.1
Garnet	tr	tr	tr		tr
Zircon	tr	tr	tr		tr
Sericite			tr	tr	tr
Sillimanite				2.6	tr
Magnetite	tr	tr	tr	tr	tr
Muscovite				1.6	tr

with biotite, muscovite, and plagioclase in a lenticular nest, suggesting a nonmagmatic relic.

The microscopic texture differs from many granites in that euhedral and subhedral crystal boundaries are very rare. Characteristically, fairly large (0.6 mm) microperthite anhedra are associated with smaller quartz crystals that have sutured borders, and are surrounded by masses of fine-grained quartz and microcline (0.5 mm). Where discernible, foliation is evidenced by a poorly oriented scattering of elongated quartz or, less commonly, feldspar crystals. The few small green or brown biotite laths may show a slight preferred orientation. The microperthite intergrowth is minute, and in a few places, the crystals are surrounded by narrow clear borders, suggesting rapakivi texture.

Within the Poundridge granite exposure along the Fire Tower Road 200 feet north of the fire tower in the Ward-Poundridge Reservation, there is a 90-degree change in strike of the foliation across a zone 300 feet in the north-south direction and 600 feet in an east-west direction. Except for the difference in orientation of the foliation and the fact that the foliation is more banded, there is little megascopic difference between this rock and the Poundridge granite. However, the banded rock contains more quartz, microcline, and biotite and much less microperthite. The texture is also different, consisting of large crystals of microcline perthite set in a fine-grained, strongly oriented groundmass of quartz microcline and brown biotite.

It is concluded that this rock may be a large, partially assimilated xenolith or a fragment of a roof pendant of Fordham gneiss.

Siscowit Granite

A large area of granite occurs in the southeastern portion of the mapped area (Pl. 1) and extends well beyond the borders of the map. This rock has been called the Thomaston granite by Agar (Balk, 1936, Pl. 1) and others, evidently correlating it with a granite of that name near Thomaston, Connecticut, described by Agar (1934, p. 363). Since this rock is not continuous with that at the type locality and bears little resemblance to it, it is here named the Siscowit granite after a reservoir within its outcrop area.

The rock is a medium- to fine-grained, light reddish gray on the fresh surface and dark reddish gray to dark gray where weathered. The outcrops tend to be rounded, and the rock massive, with the foliation visible only where close examination reveals an alignment of biotite. The uniform orientation of this structure suggests regional schistosity.

The rock consists of more than 50 per cent microcline, between 20 and 40 per cent quartz, up to 15 per cent brown biotite, and minor amounts of muscovite, oligoclase, zircon, apatite, garnet myrmekite, and magnetite. According to Johannsen's classification, it is a kali-granite (215).

The microscopic texture is dominated by medium to large (up to 1.0 mm), somewhat elongated, microcline anhedra which are poorly aligned and associated with commonly smaller, roughly aligned quartz crystals. The interstices contain small grains of quartz, microcline, and oriented laths of biotite and muscovite. The microcline contains poikilitic quartz and muscovite. Both micas tend to be concentrated in narrow irregular bands.

Bedford Augen Gneiss

The Bedford augen gneiss is exposed in a tapering belt south of the Poundridge mass 15

square miles in area extending northeast-southwest for about 6 miles (Pl. 1). It has been described by Luquer and Ries (1896), Fettke (1914), Barbour (1930), and Barth (1936, p. 811).

variety. Based on optical data (Table 4) the composition of the clinopyroxene in one specimen is (Wo_{47}, En_{32}, Fs_{21}). The optical properties and related composition of the hornblende are listed in Table 5.

TABLE 14.—ESTIMATED MODES OF THE BEDFORD AUGEN GNEISS

Minerals	38†	39A	40	41	55	90†	91	92	110†	111*	112*
Quartz	30	5	30	40	10	20	tr	25	25	5	
Andesine (An_{39-49})	25	40	45	45	50	40	40	45	65	45	20
Microcline	10							5			
Biotite	30	20	23	15	30	40	10	20	7	14	21
Chlorite	1										
Sericite		tr	tr	tr							
Garnet	2								3		
Apatite		tr	tr	tr	tr	tr	tr				
Sillimanite	tr										
Magnetite	tr				tr	tr	tr	tr	tr	tr	
Hornblende		30	tr	tr	10		50	5		25	42
Zircon		tr			tr	tr					
Pyroxene			2							7	15
Sphene			tr				1	1			2
Calcite			tr							2	
Epidote				tr		tr					
Allanite				tr							
Serpentine										2	

* Harrison (?) diorite.

† Host rock is Manhattan schist

Large pink microcline augen (maximum 1 inch) and smaller white plagioclase crystals are roughly aligned in a generally dark-gray or black, well-foliated matrix, giving the rock a distinctive appearance (Pl. 3, fig. 3). The augen are concentrated in wide bands or large lenticular patches. The microcline augen are associated with the smaller, more abundant, plagioclase augen. Most commonly only the white plagioclase augen are present as shown by the fact that only two of the nine specimens analyzed contained microcline (Table 14). Garnet porphyroblasts are widely distributed as are schistose and amphibolitic layers devoid of either type augen. Small cross-cutting pegmatites are common.

Estimated modal analyses (Table 14) indicate an andesine-quartz-biotite rock with almost universal green hornblende, irregularly distributed almanditic garnet, microcline, apatite, zircon, and sphene. About half the biotite (Table 3) is the red-brown, and half the brown

The microscopic texture is characterized by large elongated anhedra of plagioclase set in a roughly banded lepidoblastic matrix of biotite, hornblende, quartz, and plagioclase. In places a few large garnet and microcline crystals are present. The roughly segregated bands of finer-grained minerals tend to be deflected by the larger porphyroblasts. Generally the plagioclase augen show albite and carlsbad twinning and contain small quartz grains which are optically continuous within each carlsbad-twin individual. The (010) composition face of the two twin types tends to lie in the foliation. Minor myrmekitic intergrowth is present in some specimens, and small sphene crystals are concentrated in a few places. Small crystals of sillimanite, many oriented with the base parallel to the slide, were found in one specimen.

The host rock of the Bedford augen gneiss has been considered to be either the Fordham gneiss (Fettke, 1914) or the Manhattan schist (Barbour, 1930). The writer believes that the

host was in lesser part the Manhattan schist but predominantly a dioritic rock, possibly correlative with the Harrison diorite of the Stamford quadrangle to the south. This rock is apparently intrusive into the Manhattan formation, and the augen structure developed has also affected some of the bordering schist.

Diorite crops out extensively just south of the augen gneiss belt (Fettke, 1914; Luquer and Ries, 1898), and augen structure becomes noticeable toward the north. Many layers within the augen gneiss are devoid of augen and have the mineralogic composition of a diorite (Table 14, specimen 111). The matrix of most of the augen gneiss is composed of hornblende, biotite, andesine (An_{40}), quartz, and, rarely, pyroxene. It is totally different from the Manhattan schist and differs from the Fordham gneiss in the absence of orthoclase and the presence of pyroxene. A few specimens are mineralogically and texturally similar to the Manhattan schist (Table 14, specimen 38, 90, and 110), but are found principally near the borders of the augen gneiss or, rarely, within the body of the gneiss.

The diorite is exposed in a large road cut on Highway 104 two miles southeast of Bedford. Here the texture ranges from moderate to coarse, and the color from dark green to black. The rock is mostly nonfoliated. It is composed principally of green hornblende with appreciable amounts of andesine, biotite, clinopyroxene, and minor sphene (Table 14, specimen 112). It is classified, according to Johannsen, as a melanodiorite (3212). The texture is xenomorphic granular with poikilitic pyroxene in uralitic hornblende and biotite; there are also larger twinned pyroxene anhedra.

Bedford Pegmatites

Near Bedford three large pegmatite bodies, which have been quarried for feldspar, are famous for their great variety of minerals. They contain quartz, perthite, biotite, albite, allanite, apatite, autunite, beryl, bismuthinite, columbite, cyrtolite, epidote, graphite, garnet, gummite, hornblende, illmenite, magnetite, microcline, molybdenite, muscovite, orthoclase, opal, pyrite, pyrolusite, pyroxene, rutile, titanite, tourmaline, torbernite, uraconite, uraninite, uranophane, and zircon (Peter Zodac, Personal communication).

Time did not allow a detailed study of the pegmatites; hence, only a brief description is possible. The three largest pegmatites lie just southeast of Bedford within an area of 1 square mile. They are intrusive into the Bedford augen gneiss, and their long axes parallel the trend of the foliation. They appear to be mostly concordant. In outcrop area they are several hundred feet long and about 100 feet wide.

Barbour believed (1930) they were emplaced soon after a period of dynamic stress which must have been the Taconic disturbance judging from the 375-million-year age determination shown by uraninite from these dikes (Muench, 1931).

Summary of Criteria for Distinguishing Fordham Gneiss and Manhattan Schist

In southeastern New York and western Connecticut the Manhattan schist, the Fordham gneiss, and their equivalents have not been clearly distinguished or accurately correlated. A summary of the criteria used in distinguishing these rock units in the Poundridge area is presented here.

Sillimanite is present in about two-thirds of the Manhattan schist specimens, but is absent from the Fordham gneiss. Green hornblende is present in about 60 per cent of the normal Fordham gneiss and one-fifth of the migmatic phase, but is not present in the Manhattan schist. The biotite in the Manhattan schist is typically red brown, in the Fordham gneiss green and brown, as well as red brown, may be present. Garnet is more abundant in the Manhattan schist. The ratio of quartz to plagioclase in the Manhattan schist averages 1.4 to 1, while in the normal Fordham it averages 1 to 1.5.

Texturally the Manhattan is lepidoblastic with well-oriented biotite and elongated quartz crystals expressing the foliation. The biotite commonly shows optical continuity and may be concentrated in narrow fairly well defined bands. The Fordham is granoblastic with rough segregation banding which expresses a coarse foliation. Orientation of elongated minerals is poorly defined.

The bands in the Fordham gneiss, commonly

coarser than those in the Manhattan schist, are black and light gray. They are typically 2–3 inches wide, and, in many places, contorted. The Manhattan schist is schistose or more finely banded, and the color contrast between the bands is not so great. The foliation in the Manhattan may be crinkled but is not commonly folded or contorted. The Fordham gneiss weathers to black or dark gray; the Manhattan schist, to dark brown or gray. Amphibolite layers are more abundant in the Fordham gneiss. In outcrop, the Manhattan tends to be slabby, and the Fordham gneiss more massive and rounded. On the fresh foliation surface, the Manhattan schist is light gray speckled with fine-grained, black biotite, or, if sillimanite is present, has a faint purplish hue.

Of course, many of the criteria cited are functions of metamorphic grade and type and will not hold in areas of different metamorphic character.

Metamorphism

General Statement

The rocks in the Poundridge area have been subject to regional metamorphism of the highest grade. They belong to the sillimanite-almandite subfacies of the amphibolite facies or, using the zone concept, they lie beyond the sillimanite isograd. Although the Fordham gneiss and Manhattan formation are placed in the same high-grade facies and zone, the Fordham migmatite gneiss of the Poundridge mass has been somewhat more intensely metamorphosed. Its texture is coarser, and it has been more intensely metasomatized because of its close association with the Poundridge granite and numerous other granitic layers.

Facies and Zone

Using Eskola's facies classification, it is possible to assign the important metamorphic rock units to the sillimanite-almandite subfacies (Turner, 1948, p. 85) (Fig. 2). The position of the amphibolite, Fordham gneiss, and Manhattan schist are shown within the ACF diagram of the subfacies. The association of sillimanite, almandite, and orthoclase in the Manhattan schist proves that its assignment to the sillimanite-almandite subfacies is correct. Sillimanite, kyanite, and staurolite are absent from the Fordham gneiss, undoubtedly because of a lower alumina-alkali ratio. However, the presence of orthoclase, which may form in the highest grades at the expense of muscovite, and the plagioclase-hornblende-almandite association seem sufficient reason for including the Fordham gneiss in this subfacies.

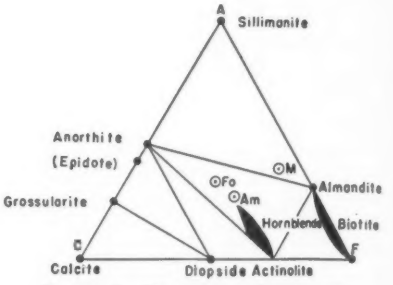

Figure 2.—Sillimanite-Almandite Subfacies of Amphibolite Facies

The position of the Manhattan formation (M), amphibolite (Am) and Fordham gneiss (Fo) is shown. The lack of sillimanite in the amphibolite and Fordham gneiss and its presence in the Manhattan formation is thus the result of bulk composition and not metamorphic grade.

In the Manhattan schist, the sillimanite occurs as inclusions in the biotite, which therefore may have contributed some potash to the formation of the orthoclase and possibly iron and magnesium to the garnet.

The amphibolites are, of course, within the amphibolite facies and are placed in the sillimanite-almandite subfacies on the basis of their intimate association with the schist and gneisses of that rank. Although the almandine-diopside-hornblende association is found in some specimens of amphibolite, the rock is not regarded as belonging in that subfacies (Turner, 1948, p. 87), because in all instances the pyroxene appears to be a relic and not an equilibrium phase. In addition epidote, a critical mineral in this subfacies, is lacking.

Silica-deficient rocks such as the Inwood marble are difficult to assign to a facies classification as now defined. Perhaps the best criterion for assuming the Inwood to be isofacial with the Fordham gneiss and the Manhattan schist is its geologic position between the two.

Also the presence of diopside in a siliceous carbonate rock indicates, with minor reservations as discussed by Bowen (1940, p. 259), that the highest pressure-temperature conditions of regional metamorphism have probably been attained.

Many petrologists prefer the concept of zones rather than that of facies in defining metamorphic intensities. Difficulties encountered in applying the facies classification in many field situations and such recent experimental work as that by Yoder (1952) strengthens this position. The argument, based on experimental evidence that indicates that while the physical principles of the facies concept are valid the facies have been improperly defined, loses some of its force when it is realized that the experimental systems are closed while it is doubtful that a perfectly closed system exists in nature.

The Poundridge metamorphic terrane is within the sillimanite zone. Minor amounts of sillimanite and orthoclase are scattered throughout the Manhattan schist. The Fordham gneiss, while it contains no sillimanite, may be assigned to the same zone, on the basis of the presence of orthoclase. Perhaps more precisely both the Fordham gneiss and the Manhattan schist lie within the orthoclase zone as defined by Heald (1950). The potash feldspar in the Fordham gneiss may have crystallized after decomposition of the muscovite and the introduction of potash from ubiquitous granitic intrusions. This can be expressed in the generalized equation: muscovite + potash → potash feldspar + water. Little muscovite occurs in the Fordham gneiss, which is in agreement with the above reaction. The lack of sillimanite in the Fordham may also be a result of that reaction since the excess alumina derived from the decomposition of muscovite is combined with metasomatic alkalies to form feldspar.

Origin of Metasediments

The possible sedimentary antecedents of the Fordham gneiss, Inwood marble, and Manhattan schist warrant some discussion. The most probable premetamorphic equivalents of these three major rock units are a graywacke, a cherty limestone with interbedded shale, and an alternating sequence of siltstone and shale. This conclusion is based principally on chemical evidence and on texture and rock associations. This is not to imply that the writer believes there is no change in chemical composition during regional metamorphism, but that those changes are, for the most part, predictable and not extensive. They involve the loss of water and carbon dioxide and the addition of various oxides, principally alkalies, in the highest grades. The more important metasomatic changes are pronounced in the Inwood marble and make the migmatite phase of the Fordham gneiss easily recognizable.

Chemical analyses were not used in the determination of chemical composition; a few analyses of these variable rocks would not give a true indication of bulk compositions. Instead the compositions were calculated from the averages of several measured modal analyses of each rock, which were determined with the integrating stage.

The volume percentages were converted to weight percentages; oxide percentages were calculated from the mineral formulae. Wherever possible optical data were used to determine mineral composition. This was not feasible for biotite and hornblende because of the poor correlation between optical and chemical data. The composition of biotite of an analyzed specimen from schist in Dutchess County analyzed by Barth (1936, Table 3, no. 2) was used together with a generalized hornblende formula. The error so introduced is considered to be less than would occur if a few scattered chemical analyses had been used. This conclusion is substantiated by the work of Chayes (Fairbairn, 1951, p. 62), who compared precision and accuracy of modal analysis and chemical analysis of a granite at Westerly, Rhode Island.

The average chemical analysis of the normal phase of the Fordham gneiss is strikingly similar to that of the average graywacke. On Table 15 the calculated mean analysis of the Fordham gneiss is compared with that of several graywacke analyses and an average shale analysis. An important characteristic of the chemical composition of graywacke is the excess of Na_2O over K_2O. This feature is shared with the Fordham gneiss in which the Na_2O:K_2O ratio is 2.05:1. This falls within the range of Na_2O-K_2O ratios found in analyzed graywackes and is

comparable to the ratio of 1.70:1 in Pettijohn's average of 11 graywackes (1949, Table 64). Also the frequency-distribution curve of Na_2O/K_2O in graywackes and shales shows two distinct maxima surrounding 3.2 in shales and 1.0 in graywackes. Thus this characteristic is not restricted to average rocks. In contrast, potash usually exceeds soda in shale, as in Clarke's average shale analysis (1924, p. 34) in which the Na_2O:KaO ratio is 1 to 0.4.

The difference in the proportion of the alkalies in graywacke and in shale is possibly a function of the degree to which chemical weathering progressed during sedimentation. According to Pettijohn (1949, p. 252), graywackes result from rapid erosion, transportation, and deposition, which limit chemical weathering. As a result, the sodium in feldspar fragments is not removed in solution as it is in shale deposition. There, chemical weathering is dominant during the erosion cycle. Potassium is also removed during the chemical weathering of igneous rocks (Pettijohn, 1949, p. 273) but is returned to shale by removal from sea water during the deposition of clay.

A comparison of the mineralogy of the Fordham gneiss with that of a metamorphosed graywacke is afforded by Ambrose's (1936) study of the Missi Series of Manitoba. Metamorphism has there reached no higher than the garnet zone, producing a quartz-oligoclase-almandite-muscovite-biotite schist. The more intense metamorphism of the sillimanite zone would alter the mineral suite to one identical to that of the Fordham gneiss. Conceivably muscovite would be converted to orthoclase, and hornblende would crystallize partially at the expense of some of the biotite (Cf. suite 3 of the chloritoid-almandite subfacies, p. 461, with a similar plot on the ACF diagram for the sillimanite-almandite subfacies, p. 457, Turner and Verhoogen, 1951). In addition, such a rock would lack sillimanite, a distinctive characteristic of the Fordham gneiss.

TABLE 15.—COMPARISON OF THE CHEMICAL COMPOSITIONS OF THE FORDHAM GNEISS AND MANHATTAN SCHIST WITH AVERAGE GRAYWACKE AND SHALE

	1	2	3	4	5	6	7
SiO_2	64.4	64.2	68.3	58.1	48.07	61.29	71.15
TiO_2	0.4	0.5	0.7	0.65	0.89	0.85	0.5
Al_2O_3	15.9	14.1	15.9	15.4	18.83	13.3	10.16
Fe_2O	2.2	1.0	1.1	4.02			
					6.91	3.94	3.72
FeO	4.4	4.2	5.7	2.45			
MnO		0.1	0.1				
MgO	1.9	2.9	2.6	2.44	3.56	3.31	1.66
CaO	3.6	3.5	1.9	3.11	4.96	5.11	3.65
Na_2O	3.5	3.4	2.1	1.3	1.17	1.32	0.86
K_2O	1.7	2.0	3.9	3.24	2.57	2.33	2.20
H_2O	0.4	2.2	0.8	5.0			
P_2O_5	0.2	0.1		0.17			
ZrO_2	0.4		0.4				
F	0.3		0.4				
CO_2		1.6		2.63			
Total.....	100.2	100.0	99.6	99.95			

1. Fordham gneiss (normal phase)
2. Average graywacke (Pettijohn 1949, p. 250)
3. Manhattan schist
4. Average shale (Clarke, 1924, p. 34)
5. Average coarse clay (Grout, 1925) ignition 10.91
6. Average silt (Grout, 1925) ignition 7.05
7. Average fine sand (Grout, 1925) ignition 5.08

Thus there appears to be acceptable chemical and mineralogical evidence pointing to a graywacke antecedent for the Fordham gneiss. The evidence is not as strong in the structural and textural characteristics and the lithologic associations. None of the typical textural features of graywacke (the gray to black color, the variable grain size and poor sorting, the rudely foliated sericite and chlorite matrix, the presence of rock fragments, and graded bedding) are inconsistent with the possible texture of the unmetamorphosed Fordham gneiss, although none of these features have survived the intense metamorphism. Layers of submarine lava commonly associated with many Precambrian graywackes could account for the amphibolites so abundantly distributed through the Fordham gneiss.

The only feature of the Fordham gneiss that is difficult to reconcile with the postulated graywacke origin is the presence of narrow marble layers which are never widely separated from the Inwood-Fordham contact. According to Pettijohn (1949, p. 243), the only carbonate associated with graywacke occurs in minor amounts as nodules. However, in the Coast Ranges of British Columbia and Alaska graywackes are interbedded with limestone and dolomites usually constituting less than 10 per cent of the section (A. E. J. Engle, Personal communication).

In considering the parent of some Grenville gneisses of the northwestern Adirondacks which resemble graywacke chemically but which are interlayered with thick, widespread carbonate zones, Engel and Engel (1953, p. 1088) have presented the alternative possibility that altered tuff or sodic shale was the premetamorphic rock. The chemical fit, including the Na_2O–K_2O ratio, is good for both tuff or sodic shale, and they may be associated with carbonate rocks. But, because they require a more restricted environment, they are less common rock types than graywacke.

It may be concluded that no sedimentary antecedent for the Fordham gneiss can be definitely established from the present data, although a graywacke seems the strongest contender. The migmatite phase of the Fordham gneiss has been strongly metasomatized and will be considered in that group.

The Inwood marble is highly metasomatized Although the rock is partially dolomitic, it can be assumed that the initial rock was a limestone. Pettijohn (1949, p. 312) summarized the preponderant evidence indicating the secondary origin of dolomitic carbonate rock. The granoblastic texture and the lack of detrital grains in the Inwood marble support this conclusion. It is probable that the original limestone contained an appreciable amount of chert. The silica, in the silicate minerals, and the quartz, comprising as much as 30 per cent of some samples, cannot be attributed entirely to metasomatism. Typically, the Inwood marble is made up of calcite, with a variable amount of dolomite, quartz, and diopside, forsterite, or tremolite. If these mineral suites are plotted in Bowen's (1940) system CO_2-SiO_2-CaO-MgO and the temperature hypothetically lowered so that reactions are reversed with attendant addition of CO_2, the original unmetamorphosed rock would be a siliceous dolomitic limestone.

The calculated average chemical composition (Table 16, specimen 4) of the Manhattan schist indicates that it was derived from a siliceous argillaceous sediment. A comparison of chemical compositions (Table 16, specimens 3, 4) shows that the Manhattan schist of the Poundridge area contains more silica and soda and less lime than the average shale. But, since the chemical composition of shale varies widely, it is more significant that the Manhattan schist has an excess of potash over soda and magnesia over lime[1] as is typical of shale. The abundance of alumina also suggests an argillaceous parent.

The high proportion of silica compared to that of the average shale indicates a rock coarser-grained than shale. Grout (1925) in studying the relation of texture to composition in clays has shown that silica content increases with increasing grain size. On Table 15 Grout's average compositions for coarse clay, silt, and fine sand are compared with that of the Manhattan schist. The 68.3-per-cent average of silica in the Manhattan schist places it between the silt and fine sand size, while the 15.9-per-cent average of alumina falls between the silt and coarse clay. Both of these values, however,

[1] Magnesia occurs in excess of lime in shale where carbonates are absent (Pettijohn, 1949, p. 273).

lie between the maximum and minimum for silt texture (Grout, 1925, Table 13), as do the amounts of all other oxides. It seems likely, then, that the original sediment was a siliceous argillite with a silt ($\frac{1}{16}$–$\frac{1}{256}$ mm) texture. Since it is based on an average composition, this represents a generalized rock type. The individual chemical analyses of Manhattan schist from other parts of Westchester County and New York City (Table 16, specimens 5–9) differ in composition. The variation in silica and alumina suggests a variation in texture from coarse clay to silt. This also undoubtedly applies in the Poundridge area where alternating siliceous and argillaceous shale probably represents the true nature of the inferred rock.

The argillaceous composition of the parent rock and the excess of K_2O over Na_2O indicates a probable depositional environment quite different from that of the Fordham gneiss. Loss of soda attests to the dominance of chemical weathering which causes the removal of both alkalies, preventing their accumulation within detrital feldspar in the resulting sediment. Potash is subsequently returned to the sediment, probably being adsorbed during clay-mineral formation, resulting in the high K_2O-Na_2O ratio in most shales. This implies a slow deposition of detritus from a distant or low-lying land mass in contrast to the possible rapid poured-in accumulation of the clastic material from a rugged land source which resulted in the "Fordham graywacke". Of course, the high Na_2O content of the Fordham may be secondary.

TABLE 16.—CALCULATED AND DETERMINED ROCK ANALYSES

	1	2	3	4	5	6	7	8	9	10
SiO_2	79.9	73.6	65.4	68.3	46.5	68.51	50.9	45.03	74.14	67.02
TiO_2	—	0.3	0.4	0.7	1.61	0.57	1.54	1.28	0.08	1.41
Al_2O_3	10.8	13.3	15.9	15.9	24.97	15.68	30.46	33.76	23.82	13.96
Fe_2O_3	0.7	0.5	2.2	1.1	2.63	0.71	1.36	—	0.62	2.36
FeO	0.6	1.8	4.3	5.7	9.58	2.32	4.59	8.19	0.46	2.37
MnO	—	—	—	0.1	n.d.	n.d.	n.d.	n.d.	n.d.	n.d.
MgO	0.1	1.1	1.9	2.6	3.7	1.42	1.09	2.75	0.19	1.27
CaO	—	1.4	3.6	1.9	2.27	3.83	0.93	1.85	—	2.69
Na_2O	2.5	3.3	3.5	2.1	3.55	4.62	1.96	2.22	0.37	3.61
K_2O	5.3	4.2	1.7	3.9	4.34	2.49	6.86	4.62	0.52	5.27
H_2O	0.1	0.3	0.4	0.8	0.9	0.14	0.54	1.07	0.54	0.38
P_2O_5	—	tr	0.2	—	n.d.	n.d.	n.d.	n.d.	n.d.	n.d.
ZrO_2	0.3	0.1	0.4	0.4	n.d.	n.d.	n.d.	n.d.	n.d.	n.d.
F	—	0.2	0.3	0.4	n.d.	n.d.	n.d.	n.d.	n.d.	n.d.
Total...	100.3	100.1	100.2	99.6	100.04	100.29	100.23	100.77	100.75	100.34

1. Poundridge granite
2. Fordham gneiss, migmatite phase
3. Fordham gneiss, normal phase
4. Manhattan schist: Biotite analysis from Barth (1936, p. 783); Garnet analysis from Barth (1936, p 786); Generalized hornblende formula used.
5. Manhattan schist, mica-feldspar schist from southeast corner of Broadway and West 116 St., New York City (Fettke, 1914)
6. Manhattan schist, gray gneissoid variety from shaft 18, Catskill Aqueduct, West 42 St. near Fifth Ave., New York City (Fettke, 1914)
7. Manhattan schist, staurolite-mica schist from Croton-on-the-Hudson, New York City (Fettke, 1914)
8. Manhattan schist, garnetiferous mica schist from Kensico, New York (Fettke, 1914)
9. Manhattan schist, kyanite schist West 120 St. east of Amsterdam Ave., New York City (Fettke, 1914)
10. Bedford augen gneiss, two-thirds of a mile southeast of Bedford along Stanford road (Fettke, 1914)

METASOMATISM

Metasomatic replacement has been important in the transformation of the Fordham gneiss,

Bedford augen gneiss, and Inwood marble. The general pattern is the introduction of the alkalies, principally potassium, and the loss of the basic ions. The Manhattan schist, except for the portion that is the host of the Bedford augen gneiss, does not show evidence of as much metasomatism as the other rocks. The rare occurrence of fresh microcline and sodic rims around plagioclase attest to minor potash and soda metasomatism in this rock.

The abundance of intrusive bodies in the area makes designation of the source of the metasomatic material in any particular place difficult to pin point. This material, particularly in the augen gneiss, need not have had a source outside the local metasediments, the transfer being effected by large-scale metamorphic differentiation.

Metasomatism seems to have had a structural control as suggested by Newhouse, Hagner, and De Vore (1949). Judging from the fact that metasomatic products may be traced for long distances parallel to the foliation but rarely across it, it may be concluded that the introducing fluids entered by migration along the foliation plane. The augen gneiss, although concentrated in a zone south of the Poundridge mass, extends in narrow fringes paralleling the foliation of the Manhattan schist for at least 2 miles northeastward.

The writer, an agnostic on the problem of granitization, presents metasomatic and magmatic alternative explanations of origin for the Poundridge granite. He feels that both alternatives fit the known facts equally well.

Barth's rock-standard cell is used in the discussion of metasomatism. This calculation does not prove that metasomatism has taken place; that fact is based on geologic and petrographic evidence. It is a convenient way, however, to show quantitatively what ions were involved in the metasomatic exchange.

The formation of the Bedford augen gneiss has been attributed (Fettke, 1914; Barbour, 1930) to the introduction of pegmatite fluids into sheared zones in the Manhattan schist; concentration of these fluids formed the large Bedford pegmatites. The evidence for this is the similarity of composition of the microcline augen and the microcline crystals in the pegmatite, and the higher concentration of augen in the vicinity of the pegmatite. However, Agar (1933, p. 9) and the writer have noted that the host rock of the Bedford augen gneiss is a complex of intrusive sheets of diorite with septa and marginal layers of Manhattan schist. This basic rock makes up a larger proportion of the augen zone than the schist. The augen are not concentrated near the Bedford pegmatites but are equally abundant several miles from these dikes. It appears that there is no need to postulate the introduction of material as complex as a pegmatite fluid to account for the change in composition necessary to produce the augen gneiss from these two hosts.

First let us consider the development of augen in the Manhattan schist. The mineral composition of this rock is presented in Table 7, specimens 38, 90, 110, and the chemical analysis on Table 16, analysis 10. This phase of the augen gneiss differs from the Manhattan schist only in having a larger proportion of plagioclase and microcline.

The shift in chemical composition which is reflected in this mineralogic change is evident from a comparison of the chemical analyses of the two rocks (Table 16). However, since metasomatism is apt to involve a volume-for-volume exchange rather than an exchange of equal weights, a weight-percentage analysis gives an inaccurate measure of the process. This does not imply that there is no mechanical volume change in the formational unit caused by stress and plastic deformation during dynamothermal metamorphism, but that, as pointed out long ago by Lindgren (1918), metasomatic replacement, even under stress, involves a volume-for-volume exchange. A truer representation of the replacement which has affected the augen gneiss is afforded by the use of Barth's (1948) rock standard cell composed of 160 oxygen ions and their associated cations. Since oxygen makes up more than 90 per cent of the volume of the lithosphere, an equal number of oxygen ions with their associated cations in any two rocks represents very nearly the same volume. For the unit cell 160 oxygen ions were selected so the number of associated cations would total close to 100. Thus a cation analysis is similar to the familiar oxide weight-per-cent analysis and shows a clear picture of the rock composition, expressed as the number of the various cations associated with 160 oxygen and hydroxyl ions.

The rock standard cell is calculated by dividing the oxide weight percentages by the molecular weight to obtain the number of moles of each oxide in 100 grams of rock. This is converted into the number of cations and oxygen ions of each oxide per 100 grams of rock by multiplying it by the appropriate subscript. The total number of oxygen ions is then divided into 160, and this number, when multiplied by the cation proportion, yields the number of cations per 160 oxygen ions.

TABLE 17.—IONS ADDED AND SUBTRACTED TO FORM BEDFORD AUGEN GNEISS FROM MANHATTAN SCHIST

Added	Subtracted
0.9 ions of Si	1.4 ions of Al
0.5 ions of Ti	1.1 ions of Fe^{++}
0.8 ions of Fe^{+++}	1.8 ions of Mg
0.7 ions of Ca	2.4 ions of H
1.6 ions of Na	
1.7 ions of K	
6.2 cations added per 160 oxygen ions representing 12^+ valences	6.7 cations lost per 160 oxygen ions representing 12^+ valence

The rock standard cells of the Manhattan schist and the Manhattan schist phase of the Bedford augen gneiss are:

$K_{4.3}Na_{3.7}Ca_{1.9}Mg_{3.5}Fe^{++}_{2.1}Fe^{+++}_{0.8}Al_{16.2}Ti_{0.5}$
$\cdot Si_{59.8}O_{150.8}(OH)_{9.2}$ Manhattan schist

$K_{6.0}Na_{6.3}Ca_{2.6}Mg_{1.7}Fe^{++}_{1.0}Fe^{+++}_{1.6}Al_{14.8}Ti_{1.0}Si_{60.7}$
$\cdot O_{156.6}(OH)_{4.4}$ Manhattan schist phase of Bedford augen gneiss

A comparison of the above reveals that the changes shown in Table 17 produced the augen gneiss from the Manhattan schist.

Although the accuracy of the data does not warrant absolute acceptance of the above values, the qualitative results appear valid. The change involved chiefly the addition of the alkalies and the loss of aluminum, magnesium, and water, a result not to be expected from the introduction of hydrous aluminum silicate pegmatite magma. Of course, the possibility of a genetic relationship between the augen and pegmatites cannot be denied. In the complex and poorly understood phase changes which probably characterize the crystallization history of magmatic pegmatites, emanations capable of producing the replacement pattern described, are certainly possible.

In thin section the feldspar augen are seen to have replaced quartz; large crystals disrupt the quartz bands and contain many quartz inclusions. In many places the augen have deflected the biotite foliation bands and commonly contain biotite inclusions. It seems possible, therefore, that the augen derived their silica largely from quartz, their aluminum and possibly some potassium from the biotite. The latter seems particularly evident in specimen 110 (Table 14) which contains the largest percentage of feldspar and the lowest of biotite.

The development of augen in the diorite produced a rock lacking garnet and sillimanite, but containing hornblende and rarely clinopyroxene. A comparison of its mineralogy with that of the unaltered (but metamorphosed) diorite (Table 14, specimens 111, 112) shows that considerably more quartz, slightly more feldspar, and less hornblende and clinopyroxene are present.

It seems logical that metamorphic differentiation, under high-grade regional metamorphism, caused rearrangement of the ions, resulting in new mineral phases and the blurring of former lithologic boundaries. Alkalies introduced from an outside source may have played a part in the formation of the feldspar augen, but much of the chemical change in the diorite and Manhattan schist can be attributed to diffusion from a local source.

To illustrate which ions must be introduced from an outside source and which may be acquired locally, a postulated origin of the plagioclase augen may be cited. In metamorphism of a gabbroic or basaltic intrusive, phase changes are induced to bring the chemical system into equilibrium with a temperature environment lower than that which existed during the crystallization of the basic igneous body. In the augen diorite this resulted, in part, in the following:

clinopyroxene $(Wo_{47}En_{32}Fe_{21})$ → common hornblende → biotite

Chemically, such a reaction involves the loss of calcium and some silicon and the addition

of water, potassium, and aluminum. Since water is expelled from shale during metamorphism and since a decrease in aluminum in the Manhattan schist has been noted (Table 17), it is conceivable that these ions constitute a partial source for the material needed in the above reaction. In addition, the calcium and silicon ions lost in the conversion of pyroxene to hornblende could combine with the aluminum to form the plagioclase porphyroblasts. Sodium and potassium are required to complete the formation of both the plagioclase and the biotite. These are the only materials which must be contributed from a source outside the local rock units.

The migmatite phase of the Fordham gneiss, which ranges from a microcline-bearing gneiss to a coarsely banded *lit-par-lit* gneiss, is more likely a product of metasomatic replacement than the result of magmatic injection. There is no evidence that the Fordham expanded as a result of migmatization. If injection had occurred the widespread unevenly distributed migmatite phase would show evidence of expansion in the form of deflected foliation planes or drag folds such as those commonly found adjacent to the injected pegmatites. The plagioclase of the migmatite phase is twinned only by the albite, carlsbad, and pericline laws, which as brought out by the studies of Turner (1951) and Gorai (1950) indicates a nonigneous origin or a recrystallized unit.

Further evidence of metasomatism is provided by a comparison of the chemical composition of the rocks involved. Again Barth's rock standard cell is calculated to allow for a comparison of equal volumes of rock. A picture of the replacement pattern which affected the Fordham gneiss is provided by the contrast in the following rock-standard cells:

$K_{1.8}Na_{6.0}Ca_{3.4}Mg_{2.8}Fe^{++}_{3.4}Fe^{+++}_{1.6}Al_{16.7}Ti_{0.3}Si_{68.9}$
$\cdot O_{160.2}(OH)_{8.8}$ Fordham gneiss (normal phase)

$K_{4.7}Na_{5.4}Ca_{1.2}Mg_{1.8}Fe^{++}_{1.4}Fe^{+++}_{0.3}Al_{15.3}Ti_{0.2}Si_{63.2}$
$\cdot O_{156.4}(OH)_{3.6}$ Fordham gneiss (migmatite phase)

Table 18 shows the ions which must be added or subtracted to form the migmatite from the Fordham gneiss.

More cations are subtracted than added, but they represent an equal number of valences. Also the total number of cations associated with 160 oxygen ions is slightly greater in the normal phase. This is a result of the addition of four-valent silicon to the migmatite phase which satisfies the valence requirements with a smaller number of ions.

TABLE 18.—CATION REPLACEMENT IN THE MIGMATITE PHASE OF THE FORDHAM GNEISS BASED ON 160 OXYGEN IONS

Added	Subtracted
4.3 ions of Si	0.1 ions of Ti
2.8 ions of K	1.5 ions of Al
	1.2 ions of Fe^{+++}
7.1 cations representing 20 valences	2.0 ions of Fe^{++}
	1.0 ions of Mg
	2.1 ions of Ca
	0.6 ions of Na
	0.6 ions of H
	9.1 cations representing 20 valences

The Fordham gneiss was migmatized by the introduction of silicon and potassium and the loss of aluminum, iron, magnesium, calcium, sodium, and water (Table 18). This is reflected mineralogically in a decrease in plagioclase, biotite, and hornblende and an increase in quartz and potash feldspar in the migmatite.

The source of the introduced silicon and aluminum was undoubtedly the Poundridge granite. There is much less assurance concerning the fate of the removed ions. Because volumes have remained constant, it cannot be assumed that the gneiss was merely diluted with granitic material, making the loss of these ions apparent only. The ions must have been displaced; their disposition is involved in the origin of the Poundridge granite.

Perhaps the most significant observation concerning the origin of the Poundridge granite involves the comparison of the chemical compositions of the Poundridge granite and the migmatite and normal Fordham gneiss. The formula for the rock standard cell of the Poundridge granite is:

$K_{5.8}Na_{4.1}Mg_{0.2}Fe^{++}_{0.5}Fe^{+++}_{0.4}Al_{10.9}Si_{68.7}$
$\cdot O_{160.8}(OH)_{1.2}$

A graphic representation of the composition of these three rocks based on their rock standard

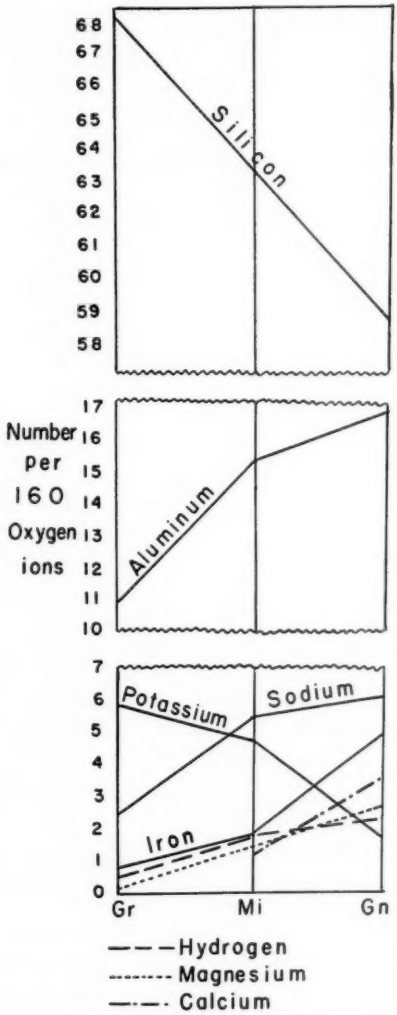

FIGURE 3.—CATION VARIATION

Per 160 oxygen ions based on the rock standard cells of the Poundridge granite (Gr), Fordham migmatite (Mi), and Fordham gneiss (Gn).

cells is presented on Figure 3. The position of the migmatite intermediate between the granite and gneiss is apparent. The change in composition from granite to gneiss shows that the silicon and potassium decrease sharply while there is a concomitant rise in aluminum, sodium, iron, hydrogen, magnesium, and calcium. The unusual increase in aluminum is a function of the low-alumina high-silica content of the alaskite. Significant is the continuance of the increase in aluminum from the migmatite to the gneiss, indicating removal of that ion from the migmatite.

The granite shows evidence of flow, and its contacts, generally concordant, are transgressive in places (Fig. 7). The rock is thus an intrusive but not necessarily magmatic. The mineralogical change between the granite and migmatite is gradational over short distances and involves a change in the type of feldspar from predominantly perthite to predominantly microcline. There is also a decrease in quartz and an increase in biotite. The texture of the granite is crystalloblastic.

These facts together with the detailed descriptions are basic to any origin postulated for the Poundridge granite.

If the Poundridge granite, although intrusive, is an end product of the same metasomatic process which produced the migmatite, the exchange of ions necessary to alter the migmatite to granite can be determined by a comparison of the rock standard cells of these two rocks.

The additions and subtractions are almost identical to those involved in the migmatization of the Fordham gneiss, a point which is further brought out by the intermediate composition of the migmatite shown on Figure 3. In the theory of granitization it may be presumed that the introduced silicon and potassium cations have been substituted for the displaced iron, magnesium, calcium, aluminum, sodium, and hydrogen, which have been removed to the surrounding rocks to form a basic front. There is nothing contradictory to this in the composition of the Fordham gneiss. These ions are abundant in the Fordham gneiss. Mineralogically they are reflected in the plagioclase, biotite, and hornblende so distinctive of that rock. It is conceivable that the addition of this material may have altered the composition of the Fordham to the extent that the inferred graywacke origin is invalid. However, when the much larger total volume of the Fordham gneiss is compared to that of the Poundridge granite, it becomes evident that these minor additions (less than 1 per cent) would not greatly affect the total chemical composition of the Fordham gneiss. Also, dissemination of these ions through

the adjacent rock would not be expected; they would be concentrated as a function of their physio-chemical environment and their rates of diffusion. In attempting to locate these ions it is more logical to look for concentrations. The

TABLE 19.—SUBSTITUTIONS NECESSARY TO ALTER THE MIGMATITE TO THE POUNDRIDGE GRANITE

Added	Substracted
5.6 Si cations	0.2 Ti cations
0.1 Fe cations	4.4 Al cations
1.1 K cations	0.9 Fe^{++} cations
	1.3 Mg cations
6.8 cations representing 23.4 valences	1.3 Ca cations
	1.3 Na cations
	1.2 H cations
	10.6 cations representing 23.5 valences

ubiquitous amphibolite layers contain heavy concentrations of all the displaced ions except sodium, which is present but not abundant. It is conceivable that the sodium migrated no farther than the migmatite and gneiss where fresh sodic rims are present around a few plagioclase anhedra. It is doubtful, however, that sufficient sodium was added to account for the high soda-potash ratio of the Fordham gneiss.

The writer regards granitization of the Poundridge granite unproved but possible. The strongest evidence in favor of granitization is the fact that certain ions have been removed from the Fordham gneiss and others added in such a pattern as to produce a migmatite which is intermediate in composition between the original gneiss and the granite. If the same ions were exchanged in the migmatite, apparently indicated by comparison of rock-standard cells (Table 19), the result would be the Poundridge granite. The composition of the Fordham gneiss is such that no radical change is necessary to produce the granite. An exchange of less than 1 per cent by volume, involving about 6 per cent of the total number of cations is all that is required. Perhaps the greatest obstacle to acceptance of granitization by ionic diffusion is the lack of a source of energy to cause this migration. The heat introduced by an intrusive magma is lacking. Other sources suggested border on pure speculation.

A different explanation of the observed facts is possible based on the assumption of a magmatic origin for the Poundridge granite. The mostly concordant pattern of the granite against the strong foliation of the Fordham gneiss indicates that the intrusive was probably synkinematic. Thus, if a granite magma intruded the complex of gneiss and amphibolite, assimilation of the bordering wall rocks was undoubtedly a factor.

Let us consider how this process could produce migmatization in the Fordham gneiss by the type of ionic replacement observed (Table 19). The Fordham gneiss is more basic than the Poundridge granite. Thus the granite magma would be incapable of dissolving the gneiss unless heat available was sufficient to keep the magma well above its melting point (Bowen, 1928, p. 198). Mineral alignment caused by flow indicates that the magma was partially crystalline at the time of emplacement and therefore contained no superheat. The magma would, however, react with this more basic material to bring its minerals into equilibrium. The plagioclase of the gneiss is more calcic than that of the granite; it would be converted to the more sodic phase with which the magma would be saturated. The heat for this reaction would be supplied by simultaneous precipitation of plagioclase of a composition in equilibrium with the magma. In the same manner, the granite magma would be saturated with biotite and supersaturated with the hornblende from the gneiss. It could not dissolve the hornblende, but would react with it to convert it to biotite. The possibility that this adjustment occurred is indicated by the more sodic plagioclase and larger percentage of biotite in the migmatite than in the normal Fordham gneiss. The migmatite may be regarded as a product of partial assimilation of the Fordham gneiss by the Poundridge granite. The more felsic segregation bands of the gneiss would become assimilated more readily than the dark ones, giving the *lit-par-lit* appearance typical of the migmatite. The incomplete assimilation can be attributed to the relatively rapid loss of heat of the comparatively small granite body. An objection may be that much of the migmatite is not in direct contact with the granite. If the mechanism suggested is valid, the granite magma and magmatic heat must have had access to the

gneiss over a wide zone adjacent to the granite contact. This is indicated by the presence of many narrow sheets of intrusive granite widely separated from the main mass. Much of the migmatite, however, is not in direct contact with any intrusive granite body. Since it is intimately associated with such material, it may have been altered by metasomatic exchanges necessitated by its attempt to reach equilibrium with the surrounding granite magma. This equilibrium was not attained, but the mineralogy of the original gneiss was altered so that the composition of the migmatite now lies between that of the normal Fordham gneiss and the Poundridge granite.

The inwood marble contains a large percentage of silicate minerals (Table 11). The part metasomatism played in the production of these minerals cannot be stated precisely for the premetamorphic composition is unknown. However, the Inwood marble was probably a dolomitized, cherty limestone. If so, alkali-alumina metasomatism could account for almost all observed mineralogy, and the same type metasomatism as in the Poundridge mass and the Bedford augen gneiss was probably active in the Inwood marble.

The great variability of the mineralogy makes estimation of the bulk composition difficult. However, the most persistent silicates are quartz and diopside, which, together with forsterite, tremolite, and serpentine, require no introduced material for their formation. The products of alkali-alumina metasomatism, microcline, orthoclase, scapolite, and biotite, are locally abundant, constituting as much as 30 per cent of one specimen. Since the scapolite is the calcium-rich variety, very little chlorine was required. Since magnesium-rich hornblende and biotite are each present in small amounts in only one specimen, iron metasomatism may be regarded as of minor importance. The small quantity of fluorine in the hornblende, biotite, and phlogopite must have been introduced.

Since Adams and Barlow (1910) showed that amphibolite could be produced by metamorphism of a limestone, the origin of these rocks has been an enigma wherever field relationship fail to indicate an exact origin. Engel and Engel (1951) stated that a solution may lie in the analysis of accessory elements in the amphibole which retain their premetamorphic igneous or metasomatic pattern.

The amphibolites of the Poundridge area reveal no positive proof of origin. However, there is evidence that metasomatism of carbonate layers and metamorphism of basic rock has contributed to their formation. Rarely can particular occurrence be assigned to an exact origin. Some of the amphibolite layers in the Manhattan schist which can be traced through the zone of the Bedford augen gneiss and into the epidiorite mass southeast of Bedford (Table 12, specimen 80) are of igneous origin. The other amphibolites in the Manhattan schist and those in the Fordham gneiss have no observable connection with an igneous body. Though the evidence is weak, their mineralogy places them in the category of amphibolites derived from a carbonate rock. Unlike most igneous amphibolites, they have a larger proportion of hornblende than plagioclase and contain appreciable amounts of quartz and biotite (Williams *et al.*, 1954, p. 243).

Additional petrographic evidence favors a sedimentary origin for some amphibolite layers in the Fordham gneiss. Two transition specimens, an amphibolite and a marble, have been studied. Specimen 49 (Table 10) from the Poundridge mass is a typical amphibolite except that it contains a small percentage of possibly relict carbonate. Specimen 96 (Table 11), from a marbel layer in the Fordham gneiss east of Lake Kitchawan, contains an appreciable proportion of diopside, scapolite, tremolite, and plagioclase in addition to the dolomite. As noted by Adams and Barlow (1910, p. 104) this could represent an early stage in the transition from marble to amphibolite. It may be significant that no marble layers were found in the Fordham near the Poundridge granite while they are common elsewhere, presumably out of range of the granite's influence.

Structural Elements

Introduction

The structural elements described together with the stratigraphy and map pattern, are the basis for the structural interpretation. In the interest of keeping fact and interpretation separate, the proposed structural solution is con-

tained in the section following those which describe the structural elements.

The geographic orientations of structural elements are read from a 360-degree scale with north at 0°. An east-west strike is thus a strike of 90°, the smaller angle being used in each case. Some features are presented in statistical diagrams (Figs. 4, 5, 6). These diagrams are the lower halves of equal-areal net projections oriented into geographic position.

Regional Setting

The foliation and formational boundaries of the New York City group strike northeastward throughout New York City and southern Westchester County. However, in northern Westchester and Putnam counties these two elements swing in large arcs of several miles radius until they are truncated by the northeast-striking Siscowit granite fault. This distortion is interpreted as the result of large-scale secondary folding in response to movement to the south or southeast.

Bedding

No feature which can definitely be ascribed to bedding was found in any rock. The position of the broad gneissic bands in the Fordham gneiss, which are probably products of metamorphic differentiation, may be controlled by original bedding. The conformable contact between the Inwood marble and the Manhattan formation gives a fairly accurate indication of the general bedding orientation within these formations. Fluhr (in a report of Board of Water Supply of City of New York, 1941, available at Engineering Societies Library) reports the presence of a bedding foliation in the Manhattan formation which is largely obscured by later schistosity, and a micaceous layering in the Inwood marble which might possibly be bedding.

This lack of definite bedding planes in an area of intense deformation and metamorphism handicaps but does not prevent the delineation of the structural picture and increases the importance of the remaining structural elements.

Foliation

Foliation is prominent in all rocks in the Poundridge area. The Manhattan formation and Inwood marble exhibit a schistosity which is considered a coarsened flow cleavage as defined by Leith (1905; 1923). In a few places this schistosity in the Manhattan formation is crinkled by incipient fracture cleavage (Leith, 1905; 1923). The cleavage planes are so distorted that a determination of their orientation is difficult. The banding of the Fordham gneiss, too coarse to be called schistosity, is referred to as the gneiss foliation. The planar flow structure of the Poundridge granite is termed flow foliation. All these foliations, except the fracture cleavage, are conformable. With minor deflections, the strikes of the foliation of all the rocks in the mapped area form a series of concentric arcs centered just to the west of the Poundridge mass (Pl. 4). Thus the strike ranges through all angles from 0° to 180°. The dip, where not vertical, is northward. This pattern is illustrated statistically in Figure 4 where 300 poles of representative foliation planes have been plotted stereographically. The breached girdle pattern indicates a variation in strike through 360°; if the girdle were rotated into the periphery of the projection, it would be continuous. The scarcity of poles in the northern portion of the projection shows the lack of dip to the south. The two maxima in the southeastern and southwestern quadrants are significant only in that they

FIGURE 4.—STEREOGRAPHIC PROJECTION OF POLES OF FOLIATION
Maxima 6 per cent

indicate the trend of the most commonly exposed rock.

These foliation trends are completely foreign to normal Appalachian structures which are characterized by strikes to the northeast.

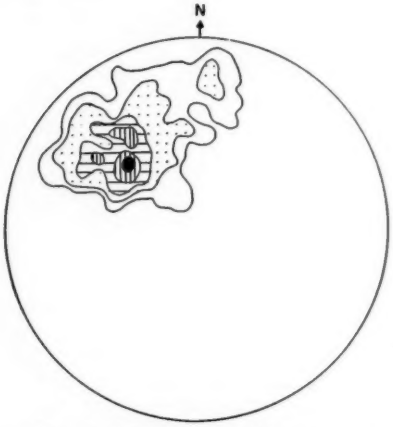

FIG. 5.—STEREOGRAPHIC PROJECTION OF LINEATION
Maximum 24 per cent

Lineation

Sander's (1930, p. 119) co-ordinate system is used: *b* is the fold axis; *a* is perpendicular to *b* in the movement plane; and *c* is perpendicular to *ab*. Fold axes will be discussed later.

The attitude of all lineations is shown statistically in Figure 5, which shows the strong preferred orientation plunging 45–50° NW. This lineation is believed to lie in *b*, the axis of latest folding, even though its position in relation to the noses of the folds in map view seems to indicate an *a* orientation. Perhaps this lineation was controlled by a thrusting movement from the northwest.

The most common lineation is alignment of elongated minerals (Pl. 3, fig. 2). In the Fordham gneiss small biotite and hornblende crystals are oriented and concentrated to produce delicate lines on the foliation planes. In the Manhattan formation this lineation is finer, the individual mineral being invisible. A strong orientation of hornblende prisms expresses the lineation in some amphibolite outcrops. In many places a light-colored mineral lineation in the Poundridge granite and Fordham gneiss consists of small quartz pencils, and commonly pods of hornblende or garnet constitute the lineation in the Fordham gneiss. A small-amplitude crinkling on the foliation surface is the most common lineation in the Manhattan formation.

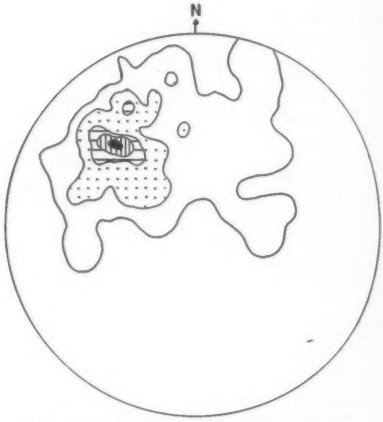

FIGURE 6.—STEREOGRAPHIC PROJECTION OF FOLD AXES
Maximum 16 per cent

Boudinage structure is found in the Fordham gneiss in several places. The boudins, usually less than a foot thick consist of amphibolite or feldspathic layers. The troughs which lie in the necks between the boudins constitute a lineation paralleling the other lineations. Boudinage is abundant near the outer contact of the Poundridge granite with the Fordham gneiss. This fact is important, since boudinage is usually a product of stretching perpendicular to the lineation. Thus, it indicates extension along the outer fringe of the Poundridge mass and tends to support the idea of axial-plane folding.

Prominent slickensides of the mullion-structure type are present on the exposed fault plane of the Siscowit granite fault.

Fold Axes

The orientation of fold axes is remarkably consistent for an area in which foliation is so variable. The statistical diagram (Fig. 6) shows a strongly preferred orientation, plunging about 45° NW., almost identical to that of the lineation. The fold axes are also considered to lie in

b, the axis of latest folding. There is again, however, the possibility that this lineation parallels the movement direction of the major thrusting from the northwest.

The orientation of these fold axes was measured directly from generally small-amplitude folds (a fraction of a foot to a few feet) on the foliation surface. A few larger folds with amplitudes up to 300 feet were noted in the Fordham gneiss.

Drag Folds

Small drag folds are common in the Fordham gneiss, and there are a few in the Manhattan formation. The study of these folds aided in elucidating the broad structural features and is a base for some of the interpretation.

The direction of shear shown by the drag folds on the northeastern portion of the Poundridge mass indicates an upward movement affecting the exterior foliation bands in relation to the interior bands. Thus, there is a strong suggestion of an anticlinal structure in the Fordham gneiss. The axis of this fold trends along the outcrop area of the Poundridge granite. If the intrusion of the granite had caused the drag folding, the shear senses would be opposite that observed. It appears likely that the granite was intruded into the core of a pre-existing anticlinal fold.

At the summit of Titicus Mountain in the northern belt of Fordham gneiss some drag folds have vertical axes. The shear indicates that the northwestern portion of this belt moved to the northeast as would result from differential slippage of foliation planes during the bending of the gneiss mass into the arcuate shape (Pl. 4).

Drag folding in the Manhattan formation half a mile south of the village of Pound Ridge indicates the position of a major synclinal axis lying along the center of the schist and Bedford augen gneiss belt, and plunging southwest. This agrees with the stratigraphic evidence that the Manhattan formation is the youngest in a synclinal fold, being flanked on both sides by older Inwood marble and Fordham gneiss.

Drag of the foliation at the contacts of many pegmatite veins indicates that intrusion was upward.

Faults

The area which was mapped in detail (Pl. 4) lies between two major faults, the Highland gneiss fault on the northwest and the Siscowit granite fault on the southeast. Deformation of the intervening area is interpreted as a result of large-scale squeezing of pre-existing structures as the Highland gneiss block moved upward and southeast toward the Siscowit granite. The granite acted in part as a buttress, but also moved in the direction of the last tectonic transport.

The reverse fault separating the Precambrian Highland gneiss from the Inwood marble (Pl. 1), although not within the area mapped in detail, has been well described (Balk, 1936, p. 737; it is of primary importance to the structural interpretation. The fault has been traced from near Danbury, Connecticut, westward to Brewster, New York, thence southwestward through Croton Falls and Lincolndale. Shears indicate a thrusting of the Highland gneiss to the southeast over the Inwood marble. The steep dip of the fault plane indicates a large vertical component.

Structural evidences of faulting are not always present along the fault trace. Strong lineations and closely spaced foliation are locally abundant near the fault, but in many places are absent. The best evidence of faulting is stratigraphic since the Precambrian Highland gneiss constitutes the hanging wall above the younger Inwood marble along the major portion of the fault.

A major fault separating the Siscowit granite on the east from the Fordham gneiss-Inwood marble-Manhattan formation group to the west was traced from a point near Ridgefield, Connecticut, southeastward as far as Highridge, Connecticut.

As shown clearly on Plate 1 the fault causes the truncation of successive belts of Inwood marble, Fordham gneiss, Inwood marble, and Manhattan formation against the Siscowit granite mass. The contacts between these formations meet the fault trace at angles of about 20°.

Structural evidence of the fault, although not abundant, is striking. Slickensiding and stretching have produced prominent mullion structure in the Siscowit granite near the fault

trace just east of Trinity Lake. The rods, up to 4 inches in diameter, plunge down the foliation plane at the maximum angle. Also the granite foliation is so closely spaced that the rock is schistose. Both features are lost and the rock becomes typically massive 100 feet away perpendicular to the strike.

This coarse lineation was also observed in a Fordham gneiss exposure near the fault. A light slickensiding on the foliation planes indicates faulting in the adjacent schist and marble.

A northwest-southeast direction of fault movement is strongly implied by the lineations near the fault, but the sense of fault displacement cannot be positively established because the relative ages of the fault blocks are not known. Since the fault planes dip northwest and the movement of the Highland gneiss block was to the southeast over the middle block, it seems somewhat more likely that the middle block also moved up to the southeast over the Siscowit granite, thus making the fault a thrust. Further work is necessary to definitely establish the movement relationships.

The probable existence of a fault separating the northern from the southern portion of the Poundridge mass is indicated by the offset Poundridge granite-Fordham gneiss contact across the east-trending valley of the Cross River (Pl. 1). The width of outcrop of the Poundridge granite is much less to the north than to the south of this line, indicating that the northern block is probably downthrown. However, there is no structural evidence of the fault; it is not known whether the fault is normal or reverse.

Fluhr (in a report of Board of Water Supply of City of New York, 1941, available at Engineering Societies Library) reported extensive evidence of shearing along the Fordham gneiss-Inwood marble and Inwood marble-Manhattan formation contacts exposed in the Croton aqueduct tunnel. Major displacement is not indicated, and evidence of this faulting is not commonly seen on the surface.

Interpretation

The area in northern Westchester and Putnam counties has undergone two distinct stages of deformation. Whether these stages are part of a single orogenic period or are widely separated in time is not known. They are characterized by deformational movements in two different directions.

From New York City to just southeast of the Poundridge area, the New York City group is isoclinally folded with the axial planes striking north-northeast and dipping to the northwest. From this point northeastward to the Highland gneiss block, the axial planes are themselves folded, causing the formational belts and foliation planes to swing in great arcs around the Poundridge mass until they abut the Siscowit granite fault (Pl. 1). To the northwest the axial planes are more tightly folded where they have been squeezed against the Highland gneiss block.

The northeasterly trend of the original isoclinal folding parallels the Appalachian fold axes and probably resulted from northwesterly tectonic movements. Later folding of the axial planes in the northern area could have resulted only from movement south or southeastward (Pl. 1). It is doubtful that the original folding is the same age as Appalachian folding, since pegmatites in the Bedford area, which were emplaced during or just following the last folding, have been dated as late Ordovician (Muench, 1931). If a large time interval separated these two deformational movements, possibly the earlier one is Precambrian, and thus the New York City group is also Precambrian. Since no data on the time interval are available, no conclusion as to the age of the New York City group is warranted, other than that it is no younger than late Ordovician.

The foliation in the Poundridge granite, although harmonious with that of the enclosing Fordham gneiss, is considered a primary flow structure. The amphibolite and less common gneiss inclusions are invariably aligned with their long dimensions paralleling the foliation strike even though in a few places they have been rotated so that their internal foliation meets that of the granite at a large angle. Large books of biotite parallel the strike of foliation at many places within the granite.

A large xenolith of partially assimilated gneiss approximately 100 by 500 feet occurs in the granite along the Fire Tower road on the eastern side of the Poundridge mass. The gneiss foliation trends east-west and makes an angle of about 70° with that of the granite and the

Fordham gneiss, attesting to considerable rotation. A discrepancy in the foliation strike in the northeastern part of the Poundridge granite (Fig. 7) probably indicates another rotated

result of an east-west movement, bending the original axial planes into broad folds.

Axial-plane folding may not be described in the same terms as normal folding since it does

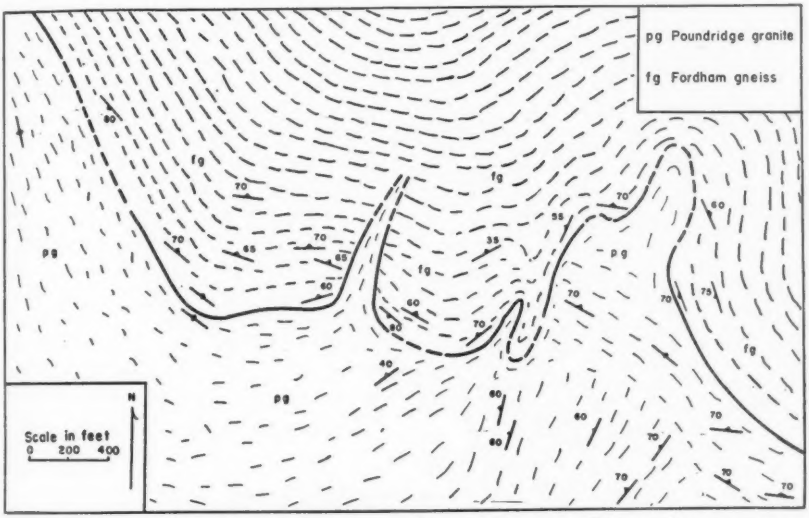

FIGURE 7.—TABLE PLANE MAP OF POUNDRIDGE GRANITE-FORDHAM GNEISS CONTACT AT THE NORTHEASTERN MARGIN OF FOUNDRIDGE MASS

Though mostly concordant, the contact in places is transgressive. The discrepancy in the foliation strike in the Poundridge granite is seen in the southeastern portion of the map.

gneiss block whose borders with the granite have become blurred.

The information obtained from drag folds in the adjacent gneiss and the overall structural interpretation lead to the conclusion that the Poundridge granite probably was intruded parallel to the folded axial plane of an anticline of Fordham gneiss. It is probable that the granite moved upward for a short distance only from its enclosing envelope of migmatite with which it is still closely associated. Whether the intruded material was magmatic or rheomorphic remains unknown. That the granite was not intruded before the final deformation of the Fordham gneiss seems definite since evidence of post-consolidation disturbance of the granite is lacking.

Figure 8 shows diagramatically the application of the concept of axial-plane folding to three formations which were originally folded so that their axial planes were vertical, striking east-west. The area has been refolded as the

not result in anticlines and synclines in the usual sense. Also, as the movements causing axial-plane folding would generally act in a roughly horizontal direction, the axes of the axial-plane folds would tend to be vertical and the terms trough and crest would lose their meaning. However, new terms need not be applied for the concept of axial-plane folding is relatively simple and may be adequately described by use of maps and sections.

Of primary importance in the interpretation of the structure resulting from axial-plane folding (Fig. 9) is the concept of the conformable stratigraphic relationship of the Fordham gneiss-Inwood marble-Manhattan formation group. If that concept is accepted, the map pattern of these formations, and additional structural evidence, allows no other interpretation. Reasons for believing that the New York City group is a conformable one need not be repeated, but it is pertinent to point out that no structural evidence of a major fault separat-

ing the Fordham and Inwood, as postulated by Balk (1936) and others, was found. Except where all three formations are faulted against the Siscowit granite, the Fordham is never

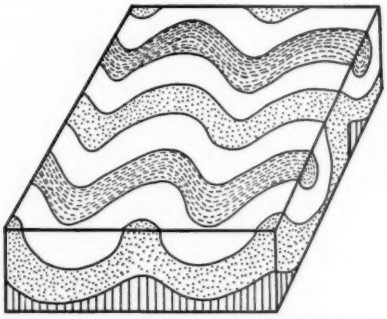

FIGURE 8.—DIAGRAMATIC REPRESENTATION OF AXIAL-PLANE FOLDING PRINCIPLE

Beds were first isoclinally folded with axes trending east-west. They were then refolded, due to east-west compression, resulting in axial-plane folds.

found in contact with any formation except the Inwood.

The existence of axial-plane folding is brought out on Plate 1 which shows the foliation and formation belts curving in large arcs around the Poundridge mass. The arcuate pattern of the anticlinal and synclinal axes is also indicated.

Additional evidence of axial-plane folding may be summarized as follows:

(1) That the belts of Fordham gneiss are anticlinal and not thrust blocks is supported by a preserved isoclinal fold a quarter of a mile east of Lake Kitchawan (Pl. 3, fig. 1). There the Fordham gneiss belt is quite narrow. In addition, the shear sense of drag folds in the Fordham gneiss in the Poundridge mass suggests that an anticlinal axis follows the crescent-shaped exposure of the Poundridge granite within the gneiss.

(2) Stretching on the outer edge of the Fordham gneiss belts as a result of bending during axial-plane folding is indicated by boudinage. This structure is found along the outer edge of the Poundridge mass particularly in the south-facing escarpment. There the lineation produced by the necks between the boudins plunges northwest. Thus, the extension which produced the structure acted in a direction paralleling the outer contact of the gneiss.

(3) The orientation of the fold axes of the axial-plane folding may be read from the numerous measurements of fold axes and lineations made throughout the area (Figs. 5, 6). The northwest plunge of these elements indicates that the axial-plane folds are tilted to the southeast.

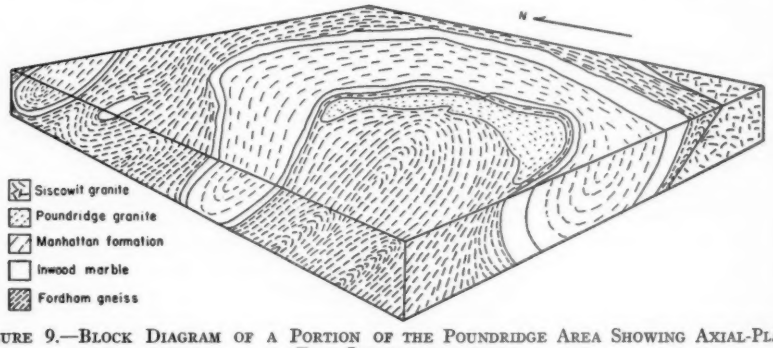

FIGURE 9.—BLOCK DIAGRAM OF A PORTION OF THE POUNDRIDGE AREA SHOWING AXIAL-PLANE FOLD INTERPRETATION

The second deformational stage, which produced axial-plane folding in the pre-existing northeast-trending isoclinal folds, appears to be the result of large-scale thrusting from the north and northwest. This movement was caused by the shifting of the Highland gneiss block south and southeastward toward the Siscowit granite mass, which may have acted as a buttress. Thus the intervening area was profoundly squeezed.

The Highland gneiss fault separating the

Highland mass from the New York City group on the south extends northeastward from Lincolndale to Brewster and then trends eastward into Connecticut. In reconstructing the movement sequence from the geologic map (Pl. 1) it appears that shifting of the Highland gneiss block was first southward causing the northern portion of the original northeast-trending isoclinal folds to be bent and displaced to the south. Later southeasterward movements resulted in the arcuate folding of these folds.

References Cited

Adams, F. D., and Barlow, A. E., 1910, Geology of the Haliburton and Bancroft areas, Province of Ontario: Canadian Dept. of Mines Mem. 6, 419 p.

Agar, W. M., 1933, Notes on the Danbury granodiorite gneiss of Connecticut: Am. Jour. Sci., v. 25, p. 1–19

— 1934, Granites and related intrusions of western Connecticut: Am. Jour. Sci., v. 27, p. 354–373

Ambrose, J. E., 1936, Progressive kinetic-metamorphism of the Missi series near Flinflon, Manitoba: Am. Jour. Sci., 4th ser., v. 32, p. 257–286

Balk, R., 1932, Structure and correlation of metamorphic rocks in southeastern New York: Nat. Acad. Sci. Proc., v. 18, p. 616–630

— 1936, Structural and petrologic studies in Dutchess County, New York, Pt. I: Geol. Soc. America Bull., v. 47, p. 685–774

Barbour, George P., 1930, Origin of the Bedford augen-gneiss: Am. Jour. Sci., 5th ser., v. 19, p. 351–358

Barth, T. F. W., 1936, Structural and petrologic studies in Dutchess County, New York, Pt. II: Geol. Soc. America Bull., v. 47, p. 775–850

— 1948, Oxygen in rocks: a basis for petrographic calculations: Jour. Geology, v. 56, p. 50–60

Bell, Gordon K., 1936, Poundridge granite (Abstract): Geol. Soc. America Proc., p. 65

Bowen, N. L., 1928, The evolution of igneous rocks: Princeton University Press, 332 p.

— 1940, Progressive metamorphism of siliceous limestone and dolomite: Jour. Geology, v. 48, p. 225–274

Berkey, C. P., 1907, Structural and stratigraphic features of the basal gneisses of the Highlands: N. Y. State Mus. Bull. 107, p. 360–378

— 1911, Geology of the Catskill aqueduct: N. Y. State Mus. Bull. 166, p. 198–199

Berkey, C. P., and Rice, M., 1919, Geology of the West Point quadrangle, New York: N. Y. State Mus. Bulls. 225, 226, 306 p.

Chayes, Felix, 1952, Note on the staining of potash feldspar with sodium cobaltinitrite: Am. Mineralogist, v. 37, p. 337

Clarke, F. W., 1924, Data on geochemistry: U. S. Geol. Survey Bull. 770, 840 p.

Clarke, J. M., 1908, Fifth report of director: N. Y. State Mus., v. 1, p. 11–12

Emmons, R. C., *et al.*, 1953, Selected petrogenic relationships of plagioclase: Geol. Soc. America Mem. 52, 142 p.

Engel, A. E. J., and Engel, C. G., 1951, Origin and evolution of hornblende-andesine amphibolites and kindred facies: Geol. Soc. America Bull., v. 62, p. 14–35

— 1953, Grenville series in the northwestern Adirondack Mountains, N. Y.: Geol. Soc. America Bull., v. 64, p. 1049–1098

Fairbairn, H. W., *et al.*, 1951, A cooperative investigation of precision and accuracy in chemical, spectrochemical, and modal analysis of silicate rocks: U. S. Geol. Survey Bull. 980, 54 p.

Fairbairn, H. W., and Podolsky, T., 1951, Notes on precision and accuracy of optic angle determination with the universal stage: Am. Mineralogist, v. 36, p. 823–832

Fettke, C. R., 1914, The Manhattan schist of southeastern N. Y. state and its associated igneous rocks: N. Y. Acad. Sci. Annals, v. 23, p. 193–260

Fluhr, T. W., 1950, The Delaware aqueduct; some geological data: N. Y. Acad. Sci. Trans., ser. 2, v. 12, p. 182–186

Folinsbee, R. E., 1941, The chemical composition of garnet associated with cordierite: Am. Mineralogist, v. 26, p. 50–53

Gorai, M., 1950, Proposal of twin method for the study of the granite problem: Geol. Soc. Japan Jour., v. 56, p. 149–156

Grout, F. F., 1925, Relation of texture and composition of clays: Geol. Soc. America Bull., v. 36, p. 393–416

Haff, J. L., 1941, Determination of extinction angles in augite and hornblende according to the method of Conrad Burri: Am. Jour. Sci., v. 239, p. 489–492

Hall, A. Jean, 1941, The relation between chemical composition and refractive index in the biotites: Am. Mineralogist, v. 26, p. 34–41

Heald, M. T., 1950, Structure and petrology of the Lovewell Mt. quadrangle, New Hampshire: Geol. Soc. America Bull., v. 61, p. 43–89

Hess, H. H., 1941, Pyroxenes of common mafic magmas. Part I: Am. Mineralogist, v. 26, p. 515–535

— 1949, Chemical composition and optical properties of common clinopyroxenes: Am. Mineralogist, v. 34, p. 621–666

Kennedy, George C., 1947, Charts for correlation of optical properties with chemical composition of some common rock-forming minerals: Am. Mineralogist, v. 32, p. 561–573

Leith, C. K., 1905, Rock cleavage: U. S. Geol. Survey Bull. 239, 216 p.

— 1923, Structural geology: N. Y., Henry Holt, 390 p.

Lindgren, Waldemar, 1918, Volume changes in metamorphism: Jour. of Geology, v. 26, p. 542–554

Luquer, L., and Ries, H., 1896, The augen-gneiss area, pegmatite veins and diorite dikes of Bedford N. Y.: Am. Geologist, v. 18, p. 239–261

Merril, F. J. H., 1902, U. S. Geol. Survey, New York City Folio 83

Muench, O. B., 1931, The analysis of cyrtolite for lead and uranium: Am. Jour. Sci., 5th ser., v. 21, p. 350–357

Newhouse, W. H., Hagner, A. T., and DeVore,

G. W., 1949, Structural control in the formation of gneisses and metamorphic rocks: Science, v. 109, p. 168–169

Percival, J. G., 1842, Report on the geology of Connecticut: New Haven, State of Conn., 495 p.

Pettijohn, F. J., 1949, Sedimentary rocks: New York, Harper, 526 p.

Prucha, J. J., 1955, Stratigraphic relationships of the Fordham gneiss in southeastern New York: Geol. Soc. America Bull., v. 66, p. 1606

Rosenzweig, A., and Watson, F. H., 1954, Some hornblendes from southeastern Pennsylvania and Delaware: Am. Mineralogist, v. 39, p. 581–599

Sander, Bruno, 1930, Gefügekunde der Gesteine: Wien, Julius Springer, 352 p.

Sanders, L. D., 1954, The status of sillimanite as an index of metamorphic grade in the Kenya basement system: Geol. Mag., v. XCI, p. 144–151

Scotford, D. M., 1951, Structure of the Sugarloaf Mountain area, Maryland, as a key to Piedmont stratigraphy: Geol. Soc. America Bull., v. 62, p. 45–76

Sundius, N., 1946, The classification of the hornblendes and solid solution reactions in the amphibole group: Sver. Geol. Undersoknung, Arsbok 40, ser. C, no. 480, 36 p.

Tröger, W. Ehrenreich, 1952, Tabellen zur optischen bestimmung der gesteinsbildenden minerale: Stuttgart, E. Schweizerbartsche Verlagsbuchhandlung, 147 p.

Tsuboi, Seitaro, 1923, A dispersion method of determining plagioclases in cleavage-flakes: Mineralog. Mag., v. 20, p. 108–122

—— 1934, A straight-line diagram for determining plagioclase by the dispersion method: Jap. Jour. Geology and Geography, v. 11, p. 325–326

Turner, Francis J., 1947, Determination of plagioclase with the four axis universal stage: Am. Mineralogist, v. 32, p. 389–410

—— 1948, Mineralogical and structural evolution of the metamorphic rocks: Geol. Soc. America Mem. 30, 342 p.

—— 1951, Observation of twinning of plagioclase in metamorphic rocks: Am. Mineralogist, v. 36, p. 581–589

Turner, F. J., and Verhoogen, J., 1951, Igneous and metamorphic petrology: N. Y., McGraw-Hill, 602 p.

Williams, H., Turner, F. J., Gilbert, C. M., 1954, Petrography: San Francisco, W. H. Freeman and Co., 406 p.

Winchell, A. N., 1951, Elements of optical mineralogy, Pt. 2, 4th ed.: N. Y., John Wiley and Co., 551 p.

Yoder, H. S., 1952, The MgO-Al_2O_3-SiO_2-H_2O system and the related metamorphic facies: Am. Jour. Sci., Bowen Volume, p. 569–627

Miami University, Oxford, Ohio

Manuscript Received by the Secretary of the Society March 13, 1955

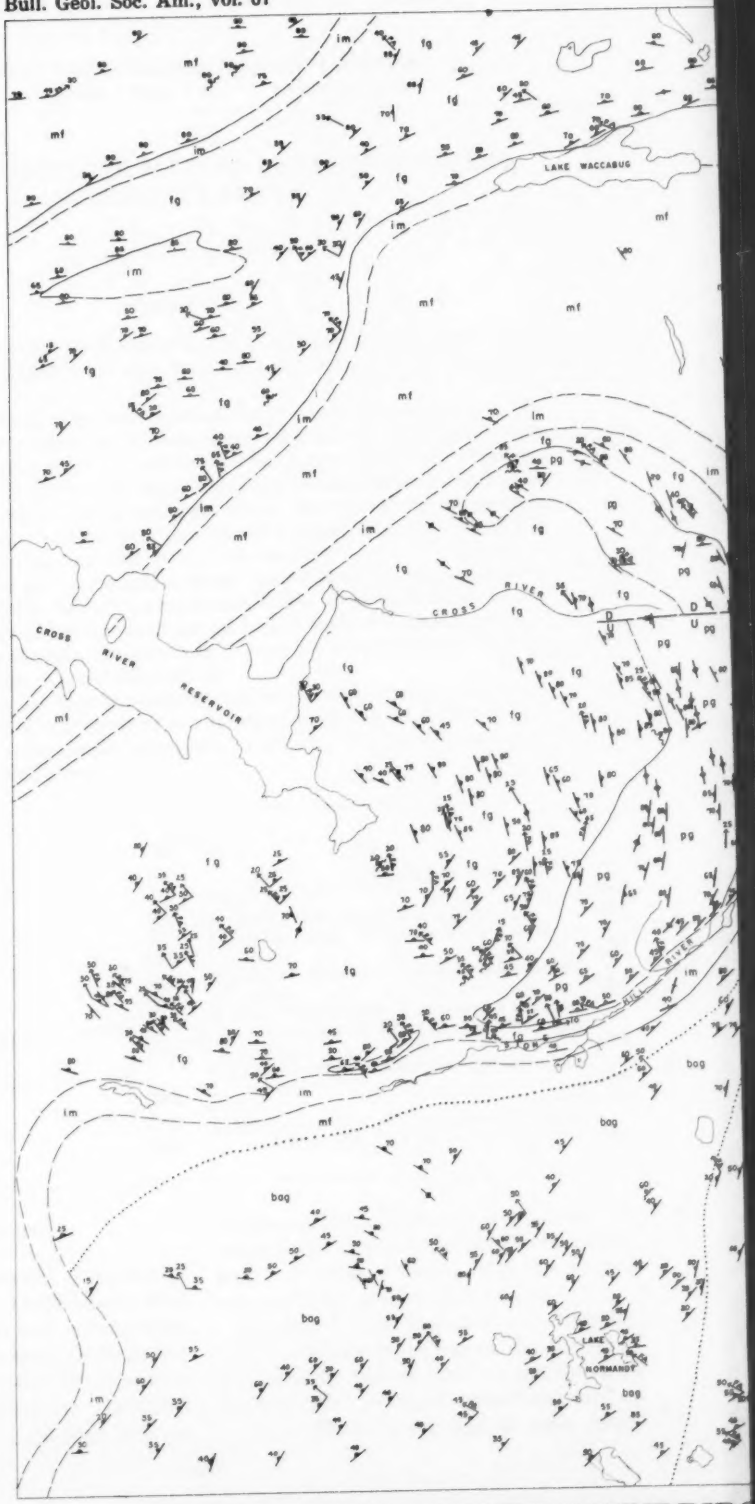

STRUCTURE MAP OF THE POUNDRIDG

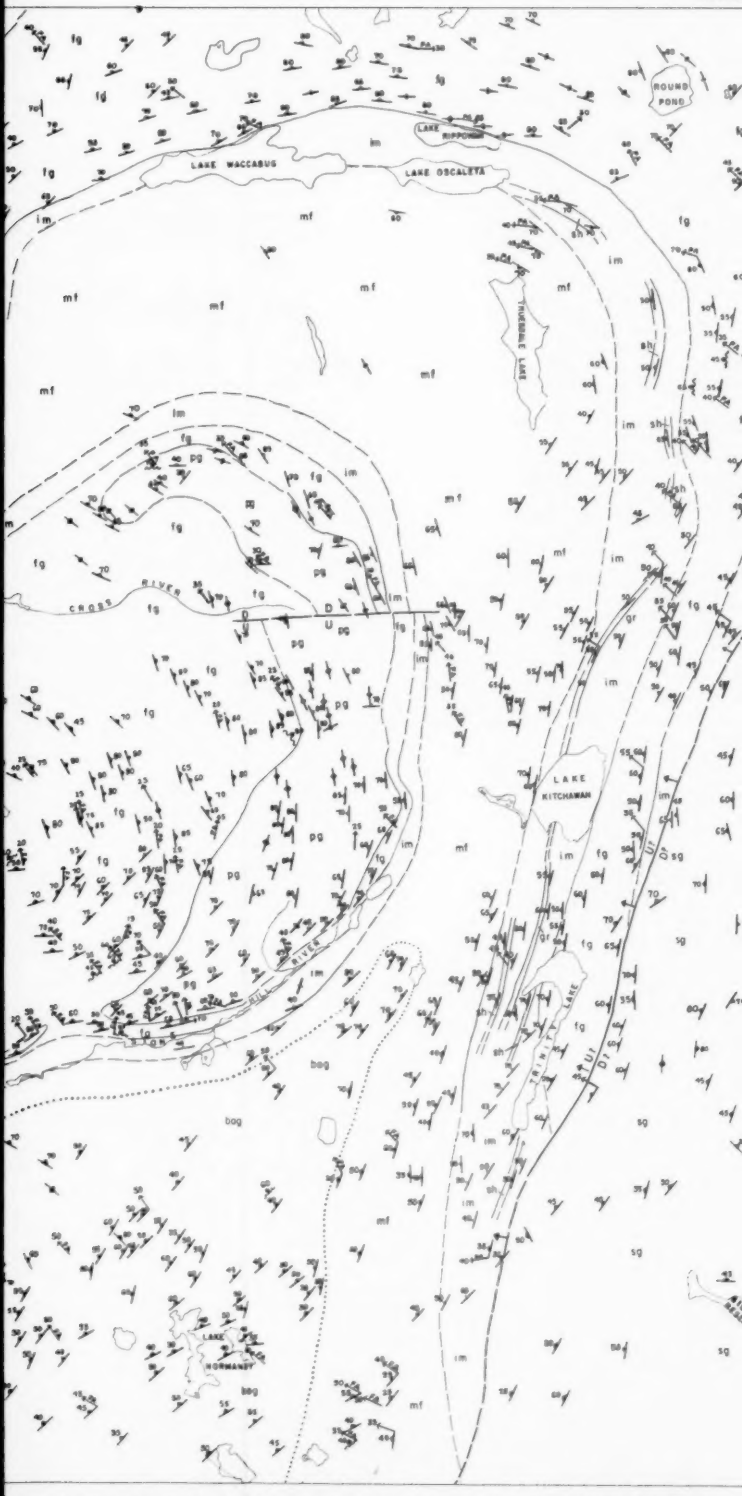

P OF THE POUNDRIDGE AREA, NEW YORK

Scotford, Pl. 4

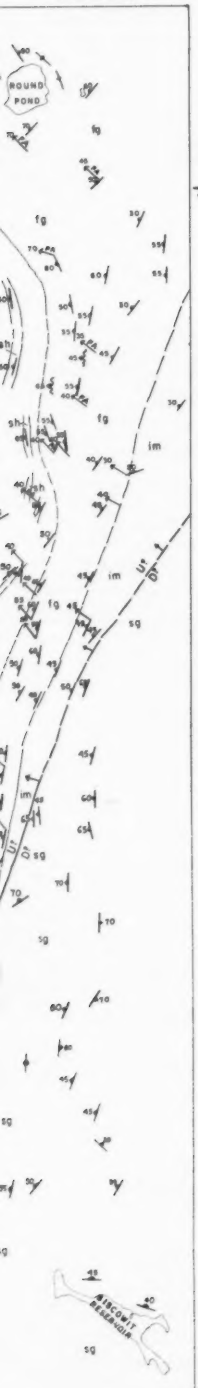

LEGEND

STRUCTURAL SYMBOLS

- Foliation in the Inwood marble
- Flow foliation
- Foliation in the schists and gneisses
- Foliation and lineation
- Foliation and fold axis
- Strike of foliation distorted
- Fault (U / D)

CONTACTS

- Accurate
- Approximate
- Gradational

FORMATION SYMBOLS

- sg Siscowit granite
- pg Poundridge granite
- bag Bedford augen gneiss
- mf Manhattan formation
- Im Inwood marble
- gr granitized unit in Inwood marble
- sh schist or gneiss unit in Inwood marble
- fg Fordham gneiss

Scale in miles

0 1

N

YORK

BULLETIN OF THE GEOLOGICAL SOCIETY OF AMERICA
VOL. 67, PP. 1199-1206, 5 FIGS., 1 PL. SEPTEMBER 1956

TILL-PEBBLE ISOPLETH MAPS OF PARTS OF MONTANA AND NORTH DAKOTA

BY ARTHUR DAVID HOWARD

ABSTRACT

An isopleth map shows the distribution of a variable by lines of equal magnitude called isopleths. Till-pebble isopleth maps show the areal distribution of pebbles of different rock types in till.

Four till-pebble isopleth maps were prepared during a reconnaissance study of the Pleistocene geology of northeastern Montana and northwestern North Dakota. Three of the maps are concerned with erratic pebbles; the fourth, with locally derived pebbles.

The isopleth maps of the erratic pebbles reveal an area in northwestern North Dakota where the erratic content of the till differs significantly from that of the till elsewhere in the region. Lithologic relations are described which suggest that the drift of this small area may differ in age from that to the north and south.

A till-pebble isopleth map of distinctive, locally derived fluvial pebbles reveals three large areas of till in which these pebbles are abundant. Two of the areas, southwest and west of extensive exposures of the source gravels, suggest that the ice moved generally southwestward across the area. The third area is unrelated to known gravel exposures and may indicate a body of gravel below the till.

The study indicates that till-pebble isopleth maps may sometimes prove useful in suggesting the possibility of multiple drifts and in helping to delimit the drifts once substantiated. They may also provide information on direction of ice movement and on the identity of concealed bedrock.

CONTENTS

TEXT

	Page
Introduction	1199
Acknowledgments	1200
Preliminary procedures	1200
Preparation of maps	1200
Interpretation of isopleth maps of erratic pebbles	1202
Interpretation of isopleth map of local rock types	1204
Conclusions	1206
References cited	1206

ILLUSTRATIONS

Figure	Page
1. Isopleth map of granitic erratics	1201
2. Isopleth map of metamorphic foliate erratics	1201
3. Isopleth map of limestone-dolomite erratics	1202
4. The Williston area in relation to the limestone-dolomite belt of the Lake Winnipeg region	1204
5. Isopleth map of Flaxville-type silica-rich rocks	1205
Plate	**Facing page**
1. Histogram map of erratic-pebble content of surface till	1206

INTRODUCTION

A study of the pebble content of the surface drift of an area of about 12,000 square miles in northeastern Montana and northwestern North Dakota was undertaken in the hope that it might contribute information on the number and distribution of the drift sheets. The results are shown on till-pebble isopleth maps. It is not the present intent to discuss the problem of the multiple drifts of the Montana-North Dakota area, but rather to discuss till-pebble isopleth maps and their possible applications.

An isopleth map (Krumbein and Pettijohn, 1938, p. 201) shows the regional distribution of a variable by lines of equal magnitude called isopleths (Gr. *isos*-equal, *plēthos*-quantity or number). Three of the isopleth maps herein

described show the regional variation in the quantity of certain erratic pebbles in the surface till of northeastern Montana and northwestern North Dakota. The fourth isopleth map shows the regional distribution in the till of the brown, water-worn quartzites, cherts, silicified igneous rocks, and other silica-rich rocks that characterize the Flaxville gravel (Miocene or Pliocene) and similar nonglacial terrace gravels. The Flaxville and similar gravels are herein collectively referred to as Flaxville-type gravels.

The wide spacing of the sample sites over most of the region was determined by the large size of the area, the reconnaissance nature of the study, and the distribution of suitable exposures. The close spacing of the sample sites in northwestern North Dakota was due to early recognition of an area of till of anomalous lithology and a desire to define its limits as accurately as possible. Some of the sample sites in this area were excavated.

Acknowledgments

The writer is indebted to Eliot Blackwelder, Gerald M. Richmond, and Paul MacClintock for review of the manuscript.

Preliminary Procedures

A total of 77 pebble counts of till were made; 65 of these were from exposures that revealed only one deposit of till below the surface. These 65 counts were used in preparing the isopleth maps. The remainder of the samples were from an underlying layer of till.

Vertical or near-vertical exposures were stripped of surface wash, and areas estimated to contain between 100 and 200 pebbles were outlined. All pebbles larger than a quarter of an inch were collected. Small chips were broken from large cobbles and boulders. Collection from a surface area rather than from a volume of the till was necessary because much of the material was firmly cemented by calcium carbonate.

The numerous lithologic types were arranged in 10 groups: granitic rocks, other plutonic rocks, acidic volcanic rocks (rhyolite and trachyte), basic volcanic rocks (andesite and basalt), quartz and quartz aggregates such as vein quartz, metamorphic foliate rocks, quartzites, limestones and dolomites, cherts and other microcrystalline or cryptocrystalline siliceous rocks, and miscellaneous types consisting largely of mudstones, siltstones, and sandstones from local Tertiary and Mesozoic formations.

Four of the groups consist exclusively of erratic types: the granitic rocks, other plutonic rocks, metamorphic foliate rocks, and the limestones and dolomites. The acidic and basic volcanic rocks and the quartz, quartzite, and chert pebbles were derived from the Flaxville and similar nonglacial gravels and are not considered erratics. Most of the nonglacial pebbles are well rounded and coated with a brown patina. Some of the Flaxville-type pebbles may have been glacially introduced from outside the area, although exposures of Flaxville-type gravels have not been reported farther north.

For each sample, the number of pebbles in each of the four groups of erratics was expressed as a percentage of the total number of erratics. The percentage of plutonic rocks other than granite was small, rarely exceeding two per cent; hence this group is not separately plotted in the diagrams.

The relative percentages of the three principal erratic groups, the granitic rocks, metamorphic foliate rocks, and limestone-dolomite, were first expressed in a histogram map (Pl. 1). The isopleth maps (Figs. 1, 2, 3), however, offer a more easily visualized picture of the regional variation of the erratic pebbles. In contrast to the histogram map which is a record of facts, the isopleth maps involve inference in the interpolation of isopleths between widely separated control points. In spite of the degree of freedom possible in sketching the isopleths, the gross characteristics of the maps remain unchanged.

Preparation of Maps

The isopleth map for each type of erratic pebble was prepared by plotting at each sample locality the relative abundance of the particular erratic, expressed as a percentage, and then drawing isopleths using the plotted percentages as control points. In the isopleth maps presented, isopleths record changes of 10 per cent

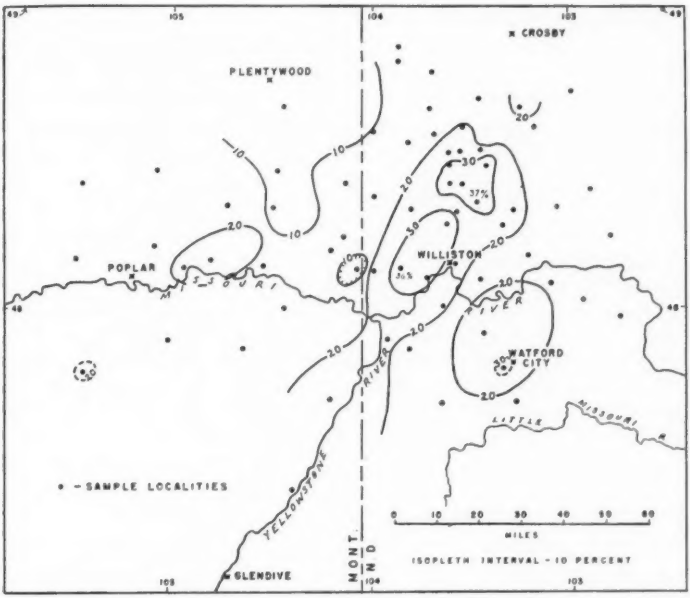

FIGURE 1.—ISOPLETH MAP OF GRANITIC ERRATICS
Interrupted isopleths enclose areas just under values indicated.

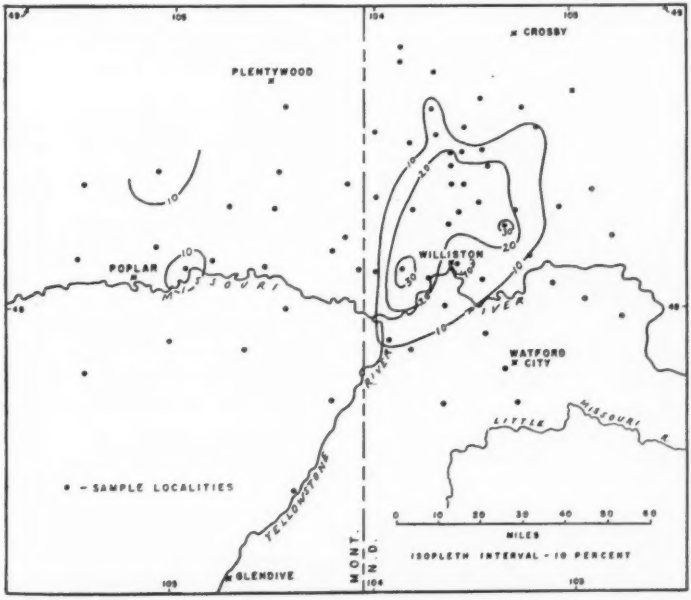

FIGURE 2.—ISOPLETH MAP OF METAMORPHIC FOLIATE ERRATICS

in the quantity of the pebbles represented (Figs. 1, 2, 3, 5).

Five of the pebble analyses used in the preparation of the isopleth maps contained fewer than 50 erratic pebbles (samples 15, 22, 23, 29, and 30, Pl. 1). Three other samples contained between 70 and 80 pebbles (samples 2, 17, and 19). All others contained 80 or more erratics, with the great majority having between 100 and 200, and a few exceeding 200.

Preparation of the isopleth map of the Flaxville-type pebbles (Fig. 5) differed only in that the percentage of these pebbles was computed against the total number of pebbles in each sample rather than against the number of erratic pebbles.

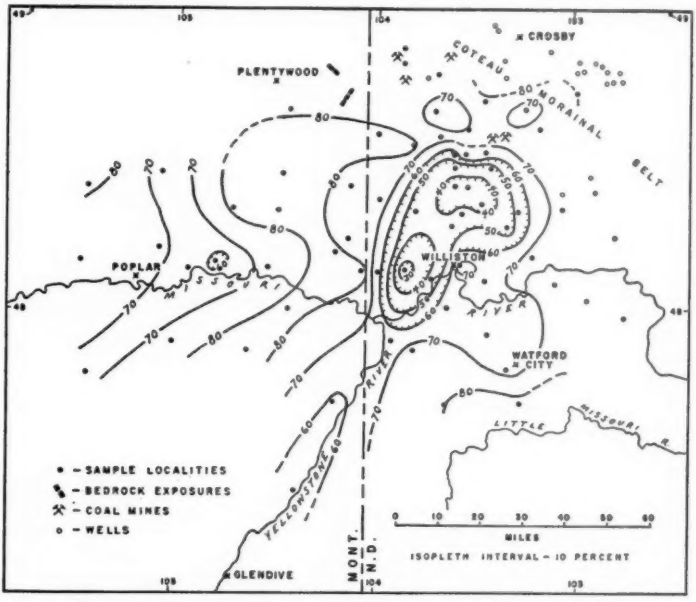

FIGURE 3.—ISOPLETH MAP OF LIMESTONE AND DOLOMITE ERRATICS

INTERPRETATION OF ISOPLETH MAPS OF ERRATIC PEBBLES

Figure 1 shows the regional variation in the content of granitic erratics. Over the greater part of the area granitic rocks constitute less than 20 per cent of the erratic pebbles of the surface till. West and north of Williston, however, the granitic-pebble content exceeds 37 per cent. At only one locality outside the Williston area did an analysis reveal close to 30 per cent of granitic pebbles. This sample, near Watford City, contained only 44 erratic pebbles after elimination of local rock types, hence its analysis is less significant than those based on larger numbers of pebbles.

Figure 2 shows the regional variation in the metamorphic foliate fraction of the erratic pebbles. Over most of the area the metamorphic rocks constitute less than 10 per cent of the glacial erratics. In the area near Williston, however, the metamorphic rocks total between 20 and 30 per cent, and exceed 30 per cent in two places. The transition to the surrounding areas of low metamorphic content is fairly abrupt.

Figure 3 shows the regional variation of the limestone-dolomite erratics. This map was first discussed by the writer in 1950. The surface portrayed by the isopleths is nearly everywhere a gently undulating plain over which the limestone-dolomite pebble content varies from about 55 to 88 per cent. A deep lithologic trough near Williston, however, contains less than 29 per cent of limestone-dolomite. The

variation in the limestone-dolomite content is not a function of duration of exposure to weathering. The drift throughout the area shows little or no leaching, and unaltered limestone and dolomite pebbles are present throughout the vertical extent of all exposures.

The margins of the lithologic trough are rather abrupt. It is unlikely that lithologic boundaries determined by the procedures outlined would appear precipitous on isopleth maps. A much closer spacing of sample localities would be needed to bring out the true declivity of lithologic slopes.

At least two drifts have long been recognized in northeastern Montana and northwestern North Dakota (Calhoun, 1906; Leonard, 1916; and Alden, 1932). Investigations by the writer and some of his colleagues on the U. S. Geological Survey seem to confirm this conclusion. Alden mapped a widespread drift of intermediate age, primarily on the basis of tenuous topographic evidence. Evidence revealed in the present investigation also indicates an intermediate drift, but of very restricted exposure north of Williston, North Dakota. Inasmuch as the present article is primarily concerned with till-isopleth maps as such, rather than with the Pleistocene stratigraphy of the region, this evidence is not discussed in detail.[1] It includes (1) the contrast in physical appearance of the till of the Williston area and the till of the rest of the region, (2) the lobelike pattern of the restricted drift, (3) the presence of a probable soil between it and an underlying till, (4) the presence of significant interdrift erosion intervals, and (5) the contrasts in degree of integration of the drainage of the drift sheets.

The pattern in the isopleth maps was primarily responsible for stimulating investigation of the possibility of a separate drift in the Williston area. The pattern seemed to offer difficulties in interpretation on the assumption that only two drifts were present. Although the difficulties were not insurmountable, they encouraged search for alternative explanations of the lithologic pattern. The drift of distinctive lithology in the Williston region will be referred to here as the anomalous drift.

If the anomalous drift is not a separate drift, it is presumably a facies of either the younger or older drifts. If it is a facies of the younger drift, then its localization and abrupt northern boundary could be due to contamination from a buried crystalline mass immediately to the north. This would account for the relative increase in the crystalline fraction of the drift and also the relative decrease in the limestone-dolomite fraction. However, numerous wells, bedrock exposures, and lignite mines reveal only the clays, silts, sands, and coals of the Fort Union formation north of the area of anomalous drift (Pl. 1). Nor does it seem likely that the isolation and abrupt lithologic boundaries of this small area of drift could be original characteristics of the younger drift.[2] The isopleth maps are based only on erratic rocks transported hundreds of miles; it seems unlikely that a mass of lithologically distinctive debris could be transported in pipeline fashion such great distances and be deposited intact in the midst of widespread contemporaneous drift of different lithology. This same difficulty applies to the assumption that there is only a single drift in the area.

If the anomalous drift is a facies of the older drift, the abrupt lithologic boundary on the north could be attributed to overlapping by the younger drift. However, in the absence of a contaminating body of crystalline rock, the restricted occurrence and the lobate pattern of the anomalous drift remain problems. Even if the anomalous drift is widespread under the cover of younger drift, the abrupt change in lithology in the direction of ice movement remains unexplained.

That the anomalous drift is a superglacial facies of the underlying drift seems unlikely because of its restriction to one relatively small area and because its lithology is no different in the silty facies than in the typical boulder-clay facies. These arguments also preclude the possibility that the change in lithology was induced by local periglacial reworking of the older drift.

If three different drifts are present, their differences in lithology may be related to

[1] The evidence is discussed in detail in a forthcoming professional paper of the U. S. Geological Survey.

[2] Anderson (1955) attributes abrupt lithologic variations in the Marseilles moraine of northeastern Illinois to contamination from adjacent source rocks, an explanation which does not apply to the present area of study.

differences in the paths taken by the several ice sheets across the belt of Paleozoic limestones and dolomites which flanks the Canadian center of ice dispersal during a single glaciation. Presumably migration would be slow, and the gradual changes in direction of ice movement

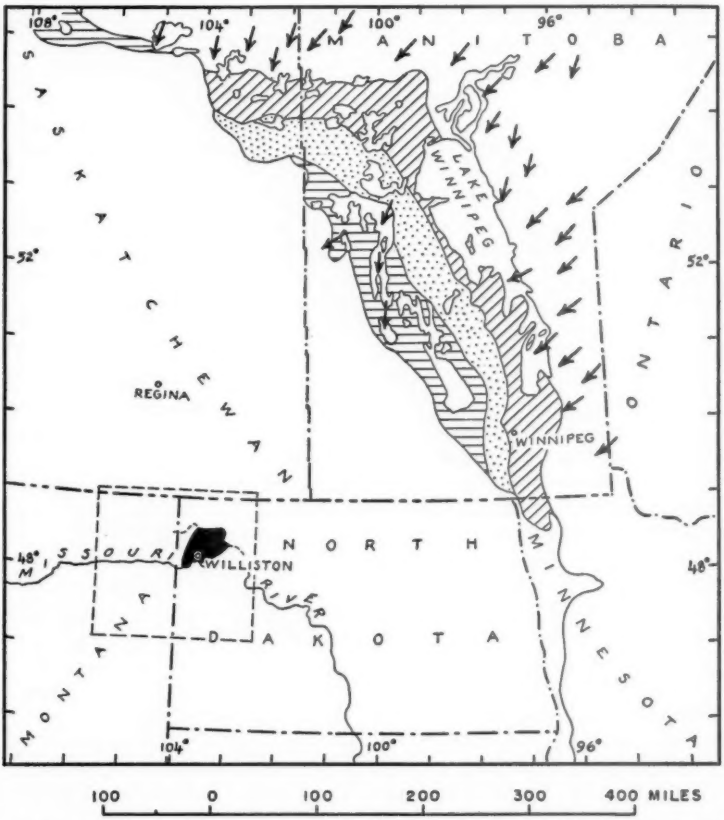

FIGURE 4.—WILLISTON AREA IN RELATION TO THE LIMESTONE-DOLOMITE BELT OF THE LAKE WINNIPEG REGION

Oblique lines—Ordovician; dots—Silurian; horizontal lines—Devonian. Arrows indicate generalized trends of glacial striations.

Shield to the northeast (Fig. 4). If the direction of advance was such that the ice crossed the belt obliquely or where the belt was broad, the limestone-dolomite content of the resulting till would presumably be high; if in a succeeding glaciation the ice crossed the belt by a more direct route or where the belt was narrow, the limestone-dolomite content would presumably be low.

It seems unlikely that the contrasts in lithology would be due to migration of the would result in gradual rather than abrupt lateral changes in lithology.

INTERPRETATION OF ISOPLETH MAP OF LOCAL ROCK TYPES

Figure 5 is an isopleth map based on the local Flaxville-type pebbles in the surface till of the region. Except in one area, the concentration of the pebbles is clearly related to the distribution of the source gravels. The high concentration

in the northwest correlates closely with the extensive fields of gravel capping the Flaxville plateaus in Montana. The eastern edge of the plateaus is indicated approximately by the overlooked in the field reconnaissance. Thus, isopleth maps of local rock types may offer clues to the identity of bedrock concealed by drift.

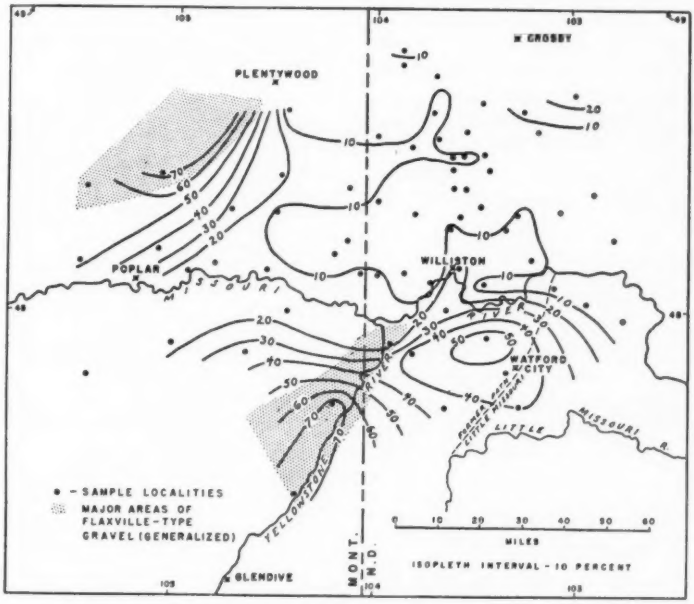

FIGURE 5.—ISOPLETH MAP OF FLAXVILLE-TYPE SILICA-RICH ROCKS

stippled area in the northwestern part of the figure. Small areas of gravel lie to the east of the plateaus but are not shown in the diagram. The high concentration of Flaxville-type pebbles in the till along the Yellowstone River is related to the extensive exposures of Flaxville-type gravels capping the uplands adjacent to Yellowstone Valley and mantling broad terraces within the valley. A third area of till with a high content of Flaxville-type pebbles is southeast of the Missouri-Yellowstone confluence. The till of this area shows a lower concentration of this pebble type than does the till of the other two areas and is not related to large areas of gravel exposure. Its eastern part straddles the ancestral path of Little Missouri River along which a few areas of Flaxville-type pebbles have been mapped. The presence of the "high", admittedly based on relatively few sample localities, suggests that additional gravels may underlie the till or may have been

Both the intermediate and the underlying drift in the central part of the map area have a low percentage of Flaxville-type pebbles suggesting the absence of source gravels under much of the central area.

Till-isopleth maps of local rock types may also furnish evidence on the direction of ice movement in areas where independent evidence is lacking.[3] In northeastern Montana and northwestern North Dakota, rocks lithologically suited to the preservation of glacial striations and other markings are practically nonexistent in the soft formations of Tertiary and Mesozoic age. The distribution of till rich in Flaxville-type pebbles southwest and west of known source areas suggests that the most widespread of the drifts (Pl. 1) was deposited by ice which

[3] Holmes (1952) concluded from a study of till-isopleth maps that the last glacier to occupy west-central New York State had its center of outflow within the Ontario basin.

advanced generally southwestward with the lines of flow possibly converging toward the west-central part of the area.

The Flaxville-type pebbles were distributed by the ice in much the same way as are the materials of a boulder train. The essential difference is that the glacial pebbles were derived from an area source rather than from a point source. The shapes of the distribution areas may vary considerably depending on the shapes of the source areas. For such broad areas of till characterized by a specific rock type the expression boulder apron may be more applicable than boulder train.

Conclusions

Till-pebble isopleth maps of erratic rock types may reveal differences in the lithology of the surface till of a region which suggest the presence of multiple drifts. Such maps may be useful in areas where drift borders are obscure and definitive evidence for multiple drifts is absent.

Till-pebble isopleth maps of local rock types may furnish clues to the identity of the buried bedrock, and may show the direction of ice movement by the distribution of boulder aprons.

References Cited

Anderson, R. C., 1955, Pebble lithology of the Marseilles till sheet in northeastern Illinois: Jour. Geol., v. 63, p. 228–243

Alden, W. C., 1932, Physiography and glacial geology of eastern Montana and adjacent areas: U. S. Geol. Survey Prof. Paper 174, 133 p.

Calhoun, F. H., 1906, The Montana lobe of the Keewatin Ice Sheet: U. S. Geol. Survey Prof. Paper 50, 62 p.

Holmes, C. D., 1952, Drift dispersion in west-central New York: Geol. Soc. America Bull., v. 63, p. 993–1010

Howard, A. D., 1950, Till isopleth map of northeastern Montana and northwestern North Dakota (Abstract): Geol. Soc. America Bull., v. 61, p. 1525

Krumbein, W. C., and Pettijohn, F. J., 1938, Manual of sedimentary petrography: N. Y., D. Appleton-Century Co., 549 p.

Leonard, A. G., 1916, The pre-Wisconsin drift of North Dakota, Jour. Geol., v. 24, p. 521–532

Stanford University, Stanford, Calif.

Manuscript Received by the Secretary of the Society October 3, 1955

Publication Authorized by the Director, U. S. Geological Survey

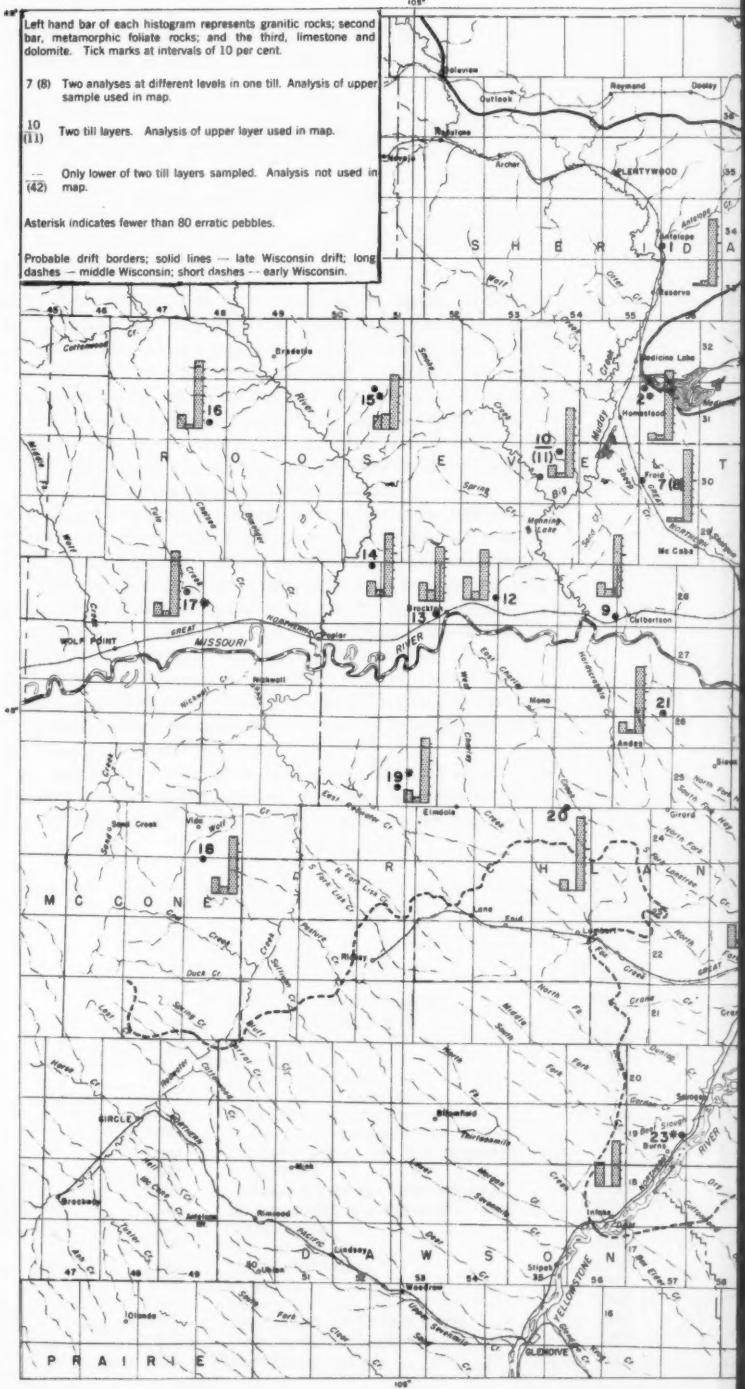
Left hand bar of each histogram represents granitic rocks; second bar, metamorphic foliate rocks; and the third, limestone and dolomite. Tick marks at intervals of 10 per cent.
7 (8) Two analyses at different levels in one till. Analysis of upper sample used in map.
10 (11) Two till layers. Analysis of upper layer used in map.
— (42) Only lower of two till layers sampled. Analysis not used in map.
Asterisk indicates fewer than 80 erratic pebbles.
Probable drift borders; solid lines — late Wisconsin drift; long dashes — middle Wisconsin; short dashes — early Wisconsin.
SHERIDAN
ROOSEVELT
MCCONE
PRAIRIE
WOLF POINT
GLENDIVE
MISSOURI
YELLOWSTONE
Outlook
Raymond
Dagmar
Archer
Antelope
Reserve
Medicine Lake
Homestead
Culbertson
Brockton
Brockway
Bloomfield
Circle
Lindsay
Woodrow
Sidney
Fairview
Plentywood
Westby
Brockton
Froid
Scobey
Girard
Richey
Vida
Elmdale
Andes
Mona
Nashua
Nickwall
Hopperstad
Poplar
Brockton
Brockway
Lambert
Culbertson
Medicine Lake
Homestead

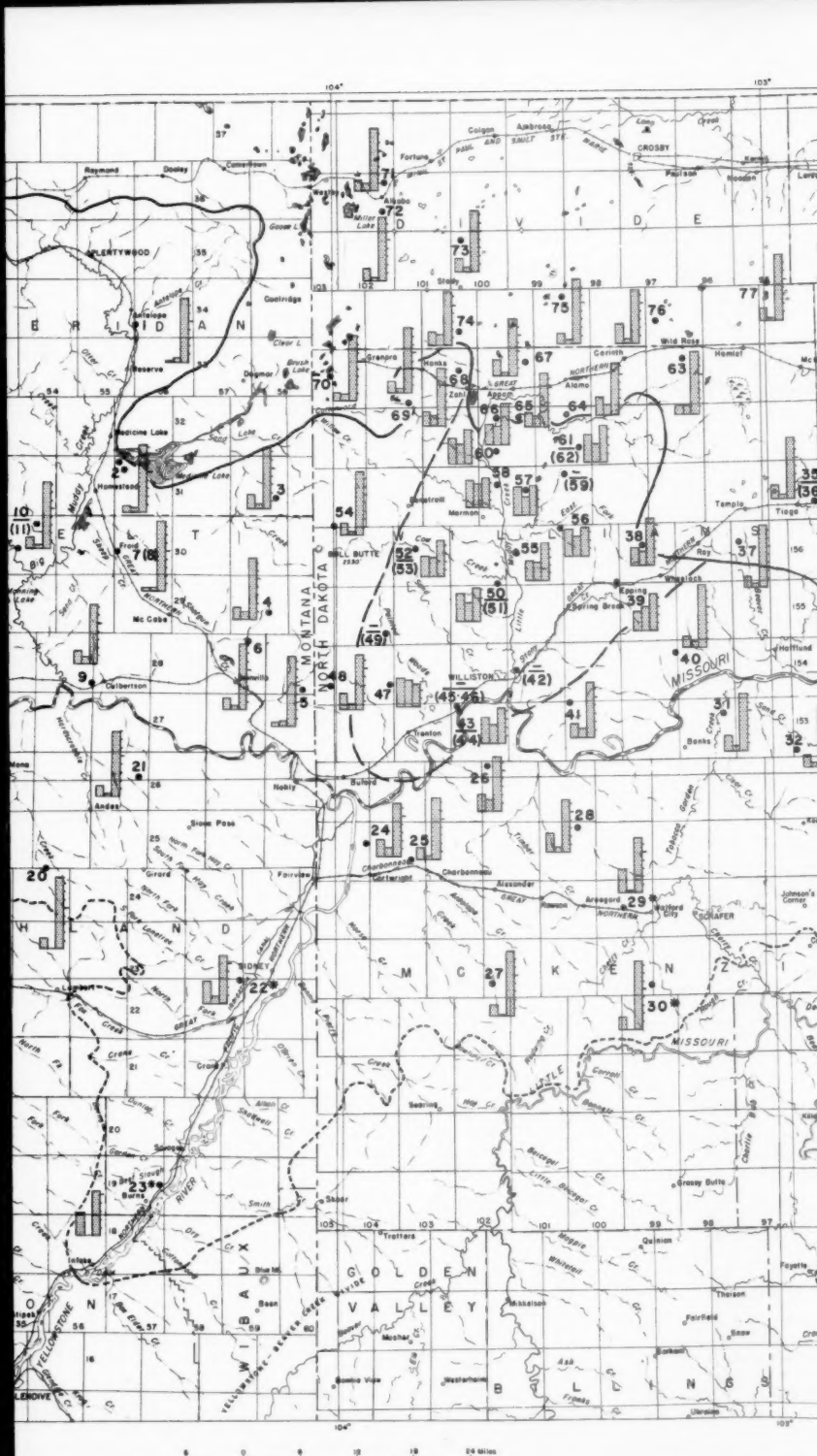
MONTANA
NORTH DAKOTA
MISSOURI
WILLISTON
WATFORD CITY
SIDNEY
CROSBY
RAY
TIOGA
STANLEY
ALEXANDER
SCHAFER
GOLDEN VALLEY
BILLINGS
MCKENZIE
WILLIAMS
DIVIDE
BURKE
MOUNTRAIL
WARD
MERCER
OLIVER
BURLEIGH
MORTON
SLOPE
HETTINGER
STARK
DUNN
MCLEAN
SHERIDAN
WELLS
FOSTER
GRIGGS
STEELE
TRAILL
CASS
RICHLAND
SARGENT
RANSOM
SIOUX
EMMONS
KIDDER
STUTSMAN
LA MOURE
DICKEY
LOGAN
MCINTOSH
DEWEY
ROBINSON
SIOUX
EDMUNDS
FAULK
SPINK
CLARK
KINGSBURY
BROOKINGS
MOODY
LAKE
MINNEHAHA
LINCOLN
UNION
CLAY
YANKTON
TURNER
HUTCHINSON
BON HOMME
CHARLES MIX
GREGORY
TRIPP
MELLETTE
TODD
BENNETT
JACKSON
PENNINGTON
CUSTER
FALL RIVER
HARDING
BUTTE
MEADE
LAWRENCE
PERKINS
CORSON
DEWEY
ZIEBACH
HAAKON
JONES
MELLETTE
TODD
TRIPP
GREGORY
LYMAN
STANLEY
JONES
HAAKON
PENNINGTON
MEADE
BUTTE
HARDING
PERKINS
CORSON
ZIEBACH
DEWEY
CUSTER
FALL RIVER
LAWRENCE
MEADE
HARDING
BUTTE
PERKINS
CORSON
DEWEY
ZIEBACH
HAAKON
JONES
MELLETTE
TODD
TRIPP
GREGORY
LYMAN
STANLEY
JONES
HAAKON
PENNINGTON

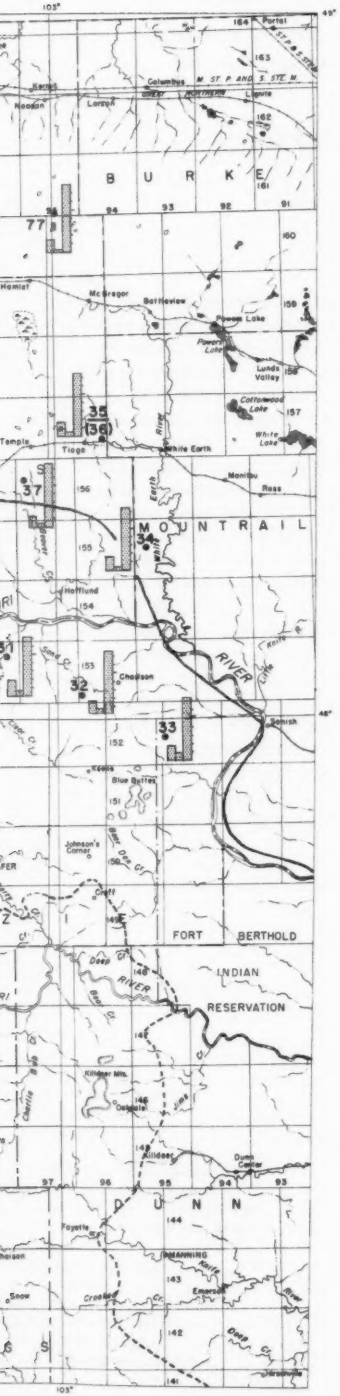
Portal
Columbus
Lignite
Kenaston
Lorraine
B U R K E
McGregor
Bottineau
Powers Lake
Lunds Valley
Cottonwood Lake
White Lake
Tioga
White Earth
Tamolo
Homlet
Mountrail
Ross
Hofflund
Chesson
Sanish
Blue Buttes
Johnson's Corner
FORT BERTHOLD
INDIAN RESERVATION
Killdeer
Dunn Center
D U N N
Manning
Emerson
Snow
Creek

TILL

Int
P
P
D
W
Ack
The
S
O
N
S
T
W
Fie
R
D
C
B

BULLETIN OF THE GEOLOGICAL SOCIETY OF AMERICA
VOL. 67, PP. 1207-1246, 25 FIGS. SEPTEMBER 1956

WRENCH-FAULT TECTONICS

BY J. D. MOODY AND M. J. HILL

ABSTRACT

Extending the work of E. M. Anderson, M. K. Hubbert, and W. Hafner on faulting, the authors develop the hypothesis that anticlinal folds, thrust faults, and *wrench faults* can be generated as a result of movement on a large wrench fault such as the San Andreas of California. Extension of this concept leads to the conclusion that for any given tectonic area, at least eight directions of wrench faulting and four directions of anticlinal folding and/or thrusting should accommodate the structural elements of that region; these directions should have a more or less symmetrical disposition relative to the direction of the primary compressive stress. The angles α, β, and γ are defined to describe the geometry of such a *wrench-fault tectonic system* relatively completely.

The authors' interpretations of tectonics in various areas indicate that wrench-fault tectonic systems do exist and are aligned systematically over large portions of the earth's crust as indicated by Hobbs, Vening Meinesz, Sonder, and others. Eight principal wrench directions are defined in terms of major elements of the earth's crust such as the Alpine fault of New Zealand. Structural elements aligned in these eight directions constitute major features of the *regmatic shear pattern* of Sonder. The authors conclude that the shear pattern may have resulted from stresses which are oriented essentially meridionally and have been acting in nearly the same direction throughout much of crustal history.

It is concluded that major wrench faults, which penetrate the entire outer crust of the earth and result in wholesale segmentation of the outer crust into polygonal blocks, constitute a fundamental type of yielding in the crust.

Possible origins of the stresses involved, formation of geosynclines, island arcs, volcanism, and crustal evolution are discussed in terms of these ideas. Some possible objections and weak points in the argument are pointed out, and suggestions for further study are included.

CONTENTS

TEXT

	Page
Introduction	1208
Purpose	1208
Principal references	1208
Definition of wrench fault	1208
Wrench-fault tectonics	1208
Acknowledgments	1209
Theory	1209
Stress ellipsoid and the angle β	1209
Orientation of stress ellipsoid	1210
Normal, thrust, and wrench faults	1210
Second-order effects and the angle γ	1211
The angle α	1212
Wrench-fault tectonics	1212
Field observations	1214
Recognition of wrench faults	1214
Dating of wrench faults	1215
California examples	1215
Basin and Range examples	1221
Pacific Northwest examples	1223
Midcontinent examples	1223
Other examples	1225
Geotectonics	1227
Regmatic shear pattern	1227
Major wrench directions	1228
Primary-stress orientation	1230
Analysis of fault pattern of France	1233
Possible origin of the regmatic shear pattern	1234
Periodic versus aperiodic orogeny	1236
Consequences of a segmented crust	1238
"Island arcs"	1240
Igneous activity	1240
Crustal evolution	1240
Conclusion	1241
Summary	1241
Suggestions for further study	1242
Possible objections to the thesis	1243
References cited	1243

ILLUSTRATIONS

Figure		Page
1.	Axes of the stress ellipsoid	1209
2.	Shear directions in homogeneous media	1210
3.	Theoretical fault orientations	1211
4.	Second-order wrench faults	1212
5.	Plan of wrench system under north-south simple compression	1213
6.	Major fault trends of California	1216
7.	Drag folds along San Andreas fault, California	1217
8.	Right-lateral stream offsets along San Andreas fault	1218
9.	Inglewood fault trend, Los Angeles area, California	1219
10.	Calaveras fault, San Ramon area, California	1220
11.	Major lineaments of western United States	1222
12.	Hillside fault, Hudspeth County, Texas	1224
13.	Thomas fault, Wichita Mountains, Oklahoma	1225
14.	Ti Valley fault, Ouachita Mountains, Oklahoma	1226
15.	New Zealand direction	1229
16.	Oca direction	1230
17.	Great Glen direction	1231
18.	Bartlett direction	1232
19.	Major tectonic directions, $\alpha = 0°$	1233
20.	Major tectonic directions, $\alpha = 345°$	1234
21.	Relation of α to latitude, for $\beta = 30°$	1235
22.	Structural pattern of the Dead Sea	1236
23.	Strain rosette for 176 faults in France	1237
24.	Diagrammatic sketch of geosyncline and geosynclinal sedimentary suite	1239
25.	Cloos' Silesian shear zone	1241

TABLES

Table		Page
1.	Theoretical wrench- and thrust-fault directions	1212
2.	Angle of drag folding, γ, along Inglewood trend, California	1219

INTRODUCTION

Purpose

New concepts of fault dynamics, evolved through re-evaluation of published data on crustal strain, mechanics of faulting, and field observations, are presented. The purpose of this paper is to develop an over-all hypothesis, based on these concepts, of the stress and strain mechanisms in the earth's crust (excluding gravity tectonics and salt tectonics).

Principal References

There are three references in the English literature on fault mechanics and faults which are fundamental to the development of principles: (1) Anderson (1942; 1951) outlined the fundamental concepts of rock fracture. (2) Hubbert (1951) corroborated Anderson's views and presented experimental and theoretical data for the value of the angle between compressional stress directions and resultant shear planes. (3) Hafner (1951) analyzed stress distribution and faulting and emphasized the necessity for considering stress distributions in attempting to understand any strain situation. The integration of the various principles and theories of fault mechanics by Billings (1954) has also been most helpful.

Definition of Wrench Fault

The term wrench fault is adopted from Kennedy (1946) and Anderson (1951) to describe ruptures in the earth's crust in which the dominant relative motion of one block to the other is horizontal and the fault planes essentially vertical. The term is translated from the German "blatt", originally used by Suess (1885), and is synonymous with strike-slip fault and transcurrent fault. The authors favor using wrench in deference to Anderson's and Kennedy's pioneer work. Wrench fault is interchangeable with lateral fault where that expression means actual rather than apparent horizontal movement. Right lateral and left lateral refer to the apparent relative movement of the two blocks viewed in plan; right lateral indicates clockwise and left lateral indicates counterclockwise separation, as described by Hill (1947). The authors extend the use of right lateral and left lateral by adding wrench, so that actual horizontal slips are implied.

Wrench-Fault Tectonics

The writers propose that large-scale wrench faults may be a dominant type of failure in the earth's crust. Large areas, probably continental in dimensions, appear to have been subjected to rather uniform stresses for ex-

tended periods. Possible orientations and origins of these regional stresses and strains are discussed. The application of these concepts to the interpretation of local and regional tectonics is considered, and many geotectonic hypotheses are re-examined in the light of wrench-fault tectonics.

Acknowledgments

This paper represents a synthesis of many previous workers' published material and countless conversations with fellow workers and friends. Particular mention is made of the many discussions and constructive criticisms by C. D. Cordry, H. D. Hedberg, and G. W. Ledingham. J. B. Currie, P. A. Grant, B. F. Hake, R. T. Hazzard, R. L. Johnston, and G. B. Lamb have contributed particularly valuable ideas and suggestions. The following have critically reviewed the manuscript, for which the writers are most appreciative: M. P. Billings, B. W. Blanpied, M. A. Hanna, R. T. Hazzard, K. C. Heald, H. D. Hedberg, M. L. Hill, G. B. Lamb, L. V. Lombardi, C. R. Longwell, C. L. Moody, H. M. Nielsen, and G. Pardo; no responsibility for any of the views presented herein is assumed by these gentlemen. The authors are indebted to the Gulf Oil Corporation and the Western Gulf Oil Company for permission to publish this paper and wish to express their appreciation to the officials of the Gulf Companies for the creation of a climate favorable to interregional exchange of ideas on a broad scale.

Theory

Stress Ellipsoid and the Angle β

A brief review of Anderson's (1951) work provides a basis for understanding fault mechanics. Fundamental to his exposition is the expression of stresses in terms of a set of three mutually perpendicular axes. In a homogeneous isotropic material under compression, the maximum compressive stress can be represented as acting in a given direction (Fig. 1, Y). The minimum-stress direction (Fig. 1, X) is then at right angles to the maximum-stress direction, and the third rectangular axis must coincide with the direction of an intermediate stress. These three stress axes are of unequal length and describe an ellipsoid which long has been termed the stress ellipsoid.

If a material of sufficient rigidity to react elastically rather than plastically is stressed

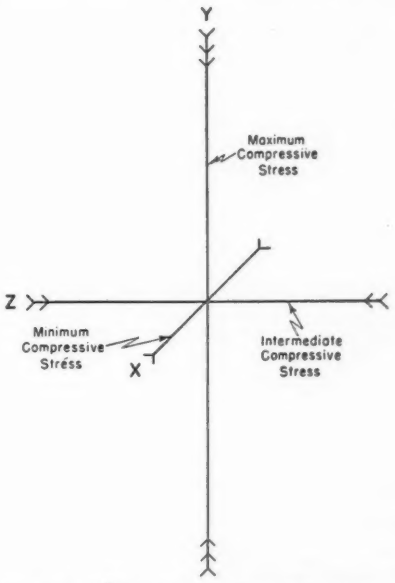

Figure 1.—Axes of the Stress Ellipsoid

beyond its strength, it will rupture. In situations such as those described above, the planes of maximum shearing stress are parallel to the intermediate stress axis and lie at angles of 45° on either side of the maximum compressive stress. The planes of actual shear do not coincide with the planes of maximum shearing stress but lie closer to the axis of maximum compressional stress and form an angle with it which is here called β, the angle of shear (Fig. 2). The factors which contribute to the deviation in direction between actual strain and theoretical strain are included in the "angle of internal friction" which is one of the controlling parameters for the value of the angle β.

Hubbert (1951) indicates that, although the value of β may vary among different materials, a good average for rocks is approximately 31°. He wrote, "For rocks, this would correspond to normal faults with hades, or reverse faults

with dips, of 31° ± 2°." Hubbert's data were for normal and thrust faults; however, the value of 31° should be applicable to wrench faulting also because of the similarity of the

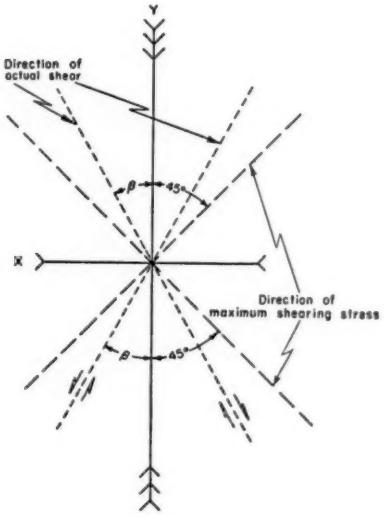

FIGURE 2.—SHEAR DIRECTIONS IN HOMOGENEOUS MEDIA

dynamics. Billings (1954) stated, ". . . the angle between the compressive force and the shear fractures is about 30°". Although the possibility of considerable variation in the value of this angle is recognized, 30° is used throughout this paper as the average value.

Orientation of Stress Ellipsoid

Hafner (1951) emphasized that the orientation of the stress ellipsoid is variable and generally must result from a complex interplay of varying stresses which are differently oriented; however, field observations of the dips of fault surfaces, which are planes of actual shear in the crust of the earth, show three frequency maxima near 90°, 60°, and 30°. For example, Hubbert (1951) cites Sax as stating that of 2102 separate faults examined in the Netherlands, 79 per cent were normal and 21 per cent were reverse; dip frequency-distribution curves plotted for these two groups showed well-defined peaks at 63° and 22° respectively. Paige (1912) said of the numerous faults of the Llano uplift in central Texas that ". . . the greater number are vertical. . . ."

Such observations can be accommodated in most cases by assuming that the stress ellipsoid is oriented with respect to the surface of the earth so that two of its axes lie very nearly in a horizontal plane; the other axis is then essentially vertical. The majority of faults must have resulted from the interplay of stresses oriented approximately horizontally (lateral compression) and approximately vertically (gravitational and other forces). Anderson (1951) stated the following principle: "Beneath country which is not Alpine in its topography one principal direction of stress is, in general, nearly vertical, and two are nearly horizontal." The air-earth interface is a surface of zero shear; hence, it must be normal to one of the principal stress directions.

The orientation of the two axes of the stress ellipsoid in the horizontal plane determines the strike of the associated shear planes.

Normal, Thrust, and Wrench Faults

This restriction on the orientation of the stress ellipsoid reduces to three the possible stress orientations, which should correspond to the three dip maxima observed. In Figure 3 the classification of shears in the crust of the earth into normal, thrust, and wrench faults is apparent. The direction of movement on each shear plane is relatively the same in each case. (Low-angle fault surfaces formed in connection with gravitational sliding are not considered shears.)

The maximum compressional stress for both thrust and wrench faults is oriented in the horizontal plane; for normal faults it is vertical. In an area under tangential compression, the stresses can be relieved along either thrust- or wrench-fault surfaces, depending only on the orientation of the minimum stress. Since the minimum-stress direction in thrust faults is vertical, thrust faulting in most cases should be a shallow phenomenon that exists only at depths where the weight of overburden is relatively small.

Normal faults require that the maximum stress be vertical, which means that the horizontal stresses are smaller than the vertical stresses. This requirement obviates the syngenetic development of normal faults with wrench or thrust faults except where normal faults are a secondary effect due to local deformation. Thus in an area of compression phenomena, normal faults can result only if the vertical stresses exceed the horizontal compressional stresses; this situation usually obtains in areas of local positive uplift, as in salt domes and igneous intrusive masses. Gravity faults at the crests of anticlines and over salt domes are examples of normal faults that result from decreased horizontal stress and consequent increased vertical stress. Dynamically, normal faults are identical with the other two types, except in the orientation of the stresses; all three are shears, and the term normal fault as used here should not be considered a result of crustal tension.

All gradations within these three classes of faults can exist because of varying stress orientations; however, the three categories should be valid for the great majority of faults.

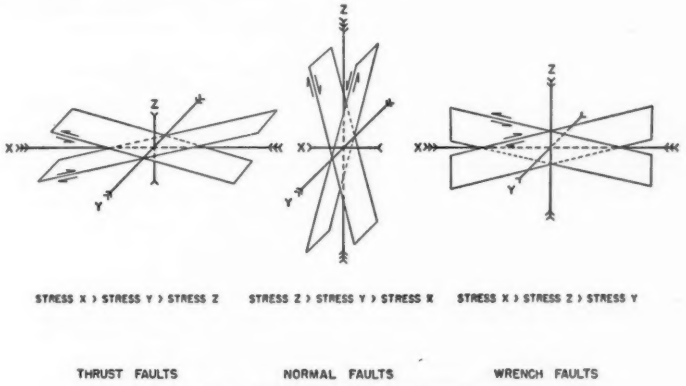

FIGURE 3.—THEORETICAL FAULT ORIENTATIONS
After E. M. Anderson (1951)

Second-Order Effects and the Angle γ

McKinstry (1953) developed a thesis of secondary strain features and discussed several known fault systems in terms of second-order shears. He wrote,

> "If movement is in progress on a main fault or 'master shear', stresses in the rock adjoining it will have such orientation as to cause failure on a new pair of mutually complementary planes, one of which will make an acute angle with the master shear."

McKinstry considered that inertial and frictional forces involved during movement on a shear plane resulted in a local reorientation of the compressional stresses. This mechanism can probably account for some second-order shears; however, as McKinstry points out, the available forces decrease rapidly and the system is not regenerative. A mechanism which is regenerative and seems more likely to explain the large-scale second-order features contemplated here was developed by Anderson (1951), based on computation by Inglis (1913). Body forces developed by movement along a fault could also yield local stress reorientation, which might result in second-order features. The idea of elastic rebound was promulgated by Lawson *et al.* (1908) to explain the movement on the San Andreas fault. A further possible mechanism for generating reoriented stresses adjacent to wrench-fault blocks may be found in the change of shape which must ensue when fault blocks are subjected to continued compression.

One or a combination of the mechanisms mentioned above results in locally reoriented compressional forces which generate new strain directions called second-order shears (Fig. 4). The principal-stress direction is indicated by the vector AB, which is equal in magnitude to

the compressive force. The vector CD is of a second order resulting from one or a combination of the mechanisms suggested above and creates second-order strain directions as indicated. Strains resulting from the stresses

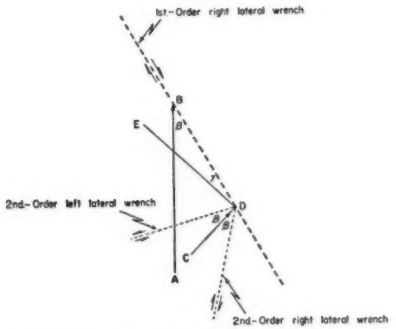

FIGURE 4.—SECOND-ORDER WRENCH FAULTS

associated with the direction CD can be second-order right and left lateral wrenches disposed on either side of CD at the angle β, or a second-order anticline or thrust fault or both oriented at right angles to CD as shown by the line DE. Such second-order anticlines, called drag folds, are normal to the direction CD and form an acute angle γ with the first-order, or parent, shear. Figure 4 shows a means of determining the strikes of the various second-order features in terms of the direction of the primary principal stress, if values for β and γ are available.

The value of the critical angle γ has not been determined satisfactorily; generally it varies between 5° and 30° with an average value of 15°. However, in some instances γ is apparently 0°, and the drag folds, in this situation called compression ridges, are parallel to the parent wrench fault. Inglis's diagram as reproduced in Anderson (1951) provides some basis for deducing values for γ.

Second-order shears of the same type can also be developed by movement on a first-order left lateral fault with corresponding orientations in mirror image to those in Figure 4. Thus, third-order shears can be developed secondary to each of the second-order shear fractures. For a single primary stress orientation there can arise two first-order shear directions, four second-order shear directions, eight third-order shear directions, and 16 fourth-order shear directions.

Second-order shears and drag folds are manifestations of stress reorientation in one fault block or a block between two parallel faults and need have no counterpart in adjacent blocks; they should terminate at the master fault. Parallel second-order strains can exist in adjacent blocks but cannot be continuous across the primary faults.

TABLE 1.—THEORETICAL WRENCH- AND THRUST-FAULT DIRECTIONS

Right or left lateral wrench			Anticlines and/or thrusts
RL	N.30° W.	First order	E.-W.
LL	N.30° E.		
RL	N.15° E.	Second order	N.45° E.
RL	N.75° W.		
LL	N.15° W.		N.45° W.
LL	N.75° E.		
RL	N.30° W.	Third order	N.-S.
RL	N.30° W.		
RL	N.60° E.		E.-W.
RL	N.60° E.		
LL	N.30° E.		N.-S.
LL	N.30° E.		
LL	N.60° W.		E.-W.
LL	N.60° W.		

The Angle α

The azimuth of the primary principal-stress direction (that is, the maximum-stress axis of the stress ellipsoid) which gives rise to first-order shears is defined as the angle α. (In the case of stress orientations resulting in normal faults, the maximum-stress axis is essentially vertical and has no azimuth.) Observed structural relations indicate that this stress direction in most instances throughout geologic time has been oriented approximately meridionally and that the value for the angle α varies from 340° to 20°; the orientation of the primary principal stress is discussed below.

Wrench-Fault Tectonics

If reasonably accurate values can be assigned to the three critical angles α, β, and γ, a

complete tectonic system can be developed in accordance with the principles presented above. If the values 0°, 30°, and 15° are assigned to

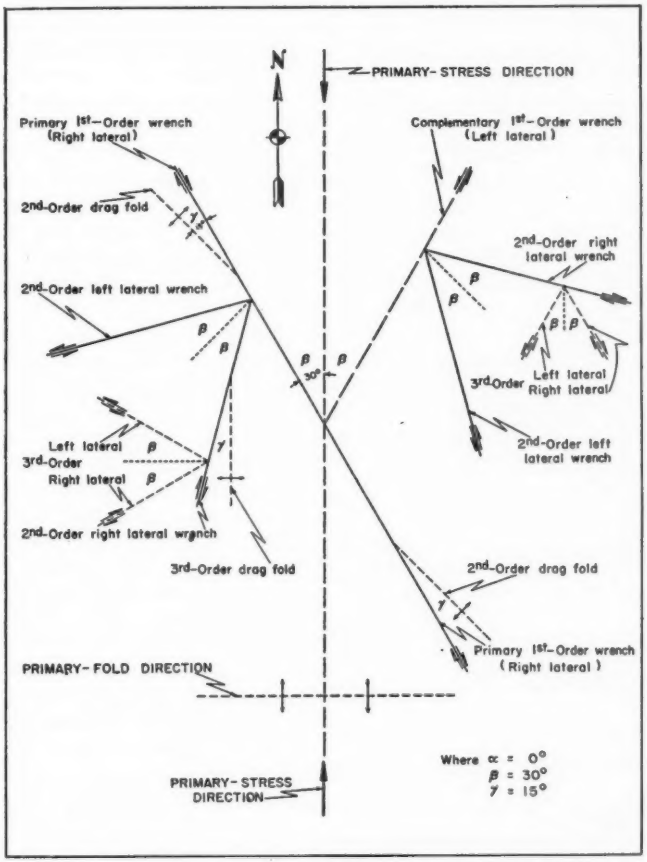

FIGURE 5.—PLAN OF WRENCH SYSTEM UNDER NORTH-SOUTH SIMPLE COMPRESSION

α, β, and γ respectively, the tectonic directions that result are shown in Table 1.

The shear and anticlinal directions are duplicated in the third order, making it impossible to distinguish fourth-order and lower directions from first-, second-, or third-order directions. Thus, an infinity of shear directions does not arise; the system is resolved into eight major wrench directions and four major anticlinal thrust-fault directions. Figure 5 illustrates a hypothetical wrench-fault system showing first-, second-, and third-order wrench faults with their corresponding drag folds. It is assumed that the right lateral wrench fractured first and is dominant; however, the left lateral could equally well be the primary fracture. An entire geometric system of strain can be developed from a single primary compressive stress orientation. Of course a somewhat different system would result in the event γ varied considerably from 15°.

The values used in Figure 5 are hypothetical and the directions indicated should not be considered rigorously. Deviations from the ideal system can result from the following:

(1) The indicated system resulted from consideration of essentially constant horizontal stresses in one direction, whereas Hafner (1951) showed that variable stresses acting in two horizontal and one vertical direction must be considered in the general case. Although

these are valid and important considerations, in most instances the result would be to impress relatively minor curvatures on the idealized surfaces. However, any orientation of the stress ellipsoid is possible.

(2) Crustal materials exhibit a wide range of inhomogeneity and anisotropy.

(3) In consequence of the above, the orientation of the stress ellipsoid with respect to the vertical, and the values of α, β, and γ probably vary horizontally and vertically.

(4) Nonelastic deformation exists in crustal materials where stresses are continuous over long periods. As Anderson (1951) points out, nonelastic behavior must contribute extensively to deviations from the ideal theoretical plane vertical-shear surfaces.

(5) A further complicating possibility is that since normal and thrust faults are also shears the same analysis must be valid. Thus Figures 4 and 5 can be regarded as vertical sections of normal or thrust faults, and the ensuing second- and third-order strains can be expected to occur in association with these types of faults also.

(6) In strongly orogenic areas subsequent deformation can alter original dips and strikes of fault surfaces.

Field Observations

Recognition of Wrench Faults

Criteria for recognition of faults have been admirably discussed by Billings (1954); the following extends his material with particular reference to wrench faults. Wrench faults are characterized by steeply dipping fault planes on which there have been appreciable strike-slip components of movement. Theoretically wrench-fault planes should be vertical; actually, any fault plane whose dip is steeper than 70° should be examined to see whether or not it might be of the wrench type, and wrench faults with much gentler dips have been described in the literature. Aerial photographs are of great assistance in identifying possible wrench faults by means of their straight traces. Cotton (1950) gave a lucid presentation of geomorphological aspects of faulting, much of which pertains to wrench faults. Variations in apparent vertical displacement along strike suggest wrench faults, as do fault planes which vary in dip from high-angle normal to high-angle reverse. Scissors faults, which show reversal of apparent dip-slip displacement along strike, might also be of the wrench type.

Evidence of strike-slip components of movement along fault planes is most frequently seen in slickensides, stream offsets, and offsets in structures and outcrop patterns. Modern movement along faults of this type in some places provides direct evidence of horizontal movement in association with earthquakes.[1]

Careful study of thicknesses, lithofacies, biofacies, and depositional fabrics can yield evidence of strike-slip movement; this approach was used by Hill and Dibblee (1953) to indicate the possibility of 350 miles of post-Jurassic strike-slip movement on the San Andreas fault in California. Mapping of subcrop contacts below unconformities should provide a more precise method of measuring horizontal components of displacement, if adequate well control is available.

It is the writers' belief that major wrenches need not have strike-slip movement of the order of magnitude indicated for the San Andreas, Alpine, and Great Glen faults. The quantitative relations existing between primary and lower-order wrenches and drag folds are not known; large-scale drag folds might develop in association with wrenches of relatively small strike-slip displacement.

The orientation of folds and thrusts furnishes a clue which can be used to delineate wrench faults, inasmuch as the wrench to which any given anticlinal fold or thrust fault is secondary should make an acute angle γ with the axis of the anticline or with the strike of the thrust-fault plane; drag folds should be asymmetric or overturned on the flank closest to the parent wrench. The apex of the angle γ should be opposed to the direction of lateral movement of the block. Structures which terminate abruptly with no apparent cause might be limited by wrench faults.

As emphasized by Anderson (1951), wrench-fault zones are characterized by the development of fault breccia along the individual

[1] A series of articles recently published by J. H. Hodgson and his associates, *e.g.*, Hodgson (1955) and Hodgson and Storey (1954), emphasize strike-slip movement associated with earthquakes.

faults. The writers believe that the large primary wrenches extend through the outer crust and thus are very deep and fundamental flaws in the crust. The result of movement along these deep faults can be expressed in the overlying sedimentary veneer more commonly by a complex zone of wrench faults and generally complicated structure than by an individual fault trace. Some deep-seated wrenches appear to be indicated at the surface only by systems of small en echelon faults or anticlines.[2] Situations of this nature have been described by Picard (1954) as disharmonic faulting in the case of the Jordan-Dead Sea rift system. A further example is the well-known zone of en echelon faulting in south-central Montana, which appears to lie in extension of the Coeur d'Alene lineament, here considered to be a left lateral wrench-fault zone. On a large wrench fault, such as the San Andreas, the zone of faulting can be several miles wide; in this zone, individual surfaces of movement anastomose in a complicated fashion resulting in a crush zone with many fault splits whose surface traces form a braided pattern, and in the development of a fault breccia throughout.

There are many difficulties inherent in the recognition of wrench faults; for example, the last increment of movement in many cases has been essentially vertical, so that the fault simulates a high-angle normal fault or high-angle thrust fault. Many wrench-fault zones are covered by secondary thrust sheets which are considered to have been built up from adjacent drag folds and moved across the parent wrench. Recognition of wrench faults has lagged far behind that of normal and thrust faults, in spite of the publication of the pioneer work of such men as Anderson (1942), Hubbert (1951), Hafner (1951), and McKinstry (1953).

Dating of Wrench Faults

Exact dating of wrench-fault movements is a difficult problem arising from the continuous activity of many of these faults through geologic time. In general, geologists determine the youngest formation offset by a fault, or the oldest rock unit unaffected by a fault, and approximate a time of rupture. This method is applicable to wrench faults only to the extent of dating the last increment of faulting. Many individual pulsations can be dated by local unconformities or buttressing of individual stratigraphic units on growing drag folds. Where stratigraphic data are available on both sides of a wrench, a progressively increasing offset of older and older units can be demonstrated by measuring facies separation; Hill and Dibblee (1953) successfully applied this principle to the San Andreas fault. In some cases an approximate date of fault inception can be determined by correlating offset portions of pre-existing deformation of known age.

Field evidence from the major wrenches studied suggests that the determination of fault inception is not clear-cut but is a function of the readable geologic history. For example, the San Andreas fault is said to have originated in the pre-Tertiary, probably Jurassic, only because the oldest rocks that contribute understandable data are probably late Jurassic and point to the presence of an ancestral San Andreas. This inference suggests that some of the major wrenches are as old as the rigid crust of the earth. On the other hand, as compression and deformation have continued through geological history, new fractures have formed in response to the increasingly complex stress distribution in the earth's crust.

California Examples

A discussion of field examples of wrench faulting should start with the San Andreas of California. An early record of strike-slip movement on faults is to be found in the discussion by Lawson *et al.* (1908) of the San Francisco earthquake, caused by movement on this fault. Figure 6 is an outline map of California on which the principal fractures have been traced, showing the San Andreas as the dominant feature. The San Andreas fault extends from Point Arena to beyond the Mexican border, about 600 miles, in a general northwest-southeast direction, with its characteristic strike N.40° W. Only two segments vary from this "normal" strike, one in the southern part, from near Maricopa to Banning (Fig. 6, M and B), where the strike approaches N.60° W., and the

[2] Wilson's (1953) paper calling attention to the relations between grabens, rifts, and wrench faults was pointed out to the authors when this manuscript was in press.

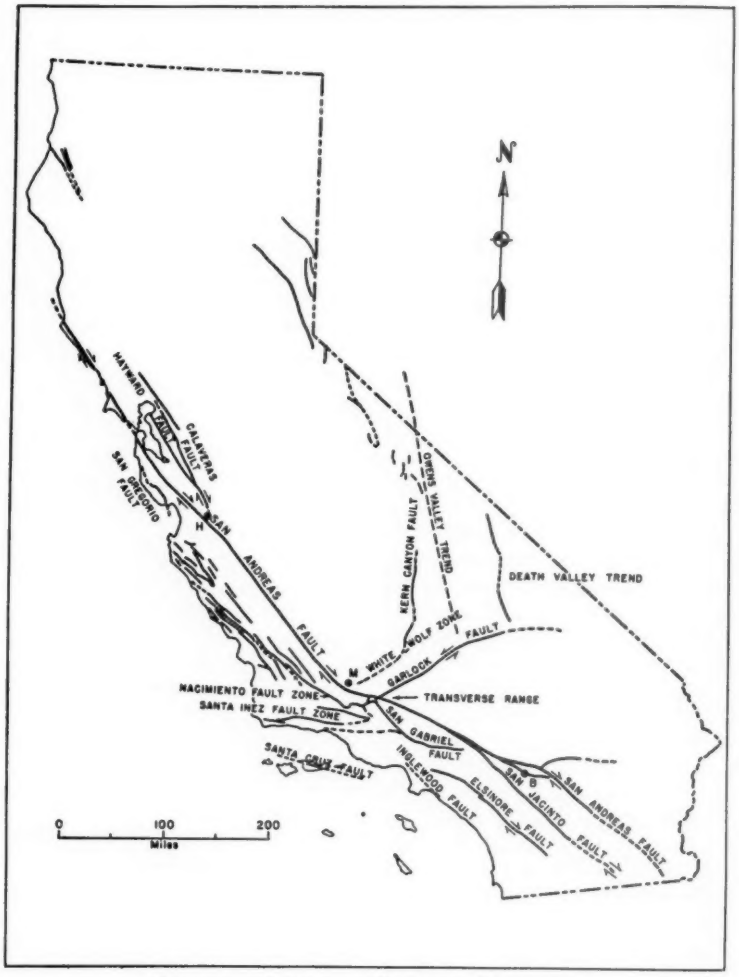

FIGURE 6.—MAJOR FAULT TRENDS OF CALIFORNIA

other a small segment near Hollister, California (Fig. 6, H), where the strike approaches N.50° W.

Hill and Dibblee (1953) described the San Andreas fault and proposed a stress orientation explaining their interpretation of the dynamics:

"The present authors believe that: (1) the San Andreas is a steep fault zone of variable width consisting of one or several nearly parallel faults; (2) its inception was quite likely pre-Tertiary, and it is now active; (3) it has probably been characterized by right-lateral displacements throughout its history; (4) it marks such an important contact that rarely can it be crossed, except in recent alluvium, without passing into significantly different rocks; and (5) its cumulative displacement of some rock units is at least tens of miles, and older rocks may have been displaced a few hundred miles."

The authors agree essentially with Hill and Dibblee. Recent detailed work at several localities along the fault substantiates the contention that the movement can be measured in tens of miles since upper Miocene time and hundreds of miles since Jurassic time.

Most authors attempt to describe the dynamics of the San Andreas fault by constructing vector diagrams surrounding its

intersection with the Garlock fault. It is important to understand the mechanism of this anomalous section, but it is equally important to define the mechanics responsible for the great extent of the fault where it is nearly a straight line. A N.40° W. orientation for the major part of the fault requires a nearly north-south direction for the principal-stress axis, or possibly a little west of north, to give right lateral movement. The drag-fold orientations illustrated in Figure 7 and many other drag folds on the west side of the fault oriented N.50°–60° W. are clear evidence of right lateral movement. The values of γ measured from the five drag folds in Figure 7 vary from 14° to 20° and average 17°. Uniform stress orientation over a wide area must exist to develop such a lengthy and uniform rupture in the crust. The authors believe that the San Andreas fault represents one of the major primary fractures of the earth's crust, responding directly to stresses of fundamental importance in crustal mechanics.

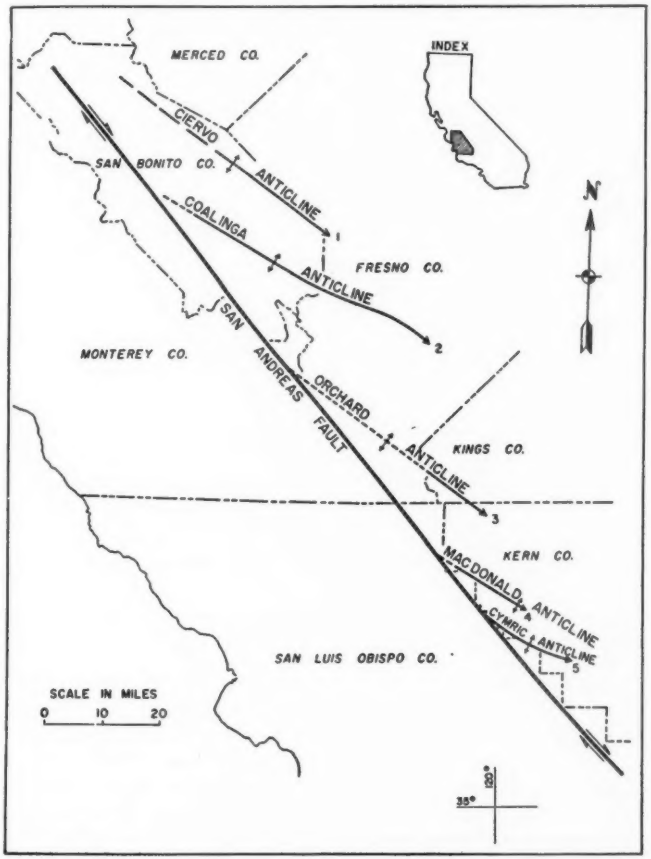

FIGURE 7.—DRAG FOLDS ALONG SAN ANDREAS FAULT, CALIFORNIA

A number of faults essentially parallel to the San Andreas are also shown in Figure 6 and probably represent the first-order wrench direction associated with the San Andreas, or possibly a part of a major rift-fault system of which the San Andreas is the most pronounced fracture. Such fractures as the San Gregorio fault south of San Francisco, the Nacimiento fault zone, the Elsinore and San Jacinto faults,

appear to be part of this major system. The Elsinore and San Jacinto faults are essentially parallel to the principal San Andreas direction and appear to be new slices caused by the fractures are shallow manifestations of a single right lateral wrench fault at depth that is part of the San Andreas system. The many oil fields along this trend are located on drag folds de-

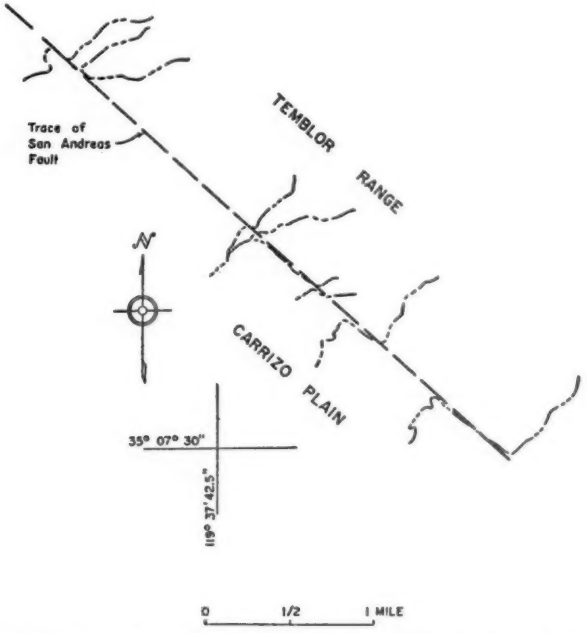

FIGURE 8.—RIGHT-LATERAL STREAM OFFSETS ALONG SAN ANDREAS FAULT

alteration of the San Andreas direction. Crowell (1952) assigns 15 to 25 miles of right lateral displacement since late Miocene time to the San Gabriel fault. Many examples of stream offsets by recent movements along these right lateral faults are visible from aerial photographs and topographic maps. Figure 8 is a sketch along the San Andreas in the Carrizo Plains area showing right lateral stream offsets varying from a few hundred to several thousand feet.

The Inglewood fault in Los Angeles County lines up exactly with the San Andreas fault and shows recent right lateral movement as exemplified by the orientation of the en echelon folds associated with it (Fig. 9). Detailed subsurface work on the oil fields of this trend does not reveal a single clear-cut fault trace, but many parallel faults are recorded in a narrow zone. The authors believe that these multiple veloped by the right lateral motion. The angle γ was measured for each of these folds (Table 2).

The average angle γ for the trend is 13.3° which compares favorably with the 17° noted above for the large drag folds adjacent to the San Andreas fault. Three of the largest folds, the El Segundo trend, the Torrance-Wilmington trend, and the Huntington Beach folds, demonstrate the largest values of γ, and the many en echelon folds along the Inglewood fault proper more nearly approach the strike of the fault itself.

The Calaveras and Hayward faults in the San Francisco area are oriented N.20° W. to N.25° W. and show right lateral movement with activity recorded in historic time. They intersect the San Andreas fault near Hollister, where its direction is altered, and appear to be part of the San Andreas rift system. Figure 10

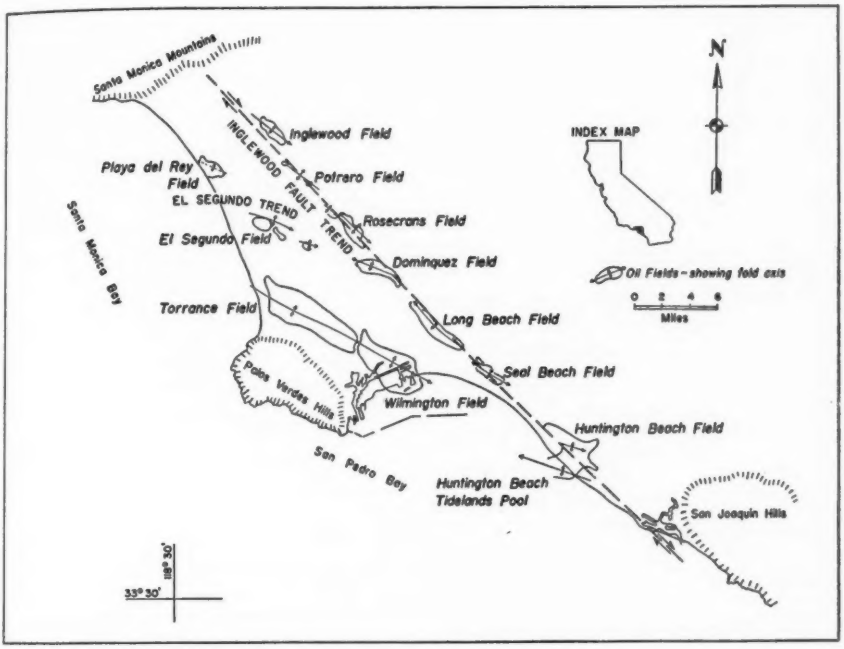

FIGURE 9.—INGLEWOOD FAULT TREND, LOS ANGELES AREA, CALIFORNIA

TABLE 2.—ANGLE OF DRAG FOLDING, γ, ALONG INGLEWOOD TREND, CALIFORNIA

Structure	Angle
1. Inglewood	10°
2. Potrero	6°
3. Rosecrans	4°
4. El Segundo trend	23°
5. Signal Hill (average)	5° (0–10°)
6. Huntington Beach	24°
7. Huntington Beach tidelands pool	24°
8. Seal Beach	10°
9. Torrance-Wilmington trend	14°
Average γ	13.3°

is a sketch of a portion of the Calaveras fault in the San Ramon-Livermore area illustrating the orientation of drag folds on both sides of the wrench. These folds demonstrate right lateral movement and give values for the angle γ from 11° to 20°. An outstanding example of drag-fold evolution is shown by the Bolinger structure where the drag fold developed beyond a simple fold, became asymmetric, and finally thrust toward the controlling wrench fault.

The Garlock fault trends N.55° E. to N.65° E. and demonstrates left lateral movement. Hill and Dibblee (1953) describe it as essentially vertical and consider it a complement to the San Andreas fault. Dynamically its orientation is not correct for the primary left lateral direction, and it would more nearly fit a theoretical position for a second-order left lateral fault, assuming north-south compression. The greatest change in direction of the San Andreas occurs near its intersection with the Garlock fault. Basin and Range structure ceases abruptly along the eastern extension of the Garlock fault, with an extremely complex structural pattern existing south of that line, as described by Hewett (1955).

Several other faults appear to be associated with the Garlock and may also have left lateral movement. These are, first, the White Wolf fault trend, N.52° E., along which the recent Arvin-Tehachapi earthquake was located. An

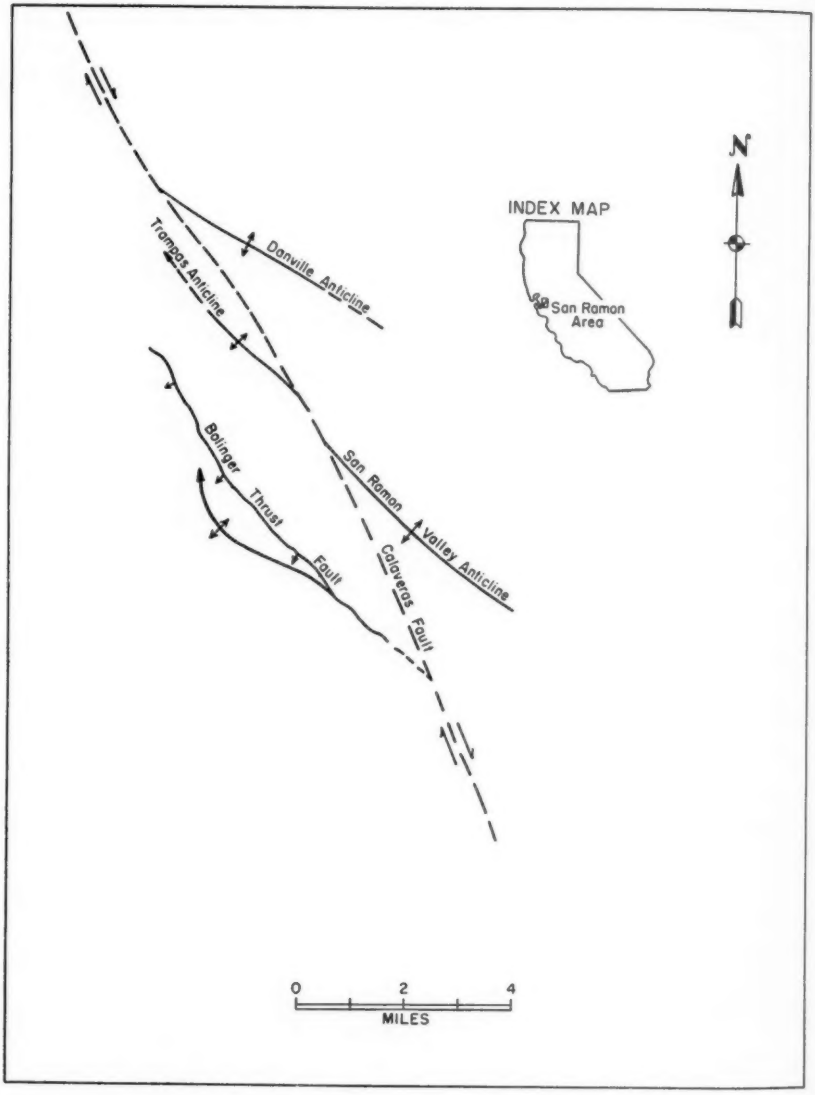

FIGURE 10.—CALAVERAS FAULT, SAN RAMON AREA, CALIFORNIA
Data from Ham (1949), Taliaferro (1951), and Johnston (Unpublished map)

excellent description of this fault and its probable relative motion is included in a report by Steinbrugge and Moran (1954). Another parallel direction is the Stockton escarpment, trending N.55° E., crossing the northern part of the San Joaquin Valley. This escarpment is known only from subsurface data which indicates that a thick section of Eocene rocks rests on Cretaceous north of the escarpment with nonmarine Miocene lying directly on Cretaceous south of the escarpment.

The Transverse Range of California occurs at

the position where the San Andreas makes its major direction change. The Transverse Range may represent the primary-fold direction, consequently shortening the crust in this area and altering the San Andreas direction. Possibly the Transverse Range is composed of drag folds related to a second-order wrench direction oriented N.65° E., or parallel to the Garlock direction. A third possibility is that the Transverse Range results from movement along the Texas lineament of Ransome (1915) and that the anomalous direction of the San Andreas system results from the intersection of these two major shear zones. Many low-angle thrusts and structural complexities obscure the true relationships in this area.

Many of these wrench directions are associated with low-angle thrusts which are probably due to reorientations of the stresses at a shallow depth. The eastern extension of the Garlock fault may pass into a thrust, the Elsinore fault appears to be associated with the Whittier thrust, the San Gabriel fault has thrust manifestations in its southern part, and the Nacimiento fault has associated thrusts in the south Cuyama area. These shallow thrusts are probably near-surface manifestations of major wrench faults which in many cases are obscured by their own shallow complexities.

Shepard and Emery (1941) discussed the tectonic origin of the submarine topography on the continental shelf off the California coast. Many of the topographic features are straight lines and parallel the major onshore faults. This topography clearly indicates the seaward extension of the Coast Range type of tectonics, at least as far west as the present continental slope. Menard (1954; 1955) discusses four major approximately east-west lineaments on the Pacific Ocean floor that no doubt have tectonic origin. There are elevation differences across them, foci of volcanism along them, and a change in character of the bottom topography between the various large lineaments. One of these major features lines up with the Mendocino escarpment (off the northern California coast) which has been genetically related to a major east-west shear zone at False Cape, Humboldt County, by Ogle (1952); another appears to be associated with the Channel Islands and Transverse Range.

Basin and Range Examples

Since Gilbert's (1874; 1875; 1928) description of the "fault-block" theory of origin for the Basin and Range structure, many geologists have been bound to a concept of "tension faulting". Other workers have long recognized the compressional aspects of the rock deformation. Many complex thrust zones, in some cases involving upper Tertiary rocks, have been described, and some have been observed by the present authors. Ferguson and Muller (1949), Ferguson, Muller, and Cathcart (1953), Roberts (1951), and Ferguson, Muller, and Roberts (1951a; 1951b) discuss areas of extreme compressional deformation in the central and northern parts of Nevada. Normal faults are recognized as subordinate features. In several cases in the literature a stratigraphic unit changes character abruptly between two exposures, suggesting facies offsets. Topographic lineaments appear to have tectonic origins, indicating that a grand fracture pattern is controlling a large area.

Locke *et al.* (1940) describe a gross tectonic pattern for the western states which includes a northwest-southeast trend parallel to the San Andreas fault, named by them the "Walker Lane". This trend is N.40° W. and has structural complexities which indicate that it is a large wrench-type shear zone with right lateral movement, as suggested by Locke *et al.* (1940). They consider the Walker Lane to be similar to the San Andreas fault. This is certainly a major right lateral wrench-fault zone comparable to the San Andreas of California (Fig. 11). Epicenters of several severe earthquakes, the most recent in December 1954, are located near Fallon, Nevada, near the central part of the Walker Lane.

Several major faults have been described along the eastern and southeastern side of the Basin and Range province. Gregory (1950) discusses the Grand Wash, Hurricane, and Sevier faults in southwestern Utah and northwestern Arizona. These faults trend N.15° E. to N.25° E. and are at the approximate location of the basinward edge of the Paleozoic shelf area (Fig. 11). The anticlinal trend described by Mackin (1955) in the Cedar City-Iron Springs area of Utah suggests drag folding. If this is

true, its relation to this fault zone would indicate left lateral movement. Kelley (1955) mentioned left lateral movement on this fault

Most of the Basin and Range province is characterized by north-south ranges classically described as bounded by large "normal" faults.

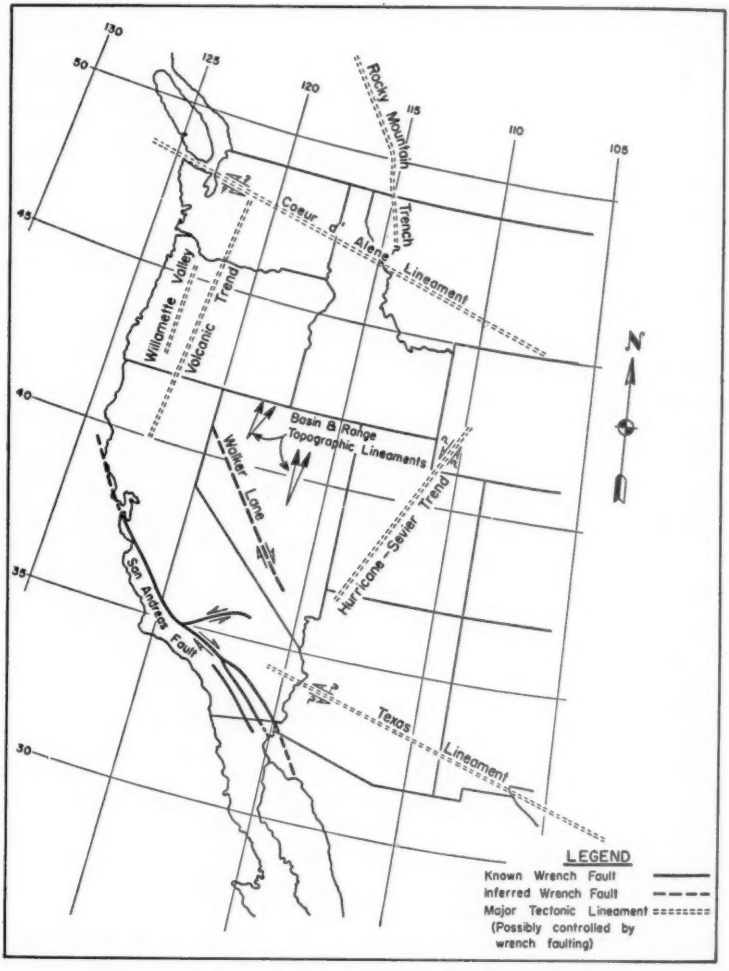

FIGURE 11.—MAJOR LINEAMENTS OF WESTERN UNITED STATES

zone which he considered the western boundary of the Colorado Plateau province. This general trend continues to the northeast along the west boundary of the Uinta uplift and makes the western boundary of the Green River basin. This trend could represent a first-order left lateral wrench direction complementary to the San Andreas-Walker Lane direction.

This trend varies from north-south to N.10° E. with a change in northwestern Nevada to N.20° E. to N.30° E. Many low-angle thrusts are involved in these mountain ranges exhibiting extreme compressional tectonism. It has been reported to the authors by several workers that some of these thrusts involve uppermost Tertiary rocks. Normal faults are

present but they are subordinate features, and the general geometry of the mountain ranges is thought to be controlled by a major wrench-fault system. The general north-south to N.10° E. orientation of these ranges suggests a second-order right lateral shear system. If the San Andreas and Walker Lane fault systems represent the western boundary, and the edge of the old shelf area represented by the Grand Wash, Hurricane, and Sevier faults is the eastern boundary, with corresponding right and left lateral movements, the greater part of the Basin and Range province should be characterized by east-west compression of a second order. The deformation exhibited reflects such compression.

Pacific Northwest Examples

Much of the area of Oregon and Washington is covered by late Tertiary volcanics which mask the effects of earlier tectonism. The most pronounced lineament consists of the chain of volcanoes extending from Mt. Shasta in California to Mt. Baker in northern Washington. This trend varies from north-south to N.18° E., the characteristic direction of the Basin and Range province. This chain of volcanoes may exist along a major wrench fault, perhaps a second-order right lateral shear. Other features which might be significant are the north-south orientation of the Willamette Valley, the northwest-southeast lineament of the Straits of Juan de Fuca, and the N.30° W. to N.35° W. orientation of the Straits of Georgia. Raisz (1945) described a pronounced series of topographic linears striking S.45° E. from the Olympic peninsula nearly to the Snake River as the Olympic-Wallowa lineament and suggested strike-slip faulting as a possible cause. Much of the east-west folding in central Washington and Oregon, reflected in the young volcanics, could represent the primary fold direction of a north-south stress system; or, in the case of the western Washington Tertiary basin, the folds extending approximately N.60° W. could be drag folds of a second-order left lateral wrench trending N.65° W., which may be part of the Coeur d'Alene lineament. Interpretation of surface mapping is hazardous in the coastal part of the Pacific Northwest because of the difficulty of seeing specific outcrops under rain-forest conditions. It is hoped that current detail work by many oil companies will contribute to the solution of the geological unknowns in this area. Sainsbury and Twenhofel (1954) suggest a strike-slip origin for several lineaments of the fiord area of southeastern Alaska. The principal directions noted are the N.10° W. alignment of Chatham Strait and the general orientation of many topographic features N.35° W., which is characteristically the San Andreas direction.

Midcontinent Examples

On the Hillside fault, which is well exposed a few miles west of Van Horn, Texas, along U. S. Highway 80, low-grade metamorphic rocks of Precambrian age are faulted against Cretaceous sandstones. The fault plane is nearly vertical, strikes N.70° W., and its trace on the surface can be followed for several miles. This fault zone, if extended northwest along its strike, would pass just south of the Sierra Blanca pluton and just north of the Malone Mountains structure. The Malone and Quitman mountains expose Jurassic and Cretaceous rocks which have been compressed into overturned and thrust-faulted folds striking generally N.45° W. The overturning and thrusting has been from southwest to northeast. The northwestern portion of the Eagle Mountains and Devil's Ridge to the east of the Quitmans constitute a similar overthrust fold. The Devil's Ridge and Quitman-Malone structural axes terminate at their intersection with the extension of the Hillside fault (Fig. 12). Farther west, the same zone is thought to be responsible for the termination of the Franklin Mountains at El Paso. Here a tilted block of little-deformed Paleozoic and Precambrian rocks standing at high elevation (the Franklins) is juxtaposed to low-lying strongly folded and faulted Cretaceous rocks which have been intruded by later porphyry (Cerro des Muleros). The entire trend from El Paso to Van Horn is a portion of the Texas or Hill lineament of Hill (1902), Ransome (1915), and Baker (1934). The interpretation of the writers is that the Hillside fault represents a large-scale left lateral wrench fault and that the Quitman-

Malone and Devil's Ridge folds are second-order drag folds relative to this wrench. The angle γ between the wrench fault and the drag folds is 29°, more or less. In the vicinity of the Sierra Blanca intrusives, overthrust sheets of the Etholen formation obscure other structural relations; these thrust sheets were probably continuous with the thrust sheets of the Devil's Ridge. North of the fault, the Cretaceous section is relatively thin and contains no rocks older than Fredericksburg (with a few minor exceptions); south of the fault, a thick sequence of pre-Fredericksburg Mesozoic sediments is present.

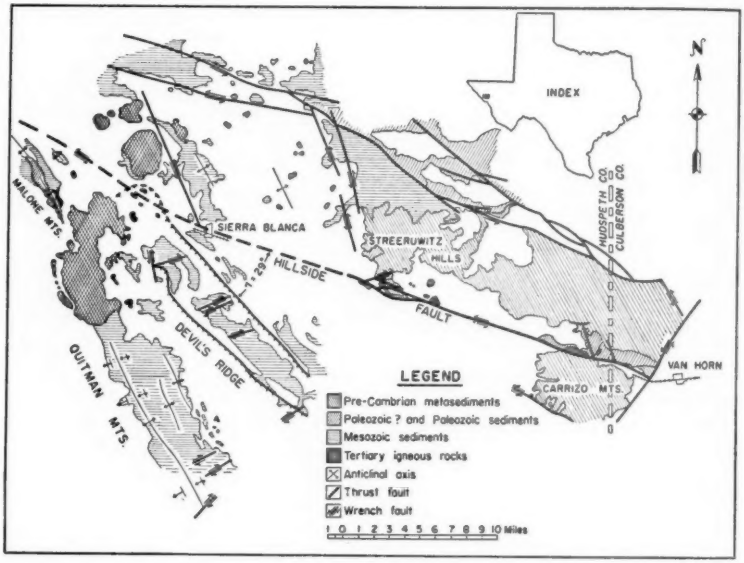

FIGURE 12.—HILLSIDE FAULT, HUDSPETH COUNTY, TEXAS

The Smoky Hills on the north side of the Wichita Mountains in southwestern Oklahoma constitute an asymmetric anticlinal fold, exposing Precambrian in its core, which strikes N.45° W. and has been called the Blue Creek Canyon anticline. The extensive Paleozoic exposures here are separated from the bulk of the Wichita Mountains to the south by the Meers Valley. A fault which has a recent scarp developed in Quaternary alluvium in this valley has long been recognized and called the Meers Valley or Thomas (*see* Harlton, 1951) fault; this fault must be nearly vertical and is considered to be one element of the boundary fault zone between the Wichita Mountain uplift to the south and the Anadarko basin to the north (Fig. 13). The Blue Creek Canyon anticline is considered to be a secondary drag fold developed from movement in Pennsylvanian time along this fault which the authors believe to be a left lateral wrench. The value of the angle γ here is 25°. The Precambrian in the core of the anticline is rhyolite porphyry, whereas most of the Precambrian of the main mountain mass south of the fault consists of granophyres and gabbroic rocks; these rocks have been cataclastically altered adjacent to the fault. However, an area of rhyolite is known in the southeastern part of the mountains.

The structural relations along the southern part of Black Knob Ridge, an Ordovician inlier in the western part of the Ouachita Mountains, Atoka County, Oklahoma, suggest wrench faulting (Fig. 14). The major fault of the area has been called the Ti Valley fault; in the opinion of Hendricks *et al.* (1947) and others, it is the surface outcrop of a very large low-angle thrust fault along which there has been extensive northwest horizontal transport. The surface trace is relatively straight, and the

fault dips at the surface are very nearly 90°. The writers believe that this portion of the Ti Valley fault is a wrench fault. The disposition of the small anticlines adjacent to this fault compressive stresses adjacent to large wrench faults.

Henson (1951, personal communication) expressed the opinion that Middle East geology is

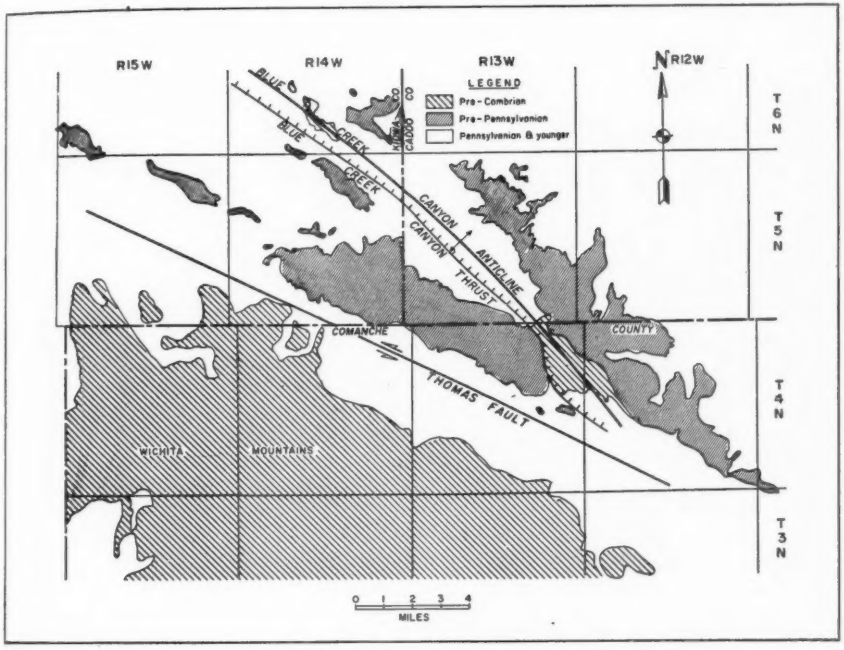

FIGURE 13.—THOMAS FAULT, WICHITA MOUNTAINS, OKLAHOMA
Adapted from Harlton (1951) and Decker (1939)

indicates that the relative motion occurred in a left lateral sense. The anticlinal axes strike N.45° E., and the trace of the fault averages N.28° E., so that the angle γ here is 17°.

Other Examples

Bucher (1933) cited the African rift system, the Rhine graben, the Triassic basins of the Appalachians, and the Great Basin country of Nevada and Utah as examples of broad-scale crustal tension. The Rhine graben which strikes roughly N.17° E. was shown by Cloos (1948) to coincide with one of his "geofractures". The four areas cited by Bucher are characterized by large-scale "high-angle normal" faulting; all may be wrench-fault zones and the associated structural features are perhaps second-order effects resulting from dominated by five major structural trends that are associated with deep-seated block faulting. He recognizes a north-south direction (the Gulf of Aquaba-Dead Sea-Jordan River trend), a northwest-southeast direction (the Red Sea and Persian Gulf shore lines), a northeast-southwest direction (the Hadhramaut coast), and two lesser subsurface directions. Cloos (1948) described the existence of an extensive system of "geofractures" in Europe which has broken the crust into blocks, which do not follow presumed fundamental structural features of the crust such as the Alps and appear to have originated far back in geologic time. From Cloos' descriptions, his "geofractures" are probably wrench faults. The Philippine fault zone as described by King and McKee (1949) appears to be a major wrench-fault zone. Wrench faulting plays an important role in

the tectonics of Taiwan (Biq Chingchang, personal communication, 1955). Extensive wrench faulting is recognized in New Zealand; Palmer's map (1940) of Cuba shows the southern coast as part of a great fault scarp which coincides in part with the north flank of

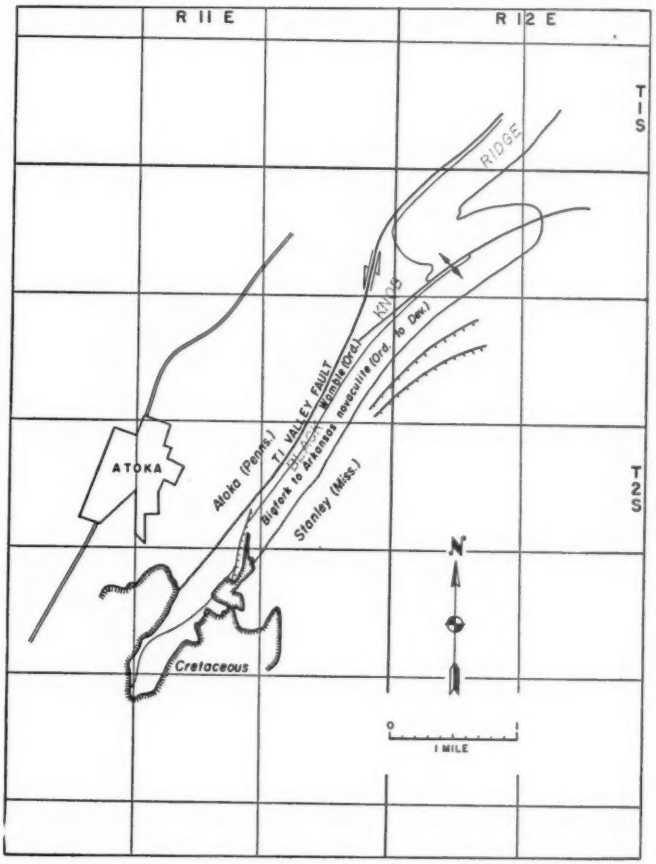

FIGURE 14.—Ti VALLEY FAULT, OUACHITA MOUNTAINS, OKLAHOMA
Adapted from Hendricks *et al.* (1947)

the Alpine fault strikes approximately N.50° E. and is a right lateral (Wellman, 1954; Gage, 1952). The "fossa magna" and "median dislocation zone" of Japan appear to have some of the characteristics of wrench-fault zones. A number of wrench faults in Britain were described by Anderson (1942). Menard's (1955) discussion of major fracture zones in the northeast Pacific suggests the existence of large wrench faults in this part of the crust.

the Bartlett trough. This great topographic feature has been considered a zone of wrench faulting by Hess (1939), Wilson (1950), and Eardley (1951); the writers concur. The Orgaños-Cayetano front in extreme western Cuba may be a wrench fault; the major fault zone extending from Cardenas to Nuevitas along the northeastern coast of the island may also be associated with left lateral wrench faulting. Many other wrench faults probably

exist in the Caribbean area. (*See* Wilson, 1940.[3]) West (1951) described major shear fractures in Alaska that the authors interpret as wrench faults. Recently Sainsbury and Twenhofel (1954) added further evidence to the existence of large-scale wrench faulting in southern Alaska. Major faulting with an important wrench component has been described in the Yellowknife area of the Canadian shield by Brown (1953; 1955). Brown (1955) states that the West Bay and associated faults are left laterals and concludes that minor faulting in the area results from movement on the West Bay system. The Rocky Mountain trench of Alberta and British Columbia in Canada is a long straight topographic feature that satisfies most of the criteria of a major wrench-fault zone. This large feature strikes N.30° W. to N.45° W. and parallels the San Andreas fault. Several recent descriptions of portions of the Grenville front in Ontario and Quebec describe tectonism which suggests large-scale wrench faulting to the present writers. (*See* Nielson, 1952; Johnston, 1954.) The system of faults extending from Bay St. George to White Bay and Notre Dame Bay in western Newfoundland as described by Betz (1943) appears to be a complex of major wrenches. Possibly the Lake Superior fault zone (Eardley, 1951) and the high-angle normal faults of eastern Missouri, southern Illinois, and western Kentucky are wrench-fault systems. A system of faults similar in many respects to the Hurricane-Sevier system of central Utah extends from El Paso to beyond Albuquerque along the Rio Grande Valley, where Kelley and Reynolds (1954) described left lateral strike-slip movement on the frontal fault of the Sandia Mountains. Jones (1952) described the distribution of volcanism and faulting in this area. Dunham (1955) described wrench faults on the northwest flank of the Arbuckle Mountains of Oklahoma and cited Ham for similar occurrences elsewhere in the Arbuckles. The Hudson and Connecticut valleys in northeastern United States and the Allegheny structural front in eastern West Virginia show features which indicate possible wrench faulting in these areas.

[3] Major wrench faults of northern Venezuela have been described in an excellent paper by Rod (1956) which appeared subsequent to the submission of this manuscript.

GEOTECTONICS

Regmatic Shear Pattern

Hobbs (1911), in a paper describing the uniformity of fractures, joints, and other lineaments throughout the world, wrote:

> "The practically uniform pattern and the like orientation within each of the orderly fracture fields, point clearly to a community of origin in stress conditions throughout an area of continental dimensions.
>
> "This recognition within the fracture complex of the earth's outer shell of an unique and relatively simple fracture pattern, common to at least a large portion of the surface, obscured though it may be in local districts through the superimposition of more or less disorderly fracture complexes, must be regarded as of the most fundamental and far reaching importance. It points inevitably to the conclusion that more or less uniform conditions of stress and strain have been common to probably the earth's entire outer shell.
>
> "The ultimate cause of this common type of deformation is presumably the continued secular cooling of the planet."

Hobbs' ideas were poorly received; however, abundant later information has been developed and published in extension of these views. Baker (1934), in summarizing his observations on the geology of Trans-Pecos Texas, wrote:

> "... brittle rocks at and near the surface, without superincumbent load of other rocks, have broken into a complicated mosaic of fault blocks by lateral slip movements in a zone under compression, producing elongated-domical or elliptical areas of uplifted ridges, the longer dimensions or axes of which are nearly parallel to the direction of lateral slippage. Therefore, they may be a consequence of thrust or shear and differ from the commonly-accepted thrust planes in that the fracturing is more nearly vertical than horizontal and the direction is more nearly parallel than at right angle to the direction of shear or thrust. Considerable rotatory or torsional effect, it would seem, would be a necessary consequence and would shatter such zones into an assemblage of angular-outlined blocks."

The investigations of Fisk (1944) in the flood plain of the Mississippi River revealed a complex system of shear-fault zones and joint systems in the unconsolidated sediments of this area.

Locke *et al.* (1940) regarded the entire crustal segment of the Sierra Nevada as part of a

regional shear zone. In discussing the tectonics of this area they said, "The answer seems to be that the longitudinal motion is fundamental, and that everything else is incidental and resultant."

Vening Meinesz (1947) described the shear pattern of the earth and investigated analytically possible origins of the required stresses. He collected information supporting Hobbs' ideas that a relatively uniform fracture pattern is common to the greater portion of the earth's surface; he implies that the stresses which yielded such a uniform shear pattern result from forces which are commonplace and worldwide. Sonder (1947), discussing Vening Meinesz's paper in connection with his own earlier publications, proposed that the worldwide shear pattern be termed the regmatic joint or shear pattern and stated,

> "I agree with Vening Meinesz that the existence of the regmatic shear pattern is a strong evidence of a rigid crust reacting elastically to tectonic forces. The strength of this force must be considerable. If this were not so, the worldwide coordination of the regmatic pattern would be impossible. The regmatic dissection runs across ocean bottoms and continental platforms as well, showing everywhere the existence of a strong, rigid, and splittable body."

Cloos (1948), describing the ancient European basement blocks, wrote:

> "The major tectonic features of our continents are generally supposed to be younger than the deformed rocks which they transgress. During the last two or three decades observations began to accumulate which prove that several, if not all, of the main fractures or fracture zones in Europe are old and have been active practically during all the tectogenetic periods of the Earth's history. This indicates that the Earth's crust was divided into polygonal fields or blocks of considerable depth or thickness during an early stage of its history. In the following, the author will speak of 'basement blocks' which are separated by 'geofractures' or 'geosutures'."

Hobbs, Vening Meinesz, and Sonder presumably included the major wrench faults as the most important surface manifestations of the regmatic joint pattern of the crust; apparently the geosutures or geofractures described by Cloos (1948) in Europe are part of the same pattern. Their evidence has been supplemented by innumerable publications covering local areas; for example, Johnston's (1954) description of a portion of the Grenville front in Ontario, Canada, may be interpreted as a major wrench-fault zone that fits into the over-all regmatic joint pattern.

Major Wrench Directions

One of the most prominent tectonic directions in the earth's crust is approximately N.30° W. to N.45° W. This direction coincides with that of major right lateral wrench faults typified by the San Andreas fault in California and is designated the San Andreas direction. (*See* Fig. 6.) The same direction is typical of the Rocky Mountain trench in western Canada, of the submarine fault scarp off the west coast of Florida, of the Red Sea, and of the west coast of Sumatra which follows major structural linears, according to Westerveld (1952).

The major tectonic directions in the Great Basin of Nevada strike from due north to N.15° E. This tectonic direction is named the Nevada direction.

The Alpine fault in New Zealand, a right lateral wrench, strikes N.50° E., as described by Wellman (1954). The tectonic direction N.45° E. to N.60° E. is therefore designated the New Zealand direction (Fig. 15). The large right lateral wrench fault in the Venezuelan Andes, extending from the Rio Santo Domingo to San Felipe and the sea, has this direction.

Another direction associated with right lateral wrench faulting is N.75° W. to N.90° W., which includes the strike of the Oca[4] fault of Venezuela and Colombia (Fig. 16). The authors refer lineaments of this strike to the Oca direction, which coincides with that of other major faults of Venezuela and Trinidad and with the southern slope of the Bay of Biscayne, the front of the Pyrenees, and the southern coast of Java. Several of the larger faults of the Transverse Range of southern California are perhaps related to this direction.

Another prominent crustal direction is approximately N.15° E. to N.35° E. as typified by the Great Glen fault in Scotland, a left lateral wrench fault; this tectonic direction is designated the Great Glen direction (Fig. 17). Other

[4] Ocoa of Sutton (1946), Rod (1956), and others. According to Gordon Young of Mene Grande Oil Company, Caracas, Venezuela, the correct spelling is Oca.

prominent tectonic features with this direction include the Grand Wash-Hurricane-Sevier fault zone of Arizona and Utah, the Ryukyu deep and the Kurile Islands, the Rhine graben in western Europe, and the Jordan-Dead Sea valley in Palestine.

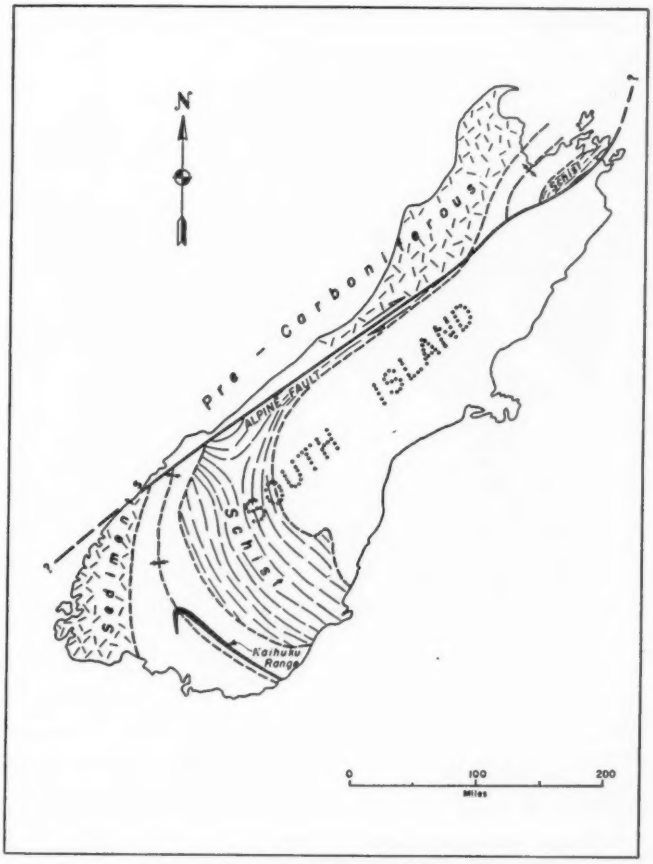

FIGURE 15.—NEW ZEALAND DIRECTION
After Wellman, Grindley, and Munden (1952)

The tectonic direction N.10° W. to N.30° W. is designated the Colombia direction since this is the strike of a large left lateral wrench fault in northern Colombia which separates the Cordillera Central from the Sierra Nevada de Santa Marta. The Oslo-Kattegat line of fractures separating Sweden from Denmark has this strike, as does the Philippine trench in the western Pacific and the Owens Valley in California. The West Bay fault system in the Yellowknife area of northwestern Canada is a left lateral wrench with this direction.

The Texas or Hill lineament, described by Hill (1902), Ransome (1915), and Baker (1934) as extending from south Texas to Los Angeles and beyond, coincides in part with a series of known or suspected left lateral wrench faults which strike N.60° W. to N.75° W. This direction is termed the Texas direction. The Hillside fault (Fig. 12) is a portion of this lineament. Other structural elements with this strike are the south flank of the Anadarko Basin in Oklahoma and the Texas Panhandle, and the Guerrero coast of Mexico.

Another well-known tectonic direction is that of the Bartlett trough in the Caribbean Sea (Fig. 18). The north flank of this deep is believed to be a fault of the left lateral type striking N.70° E.; the crustal direction N.60° E. to N.75° E. is designated the Bartlett direction. Other tectonic lines with this strike are the Guadalquivir fault in southern Spain, the Hurd deep in the English Channel, and the Bronson trough off Puerto Rico.

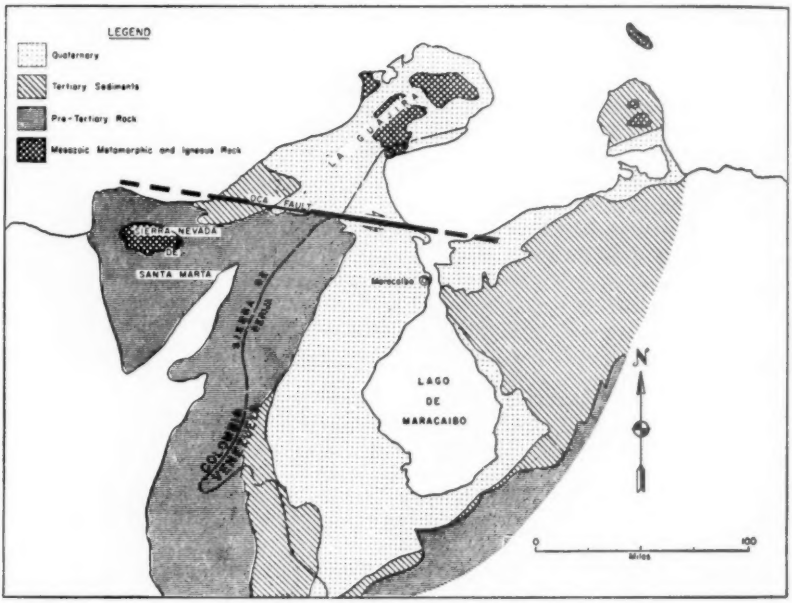

FIGURE 16.—OCA DIRECTION
Data from Geol. Soc. Amer. Map of South America (1950)

The authors believe that these eight lineament directions represent major wrench faults or geofractures along which the predominant displacement has been horizontal. Vertical movements have occurred but are of much less magnitude. The maximum elevation difference on the surface of the earth today is approximately 65,000 feet; the maximum vertical displacements on faults known to the authors are somewhat less than this. This is also the order of magnitude of the thickness of the thickest presumed conformable stratigraphic sections. On the other hand, the greatest horizontal displacement suggested for any wrench fault is 350 miles; the writers believe that vertical components of movements along elements of the regmatic shear pattern vary from as much as 50 per cent to as little as 3 or 4 per cent of the horizontal. Of course, not all wrench faults have moved hundreds of miles; on the other hand it is believed that second-order structural features of considerable proportions can be related to wrench faults where strike-slip movement is measureable in tens of miles.

Primary-Stress Orientation

The angle α has been defined above as the azimuth of the primary principal-stress direction. Anderson (1951) and Hill and Dibblee (1951) pointed out that the wrench faults observed in Britain and California respectively can have originated from a stress system which was oriented approximately meridionally (*i.e.* $\alpha = 0°$). If meridional compressional forces are assumed as generating the primary principal stresses and the primary right and left lateral wrench faults, the other six wrench directions could result as second- and third-order shears,

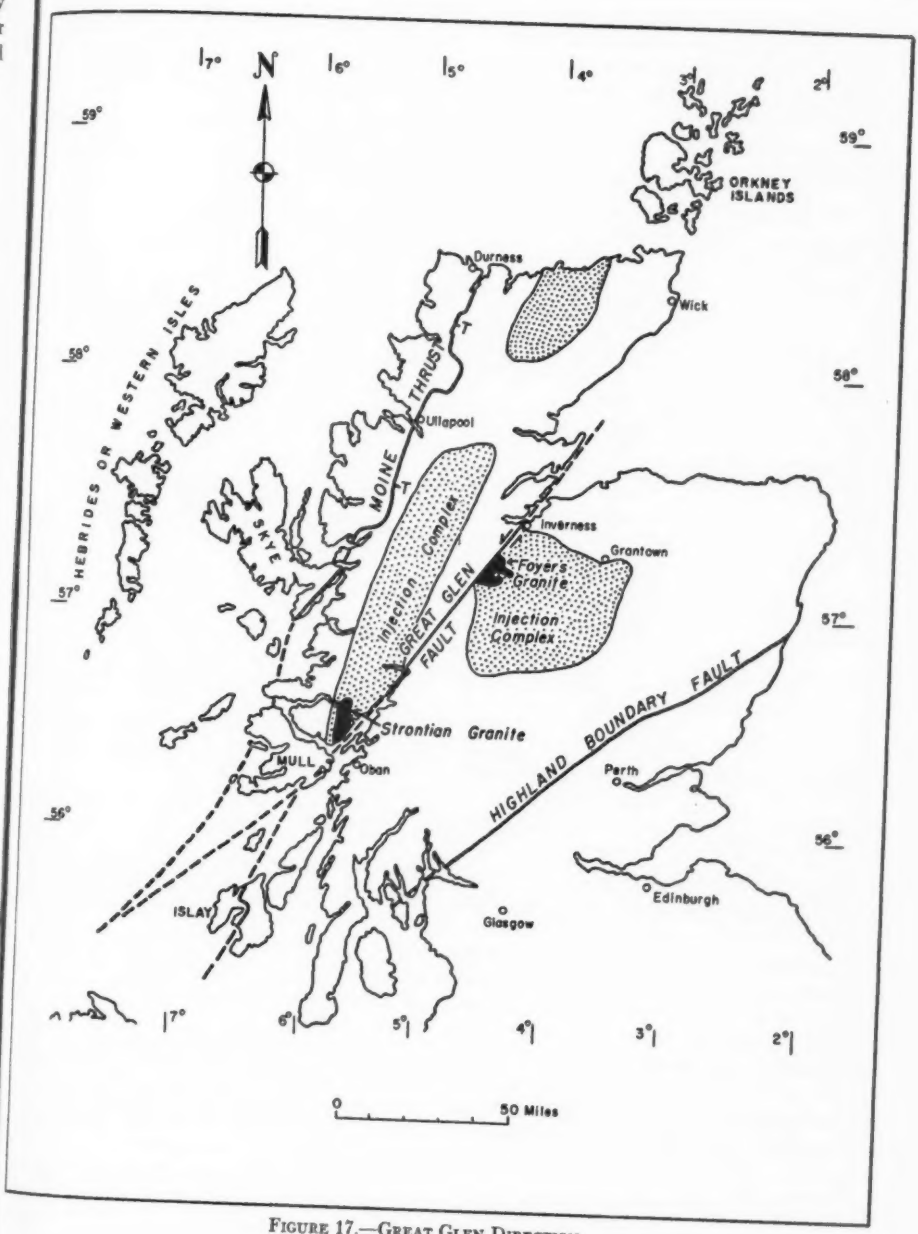

FIGURE 17.—GREAT GLEN DIRECTION
After W. A. Kennedy (1946)

as described above. Theoretically, given any direction for a primary compressional stress, there should result two first-order shears, four second-order shears, eight third-order shears, and 16 fourth-order shears. If the angle β between the principal stress and the shear remains essentially unchanged and the angle γ remains sensibly constant, the directions of the resultant lower-order shears start repeating themselves so that only eight directions result. Figure 19 shows the wrench directions which would result if the primary stress were north-south (*i.e.* $\alpha = 0°$). The prevalent directions for folding and thrusting are also shown; the second- and third-order stress directions are, of course, orthogonal to the indicated fold directions.

Figure 20 shows the resultant directions if the primary stress is oriented north-northwest ($\alpha = 345°$); the only difference is a rotation of the entire system. The direction of the primary stress may vary with latitude or perhaps other parameters. Figure 21 shows the relation between α and latitude for the Great Glen fault in Scotland, the Rhine graben in western Europe, and the Dead Sea Valley in Palestine, assuming that all three are primary left lateral wrench-fault zones. There is thus some suggestion that the wrench fault systems are gradually rotated toward the west as the equator is approached. However, in any area the relative angular relations in Figures 19 and 20 should hold.

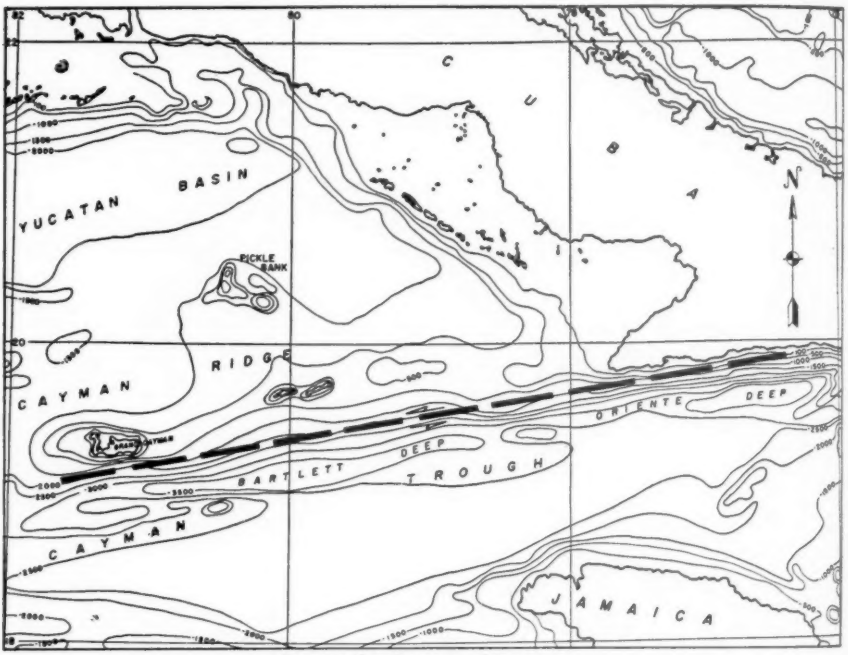

FIGURE 18.—BARTLETT DIRECTION
Depths in fathoms

The authors believe that present evidence indicates that the primary principal compressional stress direction has not varied much more than 20° to the west or east of north, and in most instances the wrench-fault systems appear to be satisfied by a primary principal-stress direction lying between due north and N.15° W. However, a symmetrical distribution of shear directions would result from primary compressional stresses oriented east-west which might exist in the earth's crust. Northwest-

southeast or northeast-southwest primary compressional stresses could generate the same shear pattern. The primary stresses may be actually east-west, or both north-south and east-west primary-stress systems may exist or have existed. However a north-south orientation for the primary principal compressional stresses seems the most reasonable in the light of the evidence at hand.

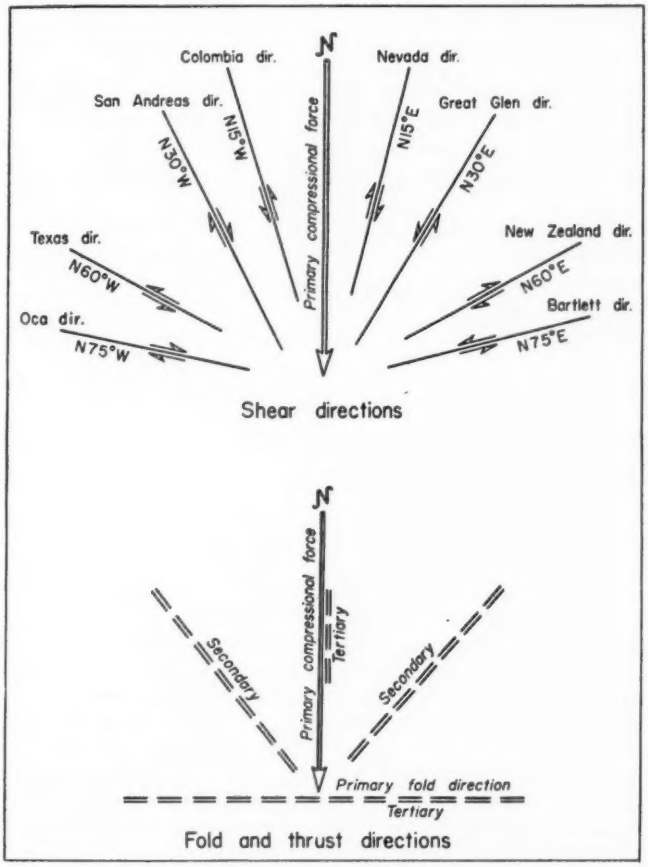

FIGURE 19.—MAJOR TECTONIC DIRECTIONS, $\alpha = 0°$

A difficult situation arises in attempting to distinguish between elements of the directions developed from primary stresses oriented so that $\alpha = 0°$ and elements which result when $\alpha \neq 0°$; the distinction can be made from the sense of the horizontal displacement only. For example, Lees' diagram (1952) of the Dead Sea Valley in Palestine (Fig. 22) shows that the relation between anticlines and faults is such that the movement must have been in a left lateral sense, so that this fault system, even though it strikes N.10° E., approximately, must be a Great Glen element resulting when $\alpha = 340°$. Such difficulties should arise only on the broadest scale, since α is thought to remain sensibly the same over fairly large segments of the crust.

Analysis of Fault Pattern of France

The directions of 176 straight faults shown on the Carte Geologique de France (1933),

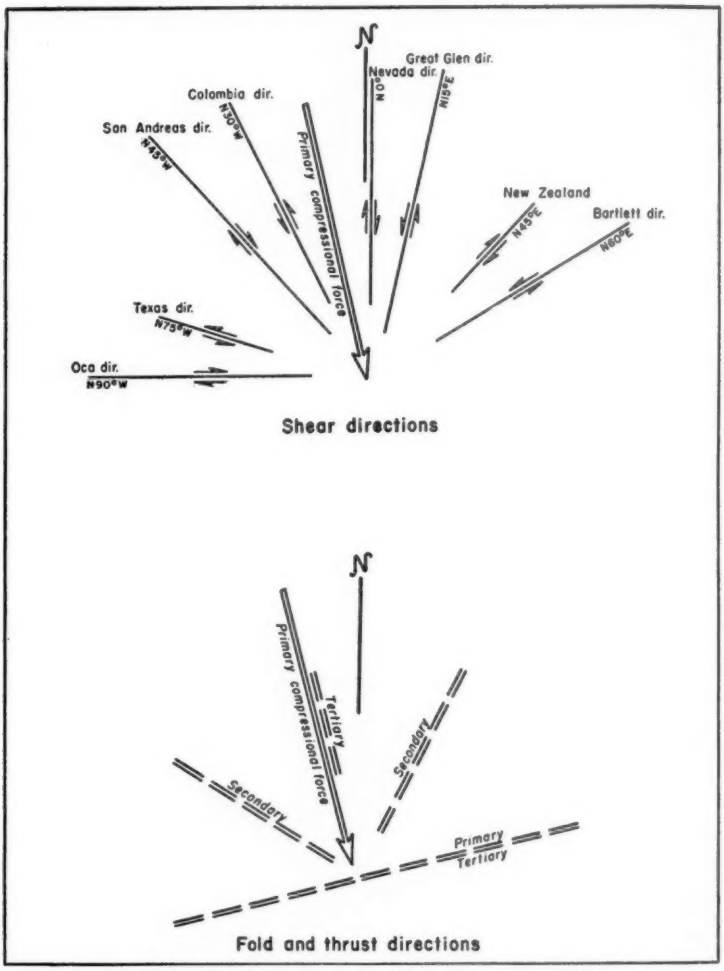

FIGURE 20.—MAJOR TECTONIC DIRECTIONS, $\alpha = 345°$

scale 1:1,000,000, are plotted on Figure 23. These measurements were not weighted for length, and it is not known how many of the included faults are normal and how many are wrench. However, the strain rosette shows five well-defined maxima with the two most prominent at N.45° W. and N.25° E. If these two maxima correspond to the primary right and left lateral directions, the primary principal-stress direction should lie halfway between them. On this basis the value for β is 35°, and the value for α is 350°. The peak at N.45° W. then corresponds to the San Andreas direction, the peak at N.25° E. corresponds to the Great Glen direction, the peak at N.50° E. corresponds to the New Zealand direction, and the peak at N.70° W. corresponds to the Texas direction.

Possible Origin of the Regmatic Shear Pattern

Apparently many major wrench faults have moved more or less continuously since their inception; in most cases they are traceable

back as far as the geologic record goes. For example, in California the San Andreas fault has been inferred to have been moving in Jurassic time; the pre-Jurassic record has been destroyed by metamorphism so that no date

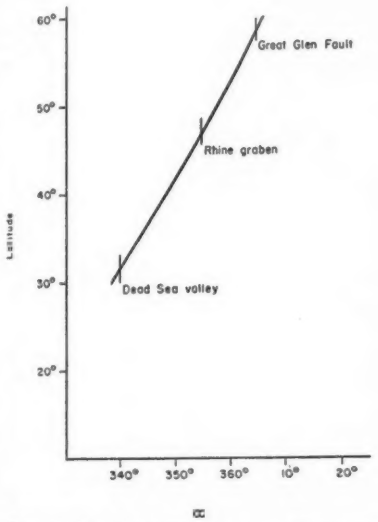

FIGURE 21.—RELATION OF α TO LATITUDE, FOR $\beta = 30°$

other than pre-Jurassic can be assigned to the origin of this fault. Cloos (1948), in describing the geofractures in Europe, states, "Great age and frequent activity can be proven for most of the central European examples." Ver Wiebe (1936) believes that the boundary fault which he postulates in the heart of the Appalachians had its inception in Precambrian time. Vening Meinesz (1947) wrote:

> "It must be realized that many of the shear planes must have been maintained throughout great parts, or perhaps the whole, of the crustal history; in all cases where forces have since worked on the crust, the chances must have been great of differential movements of the separate crustal blocks and, therefore, of new shearing along these planes. If the crust had been covered by more recent sediments, these layers must have had insufficient strength for resisting the movements, and so the shear planes must have penetrated these layers also. It may, therefore, be expected that a continuous rejuvenation of the Net has taken place at the Earth's surface. Doubtless this must have been one of the main causes of the volcanicity of the alkaline type."

There are large wrench faults which can be shown to have been active in, for example, Precambrian and Paleozoic time, on which there is no evidence of later movement. Apparently boundary faults can "heal" or lock so that no further movement occurs, and the stresses are then accommodated along other fractures. It should be emphasized that the period of geologic observations covers only a few scores of years, and it is possible that recent movements on faults believed to have been inactive since, for example, Paleozoic time may have occurred. As an illustration, the Nemaha granite ridge in Oklahoma and Kansas, believed to be associated with a major wrench-fault zone, had its main structural growth in late Paleozoic time. Lee (1954) pointed out the apparent relation between the earthquake which occurred in the area in 1952 and the outline of the Nemaha structure.

The writers believe that the origin of the regmatic joint pattern goes back to the period when the earth was very young, when the crust first evolved enough to support compression. Several different types of forces are considered to have been responsible for the genesis of the regmatic shear pattern. Subcrustal convection currents have been suggested to explain various phenomena associated with the deformation of the crust. (*See* Gutenberg, 1951; Hafner, 1951; Scheidegger, 1953; Vening Meinesz, 1954.) If subcrustal convection currents exist, they must exert a considerable drag on the base of the crust. Their orientation would perhaps be symmetrical in some fashion with the axis of rotation of the earth so that subcrustal convection currents could result in forces acting in an essentially meridional direction. Another source of compressional stress in the earth's crust is attributable to the diurnal rotation of the earth itself, possibly in association with "*Polfluchtkraft*". (*See* Gutenberg *et al.*, 1951.) Secular compression should result in consequence of cooling and contraction, as emphasized by Lees (1953), Landes (1952), and Jeffreys (1952). Possibly each of these three types of forces has had and does have large north-south components; other forces of a similar nature may be involved. These forces, which have been acting essentially continuously and in the same sense throughout geologic time, are, in the opinion of the authors, responsible

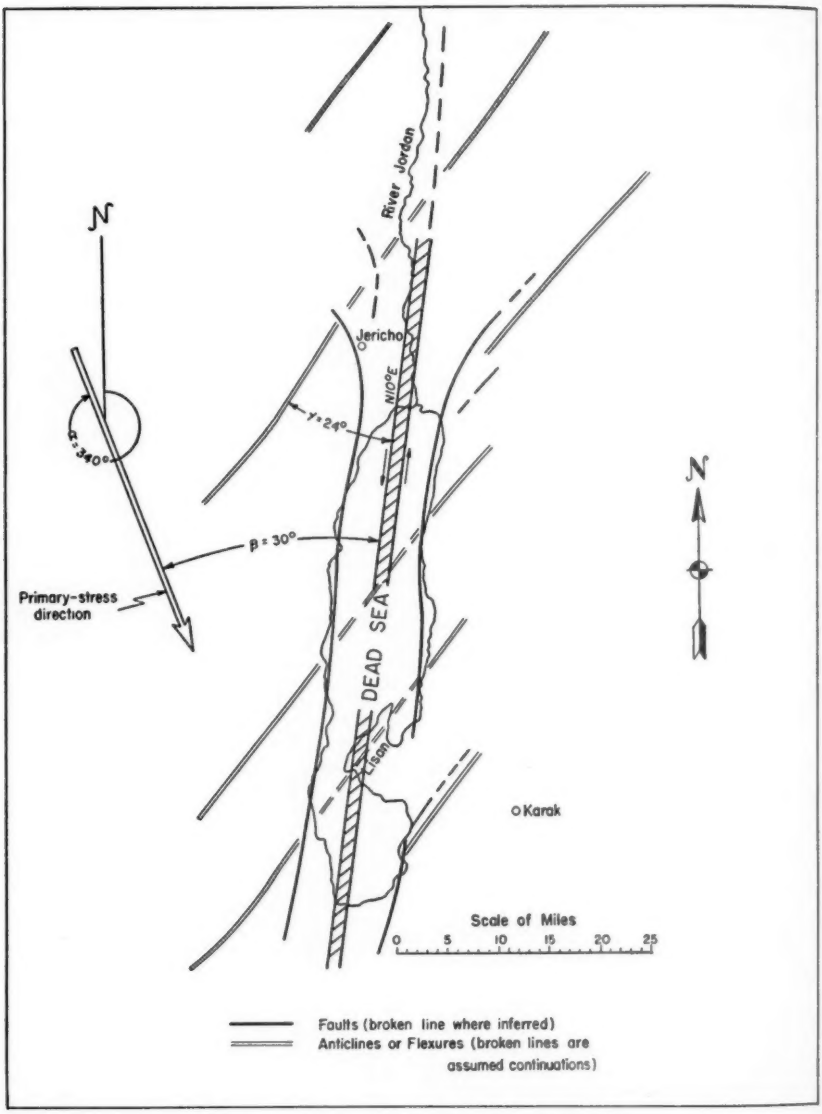

FIGURE 22.—STRUCTURAL PATTERN OF THE DEAD SEA
Modified from G. M. Lees (1952)

for the regmatic shear pattern of the earth's crust.[5]

[5] A. E. Scheidegger (1955) recently pointed out the difficulties inherent in accommodating major strike-slip movement in either the convection-current theory of orogenesis or the contraction theory as presented in the literature.

Periodic versus Aperiodic Orogeny

Gilluly (1949) stressed the aperiodic and continuing nature of crustal movement; additional support for this thesis has been developed by Spieker (1950, personal communica-

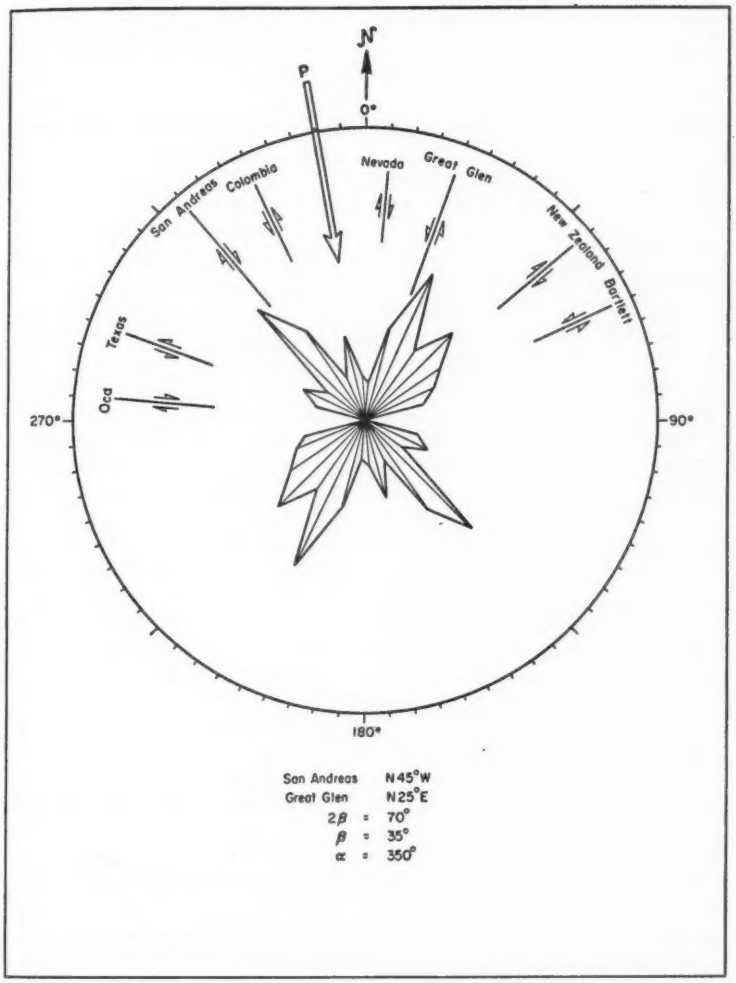

FIGURE 23.—STRAIN ROSETTE FOR 176 FAULT IN FRANCE
Taken from Carte Geologique de France (1933), scale 1:1,000,000

tion) in his studies of the Rocky Mountains. This is consistent with what might be expected if the forces of compression are associated with the rotation of the earth and related phenomena and is consistent with the extremely long history of most primary wrench faults. All the evidence indicates that compression exists and has existed continuously in a large portion of the earth's crust throughout most of geological time. Bucher (1951) wrote, "... the writer sees no escape from the conclusion that throughout recorded geological history, the earth's crust has been under tangential compression." Benioff's (1951) finding from analysis of earthquake data that energy accumulation occurs at a constant rate over periods of time of a few tens of years in a given area is consistent with this conclusion.

The culminations of crustal movement and orogeny at the end of the Paleozoic era and in later Tertiary time are well known, and orogenic cycles of less magnitude have been frequently

described in the literature. (*See* Umbgrove, 1950.) Tectonicists are thus faced with the paradox that orogeny in general is both periodic and aperiodic.

This seeming conflict can be resolved by concluding that the major crustal compression is omnipresent and results from forces derived from the rotation and precession of the earth, together with its cooling and contraction. Superimposed on this continuous force field may be a periodically variable force or group of forces which coincides with the periodic recurrence of what have been called the orogenic revolutions. It seems possible that the periodic components of compression which are required to explain the recurrence of orogenic maxima can derive from subcrustal convection currents or possibly from some extraterrestrial influence, as suggested by Umbgrove (1950).

Consequences of a Segmented Crust

The existence of a shear pattern comprised predominantly of major wrench faults results in a definite segmentation of the crust. Important components of horizontal movement on these faults, as has been demonstrated for the Great Glen fault, the Alpine fault, and the San Andreas fault, imply the existence of a surface of horizontal movement at some depth below the surface. This surface could be at Barrell's asthenosphere, or Davison's "level of no strain", or the base of the solid crust, or a zone of plastic flow. Gutenberg *et al.* (1951) give 30 to 100 km as the probable depth to the "base of the outer crust". The authors believe that the major vertical faults extend to this surface, wherever and whatever it may be, so that the solid compression-transmitting portion of the outer shell of the earth at least is divided into blocks. These blocks, bounded by major linear elements of the regmatic shear pattern, tend to be polygonal.

Hobbs (1911) mentioned as spacing between major fault components 125 miles between northeast-southwest faults, 75 miles between northwest-southeast faults, and 40 miles between north-south elements in eastern North America. Cloos (1948) suggests 175–300 miles as the breadth of major blocks in Europe. Such dimensions correspond roughly to those of areas over which isostatic adjustment is estimated to be relatively complete. The diamond-shaped block of the Philippine Basin in the Western Pacific has diagonal dimensions of roughly 1500 and 2500 miles. This shape and size are perhaps typical of megablocks bounded by two primary right lateral and two primary left lateral wrench zones.

One result of such segmentation of the crust would be that blocks or groups of blocks separated by major boundary faults could have decidedly different geological histories, as borne out in many regional geological studies.

As movement continues along the boundary faults any block could be freed from compressive forces, and thus it would be possible to have an unstressed block or blocks surrounded by stressed blocks; the unstressed block or blocks could then respond to whatever other forces to which it was subjected (for example, gravitational forces, sedimentary loading or unloading acting on its surface, or hydrostatic stresses acting on its base) and could then move vertically in response to such forces. Such a stress release could explain "isostatic adjustment" and "equilibrium" and the continued downwarping of particular crustal areas which results in what most geologists call geosynclines; it could also explain the abundant field evidence that there has been late vertical movement on vertical faults.

The development of sedimentary suites displaying most of the characteristics of geosynclinal accumulations is readily visualized (Fig. 24). Given a major boundary fault between two independent crustal blocks, minor vertical components of movement associated with the dominant strike-slip movement of the fault could be evidenced by minor tilting of these blocks so that the emergent part of one block could be apposed to the lowest part of the adjacent block. A strongly asymmetric basin would thus be formed which could accumulate sediments from two directions. Thus the fine-grained sediments accumulating from the west in the diagram could be contaminated by coarse debris eroded from the scarp of the boundary fault; this could result in mixing graywackes and conglomerates into the fine-grained clastic from the west, yielding a bimodal sediment. Major boundary faults are considered principal

avenues for movement of subterranean material upward in the crust so that volcanic and/or siliceous components could easily be added to the already complicated sediment.

A further consequence of a crust thus segmented would be that, although individual blocks or groups of blocks could show great strength, larger groups of blocks which include several major boundary faults would have very little strength insofar as vertical movements are concerned. Perhaps in this manner a second paradox which has plagued geologists for many years could be resolved.

Ver Wiebe (1936) and Weeks (1952) pointed out that most geosynclines or large basins are asymmetric and bounded on the steep flank by what Ver Wiebe termed geosynclinal boundary faults. The authors believe that these geosynclinal boundary faults are in most cases wrench faults and constitute important elements of the regmatic joint pattern. In view of the tremendous boundary fault postulated by Ver Wiebe in the Appalachian country to accommodate his stratigraphic observations, structures of the magnitude of the Appalachian chains might be related to major faults of the type described by Ver Wiebe.

One of the requirements of a contracting earth is that its surface area should decrease, as emphasized by Jeffreys (1952). In a segmented crust the surface areas of the individual blocks must decrease with continued compression; in the writers' view this contraction takes place around the edges of the major blocks in the vicinity of the boundary faults where folding and thrusting is concentrated.

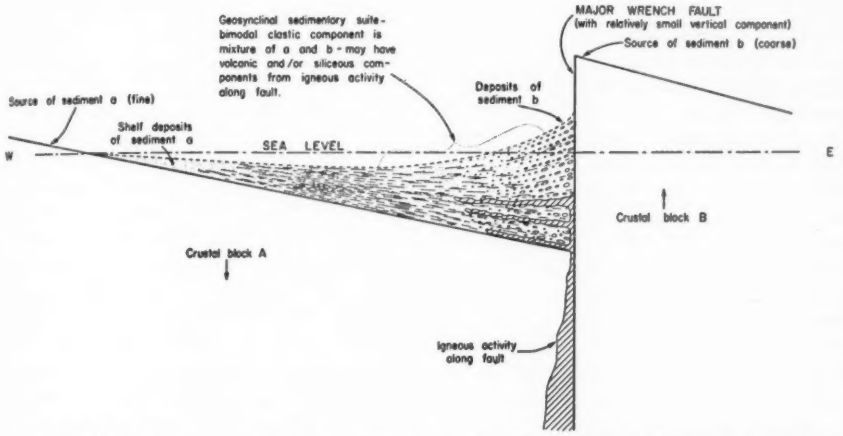
MAJOR WRENCH FAULT
(with relatively small vertical component)
Source of sediment b (coarse)
Geosynclinal sedimentary suite - bimodal clastic component is mixture of a and b - may have volcanic and/or siliceous components from igneous activity along fault.
Source of sediment a (fine)
Deposits of sediment b
Shelf deposits of sediment a
SEA LEVEL
W
E
Crustal block B
Crustal block A
Igneous activity along fault

FIGURE 24.—DIAGRAMMATIC SKETCH OF GEOSYNCLINE AND GEOSYNCLINAL SEDIMENTARY SUITE

Continued distortion of individual blocks must result in a change of shape, so that the directions of the major wrenches might vary slightly as compression continues; this is actually an increase in the angle β from the theoretical value of 31°. The magnitude of this effect is not known.

Landes (1952) developed the concept of a shrinking globe and concluded that the continental and oceanic sectors of the surface of the earth act as separate blocks or block groups and that in the course of secular cooling and accompanying contraction the oceanic blocks, or portions of them, subside while the continental blocks remain high. This would result in a deepening of the oceans and, assuming a relatively constant volume of water, the withdrawal of the seas from the continental segments. Subsequent to the subsidence of the oceanic blocks Landes considers that the continental blocks follow them down; the latter blocks are then reinundated. It is suggested that the existing average elevation difference between continental and oceanic blocks is typical of only a small portion of geologic time, and that a considerably smaller

elevation difference resulting in widespread shallow seas over large portions of the continental blocks represents a closer approach to equilibrium conditions.

These ideas are supported by the observation that practically all the sediments deposited on the continental blocks are shallow-water accumulations. The converse of this statement is apparently not true, inasmuch as recent submarine explorations have demonstrated the presence of shallow-water sediments at great depths under the oceans. At present many geologists ascribe these occurrences to turbidity currents, but some of these anomalous sediments might have accumulated more conventionally during episodes in the earth's history when the elevation differences between the continental and oceanic blocks were much less than they are now. C. L. Moody (1951), in discussing the history of the Gulf of Mexico, expressed the opinion, based on his study of the Citronelle and other formations, that during late Pliocene time at least the northern portion of the Gulf was filled with sediments. He concludes that post-Pliocene time must include 12,000 feet of collapse or subsidence in the Gulf of Mexico. M. A. Hanna (1954, personal communication) has shown, from his environmental studies of late Tertiary sediments in the Gulf coastal area, that in given localities fluctuations in depth of water on the order of 1000 feet are common.

All these effects are understandable as consequences of a segmented crust.

"Island Arcs"

In many instances the "island arcs" referred to in the literature can be resolved into sequences of straight-line segments which are believed to be associated with the regmatic joint pattern. The Aleutian Archipelago, one of the classic "island arcs", is possibly a case in point. Wilson (1950) refers to an arc along the west coast of the United States, extending from Seattle to Los Angeles, which can be resolved into two straight-line segments—one comprising the San Andreas group of wrench faults and associated structural phenomena running from Los Angeles to approximately Cape Mendocino, and the second a group of tectonic elements of the Nevada direction extending from Cape Mendocino to Seattle. (*See* Fig. 11.)

Other well-known "arcs," such as the Indonesian and Japanese groups, can be visualized as being composed in large part of linear segments which might be considered as elements of the regmatic shear pattern.

Igneous Activity

Volcanic and plutonic phenomena are known to occur in linear belts. "Serpentine" intrusives are associated in many cases with major wrench faults. Werenskiold (1953) suggested a mechanism which relates volcanic activity to large-scale geofractures. The Hawaiian Islands constitute a good example of volcanic linearity, as do the volcanoes of the Aleutians, the Solomon Islands, central Mexico, central America, and the Guinea group of West Africa. The volcanic activity of Sumatra is believed by Westerveld (1952) to be associated with the well-known longitudinal fault trough, which the writers believe is the locus of a major right lateral wrench-fault zone. Figure 25, taken from Cloos (1948), illustrates an alignment of igneous activity which includes a relatively large span of time as well as a relatively large range of composition.

The authors agree with Werenskiold that geofractures constitute the type of crustal flaws most likely to permit extensive magmatic activity.

The association of many important types of ore deposits with both major and minor vertical shears, especially with shear-zone intersections, is well known. Wallace *et al.* (1953) described the Coeur d'Alene district in Idaho and Montana in such terms, and the association of important mineralization with left lateral wrench faults in the Yellowknife area of northwestern Canada has been cited by Brown (1955). Albritton *et al.* (1954) related the ore deposits of the Goodsprings district of Nevada to faulting of the type described here.

Crustal Evolution

Lawson (1932) concluded that the "sialic" continental masses were derived from an original "simatic" crust. Bucher (1950) suggested that the primordial crust of the earth

was basic and of essentially the same composition as the stony meteorites, and that the granitic components of the crust have resulted from continued erosion, sedimentation,

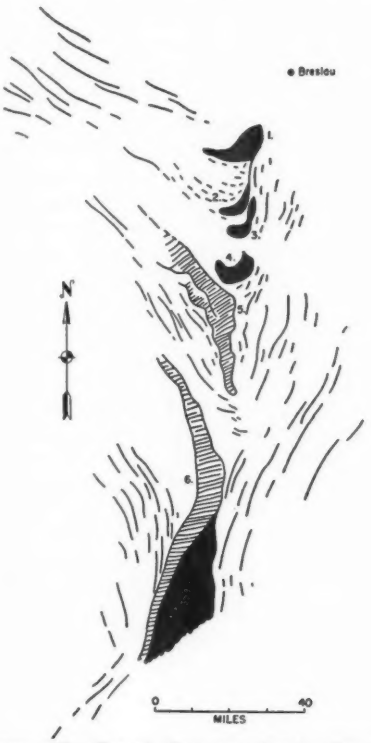

FIGURE 25.—CLOOS' SILESIAN SHEAR ZONE
Long lines are trends of the folded Paleozoic (and older?) sediments and crystalline schists:
(1) The serpentine pluton of Mount Zobten
(2) "Syenit" of Nimptsch
(3) Serpentine pluton of Frankenstein (with the well-known nickel mines)
(4) The "Syenite" of Glatz-Reichenstein
(5) The Cretaceous fault trough of the Neisse valley
(6) The Permian depression of Boskowitz
(7) The Paleozoic pluton of Brunn (Brno) in Czechoslovakia

chemical sorting, and metamorphism—metasomatism of the primary basic crust. Paige (1954) reiterated the same ideas, with which the present authors agree.

Most of what is known about geological history and geological processes could result from a crust originally of approximately stony meteoritic composition, which was and is subjected to a force field resulting from the earth's daily rotation and shifting upon its axis, the continued cooling and contraction of the earth, subcrustal convection currents, and other effects predictable from the laws of physics. The principal strains impressed upon such a crust by these forces are evidenced by the regmatic shear pattern and associated structural phenomena; horizontal movements have been predominant, and vertical movements are subordinate features which have resulted in erosion, sedimentation, and the consequent development of the geological record.

Inasmuch as the regmatic shear pattern is an observed fact, the inferences drawn above provide support for the theses that the earth is and has been a cooling and contracting body, that early in its history it was molten at the surface and later developed a solid outer crust, and that a level of no strength or at least of reduced strength exists at unknown depth.

CONCLUSION

Summary

The main concepts and conclusions presented in this paper are:

(1) Wrench faulting is much more prevalent than ordinarily supposed.

(2) There exists a regmatic shear pattern common to the entire outer crust of the earth.

(3) The major elements of this shear pattern are extremely large wrench faults which extend through the outer crust. Movement on these wrench faults has been dominantly horizontal and has resulted in wholesale segmentation of the outer crust of the earth.

(4) Second-order features developed as a consequence of movement on these large geofractures constitute a major portion of the large- and small-scale compressive phenomena of the earth's crust.

(5) Present limited data suggest that the major elements of the regmatic shear pattern tend to be aligned in eight directions. These eight directions possibly resulted from primary compressional stresses whose orientation did not vary more than a few degrees from

north-south, although this orientation is not unique.

Deductions and inferences which can be derived from the presentation are as follows:

Early in the history of formation of the crust of the earth compressional forces generated a primary pattern of major shears, which were essentially wrench faults and divided the crust of the earth into polygonal blocks. Movement on many of these boundary faults, although intermittent, has been almost continuous. The type of movement has been strike-slip with relatively small vertical components. This original segmentation of the crust into isolated blocks has controlled subsequent deformation.

Continued movements on the boundary faults have variously stressed individual blocks; in conjunction with continuous widespread compression in the crust, this has had two important results. First, the surface areas of those blocks which were supporting or transmitting crustal compression tended to reduce; second, the shapes of those same blocks tended to change from polygons with north-south elongation to polygons with east-west elongation. Both of these changes were effected by the development of lower-order strains in the individual blocks.

In general, the areal reduction took place along the edges of the blocks by means of second-order fold and thrust-fault systems. The shape change took place by megabrecciation involving lower-order wrench faults. In the event shifting of the major blocks resulted in unstressing (in a horizontal compressional sense) a given block, that block would then collapse by dominantly vertical movement along the pre-existing shear pattern comprised of lower-order wrench faults. Thus, it should be fairly common to see vertical-fault systems which satisfy the directions of a theoretical wrench-fault system but on which the later increments of movement have been essentially vertical. Such faults, having the appearance of high-angle normal or reverse faults, may have originated as wrench faults in response to horizontal compressive stresses.

In general, the parameters α (the azimuth of primary principal stress), β (the angle of shear), and γ (the angle of drag folding) determine the geometry of the wrench-fault tectonic systems in any given area. The writers believe that secondary stresses which result in variations in the orientation of the stress ellipsoid, both vertically and horizontally, and variations in the values of α, β, and γ have in most cases resulted in relatively minor deviations and curvatures impressed on the theoretically derived shear surfaces.

Suggestions for Further Study

Careful reinterpretation of mapped areas is warranted. The need for accurate measurements of the geometry of faults, anticlines, and other structural phenomena is apparent. If the concepts are correct they must stand up under critical field mapping.

Statistical analyses of the strikes of structural and topographic linears across the surface of the earth should support or refute the hypotheses presented here. Data available to the authors are too limited for any such widespread analysis.

The matter of time of genesis of faults of various directions in various parts of the crust needs to be examined carefully. Many of the large wrench faults of the regmatic shear pattern may be as old as the rigid crust of the earth, but many other wrenches have developed subsequent to the initial rupturing of the crust. The time relations of the various faults and the history of movement on each fault certainly require detailed analysis.

It is hoped that mathematical analysis can support at least some of the theses developed here. Modern electronic computers should make solutions to the partial differential equations concerning stress and strain available; Inglis' work (1913) might well be extended using various values for β (45° was used in the original work) and assuming various amounts of stress relief and varying boundary conditions.

Macelwane *et al.* (1933) made a preliminary study of earthquakes with respect to tectonism; records of tectonic earthquakes should be re-examined in the light of the concepts presented above. According to Hodgson *et al.* (1952), 11 of 18 circum-Pacific earthquakes recently investigated are related to "transcurrent" faulting, and most of the others have large transverse components.

Scale-model experimentation should yield valuable data in studying the regmatic shear pattern and determining its origins.

In view of the possibility of as much as 350 miles of horizontal movement along the larger geofractures, many stratigraphic maps (such as lithofacies maps, isopachous maps, formation-distribution maps, paleogeographic maps, paleogeological maps) should be reconstructed on "palinspastic" principles as set forth by Kay (1945).

Possible Objections to the Thesis

The large gravity anomalies associated with areas of active tectonism such as the East Indies (Vening Meinesz, 1954) have been interpreted as resulting from crustal conditions radically different from those postulated here. Although these anomalies are large in magnitude, they are not broad and probably arise from density differences in the outer crust, not more than 20 miles below the surface. Is it possible that the occurrence of large negative and positive gravity anomalies, linearly distributed as these are, arise from the juxtaposition of rocks of greatly different density by means of large-scale wrench faulting? Ewing and Worzel (1954) consider that the large negative gravity anomaly associated with the Puerto Rico trench is caused by a great thickness of sediments in the trench.

Benioff (1954) and Gutenberg and Richter (1954) interpreted the foci of shallow, intermediate, and deep earthquakes as occurring in tremendous thrust zones extending about 700 km into the earth's outer layers. Intermediate and deep foci occur at depths which are below the base of what is here considered the outer crust, and these phenomena are more likely related to subcrustal convection currents than to crustal deformation. Horizontal displacements along major wrench faults which extend to the base of the outer crust might result in anomalous velocity distributions which would have to be taken into account in plotting foci of shallow, intermediate, and deep earthquakes.

The oldest rocks whose ages have been determined (Marble *et al.*, 1952) are associated with granitic rocks, and some of the oldest sediments contain arkosic debris. This argues against the suggestion made by Lawson (1932), Bucher (1950), Paige (1954; 1955), and the present writers that the crust was originally basic and that the development of the granitic suite of rocks is a result of normal evolution of the crust. These observations are valid; however, in view of the estimated age of the earth with respect to the greatest age measured for a rock there is no reason to presume that original crustal samples should be preserved at that advanced stage in the history of the crust.

It has been objected that, with the eight wrench directions allowed in conjunction with variations of about 15° in the magnitude of the angles α, β, and γ, any shear on the face of the earth can be made to fit the hypothetical pattern. Even if this were true it would not invalidate the hypothesis but merely indicate that discretion must be exercised in assigning any shear to a type direction. Of the eight shear directions postulated, four are left lateral and four are right lateral so that, insofar as it is possible to determine the sense of movement on a wrench fault, there should be no overlapping between wrenches of the same type.

References Cited

Albritton, C. C., Jr., Richards, A., Brokaw, A. L., and Reinemund, J. A., 1954, Geologic controls of lead and zinc deposits in Goodsprings (Yellow Pine) district, Nevada: U. S. Geol. Survey Bull. 1010, 111 p.

Anderson, E. M., 1942; 1951, The dynamics of faulting: Edinburgh, Oliver and Boyd, 206 p. (rev. ed. 1951)

Baker, C. L., 1934, Major structural features of Trans-Pecos Texas: Univ. Texas Bur. Econ. Geology Bull. 3401, p. 137–214

Benioff, H., 1951, Global strain accumulation and release as revealed by great earthquakes: Geol. Soc. America Bull., v. 62, p. 331–338

—— 1954, Orogenesis and deep crustal structure—additional evidence from seismology: Geol. Soc. America Bull., v. 65, p. 385–400

Betz, F., Jr., 1943, Late Paleozoic faulting in western Newfoundland: Geol. Soc. America Bull., v. 54, p. 687–706

Billings, M. P., 1954, Structural geology: 2nd ed., N. Y., Prentice-Hall, 514 p.

Brown, I. C., 1953, Late faults in the Yellowknife area, Canada (Abstract): Geol. Soc. America Bull., v. 64, p. 1401

—— 1955, Late faults in the Yellowknife area: Geol. Assoc. Canada Proc., v. 7, p. 123–138

Bucher, W. H., 1933, The deformation of the earth's crust: Princeton, N. J., Princeton Univ. Press, 518 p.

Bucher, W. H., 1950, Megatectonics and geophysics: Am. Geophys. Union Trans., v. 31, p. 495–507
—— 1951, Fundamental properties of orogenic belts: Am. Geophys. Union Trans., v. 32, p. 514–517
Cloos, H., 1948, The ancient European basement blocks—preliminary note: Am. Geophys. Union Trans., v. 29, p. 99–103
Cotton, C. A., 1950, Tectonic scraps and fault valleys: Geol. Soc. America Bull., v. 61, p. 717–758
Crowell, J. C., 1952, Lateral displacement on the San Gabriel fault, southern California (Abstract): Geol. Soc. America Bull., v. 63, p. 1241–1242
Decker, C. E., 1939, Progress report on the classification of the Timbered Hills and Arbuckle group of rocks, Arbuckle and Wichita Mountains, Oklahoma: Okla. Geol. Survey Circ. 22, 62 p.
Dunham, R. J., 1955, Pennsylvanian conglomerates, structure and orogenic history of Lake Glassen area, Arbuckle Mountains, Oklahoma: Amer. Assoc. Petroleum Geologists Bull., v. 39, p. 1–30
Eardley, A. J., 1951, Structural geology of North America: N. Y., Harper and Bros., 624 p.
Ewing, M., and Worzel, J. L., 1954, Gravity anomalies and structure of the West Indies. Part I: Geol. Soc. America Bull., v. 65, p. 165–174
Ferguson, Henry G., and Muller, Siemon W., 1949, Structural geology of the Hawthorne and Tonopah quadrangles, Nevada: U. S. Geol. Survey Prof. Paper 216, 55 p.
Ferguson, H. G., Muller, S. W., and Cathcart, S. H., 1953, Geology of the Coaldale quadrangle, Nevada: U. S. Geol. Survey Geol. Quadrangle Map
Ferguson, H. G., Muller, S. W., and Roberts, Ralph J., 1951a, Mount Moses quadrangle, Nevada: U. S. Geol. Survey Geol. Quadrangle Map
—— 1951b, Winnemucca quadrangle, Nevada: U. S. Geol. Survey Geol. Quadrangle Map
Fisk, H. N., 1944, Geological investigations of the alluvial valley of the lower Mississippi River: War Dept., Corps of Engineers
Gage, M., 1952, Transcurrent faulting in New Zealand tectonics (Abstract): Geol. Soc. America Bull., v. 63, p. 1380
Gilbert, G. K., 1874, Preliminary geological report, expedition of 1872: U. S. Geog. and Geol. Surveys W. 100th Mer. Progress Rept., p. 48–52
—— 1875, Report on the geology of portions of Nevada, Utah, California, and Arizona, examined in the years 1871 and 1872: U. S. Geog. and Geol. Surveys W. 100th Mer. Rept., v. 3, p. 41
—— 1928, Studies of Basin-Range structure: U. S. Geol. Survey Prof. Paper 153, 92 p.
Gilluly, J. B., 1949, Distribution of mountain building in geologic time: Geol. Soc. America Bull., v. 60, p. 561–590
Gregory, Herbert E., 1950, Geology and geography of the Zion Park region, Utah and Arizona: U. S. Geol. Survey Prof. Paper 220, 200 p.
Gutenberg, B., *et al.*, 1951, Internal constitution of the earth: N. Y., McGraw-Hill Book Co., 438 p.
Gutenberg, B., and Richter, C. F., 1954, Seismicity of the earth: Princeton, N. J., Princeton Univ. Press, 273 p.
Hafner, W., 1951, Stress distributions and faulting: Geol. Soc. America Bull., v. 62, p. 373–398
Ham, C. K., 1949, Geology of Las Trampas Ridge: Calif. Div. Mines Special Rept. 22, 26 p.
Harlton, Bruce, 1951, Faults in sedimentary part of Wichita Mountains of Oklahoma: Am. Assoc. Petroleum Geologists Bull., v. 35, p. 988
Hendricks, T. A., *et al.*, 1947, Geology of the western part of the Ouachita Mountains of Oklahoma: U. S. Geol. Survey Oil and Gas Inv. Prelim. Map 66
Hess, H. H., 1939, Island arcs, gravity anomalies and serpentine intrusions; a contribution to the ophiolite problem: 17th Internat. Geol. Cong. U.S.S.R. Rept., v. 2, p. 263–283
Hewett, D. F., 1955, Structural features of the Mohave Desert region, p. 377–390 *in* Poldevaart, A. (Editor), Crust of the Earth: Geol. Soc. America Special Paper 62, 762 p.
Hill, Mason L., 1947: Classification of faults: Am. Assoc. Petroleum Geologists Bull., v. 31, p. 1669
Hill, Mason L., and Dibblee, T. W., Jr., 1953, San Andreas, Garlock and Big Pine faults, California: Geol. Soc. America Bull., v. 64, p. 443–458
Hill, R. T., 1902, The geographic and geologic features, and their relation to the mineral products of Mexico: Am. Inst. Min. Engineers Trans., v. 32, p. 163–178
Hobbs, W. H., 1911, Repeating patterns in the relief and in the structure of the land: Geol. Soc. America Bull., v. 22, p. 123–176
Hodgson, J. H., 1955, Direction of faulting in Pacific earthquakes: Geofisica Pura e Applicata (Milano), v. 32, p. 31–42
Hodgson, J. H., and Storey, T. S., 1954, Direction of faulting in some larger earthquakes of 1949: Seismol. Soc. America Bull., v. 44, p. 57–83
Hodgson, J. H., *et al.*, 1952, Progress report on the fault plane project (Abstract): Geol. Soc. America Bull., v. 63, p. 1354
Hubbert, M. K., 1951, Mechanical basis for certain familiar geologic structures: Geol. Soc. America Bull., v. 62, p. 355–372
Inglis, C. E., 1913, Stresses in a plate due to the presence of cracks and sharp corners: Inst. Naval Architects Trans., v. 55, p. 114
Jeffreys, H., 1952, The earth: 3rd ed., Cambridge, England, Cambridge Univ. Press, 392 p.
Johnston, W. G. Q., 1954, Geology of the Temiskaming-Grenville contact southeast of Lake Temagami, northern Ontario, Canada: Geol. Soc. America Bull., v. 65, p. 1047–1074
Jones, S. M., 1952, Postlaramide structural and volcanic trends in New Mexico (Abstract): Geol. Soc. America Bull., v. 63, p. 1333
Kay, M., 1945, Paleogeographic and palinspastic maps: Am. Assoc. Petroleum Geologists Bull., v. 29, p. 426–450
Kelley, V. C., 1955, Tectonic history of the Colorado Plateau (Abstract): Geol. Soc. America Bull., v. 66, p. 1583
Kelley, V. C., and Reynolds, C. B., 1954, Structure of the Sandia Mountains, New Mexico (Abstract): Geol. Soc. America Bull., v. 65, p. 1272
Kennedy, W. A., 1946, The Great Glen fault: Geol. Soc. London Quart. Jour., v. 102, p. 41
King, P. B., and McKee, E. M., 1949, Terrain dia-

grams of the Philippine Islands: Geol. Soc. America Bull., v. 60, p. 1829–1836
Landes, K. K., 1952, Our shrinking globe: Geol. Soc. America Bull., v. 63, p. 225–240
Lawson, A. C., 1932, Insular arcs, foredeeps, and geosynclinal seas of the Asiatic Coast: Geol. Soc. America Bull., v. 43, p. 353–381
Lawson, A. C., *et al.*, 1908, The California earthquake of April 18, 1906: Washington, D. C., Carnegie Inst. Washington, 451 p.
Lee, Wallace, 1954, Earthquake and Nemaha anticline: Am. Assoc. Petroleum Geologists Bull., v. 38, p. 338–340
Lees, G. M., 1952, Foreland folding: Geol. Soc. London Quart. Jour., v. 108, p. 1–34
—— 1953, The evolution of a shrinking earth: Geol. Soc. London Quart. Jour., v. 109, p. 217–257
Levorsen, A. I. (Chairman), Geologic map of South America: Geol. Soc. America
Locke, Augustus, Billingsley, Paul, and Mayo, Evans B., 1940, Sierra Nevada tectonic pattern: Geol. Soc. America Bull., v. 51, p. 513–540
Macelwane, J. B., *et al.*, 1933, Seismology: Washington, D. C., Natl. Research Council, 223 p.
Mackin, J. H., 1955, Relationship between deformation and igneous activity in the Colorado Plateau-Basin Range transition zone in southwestern Utah (Abstract): Geol. Soc. America Bull., v. 66, p. 1592–1593
Marble, J. P., *et al.*, 1952, Symposium on the measurement of geologic time: Am. Geophs. Union Trans., v. 33, p. 149–203
McKinstry, H. E., 1953, Shears of the second order: Am. Jour. Sci., v. 251, p. 401–414
Menard, Henry W., 1954, Topography of the northeastern Pacific sea floor: Am. Assoc. Petroleum Geologists Bull., v. 39, p. 236
—— 1955, Deformation of the northeastern Pacific basin and the west coast of North America: Geol. Soc. America Bull., v. 66, p. 1149–1198
Michel-Lévy, M., 1933, Carte geologique de France (echelle 1:1,000,000): Institut Cartographique de Paris
Moody, C. L., 1951, Observations on the geologic history of the Gulf of Mexico: Tulsa Geol. Soc. Digest, v. 19, p. 29–33
Nielson, J. M., 1952, Fault pattern of the Mistassini region, northern Quebec (Abstract): Geol. Soc. America Bull., v. 63, p. 1285–1286
Ogle, B. A., 1952, Major shear zone at False Cape, Humboldt Co., California (Abstract): Geol. Soc. America Bull., v. 63, p. 1341
Paige, S., 1912, Description of the Llano-Burnet quadrangles, Texas: U. S. Geol. Survey Folio, 16 p.
—— 1954, Influence of cyclic processes on the evolution of the earth's crust: Geol. Soc. America Bull., v. 65, p. 707–708
—— 1955, Sources of energy responsible for the transformation and deformation of the earth's crust, p. 331–342 *in* Poldevaart, A. (Editor), Crust of the earth: Geol. Soc. America Special Paper 62, 762 p.
Palmer, R. H., 1940, Geology and oil prospects of Cuba: 8th Ann. Sci. Cong. Proc., v. 4, p. 627–637
Picard, L., 1954, Disharmonic faulting in the Jordan-Araba graben: 19th Internat. Geol. Cong. (Algiers) Proc., fasc. 21, p. 213
Raisz, E., 1945, The Olympic-Wallowa lineament: Amer. Jour. Sci., v. 243A, p. 479
Ransome, F. L., 1915, Tertiary orogeny of the North American cordillera and its problems, chap. 6 *in* Problems of North American geology: New Haven, Conn., Yale Univ. Press, 369 p.
Roberts, Ralph J., 1951, Geology of the Antler Peak quadrangle, Nevada: U. S. Geol. Survey Geologic Quadrangle Map
Rod, E., 1956, Strike-slip faults of northern Venezuela: Am. Assoc. Petroleum Geologists Bull., v. 40, p. 457–476
Sainsbury, C. L., and Twenhofel, W. S., 1954, Fault patterns of southeastern Alaska (Abstract): Geol. Soc. America Bull., v. 65, p. 1300
Scheidegger, A. E., 1953, Examination of the physics of theories of orogenesis: Geol. Soc. America Bull., v. 64, p. 127–150
—— 1955, The physics of orogenesis in the light of new seismological evidence: Royal Soc. Canada Trans., v. XLIX, p. 65–93
Shepard, Francis P., and Emery, K. O., 1941, Submarine topography off the California coast: canyons and tectonic interpretation: Geol. Soc. America Special Paper 31, 171 p.
Sonder, R. A., 1947, Discussion of shear patterns of the earth's crust, by F. A. Vening Meinesz: Am. Geophys. Union Trans., v. 28, p. 939–945
Steinbrugge, Karl V., and Moran, Donald F., 1954, An engineering study of the southern California earthquake of July 21, 1952, and its aftershock: Seismol. Soc. America Bull., v. 44, p. 201–462
Suess, E., 1885, Face of the earth (Das Antlitz der Erde): English translation by H. B. C. Sollas under direction W. J. Sollas, N. Y., Oxford Univ. Press, 1904–1925, 5 v.
Sutton, F. A., 1946, Geology of Maracaibo basin, Venezuela: Am. Assoc. Petroleum Geologists Bull., v. 30, p. 1621–1741
Taliaferro, N. L., 1951, Geologic guidebook of the San Francisco bay counties: Calif. Div. Mines Bull. 154, 392 p.
Umbgrove, J. H. F., 1950, Symphony of the earth: The Hague, Holland, Martinus Nijhoff, 220 p.
Vening Meinesz, F. A., 1947, Shear patterns of the earth's crust: Am. Geophys. Union Trans., v. 28, p. 1–61
—— 1954, Indonesian archipelago: a geophysical study: Geol. Soc. America Bull., v. 65, p. 143–164
Ver Wiebe, W. A., 1936, Geosynclinal boundary faults: Am. Assoc. Petroleum Geologists Bull., v. 20, p. 910–938
Wallace, R. E., *et al.*, 1953, Structural setting of the Coeur d'Alene mining district, Idaho-Montana (Abstract): Geol. Soc. America Bull., v. 64, p. 1486
Weeks, L. G., 1952, Factors of sedimentary basin development that control oil occurrence: Am. Assoc. Petroleum Geologists Bull., v. 36, p. 2071–2124
Wellman, H. W., 1954, Active transcurrent faulting in New Zealand (Abstract): Geol. Soc. America Bull., v. 65, p. 1322
Wellman, H. W., Grindley, G. W., and Munden, F. W., The alpine schists and the upper Triassic of Harpers Pass (sheet S52), South Island, New Zealand: Royal Soc. New Zealand Trans. and Proc., v. 80, pt. 2, p. 213–227

Werenskiold, W., 1953, Faults and volcanoes: Am. Geophs. Union Trans., v. 34, p. 110–111

West, S. S., 1951, Major shear fractures of Alaska and adjacent regions: Am. Geophs. Union Trans., v. 32, p. 81–86

Westerveld, J., 1952, Quaternary volcanism on Sumatra: Geol. Soc. America Bull., v. 63, p. 561–594

Wilson, C. C., 1940, Los Bajos fault of south Trinidad, B. W. I.: Amer. Assoc. Petroleum Geologists, v. 24, p. 2102–2126

Wilson, J. T., 1950, An analysis of the pattern and possible cause of young mountain ranges and island arcs: Geol. Assoc. Canada Proc., v. 3, p. 141–166

—— 1953, On grabens, rifts, major wrench faults, and straight chains of islands (Abstract): Am. Geophys. Union Trans., v. 34, p. 350

Gulf Oil Corp., P. O. Box 1290, Ft. Worth, Texas; Western Gulf Oil Co., 1200 Statler Center, Los Angeles 17, Calif.

Manuscript Received by the Secretary of the Society, August 18, 1955

Publication Authorized by Gulf Oil Corporation

BULLETIN OF THE GEOLOGICAL SOCIETY OF AMERICA
VOL. 67, PP. 1247-1258, 2 FIGS. SEPTEMBER 1956

COMPOSITION OF ORGANIC MATTER IN MARINE SEDIMENTS: PRELIMINARY DATA ON HYDROCARBON DISTRIBUTION IN BASINS OFF SOUTHERN CALIFORNIA

BY WILSON L. ORR AND K. O. EMERY

ABSTRACT

As part of a program to evaluate the influence of environment on the composition of organic matter in marine sediments and the changes in composition that occur in the upper zones of sediment, cores from several basins representing different environments off southern California were examined for extractable organic matter, hydrocarbon content, and certain other properties. The data are of particular interest in considerations of the early stages of petroleum formation.

Hydrocarbon fractions were separated from extractable organic matter by chromatography on alumina. This technique permitted semiquantitative separations of a paraffin-naphthene hydrocarbon fraction and an aromatic fraction. The aromatic fraction, in the present work, contained large amounts of nonhydrocarbon aromatic compounds, and a more refined procedure seems necessary for a detailed study of aromatic hydrocarbon distribution.

While the number of samples is too small to allow definite geologic conclusions, the following are indicated:

(1) The sediment in the shallowest basin with the fastest sedimentation rate contains the highest proportion of material soluble in organic solvents and the highest hydrocarbon content even though this sediment is lowest in total organic matter.

(2) Hydrocarbons comprise 2.3–18.6 per cent of the extractable organic matter and 0.05–0.64 per cent of the total organic matter in the three basins examined. The hydrocarbon content does not differ greatly in the different basins, nor with depth (to 4 meters) in a given basin. Variations with depth appear to be random.

(3) Pyrolysis of sediments at 500° C (modified Fischer retort assay) shows only random variations with depth to 4 meters in a given basin, and the average yield of oil indicates about 7–9 per cent conversion of organic matter to oil. Compared to typical oil-shales, which give 50–75 per cent conversion, this low conversion indicates that basin sediments and oil-shales differ significantly either in the nature of the organic matter or in catalytic activity of the mineral components.

(4) The average potential oil yield, computed from hydrocarbons extracted from the sediments, is about 10 times the eventual recovery from oil fields of the Los Angeles Basin, but is only one-tenth the yield of oil obtained by pyrolysis.

(5) The proportions of hydrocarbons and more complex materials separated from the sediments differ from their proportions in petroleum. These differences may result from later changes and/or fractionation during migration from source beds.

CONTENTS

TEXT

	Page
Introduction	1248
Acknowledgments	1249
Characteristics of basins	1249
Extractable organic matter and its chromatographic separation	1250
Characterization of chromatographic fractions	1252
Assay of basin sediments by oil-shale pyrolysis method	1255
Discussion	1256
References cited	1257

ILLUSTRATIONS

Figure	Page
1. Cumulative composition of organic matter in sediments of three basins off Southern California	1250
2. Infrared curves	1254

TABLES

Table	Page
1. Basin data and core locations	1249
2. Composition of extracts	1251

Table Page
3. Average values for organic components in basin sediments 1252
4. Elemental analyses of chromatographic fractions 1253
5. Averages of oil by Fischer retort assay 1255
6. Elemental analyses of composite assay oils from cores and an organic matter concentrate 1255

Introduction

It is generally recognized that petroleum stems from organic matter deposited in marine sediments and that initially deposited organic matter must undergo considerable change or fractionation before typical petroleum accumulations are formed. The composition of organic matter initially buried in different environments is poorly understood, but the kind and abundance of contributing organisms, the depth, oxygen content, and temperature of the overlying water, and the rate of burial (total sedimentation rate) must be controlling factors. The chemical changes that occur after burial must also be functions of the nature of the initially deposited organic matter and other properties of the sediment. Knowledge of the changes in the zone of greatest bacterial activity (the upper zones of sediment) and of the composition of the remaining organic matter is necessary before the importance of slow processes such as low-temperature cracking can be evaluated. All these processes have been considered necessary for the formation of petroleum (McNab, Smith, and Betts, 1952).

Trask (1931; 1932) studied the texture and organic components of recent sediments throughout the world, including the basins off southern California, and concluded that liquid hydrocarbons, if present in sediments, must be in quantities less than 10 parts per million in the near-surface zones of sediment sampled. New techniques and advances since Trask's work permit more adequate study of the organic matter in sediments in relation to the origin of petroleum. The longer cores possible with larger and heavier coring devices permit a stratigraphic approach, whereby changes in physical and chemical properties with depth in the sediment may indicate the changes that occurred during periods of several thousand years under conditions of uniform deposition. A second advance is increased knowledge of gross properties of basin sediments (Emery and Rittenberg, 1952), circulation of basin waters (Emery, 1954), interchange of nutrients and oxygen between sediment and overlying water (Rittenberg, Emery, and Orr, 1955), and the nature of bacteria in marine sediments, their relation to environment, and the chemical changes they may be able to accomplish (ZoBell, 1946; Stone and ZoBell, 1952). Thirdly, improved methods of separation, such as chromatography, and instrumental methods of characterization, such as infrared, ultraviolet, and mass spectroscopy, allow more detailed study of the complex organic matter in sediments.

Significant amounts of hydrocarbons, and larger amounts of closely related substances that may serve as hydrocarbon precursors, occur in plants and animals and in products of their decomposition. It has been suggested that the generation of petroleum in the earth is largely a process of selection and concentration of hydrocarbons originally synthesized by the metabolism of marine plants (F. C. Whitmore, 1949, unpublished report, American Petroleum Institute Project 43). Bacteria in marine sediments are capable of destroying some hydrocarbons (as well as other organic materials) and synthesizing others in their metabolic processes. Initially deposited hydrocarbons may be altered and/or replaced by others depending on the activity of the bacteria *in situ*. Using chromatography, both aliphatic and aromatic hydrocarbons were separated by Smith (1952; 1954) from recent sediments of the Gulf of Mexico; they were shown to be of recent origin by carbon-14 dating. Although Smith's data show interesting relationships between the amounts and types of hydrocarbons and the environment, many questions remain unanswered, partly because of variations in the depositional history of these shallow sediments of the Gulf of Mexico.

A new program of study of organic matter in the southern California basin sediments was initiated because of the abundant supplementary data on these sediments, because the basins range from deep ones containing little

sediment to the now filled oil-rich Los Angeles Basin on the land, and because sedimentation in some basins appears to have been uniform for at least several thousand years.

the overlying water. The second, Catalina Basin, is deep and contains water of slightly higher oxygen content (0.40 ml/L) and sediment in which oxygen is present at the surface

TABLE 1.—BASIN DATA AND CORE LOCATIONS

	Santa Barbara Basin	Catalina Basin	Santa Cruz Basin	Santa Monica Basin
Core numbers	2622B, C 2622B, C*	2989 2616A, B*	1941	2621*
Latitude	34°13.5′	33°23.2′	33°44.2′	33°44.7′
Longitude	120°01.9′	118°49.2′	119°30.5′	118°45.5′
Sill depth (m)	475	982	1,085	737
Core depth (m)	600	1,303	1,960	912
Maximum depth (m)	627	1,357	1,966	938
Temperature at bottom (°C)	6.26	4.02	4.15	5.05
Oxygen content at bottom (ml/L)	0.30	0.40	0.80	0.25
Depth of zero Eh (cm)	0	137	132	>392
Median grain size of sediment (microns)	3.4	3.2	3.2	10.5

* Cores used for pyrolytic assay

ACKNOWLEDGMENTS

Aid in carrying out preliminary phases of the study reported here was given by Captain Allan Hancock of the University of Southern California and by a grant in aid from the Penrose Bequest of The Geological Society of America. Carbon-14 age determinations were made on sections of two cores by Magnolia Petroleum Company's Field Research Laboratories in Dallas, and pyrolytic assays by the modified Fischer retort method were made by the Petroleum and Oil-Shale Experiment Station, Bureau of Mines, Laramie, Wyoming. The authors also wish to express their appreciation to California Research Corporation, La Habra Laboratory, for use of their infrared spectrophotometer.

CHARACTERISTICS OF BASINS

Two basins were selected for study on the basis of supplementary information reported by Emery and Rittenberg (1952) and by Rittenberg, Emery, and Orr (1955). One basin, Santa Barbara, is shallow, contains water of low-oxygen content (0.30 ml/L), and has sediment of unusually uniform texture that is free of dissolved oxygen. Hydrogen sulfide present to the surface of the sediment does not occur in and absent at depth. Hydrogen sulfide is present only at depth. Properties of the basins, their sediments, and the core locations and depths are given in Table 1. Data for the Santa Cruz Basin also are included because Smith's chromatographic analyses of the extractable organic matter from this basin are available for comparison. This basin contains water of still higher oxygen content (0.80 ml/L), although its sediment is similar to that of the Catalina Basin.

Cores from these three basins show sediment of almost identical median grain diameter (Table 1; Fig. 1), suggesting uniformity of deposition. During coring operations the sediment is down-bowed and thinned in advance of the open end of the core barrel so that the length of the core is less than the length of penetration, but the shortening is proportional throughout the core length (Emery and Dietz, 1941). For the basin sediments the average ratio of core length to penetration is 51 per cent. The sections of core were sealed in glass jars and stored at 4°C until dried for analysis.

Physiographic characteristics of the basins indicate a faster rate of deposition of sediments in nearshore basins than in basins farther offshore. Considerations of supply led to an estimated rate of deposition in Santa Barbara Basin of 0.200 cm per year of sediment con-

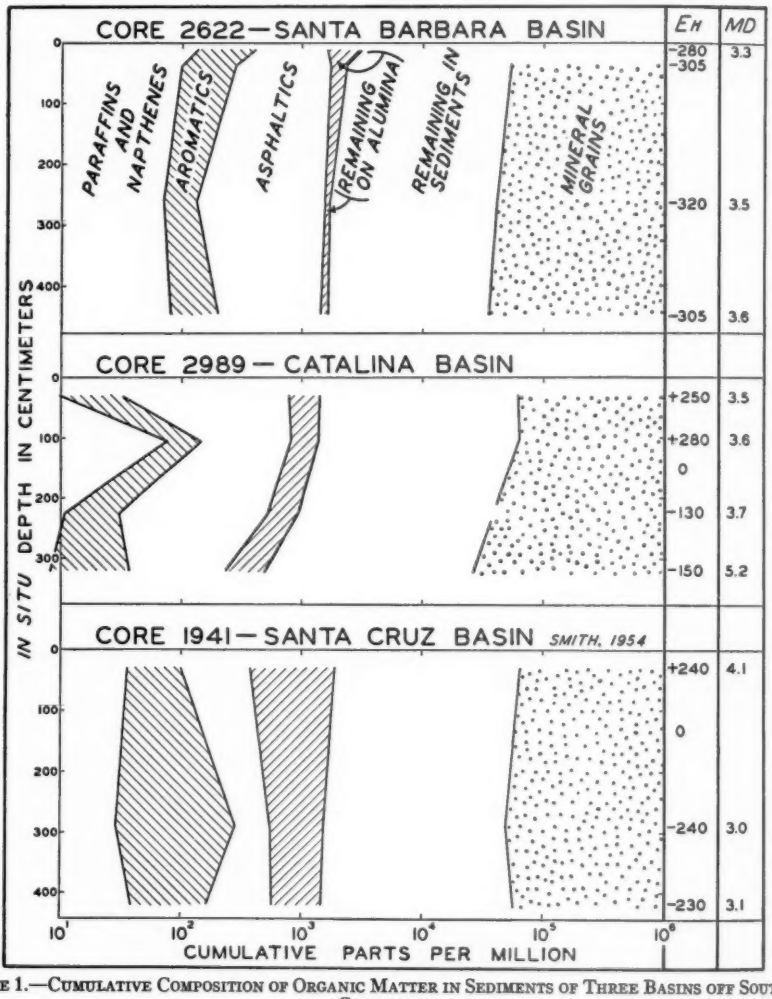

FIGURE 1.—CUMULATIVE COMPOSITION OF ORGANIC MATTER IN SEDIMENTS OF THREE BASINS OFF SOUTHERN CALIFORNIA
Note logarithmic scale

taining 65 per cent water by wet weight, or 0.091 g dry sediment per square cm per year (Emery and Rittenberg, 1952). Carbon-14 age determinations are:

Core 2622C, 76 to 91 cm, 2,380 ± 230 years
Core 2989, 170 to 188 cm, 12,750 ± 500 years

Computation of annual rates of deposition from these data require correction for core shortening and for the varying water content with depth that is produced by compaction. The rates are 0.0296 ± 0.0028 g per square cm in the Santa Barbara Basin and 0.0202 ± 0.0008 g per square cm in the Catalina Basin. Expressed as sediment having 65 per cent water by wet weight, these rates are 0.064 and 0.044 cm per year, respectively.

EXTRACTABLE ORGANIC MATTER AND ITS CHROMATOGRAPHIC SEPARATION

Most organic matter in sediments is complex high-molecular-weight material which cannot

be removed without alteration. A small portion, however, is of sufficiently low molecular weight to be extracted by organic solvents, and it is therefore suitable for study. Since the extractable organic matter is a complex mixture of chemical species, its characterization is difficult, comparable to the inadequate characterization of crude petroleum. The most reasonable approach is to attempt group separations by chromatography, a method which effects separations by selective adsorption and desorption of the various chemical species during a slow passage of the mixture (in suitable solvents) through a column of solid adsorbent. Many techniques of this type have been used for the study of petroleum fractions and are quite successful when applied to fractions of a limited boiling, or molecular weight, range. Techniques have been reported which are applicable with fair success even on crude oil and shale oil. Smith (1952; 1954) reported successful separations of the paraffin-naphthene and aromatic hydrocarbons in extracts from sediments of the Gulf of Mexico. Since the hydrocarbon distribution in sediments is of paramount importance in considerations of the origin of petroleum, two cores were examined for hydrocarbon distribution using the chromatographic procedure and technique reported by Smith.

TABLE 2.—COMPOSITION OF EXTRACTS

Sample number	Depth in core (cm)	Depth *in situ* (cm)	Organic carbon (per cent weight dry sediment)	Per cent of total organic matter (1.7 x carbon) extracted	Grams organic matter extracted per 100 g dry sediment	Per cent paraffins and naphthenes	Per cent aromatics	Per cent asphaltics	Per cent extract remaining on alumina	Ratio of aromatics to paraffin-naphthenes	Ratio of asphaltics to paraffin-naphthene-aromatics
Santa Barbara Basin—Core 2622B, C											
1	0–8	0–16	3.75*	4.70	0.301	4.4	8.2	39.9	47.5	1.9	3.2
2	16–30	32–60	3.24	4.35	0.239	4.2†	7.2†	61.5	27.1	1.7	5.4
3	124–137	248–274	2.40	4.28	0.175	4.1	3.5	81.4	11.0	0.9	10.7
4	209–239	418–478	2.06	4.75	0.166	4.9†	7.2†	74.3	13.6	1.5	6.2
Catalina Basin—Core 2989											
5	0–30	0–60	3.63	2.28	0.141	0.7†	1.6†	52.8	44.9	2.3	23.0
6	30–74	60–148	3.66	2.22	0.138	5.6	5.0†	48.4	41.0	0.9	4.6
7	103–125	206–250	3.50*	1.55	0.092	1.2†	2.0	52.7	44.1	1.8	16.5
8	147–170	294–340	1.63	1.73	0.048	1.8	4.6	40.8	52.8	2.6	6.4
Santa Cruz Basin—Core 1941 (Smith, 1954)											
9	12–18	24–36	3.76	2.94	0.188	1.9	3.4	14.7**	80.0	1.8	2.8
10	137–152	274–304	2.91	2.97	0.152	1.9	16.7	17.9	63.5	8.8	1.0
11	198–221	396–442	3.36	2.61	0.149	2.6	8.4	27.4	61.6	3.2	2.5
Crude Oil, Los Angeles Basin—Domínguez Field (4775 feet) Lower Repetto Pliocene Age††											
12	.....	.....	.....	.....	.....	41.8	18.9	17.5	21.8	0.45	0.3

* Two organic carbons from earlier cores

† Values uncorrected for sulfur

** Per cent asphaltic fractions are larger, and per cent remaining on alumina smaller in present work than in Smith's owing to difference in procedure.

†† Crude oil was topped at 56°C at 2 mm, as were the sediment extracts.

Finely ground dried sediment was extracted with a mixture of 70 per cent benzene, 15 per cent methanol, and 15 per cent acetone in a soxhlet extractor for 8 days. This proved more convenient than batch-wise extraction and extracted slightly more organic material. The solvents must be carefully redistilled and checked to ensure a negligible residue upon evaporation. Acetone and methanol were stripped from the extract, and inorganic salts were removed by washing the remaining benzene solution with water. The residue from the benzene solution (dried at 56°, 2 mm), a reddish-brown tar, was analyzed for hydrocarbons by the chromatographic technique as given by Smith except for the use of more acetone and methanol in the final washing. The residue is thereby separated into fractions, designated as (1) paraffin-naphthene hydrocarbons, (2) aromatic hydrocarbons, (3) asphaltic materials that contain oxygen, nitrogen, and sulfur compounds, and (4) the strongly adsorbed material which cannot be removed from the alumina with reasonable amounts of solvents. The separation between fractions 3 and 4 is arbitrary, depending on the amount of solvent used in the final washing, and the writers' separations (using more acetone and methanol) increase 3 and decrease 4 relative to Smith's separations. Smith's data for the Santa Cruz Basin sediment are compared to data for Santa Barbara and Catalina Basins and for a Pliocene crude oil from the Los Angeles Basin (Tables 2, 3; Fig. 1). As discussed in the next section, the designation of aromatic hydrocarbons for fraction 2 is not entirely appropriate since, in samples examined, this fraction contains large amounts of nonhydrocarbon impurities.

Characterization of Chromatographic Fractions

The chromatographic fractions examined by elemental analysis, infrared and ultraviolet spectra confirm the designations given fractions 1 and 3 but indicate disturbing amounts of nonhydrocarbon impurities in fraction 2. The small size of the fractions (2 to 60 mg of hydrocarbons) greatly curtail the number of methods and operations that may be applied to a single fraction and examination has not been sufficient to disclose fine differences which may exist between corresponding fractions from different samples. Paraffin-naphthene fractions are colorless waxy solids which melt sufficiently to flow at temperatures below 50°C. The only fraction which was liquid at room temperature was sample 8, the deepest sample from the Catalina Basin The aromatic fractions are pale yellow waxy solids, showing strong fluorescence under ultraviolet light.

Elemental sulfur appears in the paraffin-naphthene and aromatic hydrocarbon fractions in variable amounts, and its removal without loss of hydrocarbon has offered difficulty. Smith also noted the presence of sulfur in his samples. Methods of sulfur removal from these small fractions are under investigation and a successful method, when developed, should increase the accuracy of the hydrocarbon analysis. To date, the bulk of the sulfur has been removed from the paraffin-naphthene

Table 3.—Average Values for Organic Components in Basin Sediments
Ppm of dry sediment

	Santa Barbara Basin	Catalina Basin	Santa Cruz Basin	Santa Monica Basin	Grand Average
Paraffins and naphthenes	97	27	35	.....	53
Aromatics	149	33	148	.....	110
Asphaltics	1,330	520	320	.....	720
Remaining on alumina	620	470	1,130	.....	740
Remaining in sediment	46,400	51,700	55,200	.....	51,100
Total organic matter*	48,600	52,800	56,800	30,000	52,700
Oil by pyrolysis	4,600	5,000		2,300	3,970

* 1.7 times organic carbon

fractions by quantitative transfers of the hydrocarbon with a minimum of n-heptane through a small glass-wool plug. Complete sulfur removal is not easily accomplished in this manner but it is reduced to a low percentage of the hydrocarbon fraction (*see* Table 4). The sulfur in the aromatic fractions does not crystallize well enough to allow effective separation in this manner so these fractions were analyzed without attempting sulfur removal. Weights of the aromatic fractions were corrected to a sulfur-free basis, assuming all sulfur is elemental sulfur although it is probable that some organic sulfur compounds are present. The weights of samples not analyzed for sulfur (Table 2) may be from 2 to 20 per cent high depending on their sulfur content.

TABLE 4.—ELEMENTAL ANALYSES OF CHROMATOGRAPHIC FRACTIONS*
In per cent

Fraction	Sample number	Carbon	Hydrogen	Sulfur	Nitrogen	Summation C, H, S	Ratio H/C
(1) Paraffin-naphthene	1	81.25	12.63	1.59	.....	95.47	1.87
	3	86.26	13.66	.....	.....	99.94	1.90
	6	86.24	13.80	.....	.....	100.04	1.92
	12	86.53	13.48	.....	.....	100.01	1.86
(2) Aromatic	1	74.98	9.62	10.49	.....	95.09	1.55
	3	86.17	12.23	1.59	.....	99.99	1.71
	4	73.83	9.67	11.89	.....	95.39	1.57
	7	69.98	10.07	7.00	.....	87.05	1.78
	8	65.17	8.77	21.75	.....	95.69	1.62
	12	85.70	10.29	3.05	0.53	99.04	1.43
(3) Asphaltic	3	68.01	10.17	2.32	1.09	80.50	1.79
		(0, 18.40, by difference)					

*Microanalyses by Adalbert Elek

Elemental analyses (Table 4) for the paraffin-naphthene fractions confirm the absence of nonhydrocarbon impurities, except for the sample still containing sulfur, and the atomic H/C ratios around 1.9 are reasonable values for paraffin-naphthene mixtures.

Elemental analyses of the aromatic fractions indicate that satisfactory separation of aromatic hydrocarbons were not obtained. Except for one sample, the total of carbon, hydrogen, and sulfur is considerably less than 100 per cent, and the deficiency must be due to nitrogen, oxygen, or inorganic materials. Although extreme care was used, the possibility of contamination by traces of very fine alumina has not been eliminated. This may also account for the deficiency in the paraffin-naphthene fraction from sample 1. However, in the larger petroleum sample (12), this possibility was eliminated, and nitrogen is present. The sulfur in this sample is probably largely organic sulfur, and a small percentage of oxygen may be present. Some organic sulfur, nitrogen, and oxygen compounds are believed to be present in the aromatic hydrocarbon fractions from the sediments, but the deficiency is probably due partly to inorganic contamination. These impurities may not be introduced in the last part of the benzene eluate since the benzene elution was intentionally cut about 5 per cent short in sample 7 and this fraction showed more impurities than any other fraction. Since the separation depends on the adsorption characteristics of the compounds, it is not surprising that some nonhydrocarbon materials are eluted before some of the more complex aromatic hydrocarbons in these mixtures which have a wide molecular-weight range. It is not clear whether failure to obtain clean separations of the aromatic hydrocarbon fraction is due to differences in the nature of the samples or to differences in technique. However, the writers are investigating the separation in more detail by use of larger samples, a more gradual elution of the aromatic fraction (with weaker desorbants than pure benzene), and separation into a number of fractions for separate examination.

The atomic H/C ratios of the aromatic fractions range from 1.55 to 1.78, which are reasonable values for aromatics having a high content of paraffin side-chains or condensed naphthene rings, but many nonhydrocarbon impurities would have similar ratios. Smith reported a ratio of 1.55 for a single aromatic fraction from the Gulf of Mexico.

The ultraviolet spectra of paraffin-naphthene fractions show low absorptivities characteristic of saturated hydrocarbons mixed with less than 5 per cent of mono-nuclear aromatics. The aromatic fractions show high absorptivities extending to long wave lengths and indicate a complex mixture of aromatics including large amounts of polycyclic aromatics. Some saturated hydrocarbons are probably included in the aromatic fractions, but none of the methods used are applicable for their detection.

The infrared spectra (Fig. 2) confirm the structural nature of the fractions and show the similarity of corresponding fractions separated from the sediments and crude oil. Although only one example of the spectra of each fraction from sediment and from the crude oil are shown in the figure, all spectra of corresponding fractions are quite similar; some differences around the 6-μ region exist in the aromatic fractions, and differences above 8 μ may be expected, although this region was not run on most samples. The 6.25-μ band due to aromatic rings is evident in all aromatic fractions and absent in paraffin-naphthene fractions. On some of the aromatic fractions the aromatic band near 6.70 μ appears

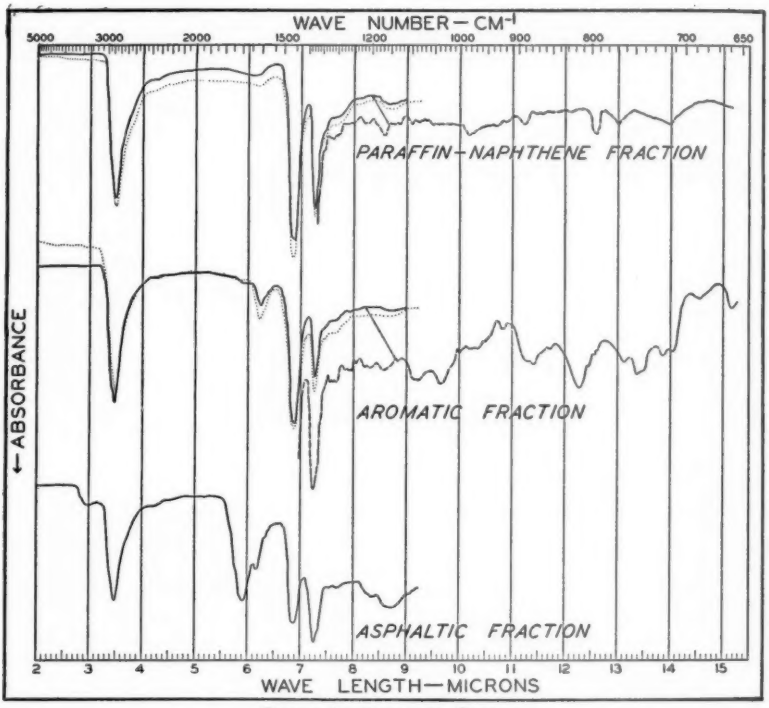

FIGURE 2.—INFRARED CURVES

Typical infrared curves for paraffin-naphthene, aromatic, and asphaltic fractions from basin sediments (sample 4) and from a Pliocene crude oil (sample 12) from the Los Angeles Basin. Solid line—spectra in carbon tetrachloride solution; dashed line—film on silver chloride disk; dotted line—petroleum fractions in carbon tetrachloride. (Perkin-Elmer Model 21 Infrared Spectrophotometer, NaCl prism, solvent absorbance eliminated.)

TABLE 5.—AVERAGES OF OIL BY FISCHER RETORT ASSAY

Basin	Number of samples	Oil yield per cent of dry sediment		Per cent of total organic matter converted to oil
		Range	Average	
Santa Barbara	12	0.1–0.6	0.46	9.5
Catalina	9	0.1–1.0	0.50	9.5
Santa Monica	6	0.0–0.7	0.23	7.7

be obtained with the small samples and cells which were available.

With regard to the impurities in the aromatic fractions, it should be noted that indicated trends on distribution of hydrocarbons in the sediments with depth and from basin to basin (Fig. 1) are not seriously affected by the inadequate separation of the aromatic fraction. The true aromatic hydrocarbon content of the sediments is less than the data indicate, but the limited geological conclusions which can be

TABLE 6.—ELEMENTAL ANALYSES OF COMPOSITE ASSAY OILS FROM CORES AND AN ORGANIC MATTER CONCENTRATE*

In per cent

Samples	Carbon	Hydrogen	Sulfur	Nitrogen	Oxygen†	Atomic H/C ratio	Specific gravity 60°/60°F
Assay oils (Composite of all core sections)							
Catalina Basin	75.94	8.54	1.98	6.12	7.42	1.34	1.030
Santa Barbara Basin	73.98	8.52	6.66	5.32	5.52	1.37	1.006
Santa Monica Basin	74.17	8.52	n.d.	n.d.	n.d.	1.37	n.d.
Colorado oil-shale	84.59	11.53	0.61	1.96	1.31	1.62	0.916
Concentrate of organic matter**							
Catalina Basin	66.20	5.29	2.50	4.23	21.78	0.95	.....
Colorado oil-shale	77.66	9.58	0.67	2.58	9.51	1.48	.....

* Samples prepared and analysed by Bureau of Mines

† Oxygen by difference

** Concentrate of organic matter made by removal of minerals with HCl and HF. Pyrite, excess ash, and chlorine in concentrate are eliminated in computations.

as a shoulder on the strong CH deformation band centered at 6.85 μ. No bands indicative of impurities appear in the curves for the paraffin-naphthene fractions, but a weak to fairly strong band at 5.85 μ, possibly due to the carbonyl group (>C=O), appears in several of the aromatic fractions. This band, however, is evidently not due to a major impurity since there is no correlation between the intensity of the band and the nonhydrocarbon impurities as indicated by elemental analysis. The lack of correlation is evident in samples 1, 3, and 4; the 5.85-μ band is considerably stronger than the 6.25-μ band in sample 1, is slightly stronger in 3, and is hardly evident in sample 4. More detailed infrared spectra in the 5 to 7- and 9 to 15-μ regions would be interesting but could not drawn from these few samples would not be changed by better analyses.

ASSAY OF BASIN SEDIMENTS BY OIL-SHALE PYROLYSIS METHOD

The Bureau of Mines Petroleum and Oil-Shale Experiment Station assayed 27 samples from three basins by the modified Fischer retort method (Stanfield and Frost, 1949) which is used for the evaluation of oil shales. By this method the organic matter in the sediment or shale is converted to oil, gas, and a carbonaceous residue by pyrolysis at 500°C. Oil yields range from 0.0 to 1.0 per cent of the dry sediment but fail to show any consistent change with depth. The average for each basin, however, shows a

close correspondence to the average total organic matter, with 7.7–9.5 per cent of the total organic matter being converted to oil (Table 5). This conversion of organic matter to an oil is low compared to assays of Green River oil shales of Colorado (Stanfield, Frost, McAuley, and Smith, 1951), which show 50 to 75 per cent conversion. This large difference would seem to indicate that the basin sediments and oil shales differ significantly in either the nature of the organic matter or the catalytic activity of the mineral components.

This difference is also shown by comparison of elemental analyses of assay oils from the sediments and Colorado oil shale (Table 6). Assay oils from sediments are higher in nitrogen, sulfur, and oxygen than those from the oil shale. The hydrocarbon content of the assay oils was not determined but must be lower for oils from the sediments, owing to the higher content of nitrogen, sulfur, and oxygen.

The desirable comparison of organic matter in sediments and shales would be by complete elemental analysis of the total organic matter, but the complete separation of minerals from the organic matter, without altering the latter, cannot be effected. Nevertheless a concentrate of organic matter in the core from the Catalina Basin was prepared by the Bureau of Mines by dissolving most of the minerals in hydrochloric and hydrofluoric acid. After elimination of pyrite, excess ash, and chlorine, the residue comprised 3.17 per cent by dry weight of the original sediment, in contrast to 5.64 per cent organic matter in the original sediment as computed from its organic carbon content. Thus, about 44 per cent of the organic matter was lost during its concentration. Analysis of the final organic concentrate (Table 6) shows a higher carbon/nitrogen ratio than in the original sample (15.6 versus 9.5), indicating a loss of 63 per cent of the nitrogen during the concentration. This preferential loss of nitrogen by the acid extraction is to be expected if appreciable amounts of basic nitrogen compounds are present.

Discussion

Santa Barbara Basin, a reducing environment, has the highest average content of extractable organic matter even though it is the lowest in average total organic matter (Tables 2, 3). The percentages of the total organic matter extracted range from 4.3 to 4.7. For the Catalina and Santa Cruz cores the corresponding ranges are 1.5–2.3 and 2.6–3.0, respectively. These differences may be due to the fact that the organic debris settles through a shorter water column in the Santa Barbara Basin, is buried more rapidly owing to a faster total rate of sedimentation, and therefore has not been oxidized as much as the material in the other two basins. A higher percentage of easily oxidizable material could readily exhaust the oxygen in the sediment, accounting for the negative Eh at the sediment surface in this basin.

While the fraction of the total organic-matter which is extractable appears to show differences owing to the sedimentary environment, differences in the composition of the extractable organic matter are less definite. The hydrocarbon content of the extractable organic matter appears to be highest in the Santa Barbara Basin (Table 2). Variations in the composition of the extractable organic matter with depth are not clear from the present data. The first three samples of the Santa Barbara Basin sediment show a small decrease in percentage of hydrocarbons with depth, but the percentage in the bottom sample increases again to near that of the top sample. It may be significant that this bottom sample was from a separate core taken less than a tenth of a mile away. In the other two basins the variations with depth appear random with the highest hydrocarbon content occurring at intermediate depths. More cores and more samples in a single core will be required to establish a trend or lack of trend in the total hydrocarbon content with depth.

Changes in composition within corresponding fractions may be more significant than variations with depth of the absolute amount of each fraction. It is interesting to note that the only liquid paraffin-naphthene fraction was from the deepest sample in the Catalina Basin. Perhaps the most significant observation of this type yet reported is that of Rosenfeld (1948) in which the fatty acid content showed no trend with depth, but the degree of unsaturation of the fatty acids showed a decrease with depth of burial.

It is interesting to note the magnitude of the

hydrocarbon content of these sediments in relation to potential petroleum production. As shown by Emery and Rittenberg (1952), past and proved-future reserves in the Los Angeles Basin amount to 0.077 per cent of the original content of organic matter. Since original organic content was about 5 per cent (about the same as in the Santa Barbara Basin), the petroleum production and reserves amount to about 40 ppm of sediment. If average hydrocarbon content in this petroleum is assumed to be 60 per cent, the Santa Barbara Basin sediment already contains hydrocarbons equivalent to 410 ppm of petroleum, or about 10 times the estimate for actual oil field production; this figure would be lowered somewhat by correction for the impurities in the aromatic fractions. Other organic material present may serve as source material for further oil formation as shown by the oil yield by pyrolysis, but of course the pyrolysis experiments bear no relation to conditions occurring in nature.

As pointed out by Hunt and Jamieson (1956) and by Stevens, Bray, and Evans (1956) and as shown also by Table 2, the organic materials extracted from the sediments differ from petroleum in several respects. In terms of total extract, the percentage of hydrocarbons is lower and the percentages of the asphaltic fractions and of material remaining on alumina are much higher in the sediment extracts than in crude oil. The importance of these differences is difficult to evaluate since these are the differences that would be expected from the fractionation by preferential adsorption during migration. Nevertheless, it is probable that further formation of liquid hydrocarbons is necessary before efficient migration can occur. Further study, particularly more detailed knowledge of the composition of the chromatographic fractions from the sediments at various depths and from the Los Angeles Basin, may allow more definite conclusions as to the part that these initial hydrocarbons play in petroleum formation.

References Cited

Emery, K. O., 1954, Source of water in basins off southern California: Jour. Marine Research, v. 13, p. 1–21

Emery, K. O., and Dietz, R. S., 1941, Gravity coring instrument and mechanics of sediment coring: Geol. Soc. America Bull., v. 52, p. 1685–1714

Emery, K. O., and Rittenberg, S. C., 1952, Early diagenesis of California basin sediments in relation to origin of oil: Am. Assoc. Petroleum Geologists Bull., v. 36, p. 735–806

Hunt, J. M., and Jamieson, G. W., 1956, Oil and organic matter in source rocks of petroleum: Am. Assoc. Petroleum Geologists Bull., v. 40, p. 477–488

McNab, J. G., Smith, P. V., Jr., and Betts, R. L., 1952, Evolution of petroleum: Indus. and Eng. Chemistry, v. 44, p. 2556–2563

Rittenberg, S. C., Emery, K. O., and Orr, W. L., 1955, Regeneration of nutrients in sediments of marine basins: Deep-Sea Research, v. 3, p. 23–45

Rosenfeld, R. W., 1948, Fatty acid transformations by anaerobic bacteria: Archives of Biochemistry, v. 16, p. 263–273

Smith, P. V., Jr., 1952, The occurrence of hydrocarbons in recent sediments from the Gulf of Mexico: Science, v. 116, p. 437–439

—— 1954, Studies on origin of petroleum: Occurrence of hydrocarbons in recent sediments: Am. Assoc. Petroleum Geologists Bull., v. 38, p. 377–404

Stanfield, K. E., and Frost, I. C., 1949, Method of assaying oil shale by a modified Fischer retort: U. S. Bur. Mines Rept. Inv. 4477, p. 1–13

Stanfield, K. E., Frost, I. C., McAuley, W. S., and Smith, H. N., 1951, Properties of Colorado oil shale: U. S. Bur. Mines Rept. Inv. 4825, p. 1–27

Stevens, N. P., Bray, E. E., and Evans, E. D., 1956, Hydrocarbons in sediments of Gulf of Mexico: Am. Assoc. Petroleum Geologists Bull., v. 40, p. 975–983

Stone, R. W., and ZoBell, C. E., 1952, Bacterial aspects of the origin of petroleum: Indus. and Eng. Chemistry, v. 44, p. 2564–2567

Trask, P. D., 1931, Sedimentation in the Channel Islands region, California: Econ. Geology, v. 26, p. 24–43

—— 1932, Origin and environment of source sediments of petroleum: Houston, Gulf Publishing Co., p. 1–323

ZoBell, C. E., 1946, Marine microbiology, a monograph on hydrobacteriology: Waltham, Mass., Chronica Botanica Co., 240 p.

University of Southern California, Los Angeles, Calif.

Manuscript Received by the Secretary of the Society October 4, 1955

Allen Hancock Foundation Contribution No. 176

Project Grant 623-53

BULLETIN OF THE GEOLOGICAL SOCIETY OF AMERICA
VOL. 67, PP. 1259-1294, 19 FIGS., 5 PLS. SEPTEMBER 1956

DEFORMATION OF YULE MARBLE. PART VII: DEVELOPMENT OF ORIENTED FABRICS AT 300°C-500°C

BY FRANCIS J. TURNER, DAVID T. GRIGGS, R. H. CLARK, AND ROBERTA H. DIXON

ABSTRACT

Yule marble has been deformed at 400° and 500° C and a confining pressure of 5000 atmospheres. Its strength, relative to that at room temperature, is 47 per cent at 400° C and 41 per cent at 500° C, measured in all cases at 3 per cent strain. Textures of the deformed rock are similar to those of marble comparably deformed at 300° C.

Sander's method of "axial-distribution analysis" has been used to test homogeneity of fabric in the original marble and in a specimen shortened 19 per cent at 300° C. In both cases aggregates of a few tens of grains show local very strong preferred orientation of the lattice. In this respect there is no effect that can be correlated with deformation.

Petrofabric analysis of specimens shortened 40 per cent or elongated 90–120 per cent demonstrates strong preferred orientation of the *c* axis at 10°–30° to the axis of compression or at 60°–80° to the axis of extension. The symmetry of the deformed fabrics corresponds with the symmetry of strain, which is determined by the orientation of the axis of extension or compression in relation to the preferred orientation pattern of the original fabric.

Behavior of grains is predicted on the basis of a hypothesis of approximately homogeneous deformation, involving twin gliding on $\{01\bar{1}2\} = e$ and translation gliding on $\{10\bar{1}1\} = r$. Behavior of individual grains is also reconstructed from evidence of observed internal rotation of early *e* lamellae, interpreted in the light of previous observations on single crystals of calcite. The same data are used to compute shortening or elongation of individual grains parallel to the axis of applied force. The behavior and strain so deduced and the details of observed preferred-orientation patterns agree with prediction. It should prove possible to compute strain in geologically deformed rocks on the basis of petrographically measured effects of internal rotation. However, at present this can be attempted only for those few minerals, such as calcite and dolomite, whose glide systems have been ascertained experimentally. Possible analogy between a natural marble fabric and a fabric resulting from experimental compression is noted.

CONTENTS

TEXT

	Page
Introduction	1260
Acknowledgments	1260
Experimental data	1261
Laboratory procedure	1261
Effect of temperature on strength	1261
Effect of strain rate on strength	1262
Homogeneity of fabric	1263
Fabric of strongly deformed marbles	1265
General statement	1265
Symmetry of deformation	1269
Results of petrofabric analysis	1269
Marble deformed by compression	1269
Marble deformed by extension	1271
Evidence of possible recrystallization	1272
The orienting mechanism	1273
Relation between single crystals and aggregates	1273
Predicted behavior of individual grains	1278
Basic assumptions	1278
Behavior of grains during twin gliding on $\{01\bar{1}2\}$	1281
Behavior of grains during translation gliding on $\{10\bar{1}1\}$	1281
Petrofabric confirmation of the orienting mechanism	1284
Evidence from preferred orientation data	1284
Evidence from individual grains	1286
Concluding statement	1289
Geological applications	1290
References cited	1292

ILLUSTRATIONS

Figure	Page
1. Stress-strain curves for Yule marble	1262
2. Orientation diagrams for *c* axes of calcite in Yule marble	1263

Figure — Page
3. Key to axial-distribution analysis 1264
4. Axial-distribution diagrams 1266
5. Axial-distribution diagram 1267
6. Orientation diagrams for *a* axes of calcite .. 1268
7. Orientation diagrams for *a* axes of calcite .. 1270
8. Symmetry of deformation and of fabric .. 1274
9. Orientation diagrams for *c* axes and *e* lamellae of calcite, Yule marble deformed by compression 1275
10. Orientation diagrams for *c* axes and *e* lamellae of calcite, Yule marble deformed by extension 1276
11. Orientation diagrams for *a* axes of calcite in deformed Yule marble 1277
12. External rotation of calcite crystal in relation to applied force 1279
13. Twin gliding on *e* and external rotation of calcite crystal in relation to applied force 1280
14. Translation gliding on *r* and external rotation of calcite crystal in relation to applied force 1282
15. Stable orientations of twinned calcite 1284
16. Projection illustrating kinematic interpretation of fabric resulting from diagonal shear 1285
17. Projections illustrating behavior of individual grains as deduced from internal rotation of *e* lamellae 1291
18. Projection illustrating repeated complete twinning of calcite 1292
19. Possible local recrystallization effects, specimen 409 1292

Plate — Following page
1. Photomicrographs
2. Photomicrograph 1272
3. Photomicrographs
4. Photomicrograph

Facing page
5. Photomicrographs of individual grains 1278

TABLES

Table — Page
1. Strain and external rotation induced by twin gliding on $\{01\bar{1}2\}$ 1281
2. Values of S_O at successive stages of external rotation during translation on $\{10\bar{1}1\}$ 1283
3. S_O for $\{10\bar{1}1\}$ glide systems for stable orientations of calcite 1284
4. Universal-stage measurements for individual grains 1287
5. Data on observed internal rotation and calculated strain for individual grains 1288

Introduction

At 300°–500° C and confining pressure of 5000 atmospheres, Yule marble is so ductile that a cylinder 1 inch long by 0.5 inch in diameter may be shortened as much as 40 per cent of its initial length without rupture. Local elongation of more than 100 per cent may be achieved in the necked region of a cylinder deformed by extension. The highly strained marble affords excellent material for investigating the evolution of preferred orientation of the component calcite grains as deformation proceeds. Among the questions for which answers are sought are these: How homogeneous is the fabric of marble deformed at high temperature? What is the significance of maxima (concentrations of *c* axes) in *c*-axis diagrams constructed for 100 or for several hundred grains of a deformed specimen? What correlation exists between strength of such maxima and degree of strain? Does the preferred orientation pattern that existed before deformation influence the pattern observed in highly deformed specimens? What are the relative roles played by plastic deformation of grains and by recrystallization respectively? What is the behavior of individual grains during progressive deformation of the polycrystalline aggregate?

With these questions in mind we have carried out petrofabric analyses of representative specimens and have examined in detail the internal structures—especially all visible lamellae—in many individual grains. These have been interpreted in the light of recent work on single crystals of calcite deformed experimentally under like conditions (Turner, Griggs, and Heard, 1954). Homogeneity of fabric has been tested by Sander's (1950, p. 161–217) method of *Achsenverteilungsanalyse* (*AVA*).

Acknowledgments

We gratefully acknowledge financial support from the Office of Naval Research of the United States Navy (Project grant N 6 onr-27511, Project NR 081-101), the National Science Foundation (Grant S-996), and the Penrose Bequest of The Geological Society of America (Project 615-53). A travel grant from the Carnegie Trust for the Universities of Scotland made it possible for Clark to work with the other authors in California. Mr. Hugh Heard

performed the experiments at 400° C and greatly assisted in developing the apparatus for work at 500° C. Some of the fabric analyses were done by Dr. Iris Borg, and the thin sections were prepared by Mr. J. de Grossé.

Experimental Data

Laboratory Procedure

Five experiments at 400° C, 3000 atmospheres confining pressure, were done in the apparatus described earlier in this series (Griggs *et al.* 1953). 3000 atmospheres was the limit that the old cylinder could withstand without excessive creep at 400° C.

A new cylinder and accessories have been used for eight more experiments on the Yule marble at 500° C, 5000 atmospheres confining pressure. This cylinder employs a Newhall "controlled-leak" packing around the piston to minimize friction. The measurement of differential force applied to the specimen is thus much more accurate than in previous work. CO_2 is used to supply the confining pressure, which is maintained constant by a servo-controlled pump driven from a self-balancing Carey-Foster bridge which measures pressure from the change in resistance of the manganin pressure cell. The pump compresses CO_2 in one stage from tank pressure to 5000 atmospheres. This automatically controlled confining pressure permits measurements at low strain rates with a precision which was hitherto impossible. The cylinder and external furnace have also been designed to minimize temperature gradients so that the temperature of the specimen is more accurately known.

The probable error in temperature is 1° C, in pressure 0.5 per cent, in stress 30 kg/cm², and in strain 0.1 per cent. The stress and strain are only known to this accuracy for strains of a few per cent. At higher strains the inhomogeneity of deformation causes much greater uncertainties. These figures apply only to the experiments at 500° C.

The method of jacketing the specimen with thin-walled copper tube is described in Griggs *et al.* (1953, p. 1328).

Effect of Temperature on Strength

Figure 1A shows the stress-strain curve of a 1 cylinder of Yule marble at 500° C, 5000 atmospheres confining pressure, compared to curves for experiments at lower temperatures with the same confining pressure. This curve for 500° C is the average of three tests. The average departure of these three from their mean is 1.5 per cent. J. W. Handin, of the Shell Development Company, has checked these results for Yule marble up to 300° C, 5000 atmospheres.

Robertson (1955) found an *increase of rupture strength* with temperature for Solenhofen limestone in experiments on the collapse of cylindrical shells under external pressure. We have found that increase in temperature from 25° C to 500° C is accompanied by *lowering of strength* (measured at a given strain) by a factor of 2 in specimens of Solenhofen limestone[1] tested at 5000 atmospheres in compression and extension. We checked Robertson's results for compression at 25° C, 4000 atmospheres to about 5 per cent in stress at a given strain.

Handin and Fairbairn (1955) found that the strength of Hasmark dolomite rock, measured at a given strain, decreases very slightly from 20° C to 300° C. Handin (Personal communication) found a similar effect in dolomite single crystals, in marked contrast to observations of great decrease in strength of calcite crystals with increase in temperature (Turner, Griggs, and Heard, 1954, p. 893). We have done experiments on Dover Plains dolomite rock and on dolomite single crystals supplied by Handin; these confirm the results reported by Handin and Fairbairn.

In Robertson's tests, the central hole of the shell was nearly at atmospheric pressure, and the external pressure required to cause rupture increased with increasing temperature up to 600° C. This rupture begins at the inner surface, where there is a very low normal pressure. Robertson found, as we have, that ductility is markedly increased by increased temperature. The increase of ductility may be more important in raising the rupture strength in his experiments than is the lowering of the stress-strain curve. In our experiments, rupture strength was not measured, since all ruptures are believed to be caused by a failure of the jacket at high deformations. Specimen 459

[1] These were kindly supplied to us by Dr. Robertson.

was elongated 120 per cent without rupture. The final stress at the neck was 2700 kg/cm². At room temperature, specimens of similar orientation have been stressed to more than 6000 kg/cm² at much lower strains.

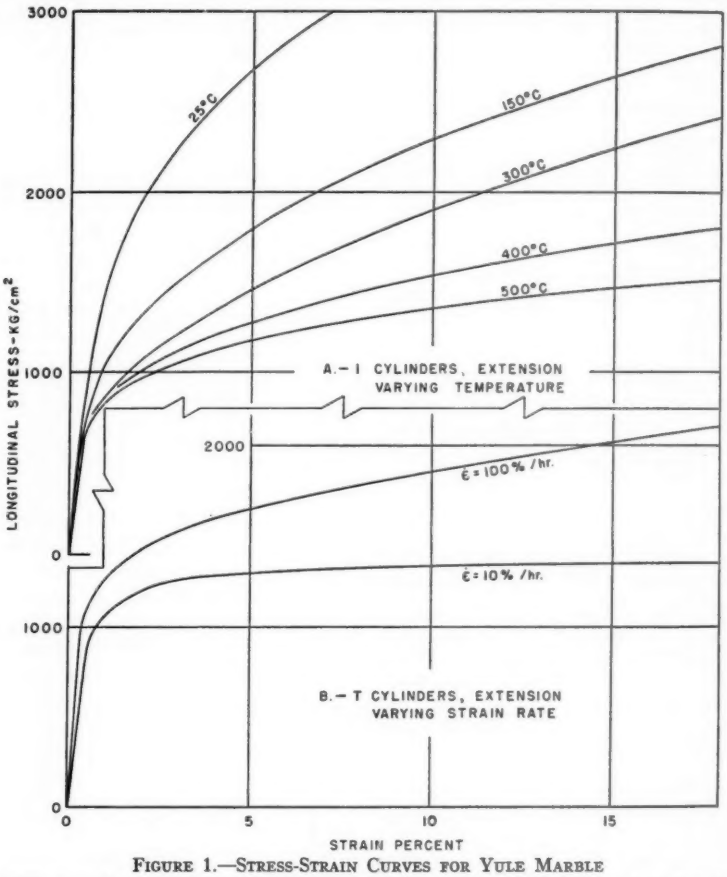

FIGURE 1.—STRESS-STRAIN CURVES FOR YULE MARBLE
All at 5000 atmospheres confining pressure, except 400° C curve (3000 atmospheres). Jacketed, dry.

Effect of Strain Rate on Strength

Figure 1B shows the effect of rate of strain on *T* cylinders of Yule marble in extension at 500° C, 5000 atmospheres. Similar effects have been observed at lower temperatures, although quantitative data are not available to permit a comparison of this effect as a function of temperature. Four experiments at the low strain rate were performed. One, 520, was stretched 40.5 per cent over-all, in an attempt to duplicate 459; a *T* cylinder extended 40.7 per cent at the normal strain rate, with other conditions the same. The degree of necking in 520, however, was much less. The maximum strain at the neck in 520 was 74 per cent versus 118 per cent in 459. The reason for this difference is not known.

Experiments at 400° C and 500° C provided further confirmation of trends observed at 25°, 150°, and 300° C. The principal effort in these experiments was to provide very highly strained specimens for fabric study.

HOMOGENEITY OF FABRIC

Experience has confirmed the earlier opinion (Turner and Ch'ih, 1951, p. 891) that measure-

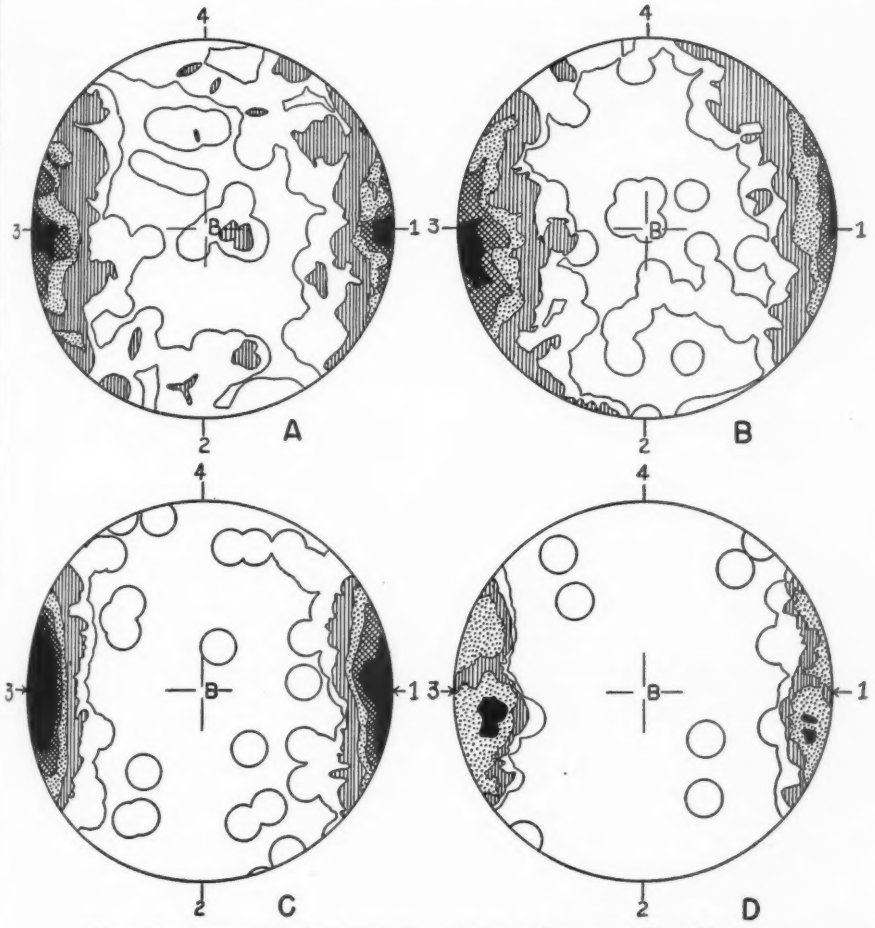

FIGURE 2.—ORIENTATION DIAGRAMS FOR *c* AXES OF CALCITE IN YULE MARBLE

Projections on plane normal to foliation (*NS*)

A. Specimen 172 undeformed. 300 axes measured in upper half of Figure 4A. Contours 0.3%, 1%, 3%, 5%, 7%, per 1% area.

B. Specimen 172 undeformed. 300 axes measured in lower half of Figure 4A. Contours as in A.

C. Specimen 295 shortened 19 per cent normal to foliation (compression indicated by arrows). 550 axes measured in Figure 4B. Contours as in A.

D. Specimen 295, same section as C. 100 axes measured in linear traverses. Contours 1%, 3%, 5%, 10%, per 1% area.

ment of a random sample of 100 calcite grains brings out the essential pattern of preferred orientation of *c* axes. In the initial fabric this is characterized by a concentration of *c* axes at high angles to the foliation (Fig. 3, plane 1). Maxima within this general area of concentration are not reproducible in diagrams based on 100 grains; they disappear when as many as 300 axes are plotted on one diagram (Fig. 2A, B). There is no consistent pattern of *a* axes in the initial fabric as a whole. A faint tendency for preferred orientation of *a* previously reported (Turner and Ch'ih, 1951, p. 895) is not confirmed by later work.

The fabric of a cylinder (295) shortened 19 per cent by compression normal to the foliation (Fig. 3, plane 1) at 300° C shows a strengthening of the original *c*-axis maximum around

the axis of compression. As in diagrams for the initial fabric, the local maxima in diagrams for 100 axes do not persist in diagrams for 300 axes (Fig. 2C, D). In a random sample of 100 grains there is no obvious preferred orientation of the *a* axes such as may be detected in more highly deformed marble. (*Cf.* Fig. 11.)

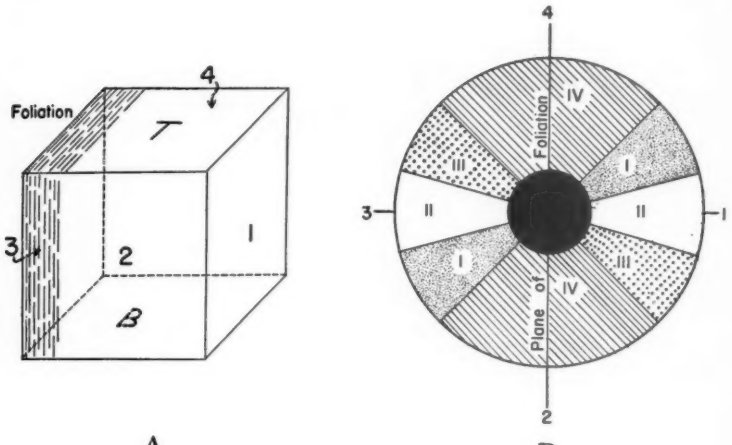

FIGURE 3.—KEY TO AXIAL-DISTRIBUTION ANALYSIS (AVA)

A. Orientation of numbered faces of the marble block in relation to foliation.

B. Equal-area projection on the *T* plane, showing five ranges of orientation of *c* axes specified for axial-distribution analysis of marble.

Before and after deformation the fabric of the marble is so homogeneous that a reproducible orientation pattern may be obtained in any sample of 300 contiguous grains. These occupy an area of 8 mm by 3 mm in a thin section or a volume (allowing average grain thickness of 0.3 mm) of less than 0.007 cc. However, local fluctuations shown by aggregates of a few contiguous grains whose *c* axes tend to be mutually parallel, have long been obvious (Turner and Ch'ih, 1951, p. 895). Local inhomogeneity of this kind has now been investigated by axial-distribution analysis (AVA of Sander) of two thin sections cut respectively from undeformed marble (specimen 172) and from a cylinder (specimen 295) shortened 19 per cent normal to the initial foliation, at 300°C and 5000 atmospheres.

Both thin sections are parallel to plane T of Figure 3. Grains are arbitrarily divided into five orientation groups (Fig. 3B) according to orientation of the *c* axis. Group I includes grains whose *c* axes lie in the finely stippled sectors of Figure 3B, group V those with *c* axes in the central black area, and so on. It is clear from the orientation diagrams (Fig. 2A, B) that group II has more grains than any other group. In Figure 4, A and B, grains are individually marked to correspond with the five orientation groups similarly marked in Figure 3. Sander (1950) found that in strongly deformed rocks quartz grains of one orientation group may be concentrated in streaks that trend parallel to the foliation or to other *S* planes in the fabric. No such tendency is clearly defined in Figure 4A or 4B. However there is a decided tendency for grains of one orientation group to be associated mutually in space as aggregates of between 5 and 30 grains.

Figure 6A shows 258 *a* axes in 86 grains of orientation group II occurring in four local aggregates in the undeformed marble. No preferred orientation of *a* is obvious. This is true also for a plot of 87 *a* axes in 29 grains that make up one of these aggregates (Fig. 6B). But when the *a* axes of 12 large grains in the same aggregate are plotted separately (Fig. 6C), an orientation pattern characterized by 3 maxima 60° apart is obvious. This is

true in general for the *a* axes of all large grains in any local aggregate of grains belonging to one orientation group (Fig. 6C-F). Similar results (Fig. 7) have been obtained from investigating orientation of *a* axes in the deformed specimen, 295. In each of the diagrams representing a grain aggregate, one of the three maxima is normal to the axis of compression.

Axial-distribution analysis has yielded no significant information bearing on the mechanism of deformation. It brings out the following features shown by undeformed and deformed fabrics alike:

(1) Irregularly bounded aggregates of between 5 and 30 grains show local strong preferred orientation of *c* axes and give rise to fluctuations within the general preferred-orientation pattern that characterizes the fabric as a whole.

(2) There is no obvious preferred orientation of *a* axes either in a random sample of grains of one orientation group (defined by *c*-axis orientation) or in a sample composed of all grains constituting one of the aggregates described under (1).

(3) The larger grains of any such local aggregate, however, commonly show a strong preferred orientation of *a* axes. Such orientation varies from one aggregate to another even within one orientation group.

Axial-distribution analysis of the most highly deformed marble available (specimen 459, locally extended 118 per cent at 500° C) shows similar inhomogeneity (Fig. 5). Preferred orientation of *a* axes in each orientation group (Fig. 11C, D) is stronger and more consistent than in less-strained material.

Fabric of Strongly Deformed Marbles

General Statement

Five strongly deformed specimens have been subjected to fabric analysis:

409: *1* cylinder, shortened 39.9 per cent, 400° C, 3000 atmospheres; maximum shortening 46 per cent; one-tenth normal strain rate.

443: *T* cylinder, shortened 40.7 per cent, 400° C, 3000 atmospheres; maximum shortening 44 per cent.

459: *T* cylinder, elongated 40 per cent, 500° C, 5000 atmospheres; maximum elongation in necked area, 118 per cent.

520: *T* cylinder, elongated 40.7 per cent, 500° C, 5000 atmospheres; maximum elongation in necked area, 74 per cent; one-tenth normal strain rate.

477: *1* cylinder, elongated 48 per cent, 500° C, 5000 atmospheres; maximum elongation in necked area, 93 per cent.

With these is compared a *1* cylinder (400) strongly deformed by compression at 300° C and 5000 atmospheres (Griggs *et al.*, 1953, p. 1340–1341). In two experiments (443 and 477) most of the grains initially were oriented to permit twinning on $\{01\bar{1}2\}$.

The five specimens have several features in common: Strain is concentrated in a central sector of the cylinder, which is free from restriction by the steel end cups. (*Cf.* Pl. 1, fig. 1; Pl. 2; Pl. 3, fig. 1.) The mean grain size is distinctly reduced, especially in specimens in which twinning on $\{01\bar{1}2\}$ has been prevalent (Pls. 2, 4). Grains are greatly elongated or flattened and commonly show undulatory extinction. These latter effects are most conspicuous in specimens in which few grains have been completely twinned on $\{01\bar{1}2\}$. (*Cf.* Pl. 1, fig. 1; Pl. 3.) Dark $\{01\bar{1}2\}$ lamellae are conspicuous in most grains and show obvious preferred orientation.

For each specimen a thin section cut parallel to the axis of compression or extension was used for petrofabric analysis. Within the deformed sector of each section 100 grains in widely separated traverses were measured. The *c* axis and one or more prominent sets of $\{01\bar{1}2\}$ lamellae or $\{10\bar{1}1\}$ cleavages were located in a restricted part of each grain—a procedure dictated by variation in optic orientation (shown by undulatory extinction) in many grains. Many of the lamellae recorded as $\{01\bar{1}2\} = e$[2] have been internally rotated through the grain by extensive translation gliding on $\{10\bar{1}1\} = r$, as have the anomalous orientations that have elsewhere been designated L_1 and L_7 (Turner, Griggs, and Heard, 1954, p. 910, 930).

[2] Following recently established usage (Turner, Griggs, and Heard, 1954, p. 886), planes $r = \{10\bar{1}1\}$, $e = \{01\bar{1}2\}$, and $f = \{02\bar{2}1\}$ that are cozonal with one another and with $\{0001\}$ are designated with a common subscript—*e.g.*, r_1, e_1, and f_1.

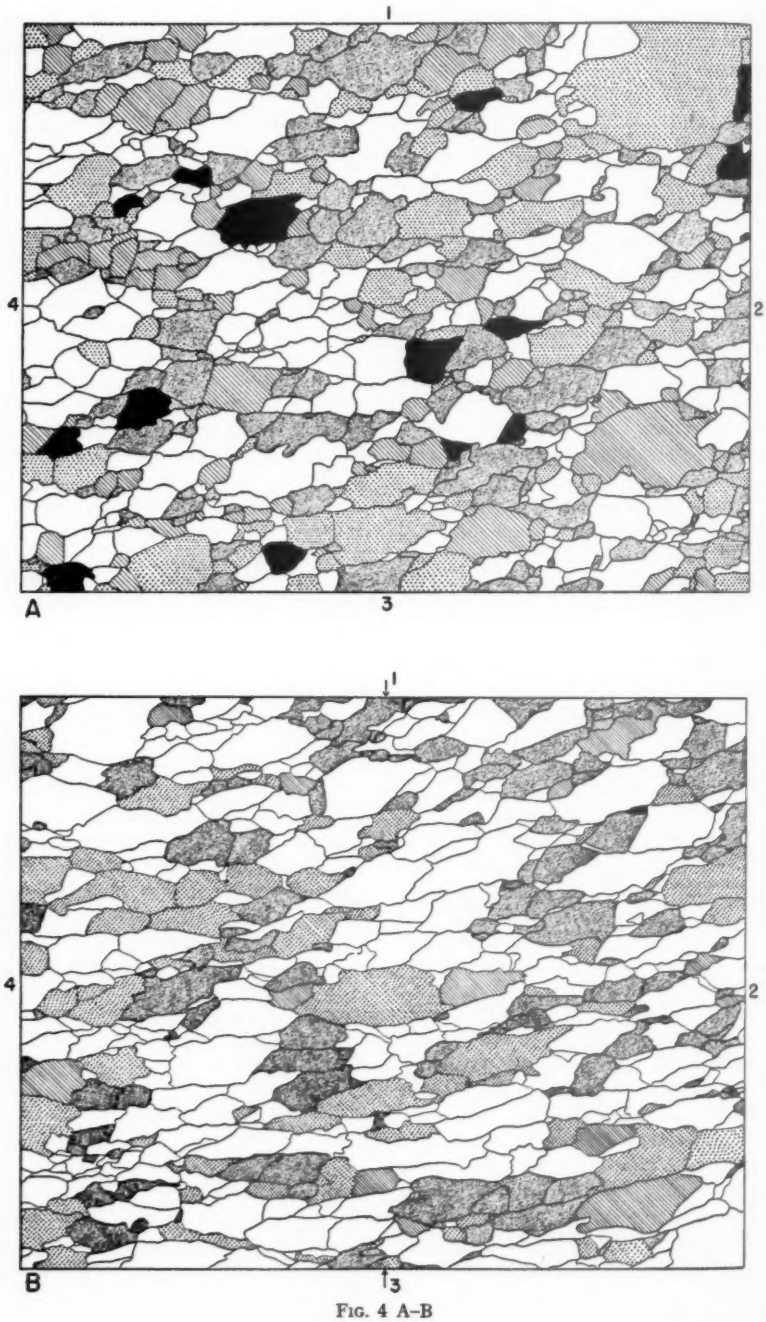

FIG. 4 A–B

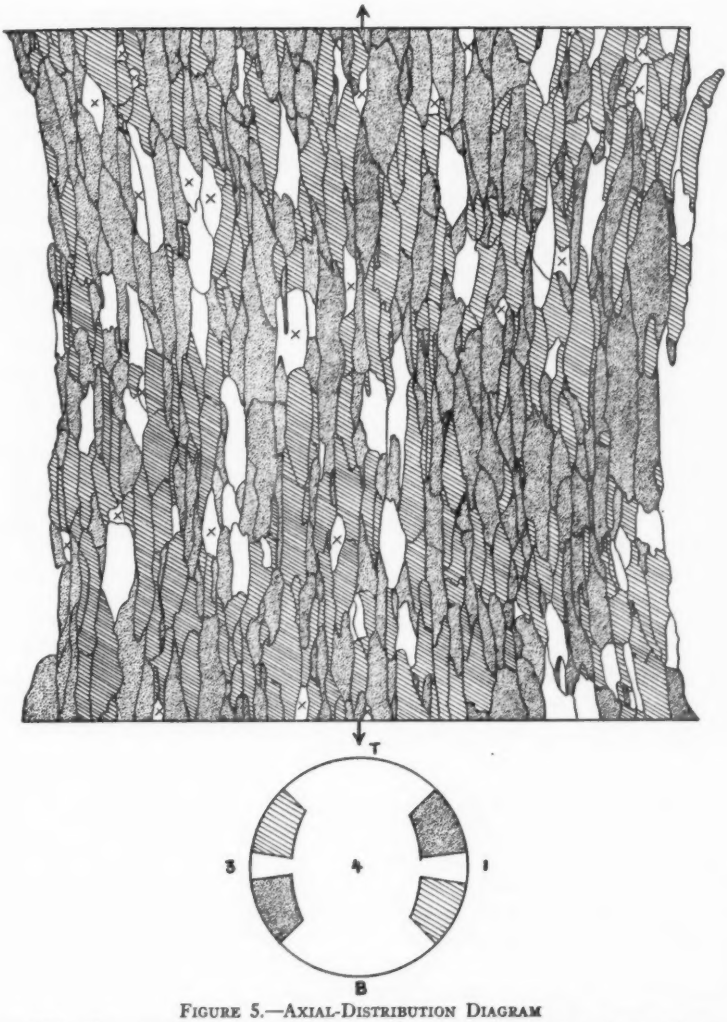

FIGURE 5.—AXIAL-DISTRIBUTION DIAGRAM

Specimen 459 locally extended 118 per cent at 500° C. Tracing of photomicrograph of section cut parallel to 2 in necked zone. Lower diagram shows orientation of specimen and of *c* axes. (*Cf.* Fig. 10, A and B.) In upper diagram grains are shaded to correspond to the orientations similarly shaded in the lower figure. Crosses indicate grains whose orientations could not be measured. Arrows indicate extension axis.

FIGURE 4.—AXIAL-DISTRIBUTION DIAGRAM

Tracings of photomicrographs of sections cut parallel to *T*; orientation is indicated by numbers at margins. Each grain is shaded to indicate orientation of the *c* axis in the corresponding sector of Figure 3. Magnification × 1.5.

A. Specimen 172, undeformed

B. Specimen 295, shortened 19 per cent parallel to arrows. Note virtual elimination of unstable orientations (ruled or black).

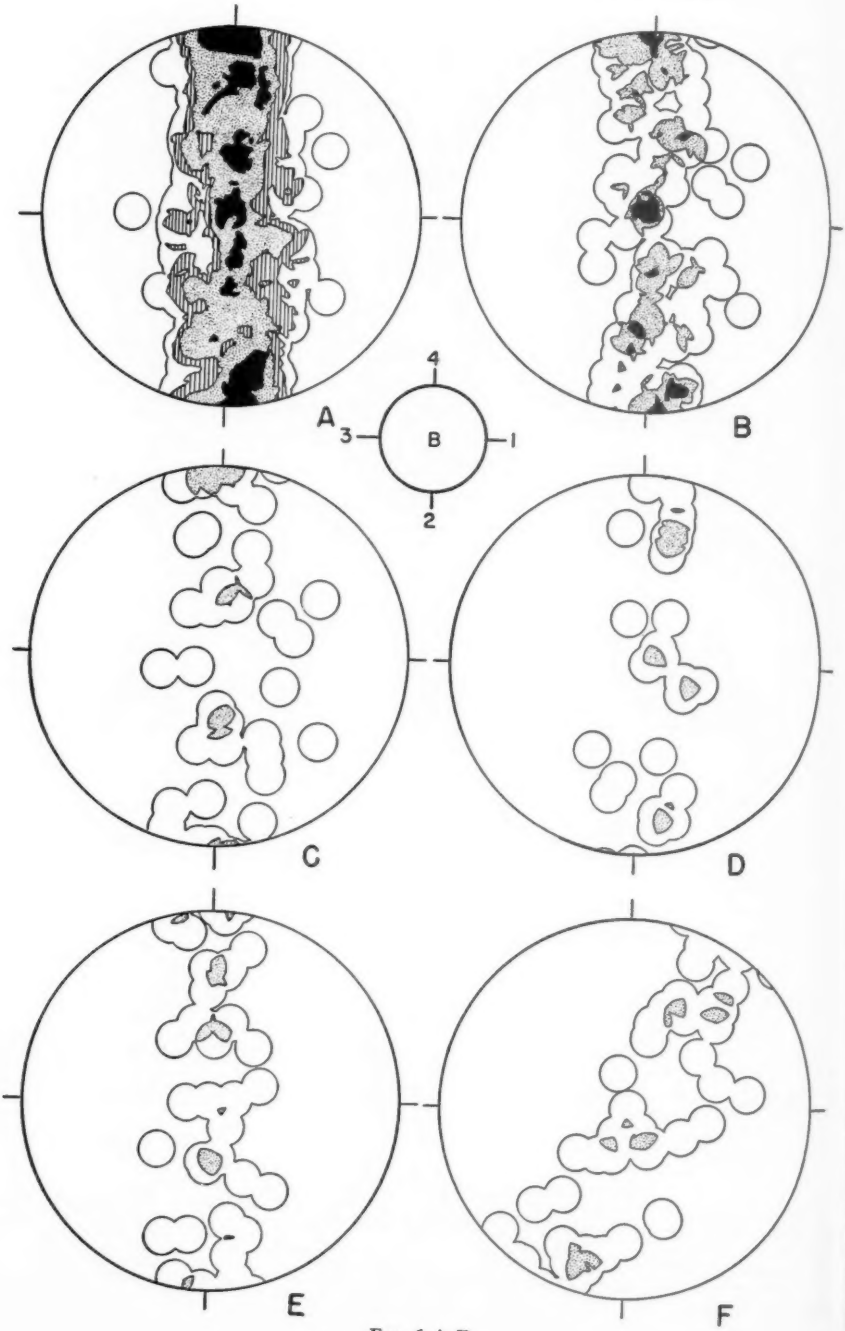

FIG. 6 A–F

Symmetry of Deformation

In both compression and extension experiments the ideal symmetry of the load system is polar. There is a principal plane of symmetry normal to the axis of loading; parallel to this axis is an infinite number of planes of symmetry. Ideal polar symmetry of load was approximated in experiments 409, 443, 459, and 477. (*Cf.* Fig. 8A, B.) On the other hand experiment 400 is typical of several in which unintentional slight eccentricity of loading induced diagonal shear (Fig. 8C), and here the symmetry of load is monoclinic. There is a single symmetry plane parallel to the axes of loading and normal to the shear plane; normal to this symmetry plane is an axis of two-fold symmetry.

The pattern of preferred orientation of calcite grains in the initial fabric has polar symmetry. A concentration of *c* axes normal to the foliation defines the polar symmetry axis, and the foliation plane is the principal plane of symmetry.

The symmetry of deformation in any experiment can be deduced from the geometrical shape of the deformed cylinder. In every instance it combines the symmetry of load with the symmetry of the initial fabric. When the axis of compression or extension is normal to the initial foliation (experiments 409 and 477) the polar symmetry axis of load coincides with that of the initial fabric; the deformed cylinder remains almost circular in cross section (Fig. 8D, E); the symmetry of deformation is polar. When the axis of compression or extension lies in the plane of initial foliation (experiments 443 and 459) the polar axes of load and initial fabric are mutually perpendicular, the cross section of the deformed cylinder is elliptical (Fig. 8G, H), there are three mutually perpendicular symmetry planes intersecting in three symmetry axes, and the symmetry of deformation accordingly is orthorhombic. In experiment 400 the polar symmetry axis of the initial fabric lies in the single symmetry plane of the eccentric load system, the shear band is elliptical in cross section, and the symmetry of deformation for the specimen as a whole is monoclinic (Fig. 8C, F).

Results of Petrofabric Analysis

Marble deformed by compression.—In Figure 9 are three pairs of orientation diagrams, for *c* axes and for most prominent *e* lamellae in the same grains measured in three cylinders deformed by compression. The symmetry of each pair of diagrams corresponds with that of deformation as indicated by change in shape of the cylinder:

Figure 9A, B (specimen 409): polar symmetry; compression axis is principal axis of symmetry.

Figure 9C, D (specimen 443): orthorhombic symmetry; three axes of two-fold symmetry respectively parallel to compression axis, normal to initial foliation, and normal to both these directions.

Figure 9E, F (specimen 400): monoclinic symmetry; deformation plane (plane of orientation diagrams) is sole plane of symmetry.

All three *c*-axis diagrams show preferred orientation of axes inclined at between 10° and 30° to the axis of compression. In Figure 9A they are distributed through a ring maximum. In Figure 9C the *c* axes are concentrated in a pair of maxima symmetrically situated in the plane containing the axis of compression and the initial direction (1–3) of preferred orientation of *c* axes. Figure 9E shows a single *c*-axis maximum lying between the axis of compression and the normal to the diagonal shear zone that has formed (*SS* in Fig. 8C).

FIGURE 6.—ORIENTATION DIAGRAMS FOR *a* AXES OF CALCITE

Specimen 172, undeformed. Equal-area projections, lower hemisphere; orientation shown in inset.

A. 258 axes in 86 grains in four aggregates, orientation group II (Fig. 3). Contours 0.4%, 1%, 2%, 4%, per 1% area.

B. 87 axes in 29 grains forming one aggregate, orientation group II. Contours 1%, 3.5%, 5.5%, per 1% area.

C. 36 axes in 12 large grains of same aggregate as B. Contours 2.5%, 8%, per 1% area.

D. 24 axes in 8 large grains of another aggregate, orientation group II. Contours 4%, 12.5%, per 1% area.

E. 33 axes in 11 large grains of another aggregate, orientation group II. Contours 3%, 9%, per 1% area.

F. 39 axes in 13 large grains forming one aggregate, orientation group III. Contours 2.5%, 7.5%, per 1% area.

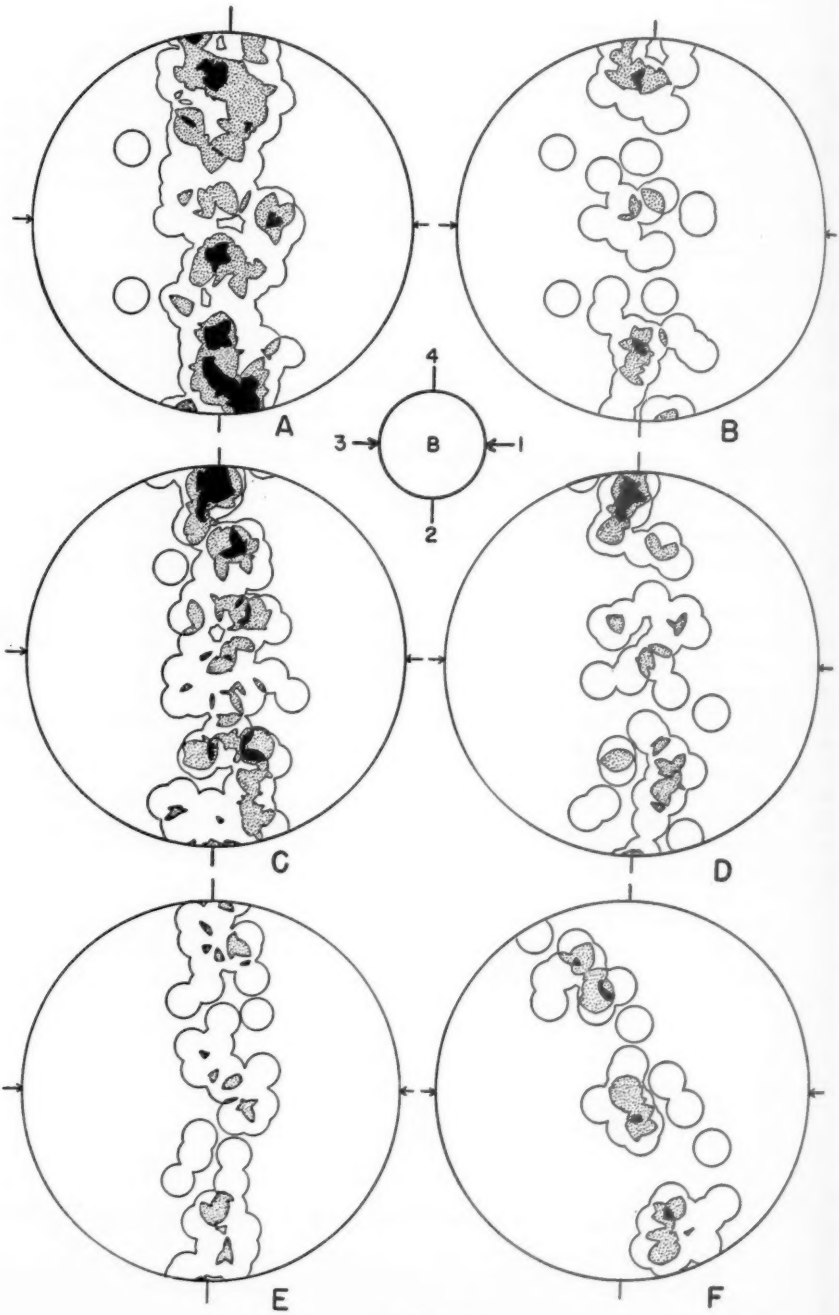

FIG. 7 A–F

In the single compression specimen examined, the *a* crystal axes in one sample have distinct preferred orientation; one axis is normal to the axis of compression (Fig. 11A). This is local, however, and is not obvious in another sample of grains (Fig. 11B).

Poles of most prominent *e* lamellae (one set per grain) likewise show strong preferred orientation. In Figure 9, B and D, there is a single lamella-pole maximum coinciding with the axis of compression. It is much more sharply defined in Figure 9B than in Figure 9D. In Figure 9F the lamella-pole maximum is situated between the axis of compression and the normal to the shear zone. In all three fabrics the lamella-pole maximum coincides with the normal to the average plane of flattening of calcite grains, *i.e.*, there is marked preferred orientation of *e* lamellae in the newly developed plane of foliation. (*Cf.* Pl. 1.)

The plotted *e* lamellae of most grains are obviously the result of twinning. In some grains the presence of a few conspicuous dark L_2 or L_3 lamellae shows that twinning is almost or quite complete (*cf.* Turner, Griggs, and Heard, 1954, p. 902), but the twin plane may or may not correspond to the most prominent set of *e* lamellae in such grains. Twinned grains are much more numerous in specimen 443 than in the other two specimens. Indeed the profound change in preferred orientation of *c* axes in 443 shows that the dominant lattice in most grains is twinned in relation to the initial, now subordinate, lattice of the grain. Many of the lamellae recorded and plotted as *e* are inclined to the *c* axis at anomalous angles and belong to the category of internally rotated lamellae designated L_1 and L_7 (Turner, Griggs, and Heard, 1954, p. 930).

Marble deformed by extension.—Figure 10 shows orientation diagrams for *c* axes and for poles of most prominent lamellae (one set per grain) in two specimens deformed by extension. In each specimen measurements were confined to the highly deformed necked region. In specimen 459 (Fig. 10A–C) symmetry of fabric as shown by the orientation diagrams corresponds exactly with that of deformation: orthorhombic symmetry; three axes of binary symmetry, (1) parallel to extension axis, (2) normal to initial foliation, (3) normal to (1) and (2). In specimen 477 it is impossible to locate some *c* axes and all *e* lamellae whose poles would fall in the central portion of the projections. Consequently the orientation diagrams (Fig. 10D, E) only imperfectly depict the state of preferred orientation. Both diagrams are consistent with, but do not clearly demonstrate, polar symmetry of fabric, with the extension axis as principal axis of symmetry.

In both specimens the great majority of *c* axes are inclined 60° to 80° to the axis of extension. In Figure 10A, B they are restricted to two very strong concentrations, symmetrically located in the plane that contains the axis of extension and the initial direction of preferred orientation of *c* axes (horizontal diameter). The patterns of preferred orientation for a strain of 118 per cent in the central neck (Fig. 10B) and for a strain of 80–90 per cent in an adjoining region of the same specimen (Fig. 10A) are identical. Specimen 520, strained under the same conditions but at one-tenth the normal rate, shows an identical pattern of preferred orientation of *c* axes (not reproduced here). In Figure 10D the *c* axes tend to be more evenly distributed through a cleft girdle whose axis is the axis of extension.

FIGURE 7.—ORIENTATION DIAGRAMS FOR *a* AXES IN CALCITE

Specimen 295, shortened 19 per cent, 300° C. Equal-area projections, lower hemisphere; orientation shown in top circle; axis of compression shown by arrows.

A. 99 axes in 33 grains forming one aggregate, orientation group II (Fig. 3). Contours 1%, 3%, 5%, per 1% area.

B. 45 axes in 15 large grains of same aggregate as A. Contours 2%, 7%, 11%, per 1% area.

C. 81 axes in 27 grains forming another aggregate, orientation group II. Contours 0.8%, 4%, 5.6%, per 1% area.

D. 45 axes in 15 large grains of same aggregate as C. Contours 2%, 7%, 11%, per 1% area.

E. 39 axes in 13 large grains of another aggregate, orientation group II. Contours 2.5%, 7.5%, per 1% area.

F. 39 axes in 13 large grains of another aggregate, orientation group I. Contours 2.5%, 7.5%, 11%, per 1% area.

If allowance is made for grains whose *c* axes could not be measured but would fall somewhere in the central partially blind spot, the actual distribution of *c* axes in the fabric must be more regular than that shown.

Figure 11C and D shows distinct preferred orientation of the three *a* crystal axes at 10°, 45°, and 65° to the axis of extension. Maxima *X*, *Y*, and *Z* are 60° apart.

Most prominent *e* lamellae are subparallel to the axis of extension. (*Cf.* Pl. 3.) The strong maximum in Figure 10C is real, for in this case the *c* axes of almost all grains are so oriented that it is possible to measure all three *e* planes in each. In Figure 10E, however, all three *e* planes of many grains are inaccessible, and the central portion of the diagram is necessarily a blind spot. As in compressed specimens, the most prominent *e* lamellae of 459 and 477 commonly are the result of twinning. Completely twinned grains with obvious L_3 lamellae are present in both sections (dark lamellar grains in Pl. 3, 4). They are much more numerous in specimen 477 than in 459 and testify to the relatively important role of twinning in deformation of 477.

Evidence of Possible Recrystallization

Marble deformed at 300° C yielded petrographic indications of intergranular flow and boundary recrystallization that were not present in specimens similarly deformed at room temperature (Griggs *et al.*, 1953, p. 1327, 1342). It was anticipated that recrystallization would become much more active at higher temperatures. Actually there is little evidence to this effect in specimens deformed at 400° C and 500° C. Plastic deformation of individual grains, accompanied by appropriate external rotation and differential movement along grain boundaries, and local development of smaller subgrains together can account for most observed textures and all the preferred-orientation data.

One possible indication of incipient recrystallization was first observed in specimen 409, which was deformed under conditions designed to promote crystallization. This specimen was shortened by 39.9 per cent in 400 minutes (one-tenth the normal strain rate) and was then held for 12 hours at the temperature and pressure of deformation (400° C, 3000 atmospheres). In many grains (*e.g.* Pl. 5, fig. 4; Fig. 19) there are small sharply bounded lobes and discontinuous lensoid streaks whose orientation differs notably from that of the host grain. No matter how the host is oriented, the *c* axes of the lobes are very strongly oriented parallel to the axis of compression. This may be an effect of incipient recrystallization. If so, it is accompanied by reorienting of the lattice with the *c* axis parallel to the axis of compression.

A similar effect has been observed in two specimens (459 and 520) highly elongated at 500° C. Here there is a distinct tendency for the "recrystallized" streaks to be oriented with the *c* axis at 80°–90° to the axis of elongation. In a few instances the "recrystallized" portion may rival the remainder of the grain in size, and its true nature can be recognized only by the absence of sharply defined intergranular boundary such as that which invariably separates grains of independent origin.

An attempt was made to induce recrystallization in Yule marble which had been deformed previously. A specimen which had been compressed 12 per cent normal to the foliation was broken in two. Dr. G. C. Kennedy subjected one half to 300 atmospheres of H_2O plus 300 atmospheres of CO_2 for 2 weeks at 450° C. Both

---

PLATE 1.—PHOTOMICROGRAPHS

Specimen 409. *1* cylinder, shortened 39.9 per cent; section cut parallel to *T*; compression axis vertical.

FIGURE 1.—Complete longitudinal section of cylinder. Magnification ×6

FIGURE 2.—Circled area in *A*, showing alignment of $\{01\bar{1}2\}$ lamellae normal to compression axis. Magnification ×50

PLATE 2.—PHOTOMICROGRAPH

Specimen 443. *T* cylinder, shortened 40.7%; complete section cut parallel to *2*; compression axis vertical. Note reduction in grain size as compared with relatively undeformed marble at ends. Magnification ×9

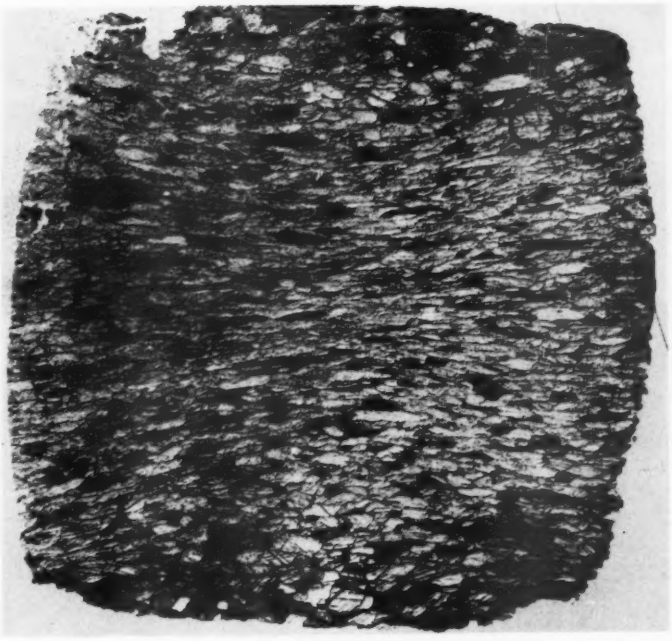

FIGURE 1

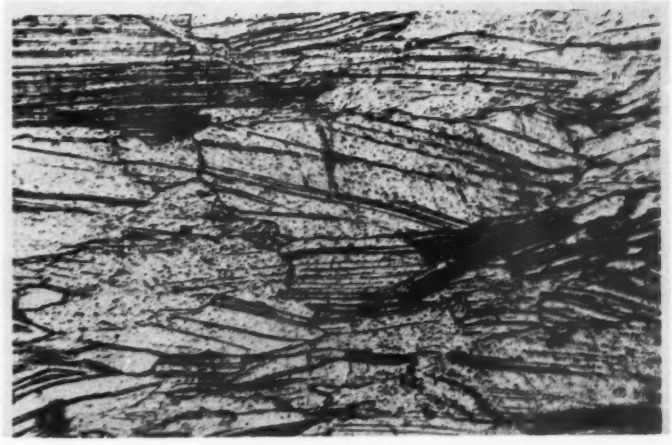

FIGURE 2

PHOTOMICROGRAPHS

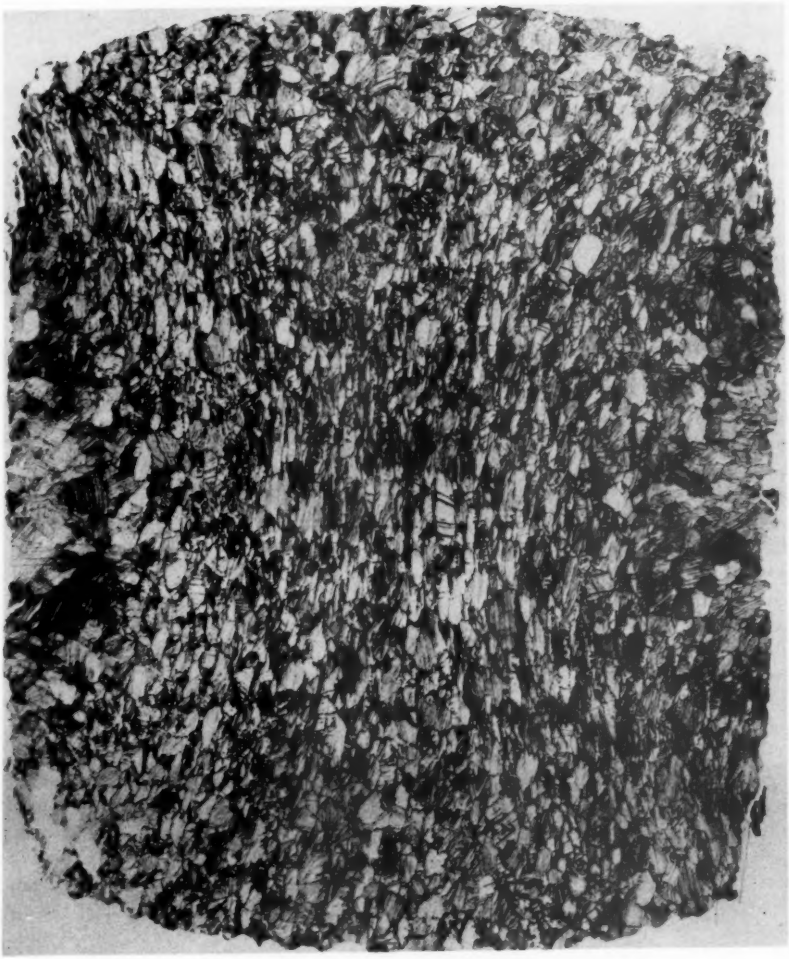

PHOTOMICROGRAPH

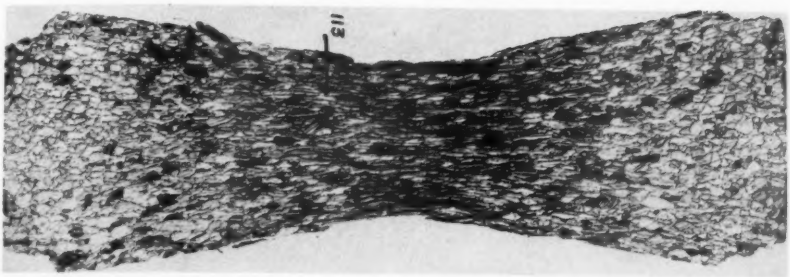

FIGURE 1

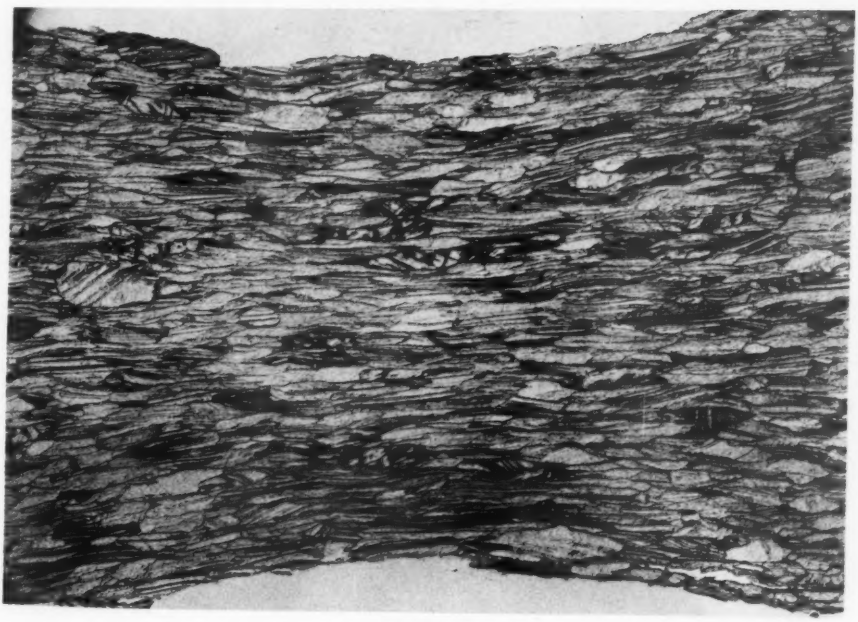

FIGURE 2

PHOTOMICROGRAPHS

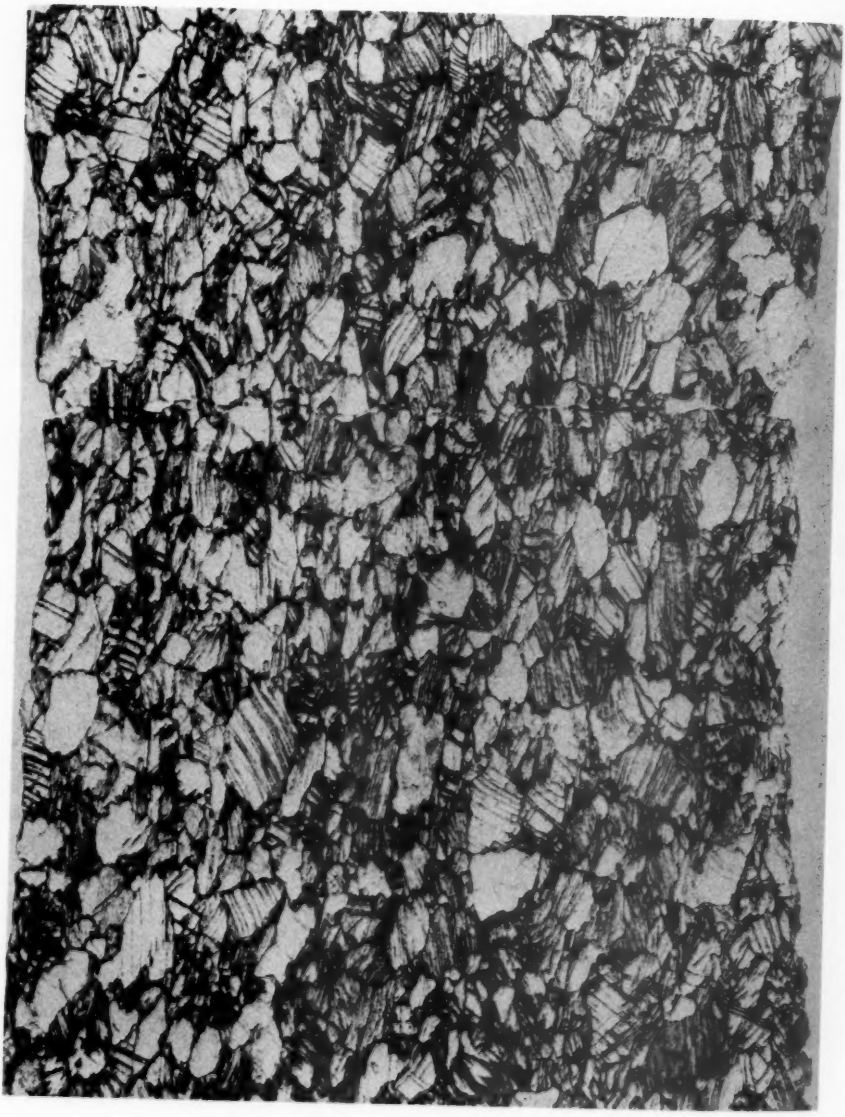

PHOTOMICROGRAPH

pieces were then sectioned and studied. There was no difference between them.

The Orienting Mechanism

Relation between Single Crystals and Aggregates

When the mechanisms of deformation of single crystals are known, it should be possible to predict both the stress-strain curves and the changes in preferred orientation of polycrystalline aggregates. Students of metals have long sought to do this with varying success. Outstanding among these is Taylor's (1938) treatment of aluminum aggregates. Aluminum has high symmetry and can glide with equal ease in both senses on each of 24 glide systems. Because of this high symmetry, the angle between glide planes and lines having maximum resolved shear stress in each of two adjacent crystals must always be small. Presumably because of this, there is little difference between the stress-strain curves of single crystals and those of aggregates in aluminum.

Taylor (1938) assumed, for the purposes of calculation, that the deformation of each grain in an aggregate is exactly the same as that of the material as a whole. In order to achieve this it is necessary that five glide planes operate simultaneously. He deduced which planes would function in a stressed aggregate from the principle of least work. He obtained a predicted stress-strain curve for an aluminum aggregate which was in good agreement with observations. He also predicted changes in the preferred orientation of grains which qualitatively agreed with those observed. Barrett and Levenson (1940) showed, however, that the actual directions of rotation are different from that predicted in about one-third of the grains.

There is abundant evidence from metals that grain deformation is not strictly homogeneous. This has led to a wide range of individual views among metallurgists between Taylor's extreme on the one hand and the hypothesis of Cox and Sopwith (1937) who assumed that no restriction is imposed on the deformation of a grain by its neighbors.

Handin and Griggs (1951) tested these two hypotheses, with respect to the Yule marble, by predicing fabric changes which were then compared with observed changes. The predictions based on Taylor's "homogeneous" hypothesis agreed closely with observations, while those based on the "heterogeneous" hypothesis were grossly different. Handin and Griggs' treatment was based on one assumption now known to be in error: that *e* translation was the complementary glide system in addition to *e* twinning. This error does not, however, affect this test of the homogeneous hypothesis, since the important orientation changes for the relatively low deformations that they considered were due to *e* twinning. This will be only slightly affected by substituting *r* translation for *e* translation as the second mechanism of deformation. (*Cf.* Turner, Griggs, and Heard, 1954.)

The earlier data recorded by Griggs and Miller (1951) and by Handin and Griggs (1951) also appeared to provide a test for the homogeneous hypothesis in correlating the anisotropy of the stress-strain curves with that of the original fabric. This apparent correlation was misleading, since it is now found to be insensitive to the mechanism of deformation assumed. There exists no basis for correlating the stress-strain curves of the aggregate with those of the single crystals, because it is impossible to assess the effects of grain boundaries.

Plate 3.—PHOTOMICROGRAPHS

Specimen 459. *T* cylinder, elongated 40%, maximum elongation in neck = 118%; section cut parallel to *2*; extension axis vertical. Note rarity of dark completely twinned grains.

Figure 1. Complete section. Position of grain 113 is shown. Magnification ×3.7

Figure 2. Necked region. Magnification ×9

Plate 4.—PHOTOMICROGRAPH

Specimen 477. *1* cylinder, elongated 48 per cent, maximum elongation in neck is 93 per cent; section cut parallel to *T*; extension axis vertical. Magnification ×12

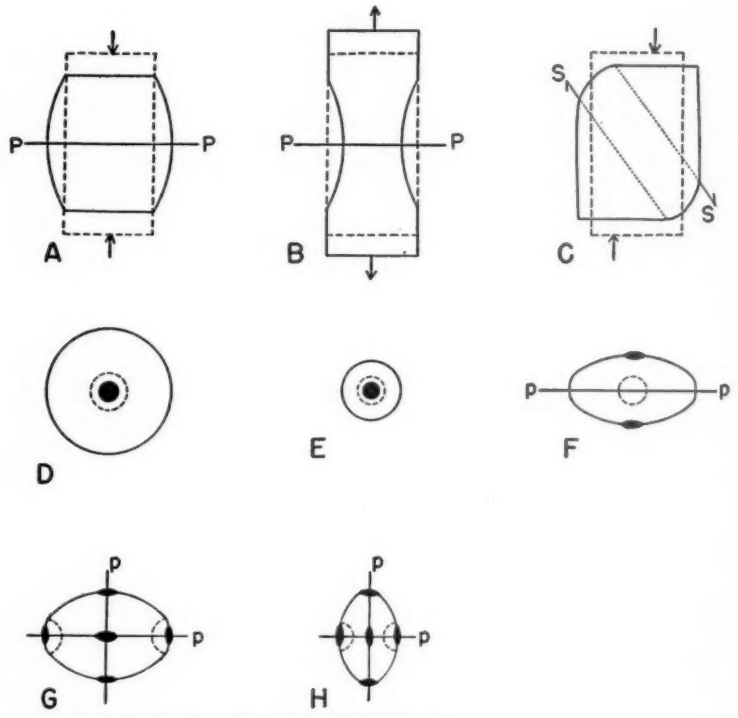

FIGURE 8.—SYMMETRY OF DEFORMATION AND OF FABRIC

A–C. Longitudinal sections through cylinders showing applied force (arrows), original outline (broken lines), and outline after deformation (full lines).

A. Compression; 409, 443.

B. Extension; 459, 477.

C. Diagonal shear under eccentric compression; 400.

D–H. Cross sections of deformed cylinders. Broken circles show concentration of *c* axes of calcite in undeformed marble fabric. Solid circles—axes of polar symmetry; solid ellipses—axes of two-fold symmetry; full lines—planes of symmetry in deformed fabric.

D. Compression, 409, *1* cylinder.

E. Extension, 477, *1* cylinder.

F. Diagonal shear, 400, *1* cylinder.

G. Compression, 443, *T* cylinder.

H. Extension, 459, *T* cylinder.

FIGURE 9.—ORIENTATION DIAGRAMS FOR *c* AXES AND *e* LAMELLAE OF CALCITE, YULE MARBLE DEFORMED BY COMPRESSION

Equal-area projections, lower hemisphere; axis of compression shown by arrows; mean elongation of grains—*EE*; initial foliation is *NS*, normal to plane of projection.

A. Specimen 409, *1* cylinder, shortened 39.9 per cent. 100 *c* axes. Contours 1%, 5%, 10%, per 1% area.

B. Specimen 409. Most conspicuous *e* lamellae (1 per grain) in 100 grains. Contours 1%, 5%, 20%, per 1% area.

C. Specimen 443, *T* cylinder, shortened 40.7 per cent. 100 *c* axes. Contours 1%, 5%, 8%, per 1% area.

D. Specimen 443. Most conspicuous *e* lamellae (1 per grain) in 100 grains. Contours 1%, 5%, 8%, per 1% area.

E. Specimen 400, *1* cylinder shortened 37% by diagonal shear parallel to SS. 100 *c* axes. Contours 1%, 5%, 10%, per 1% area.

F. Specimen 400. Most conspicuous *e* lamellae (1 per grain) in 100 grains. Contours 1%, 5%, 10%, 20%, per 1% area.

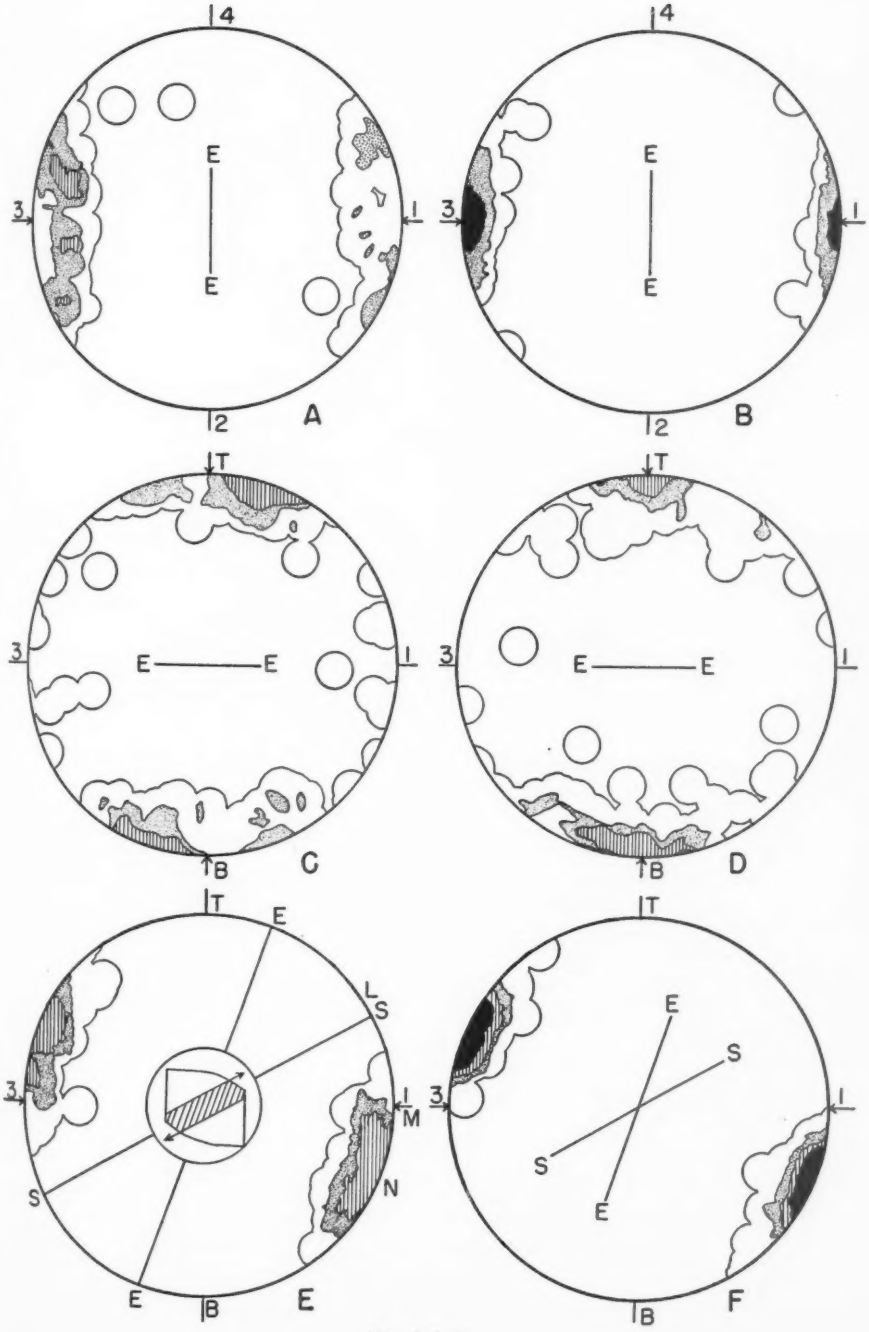

FIG. 9 A–F

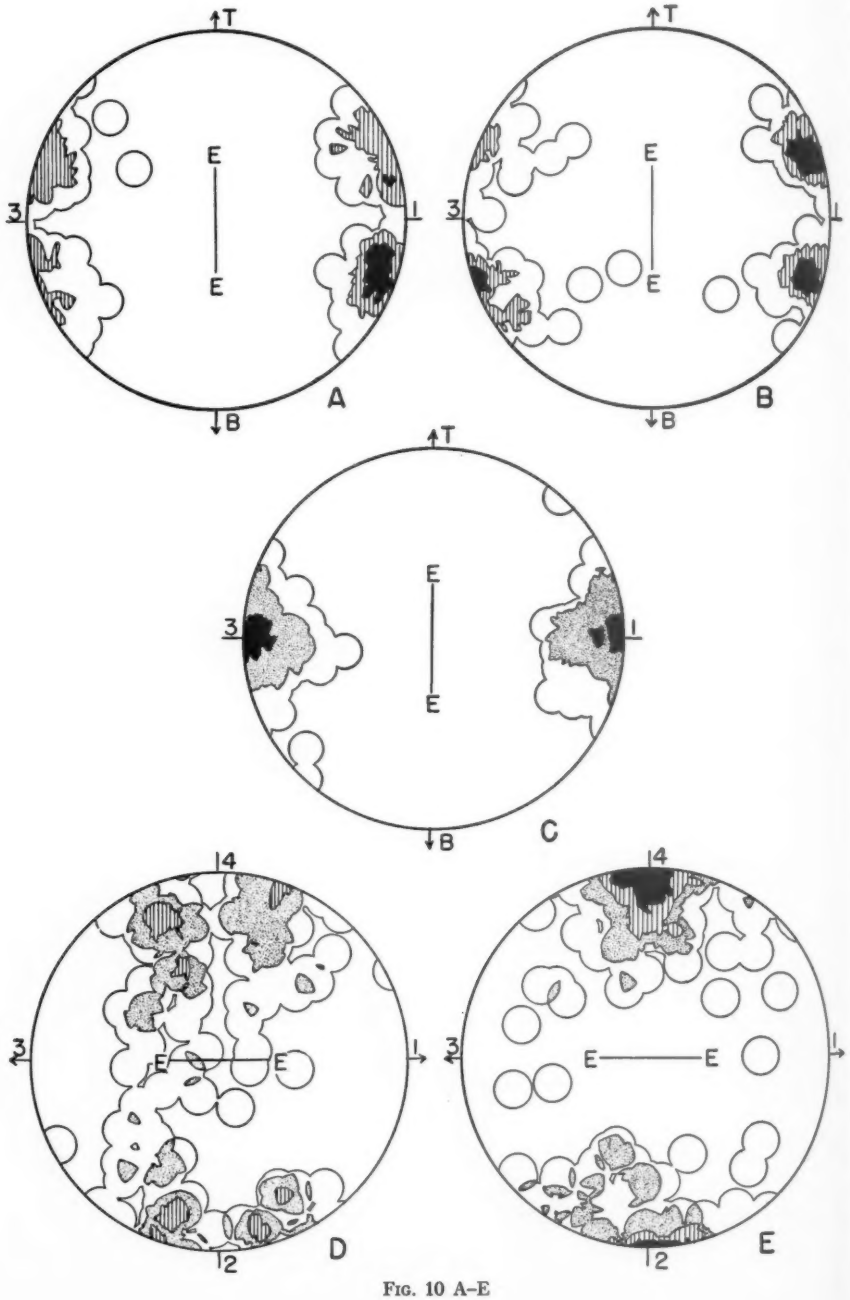

FIG. 10 A–E

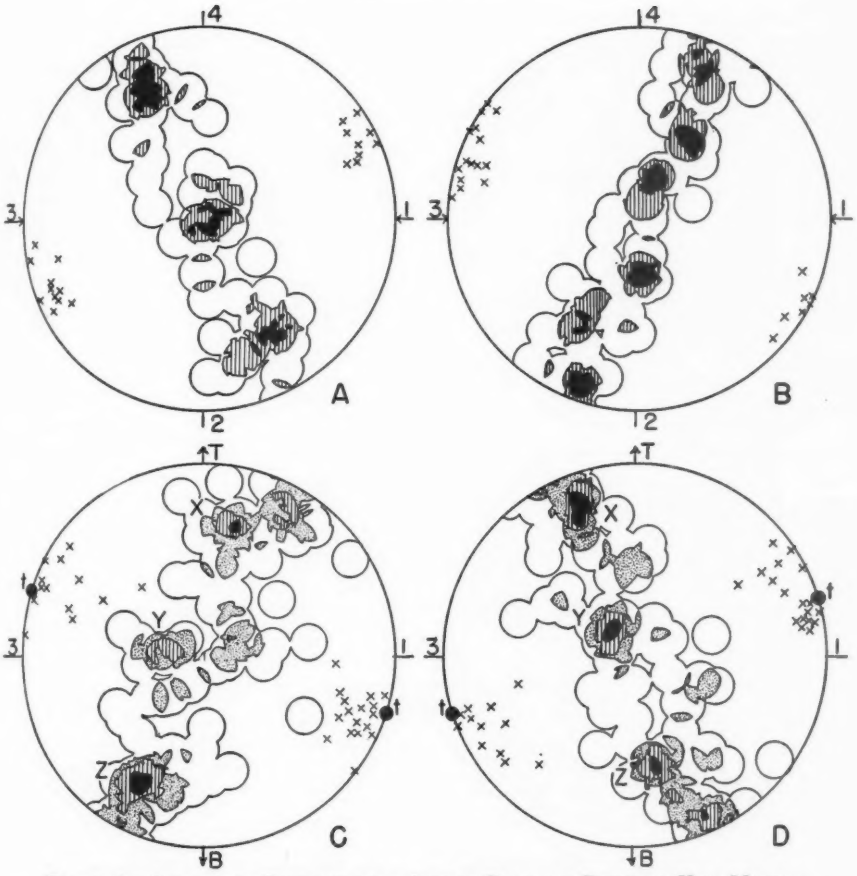

FIGURE 11.—ORIENTATION DIAGRAMS FOR *a* AXES OF CALCITE IN DEFORMED YULE MARBLE

Equal-area projections, lower hemisphere; axis of applied force shown by arrows, initial foliation is *NS*, normal to plane of foliation; *c* axes of measured grains shown by crosses. Each diagram shows 90 *a* axes in 30 grains; contours 1.1%, 3.3%, 5.5%, 8.8%, per 1% area.

A and B. Specimen 409, *1* cylinder shortened 39.9 per cent.

C and D. Specimen 459, *T* cylinder elongated 40 per cent. Grains were measured in neck where elongation is 118 per cent. Theoretically stable orientation of *c* axis (T, Figure 15) is shown at *t*; corresponding positions of 3 *a* axes in the stably oriented lattice coincide with *X*, *Y*, *Z*.

FIGURE 10.—ORIENTATION DIAGRAMS FOR *c* AXES AND *e* LAMELLAE OF CALCITE, YULE MARBLE DEFORMED BY EXTENSION

Equal-area projections, lower hemisphere; axis of extension shown by arrows; mean elongation of grains—*EE*; initial foliation is *NS*, normal to plane of projection.

A. Specimen 459, *T* cylinder elongated 40 per cent. 100 *c* axes measured near top of necked zone (local elongation 80–90 per cent). Contours 1%, 5%, 10%, per 1% area.

B. Specimen 459. 100 *c* axes measured in middle of necked zone (local elongation 118 per cent). Contours 1%, 5%, 10%, per 1% area.

C. Specimen 459. Most conspicuous *e* lamellae, 152 in 100 grains. Contours 0.6%, 3.3%, 13%, per 1% area.

D. Specimen 477, *1* cylinder elongated 48 per cent. 125 *c* axes in necked zone (local elongation 90 per cent). Contours 0.8%, 2.4%, 5%, per 1% area.

E. Specimen 477. Most conspicuous *e* lamellae, 110 in 100 grains. Contours 1%, 3%, 5%, 10%, per 1% area.

Yule marble *1* cylinders have an initial preferred orientation qualitiatively similar to cylinders cut from single crystals parallel to the *c* axis. The latter are 10 times as strong in compression as in extension, whereas the marble is only 50 per cent stronger in compression.

Internal rotation of *e* lamellae in calcite provides a basis for determining the strain and the deformation history of individual grains. This permits a further test of the "homogeneous" hypothesis in Yule marble. It also can provide details of the development of preferred orientation.

Predicted Behavior of Individual Grains

Basic assumptions.—It has been shown experimentally (Turner, Griggs, and Heard, 1954) that at 300° C–400° C there are two gliding mechanisms for calcite: (1) twin gliding on $\{01\bar{1}2\} = e$, with the edge $[e_1{:}r_2]$ as glide direction, sense of shear positive;[3] (2) translation gliding on $\{10\bar{1}1\} = r$, with the edge $[r_1{:}f_2]$ as glide direction, sense of shear negative[4] (Turner, Griggs, and Heard, 1954).

At 300°–500° C the critical resolved shear stress for *r* translation at the yield point is still several times greater than that which induces twin gliding on *e*.

Students of metal fabrics (*e.g.* Taylor, 1938; Barrett, 1952, p. 448–457) have predicted the behavior of individual grains during deformation of polycrystalline metals whose glide mechanisms are known. A similar prediction has been made for calcite grains in marble on the basis of three assumptions: (1) Deformation is homogeneous. (2) The law of maximum resolved shear stress determines which $\{01\bar{1}2\}$ or $\{10\bar{1}1\}$ glide system or systems shall predominate in deformation. (3) Twin gliding on $\{01\bar{1}2\}$ will occur rather than translation on $\{10\bar{1}1\}$ wherever the resolved shear-stress coefficient, S_O, for one $\{01\bar{1}2\}$ system exceeds some limiting value, with the sense of shear positive. $S_O = 0.05$ has been selected arbitrarily as this limiting value. None of these assumptions can be expected to hold true rigorously for every grain in the strained aggregate. The extent to which predicted behavior and fabrics depart from those actually observed will provide some measure of the general validity of the three assumptions.

A necessary consequence of homogeneous deformation by gliding on one system per crystal is that every grain rotates bodily (external rotation) in the sense opposite to that of gliding (internal rotation). Thus there is close analogy between the ideal rotation of each grain in the aggregate and the rotation actually observed in experimentally deformed single crystals. (*Cf.* Turner, Griggs, and Heard, 1954, p. 898–899.) Somewhat as kink bands develop in single crystals, so many grains of the marble aggregate develop extinction bands differing as much as 5°–20° in crystallographic orientation. The boundaries between adjacent bands may sharpen to the point where the grain becomes divided into subgrains (*cf.* Beck, 1954, p. 269), thus reducing the mean grain size of the aggregate. External rotation may affect subgrains rather than the parent grain as a whole. Development of extinction bands and

[3] Where the upper layers of the crystal are displaced upward toward the *c* axis the sense of shear is said to be positive.

[4] In all experiments where translation on *r* occurred the sense of shear was negative. In other experiments, where the crystal was so oriented that shear could occur on *r* with a positive sense, twin gliding on one or more *e* planes was also possible and actually took place in preference to *r* translation, because of the greater ease of twinning.

PLATE 5.—PHOTOMICROGRAPHS OF INDIVIDUAL GRAINS

Specimen 409. *1* cylinder, shortened 39.9 per cent; section cut parallel to *T*. Magnification ×130

FIGURE 1.—Grain 6, in central part of top half of photograph; rotated *e* lamellae are L_3' trending northeast and L_7 trending northwest. Grain 23, at lower margin of photograph, shows strong lamellar twinning on e_3, trending west-northwest.

FIGURE 2.—Grain 11, completely twinned on $e_2 = L_1$ (nearly horizontal lamellae); dark nearly vertical bands are rotated L_3 lamellae, L_3'.

FIGURE 3.—Grain 22, completely twinned on e_2 (not visible); dark bands are L_3 lamellae inclined at 38° to plane of section and showing surface striation parallel to intersection with e_1 and e_2; subhorizontal lamellae are e_1.

FIGURE 4.—Grain 10, occupying top two-thirds of photograph. Subhorizontal discontinuous streaks with dark outlines are possibly recrystallized calcite with *c* axis parallel to compression axis. (*Cf.* Fig. 19.)

PHOTOMICROGRAPHS OF INDIVIDUAL GRAINS

FIGURE 2

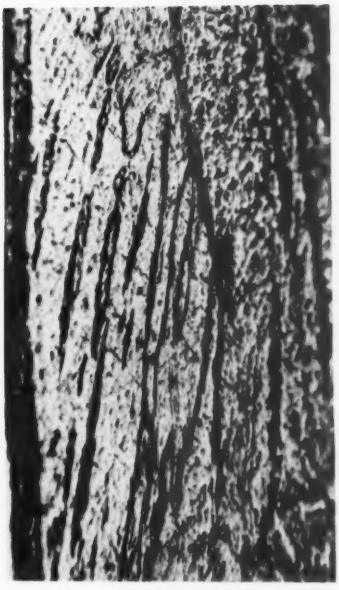

FIGURE 4

FIGURE 1

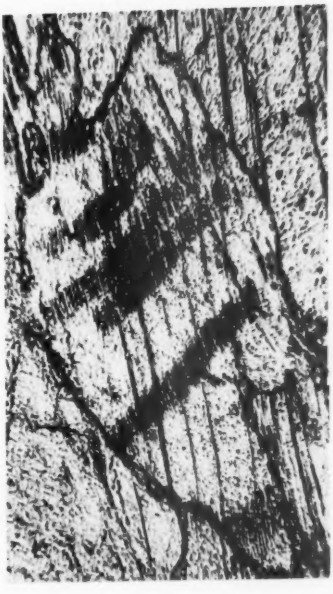

FIGURE 3

subgrains obviously is a departure from one of the primary assumptions, that of homogeneous deformation.

External rotation of a grain can be described as migration of the axis of applied force in relation to the crystal lattice. With progressive rotation, the angle between the single active glide plane and the axis of extension approaches zero; the angle between the glide plane and the axis of compression approaches 90°. In experiments on single crystals of metals and of calcite the precise path along which the axis of applied force migrates through the crystal lattice depends on conditions of experiment. For deformation by gliding on only one set of glide planes, three cases have been recorded (*cf.* Fig. 12):

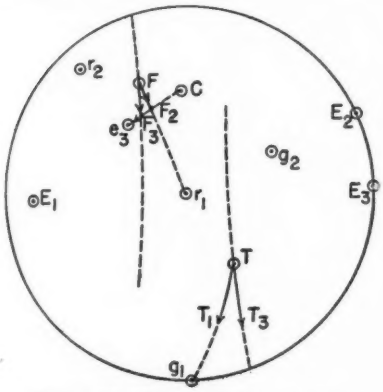

FIGURE 12.—EXTERNAL ROTATION OF CALCITE CRYSTAL IN RELATION TO APPLIED FORCE

Equal-area projection on plane of gliding, r_1.g_1 = glide direction in r_1; g_2 = glide direction in r_2. External rotation is shown as migration of the axis of compression (F) or extension (T) about one of three alternative rotation axes:

E_1: rotation of T to T_1 toward g_1

E_2: rotation of F to F_2 toward r_1

E_3: rotation of T toward T_3 or of F to F_3 on small circle of the projection net

Duplex gliding on r_1 and r_2 gives rotation from F_2 to F_3 to stable orientation coinciding with e_3.

(1) In tension experiments, where the ends of the specimen are constrained to remain coaxial, the axis of tension approaches the glide direction (Schmidt and Boas, 1950, p. 58). The axis of external rotation (Fig. 12, E_1) is the normal to the plane containing the tension axis and the glide direction.

(2) In compression experiments the ends of the specimen are free to move laterally parallel to their line of intersection with the glide plane, and the axis of compression moves directly toward the normal to the glide plane (Schmidt and Boas, 1950, p. 62). The axis of external rotation (Fig. 12, E_2) lies in the glide plane and is normal to the compression axis.

(3) In kink bands, whether developed during compression or extension, the axis of external rotation (Fig. 12, E_3) lies in the glide plane and is normal to the glide line.

It is unlikely that all the grains of a multicrystalline aggregate precisely follow any of these rules in a given experiment. But, if deformation of the specimen is more or less homogeneous, there should be a strong statistical tendency for grains to rotate in order to increase the angle between the active glide plane and the compression axis or to reduce the angle between the glide plane and the axis of extension. Since the longest dimension of the strain ellipsoid in any grain progressively approaches the active glide plane, grains in a highly strained aggregate will have a pronounced tendency to be aligned with their longest dimensions parallel to the axis of extension or normal to the axis of compression. In the analysis which follows it is assumed that the grains of the aggregate behave individually in the manner described under (1) and (2) above. Relations between strain, shear, orientation, and rotation are expressed as follows. (*Cf.* Schmidt and Boas, 1950, p. 57–63.)

For extension,

$$\frac{l_1}{l_0} = \frac{\sin \chi_0}{\sin \chi_1} = \sqrt{1 + 2sS_O + s^2 \sin^2 \chi_0}$$

For compression,

$$\frac{l_0}{l_1} = \frac{\cos \chi_0}{\cos \chi_1} = \sqrt{1 + 2sS_O + s^2 \cos^2 \lambda_0}$$

where χ_0 and χ_1 = angle between glide plane and axis of applied force before and after deformation,

λ_0 = angle between glide direction and axis of applied force before deformation,

S_O = coefficient of resolved shear stress for glide system,

s = shear,

l_0 and l_1 = length of crystal before and after deformation

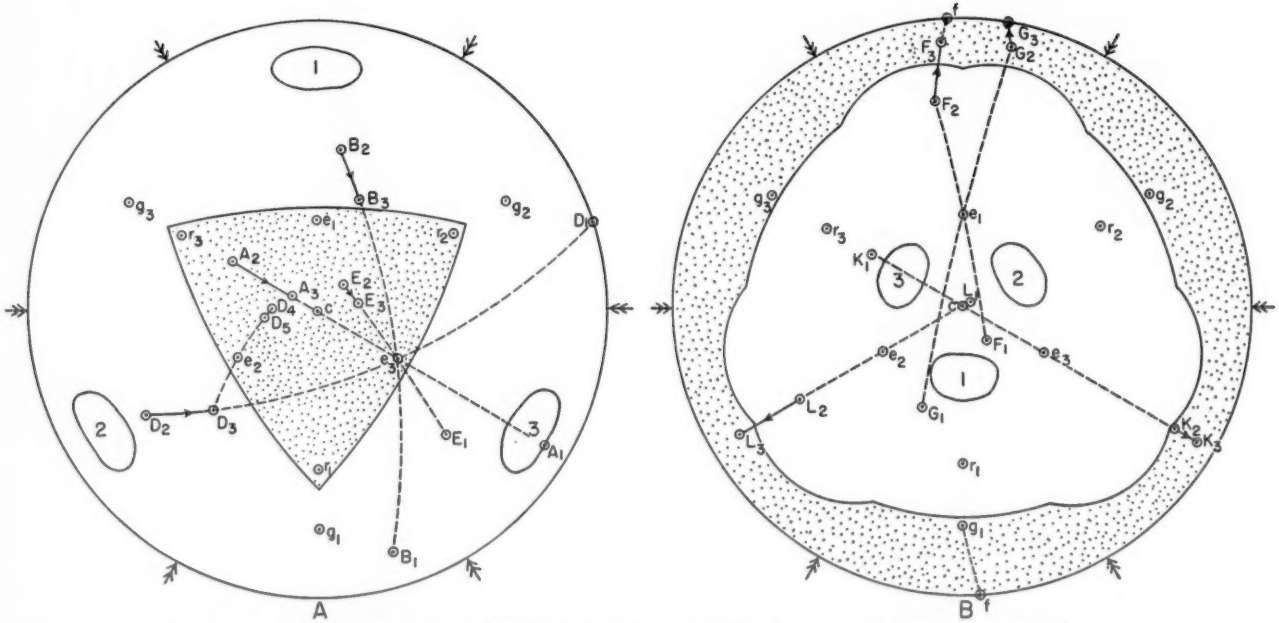

FIGURE 13.—TWIN GLIDING ON *e* AND EXTERNAL ROTATION OF CALCITE CRYSTAL IN RELATION TO APPLIED FORCE

Equal-area projections, lower hemisphere, on plane normal to *c* axis of calcite.

A—conditions for compression. *B*—conditions for extension. Twin gliding can occur if the applied force falls within the blank area. Ellipses show orientations of applied force for which $S_O = 0.45$ for (1) e_1, (2) e_2, and (3) e_3 respectively. Glide lines in e_1, e_2, and e_3 are g_1, g_2, and g_3 respectively. Broken arcs indicate change of orientation by reflection due to twinning; full arcs indicate accompanying external rotation of applied force in relation to the calcite crystal.

Behavior of grains during twin gliding on $\{01\bar{1}2\}$.—Figure 13, A and B, shows projections of a calcite crystal upon which are plotted fields embracing all orientations of applied force permitting twin gliding on at least one of the three *e* planes. The outer limits of these fields are drawn arbitrarily where $S_O = 0.05$. Doubtless this is less than the average critical value for twinning on *e* in preference to translation on *r*. The field within which twinning is likely to occur must therefore be more restricted than shown in Figure 13, A and B.

TABLE 1.—STRAIN AND EXTERNAL ROTATION INDUCED BY TWIN GLIDING ON $\{01\bar{1}2\}$

(*Cf.* Fig. 13.)

Applied force	Initial orientation	χ_0	λ_0	S_O	$\frac{L_0}{L_1}$	χ_1	External rotation*
Compression (Fig. 13A)	A_1	36°	36°	0.48	1.41	55°	19°
	B_1	32°	58°	0.28	1.24	47°	15°
	D_1	18°	53°	0.24	1.23	39°	21°
	E_1	64°	66°	0.36	1.33	71°	7°
	D_3	74°	76°	0.23	1.18	76½°	2½°
					$\frac{L_1}{L_0}$		
Extension (Fig. 13B)	F_1	55°	55°	0.47	1.41	35½°	20°
	G_1	35°	37°	0.46	1.34	25°	11°
	K_1	34°	34°	0.46	1.33	25°	9°
	L_1	62°	62°	0.41	1.39	39°	23°

* For compression the angle of external rotation is $\chi_1 - \chi_0$. For extension the angle of external rotation is $\chi_0 - \chi_1$ only when the axis of extension lies on the great circle containing the glide direction and the pole of the glide plane (*e.g.* *K* and *L* in Figure 13B); for other orientations (*e.g.* *F* and *L*) the angle of external rotation is somewhat greater than $\chi_0 - \chi_1$.

Figure 13A illustrates the changing orientation of a crystal in relation to the axis of compression during progressive deformation by twin gliding on e_3. Four initial orientations of the axis of compression are shown by points A_1, B_1, D_1, and E_1. New orientations resulting from complete twinning on e_3[5] are A_2, B_2, D_2, and E_2; but accompanying external rotation (*cf.* Table 1) changes the final orientations to A_3, B_3, D_3, and E_3. In most cases this final orientation must lie within the field (stippled area of Fig. 13A) where further twinning is impossible. But for a restricted range of orientation, with the axis of compression nearly perpendicular to the *c* crystal axis, twinning may be repeated, as in D_1, which changes to D_3 by twinning on e_3 and then is reoriented to D_5 by twinning on e_2.

Reorientation accompanying twinning induced by extension is illustrated in Figure 13B. Reorientation from F_1 to F_2 with accompanying external rotation to F_3 results from twinning on e_1. Similarly K_1 is reoriented to K_3 by twinning on e_3, and so on. There is no initial orientation permitting repeated twinning. Even if the axis of extension is initially almost parallel to the *c* axis of the crystal (L_1) external rotation (L_2 to L_3) carries the crystal outside the field of possible twinning.

Behavior of grains during translation gliding on $\{10\bar{1}1\}$.—During translation gliding, external rotation alone is responsible for changes in orientation. Figure 14A illustrates migration of the axis of compression in relation to the crystal lattice of calcite. The field of translation gliding is divided into three pairs of sectors according to whether gliding begins on r_1 (blank), r_2. (stippled), or r_3 (ruled). If A_1 represents the initial orientation of the compression axis, gliding begins on r_1, and the orientation changes from A_1 to A_2. At this point S_O has the same value for r_1 and r_2 (0.43; *cf.* Table 2, column 2), and duplex glide on these two planes ensues. The orientation now changes from A_2 to A_3. Other typical paths are $B_1 \rightarrow B_2 \rightarrow B_3$ and $E_1 \rightarrow E_2$. Changing values of S_O on all three *r* glide systems for these and other paths of migration in Figure 14 are given in Table 2. With further rotation beyond A_3, E_2, or G_1 the orientation would enter the field of possible twin gliding on $\{01\bar{1}2\}$. The possibility of twin gliding occurring at this stage and at a comparable stage of extension is discussed below.

For most grains, whether initially oriented in the translation field or reoriented into that field by preliminary *e* twinning, gliding on one *r* system is followed by duplex glide on two *r* systems until orientation of the compression

[5] In Figure 13 these orientations refer to the new lattice resulting from twinning.

FIGURE 14. TRANSLATION GLIDING ON r AND EXTERNAL ROTATION OF CALCITE CRYSTAL IN RELATION TO APPLIED FORCE

Equal-area projection, lower hemisphere, on plane normal to c axis of calcite.

A—conditions for compression. *B*—conditions for extension. Glide lines in r_1, r_2, and r_3 are g_1, g_2, and g_3 respectively. Arrows indicate typical paths of migration (external rotation) of axis of applied force, $A_1 \rightarrow A_2 \rightarrow A_3$, $D_1 \rightarrow D_2$, $L_1 \rightarrow L_2 \rightarrow L_3$, etc. The fields of translation gliding on r_1, on r_2, and on r_3 are blank, stippled, and ruled respectively.

axis normal to e is ultimately achieved. Exceptions are exemplified by D_1, F_1, and G_1. Where the compression axis initially falls on the great circle connecting two r poles, gliding on one r system finally brings the grain normal to e (*e.g.* $G_1 \rightarrow G_2$). Where the compression axis initially falls on a sector boundary there is duplex gliding from the outset ($E_1 \rightarrow E_2$). But if the compression axis lies between c and the pole of r_3, it is rotated by duplex gliding on r_1 and r_2 until it coincides with c, a theoretically stable orientation allowing simultaneous gliding on all three r systems. The paths $D_1 \rightarrow D_2 \rightarrow c$ and $F_1 \rightarrow c$ illustrate this condition, which probably has little or no practical significance. Temporary fluctuations of stress are likely to divert the compression axis into one of the adjoining sectors of Figure 14A; with ensuing gliding on one r system, migration continues along a course such as $F_1 \rightarrow F_2 \rightarrow F_3$.

TABLE 2.—VALUES OF S_O AT SUCCESSIVE STAGES OF EXTERNAL ROTATION DURING TRANSLATION ON $\{10\bar{1}1\}$

Initial orientation	Glide plane	S_o at successive stages		
		1	2	3
Compression (Fig. 14A)				
A_1	r_1	*.43*	*.43*	*.37*
	r_2	.38	*.43*	*.37*
	r_3	.39	.39	.30
B_1	r_1	*.47*	*.46*	*.37*
	r_2	.43	*.46*	.37
	r_3	.43	.43	.30
D_1	r_1	*.40*	*.47*	*.50* at C
	r_2	.32	.45	*.50* at C
	r_3	*.40*	*.47*	*.50* at C
E_1	r_1	*.47*	*.37*	.....
	r_2	.45	.30	.....
	r_3	*.47*	*.37*	.....
F_1	r_1	*.34*	*.42*	*.43*
	r_2	*.34*	.37	.39
	r_3	.25	.38	*.43*
Extension (Fig. 14B)				
K_1	r_1	.10	.03	.01
	r_2	*.23*	*.47*	*.40*
	r_3	.13	.26	.12
L_1	r_1	.09	.04	.01
	r_2	.13	.24	.15
	r_3	*.25*	*.50*	*.39*
M_1, M_1'	r_1	.08	0	.....
	r_2	*.24*	0	.....
	r_3	*.24*	*.38*	.....
P_1	r_1	0	.10	.05
	r_2	*.31*	*.50*	*.39*
	r_3	0	.10	.05

* *Italics* for S_o values designate active glide planes.

Figure 14B illustrates external rotation in extension experiments; corresponding values of S_O on all three r systems are given in the lower half of Table 2. The field of r translation is divided into three pairs of sectors according to whether the active glide system is r_1 (blank), r_2 (stippled), or r_3 (ruled). Typical paths of migration of the extension axis toward the glide direction of the active system are $K_1 \rightarrow K_2 \rightarrow K_3$, $L_1 \rightarrow L_2 \rightarrow L_3$, $P_1 \rightarrow P_2 \rightarrow P_3$. The changing values of S_O (Table 2) are such that duplex gliding never occurs. Simple gliding eventually brings the extension axis to the boundary of the field of possible e twinning (row of arrows in the upper blank sector). The only exception is where the axis of extension initially lies on a sector boundary. Here it migrates, during duplex gliding, to a theoretically stable orientation coinciding with one of the a crystal axes (*e.g.* $M_1 \rightarrow M_2$; $M_1' \rightarrow M_2$). This has little practical significance, since fluctuations in stress would divert the axis of extension into one of the adjoining sectors, and simple gliding on one r would then ensue.

In both compression and extension experiments, all grains of a highly strained aggregate ultimately reach the boundary of the field where e twinning is possible. This applies to the majority of grains in the most highly strained specimens. Assuming shortening by 50 per cent in compression, values of external rotation have been computed, starting from representative initial orientations in the triangle r_3cr_1 of Figure 14A. The ultimate orientations so computed fall within the narrow range between E_3 and g_2. For twin gliding on e_2, S_O lies between 0.10 at E_3 and 0.31 at g_2; corresponding values of S_O for gliding on r_1 and r_3 are 0.32 at E_3 and 0.20 at g_2.

For elongation of 100 per cent in extension experiments, it can similarly be shown that initial orientations lying within the stippled field of Figure 14B will change to final orientations lying within the doubly ruled sector bounded by $m'kpq'$. For points between K_3

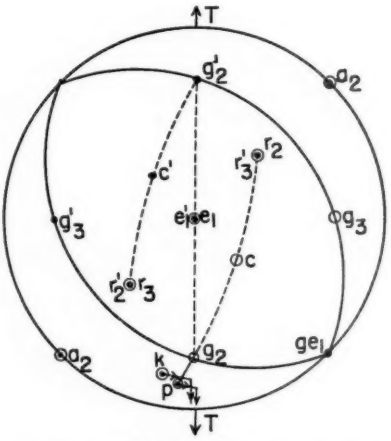

FIGURE 15.—STABLE ORIENTATIONS OF TWINNED CALCITE

Equal-area projection of initial calcite lattice (open circles, c, r_2, r_3, etc.) in relation to lattice formed by twin gliding on e_1 (solid circles, c', r'_2, r'_3, etc.). Points are lettered to correspond with Figure 14. Solid arcs are projections of the two r translation planes common to both lattices. Glide directions in the r translation systems are designated g_2, g_3, g'_2, and g'_3. Direction of twin gliding in e_1 is g_{e_1}. The system is stable for compression normal to e_1 (*i.e.*, normal to plane of projection) or extension parallel to T or to a.

TABLE 3.—S_O FOR $\{10\bar{1}1\}$ GLIDE SYSTEMS FOR STABLE ORIENTATIONS OF CALCITE

(*Cf.* Fig. 15.)

Orientation	S_O for $\{10\bar{1}1\}$		
	$r_1(r_1')$	$r_2(r_2')$	$r_3(r_3')$
1. Compression normal to e_1	0.30	0.37	0.37
2. Extension parallel to a_2	0	0.38	0.38
3. Extension parallel to T, 45° to a_2	0.16	0.38	0

and P_3, S_O for translation on r_2 (0.40) greatly exceeds S_O for twinning on e_1 (0.05); for extreme orientations between k and p, S_O for the two systems becomes approximately equal (0.19 ± 3).

In strained metallic aggregates all grains ultimately approximate a stable orientation in which the active glide systems are symmetrically oriented in relation to the stress system, so that external rotation ceases. (*Cf.* Barrett, 1952, p. 371, 372.) For calcite various stable orientations are possible for grains which, following reorientation during r translation as described above, have then become half-twinned. If the twin plane is e_1, each stable orientation must fulfill the following conditions (*cf.* Fig. 15): (1) the axis of compression is perpendicular, or the axis of extension parallel to e_1; (2) the axis of compression or extension is oriented symmetrically with reference to the active systems $r_2(r'_2)$, $r_3(r'_3)$ of translation gliding; S_O on these systems of translation gliding must be high and must exceed S_O for r_1. There are three such orientations: (1) compression normal to e_1; (2) compression parallel to the a axis that is common to both lattices (a_2, Fig. 15), if all four glide directions are active; (3) extension parallel to e_1 and at 45° to a_2 (T, Fig. 15), if only two glide directions, g_2 and g'_2, are active. Values of S_O for active glide systems r_2 and r'_2 for these three orientations are given in Table 3. Orientation (1) would be reached as soon as a grain becomes half-twinned in compression. Grains which have become reoriented into the field of twinning by r translation induced by extension (*e.g.* k and p, Fig. 15) are remote from orientation (2) but close to (3). Moreover, external rotation accompanying partial twinning on e_1 and subsequent translation on r_1, as shown by the arrows in Figure 15, would cause even closer approach to orientation (3). This, therefore, is the stable orientation predicted for extension (T, Figs. 14B, 15).

Petrofabric Confirmation of the Orienting Mechanism

Evidence from preferred-orientation data.—Orientation diagrams (Figs. 9–11) based on petrofabric analysis of highly strained cylinders show several characteristics that are completely in harmony with the orienting mechanism just described:

(1) c axes have been almost eliminated from regions where e twinning is possible.

(2) c-axis diagrams have strong concentrations at 10°–30° to the axis of compression or at 60°–80° to that of elongation. This is the range of orientation adjoining the fields of e twinning in Figures 13 and 14. At the predicted

stable orientations of Figure 15, *c* makes an angle of 26° to the axis of compression or 72° to that of elongation.

(3) The most prominent set of *e* lamellae per grain tends to be normal to the axis of compression or parallel to that of elongation. (*Cf.* Pl. 1, 3.) Commonly these are broad lamellae, clearly recognizable as twins; their rational orientation in the grain lattice shows that they have formed in the latest stage of deformation, as would be expected of grains that have become rotated into the stable orientations of Figure 15. As would be predicted for strains of the magnitude observed, not many grains have reached the half-twinned state requisite for complete stability. The orientation of well-developed *e* lamellae in highly strained marble accords with previous observations on orientation of edges [*e*:*e*] and on spacing index of *e* lamellae in specimens deformed less strongly at 20°–300° C (*e.g.* Turner and Ch'ih, 1951, p. 898–900; Griggs *et al.*, 1953, p. 1380).

(4) Preferred orientation of *a* crystal axes is less readily demonstrated by petrofabric analysis than is that of *c* axes, largely because there are three identical *a* axes per grain. On the whole, however, observations agree well with prediction. Axial-distribution analysis of a specimen shortened by only 20 per cent has established distinct preferred orientation of *a* for large grains of local aggregates having subparallel *c* axes (Fig. 7, D–F). In each aggregate one *a* axis tends to be normal to the compression axis, as would be expected for grains approaching the stable orientations normal to *e*. (*Cf.* A_3 and E_2, Fig. 14A.) In highly strained specimens preferred orientation of *a* is more pronounced and consistent. Again one *a* axis tends to be oriented normal to the compression axis (Fig. 11A). In specimens deformed by extension the three *a* axes are consistently inclined at 10°, 45°, and 65° to the axis of extension (Fig. 11C, D, maxima *X*, *Y*, *Z*), precisely as required for a grain in the stable orientation *T* of Figure 15 (t, Fig. 11C, D).

(5) The variable extent to which the initial fabric has become reoriented under different conditions is also consistent with prediction. As an orienting mechanism twinning must be much more effective, for a given strain, than translation gliding. Where specimens were so oriented that most grains could twin on *e* (Figs. 9C, 10D), reorientation of the fabric has been much more drastic than in specimens whose orientation minimized the possibility of twinning (Figs. 9A, 10A, B).

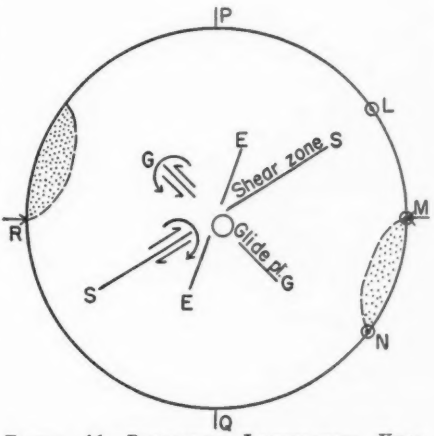

FIGURE 16.—PROJECTION ILLUSTRATING KINEMATIC INTERPRETATION OF FABRIC RESULTING FROM DIAGONAL SHEAR

Specimen 400. Axis of compression—*MR*; shear zone—*SS*; elongation of grains—*EE*; orientation of typical active glide plane *r*—*GG*; zone of concentration of *c* axes shown stippled. Arrows show senses of shear and accompanying rotation on *SS* and *GG*.

Further light is thrown upon the orienting process by the fabric of specimen 400 which yielded under compression by diagonal shear. The grains constituting the original fabric fall into three categories (*cf.* Fig. 9E): (1) A minority, originally oriented to permit *e* twinning, have been completely reoriented so that the field of twinning is vacant. (2) Numerous grains initially oriented with their *c* axes adjacent to the arc *MN* (Fig. 9E) retain their aggregate orientation, so that reorienting of individual grains cannot have been profound. (3) Equally numerous grains whose *c* axes initially fell adjacent to the arc *LM* have been reoriented into the sector *MN* by clockwise external rotation. In these grains the sense of translation on *r* must have been counterclockwise. Under the stress system of this particular experiment this was possible only for glide planes whose poles lie in quadrants *POM* and *ROQ* of Figure 16.

Thus in at least half of the original grains, including all those whose behavior can be reconstructed, the active *r* glide planes (*e.g.*, *GG*, Fig. 16) were transverse to the zone of shear (*SS*, Fig. 16). It would seem that in this experiment intragranular gliding on *r* was controlled by the clockwise sense of shear in the deformed zone *SS*. This caused clockwise external rotation of individual grains and complementary counterclockwise gliding within the grains, restricting the active glide planes to orientations transverse to the shear zone. As in simple extension and compression fabrics, many grains ultimately have become oriented so that the sense of shear on an *e* plane favors twinning. Such grains show obvious late twin lamellae inclined at 75°–90° to the axis of compression (Fig. 9F).

Evidence from individual grains.—The individual behavior of many grains can be traced in considerable detail on the basis of petrographic evidence of internal, and to a lesser extent external, rotation. (*Cf.* Borg and Turner, 1953, p. 1346–1350; Turner, Griggs, and Heard, 1954, p. 898–902, 929, 930.) It is usually necessary to spend several hours on each grain. Some 70 grains distributed in several specimens have been examined. Some yield ambiguous results, but in the majority the present orientation or the reconstructed behavior or both are consistent with the hypothesis of orienting outlined above.

From data relating to internal rotation of early formed *e* lamellae it is also possible to estimate quantitatively the strain in individual grains. If allowance is made for inaccuracies of 1°–2° which unavoidably attend microscopic measurement of internal rotation, the strain calculated for individual grains agrees well with that recorded experimentally for the whole specimen. The procedure followed is to determine the glide system responsible for rotation, then to calculate the shear s on the active glide system, and finally to determine the ratio $\frac{l_1}{l_0}$ (for extension) or $\frac{l_0}{l_1}$ (for compression), using the equations given above. The value of s is given by the equation (Turner, Griggs, and Heard, 1954, p. 900)

$$s = \frac{\cot \alpha - \cot \beta}{\sin \gamma}$$

where α and β are the angles between the active glide plane and the rotated lamella before and after deformation ($\alpha < \beta$), and γ is the angle between the glide direction and the axis of internal rotation.

Where complete twinning on *e* has been followed by translation on *r* of the twinned lattice, the initial length of the grain is designated l_0, the length after twinning is l_1', and the length at the close of deformation is l_1. The ratios $\frac{l_0}{l_1}$ and $\frac{l_1'}{l_1}$ are determined separately, and the total strain, ϵ, can be calculated from the product $\frac{l_0}{l_1}$. For extension,

$$\epsilon = \frac{l_1}{l_0} - 1$$

For compression,

$$\epsilon = 1 - \frac{l_1}{l_0}$$

The photomicrographs (Pls. 1–4) show a close correlation between incidence of complete twinning and orientation of the specimen in relation to the applied force. Grains that have been completely twinned usually have a few dark conspicuous L_3 lamellae (original e_1 lamellae internally rotated to $\{11\bar{2}0\}$ of the new lattice during twinning on e_2). Where orientation of the specimen should favor twinning in many grains (*e.g.* Pls. 2, 4), numerous grains show L_3 lamellae; where orientation is unfavorable for twinning (Pl. 3), grains with L_3 are few and stand out conspicuously.

Details of a few representative grains are recorded below. Orientation data for each grain are given in Table 4, and data for internal rotation and calculated strain are summarized in Table 5.

SPECIMEN 409, GRAIN 23;[6] FIGURE 1 OF PLATE

[6] A record of measured grains, numbered on photomicrographs, is on file in the Department of Geology, University of California.

5, LOWER MARGIN: In this grain, typical of many in specimen 409 (Pl. 1, fig. 1), there is strong lamellar twinning on one set of *e* planes

TABLE 4.—UNIVERSAL-STAGE MEASUREMENTS FOR INDIVIDUAL GRAINS

Specimen	Grain	Figure	Measured face or direction	Innermost circle	Tilt	
					on EW	on NS
409	23	17A	*c* axis	66°	..	7°→
			e_3	358°	3°↓	..
409	6	17B	*c* axis	73°	..	20°→
			e_1	353°	5°↓	..
			L_7	315°	18°↑	..
			L_3'	40°	11°↓	..
				45°	9°↓	..
409	11	17D	*c* axis	100°	..	7°→
			e_1	353°	5°↑	..
			r_1	63°	4°↑	..
			L_1	20°	12°↑	..
			L_3'	88°	18°↓	..
409	22	17C	*c* axis	303°	..	8°→
			e_1	8°	2°↑	..
			L_1	22°	13°↓	..
			L_3	312°	52°↑	..
459	113	17E	*c* axis	340°	..	17°←
			r_3	42°	17°↓	..
			e_2	42°	19°↑	..
			e_1	79°	10°↓	..
			L_1	90°	3°↑	..
459	205	17F	*c* axis	342°	..	11°→
			e_1	46°	7°↓	..
			e_3	89°	12°↑	..
			L_1	74°	8°↓	..
			L_3'	10°	37°↑	..
			L_3''	348°	44°↓	..

(e_3, Fig. 17A). The orientation approximates the stable position A_3 or E_2 of Figure 14A. The values of S_O on r_1 and r_2 are equal (0.40) and are higher than that for r_3 (0.33); in the twinned lattice, S_O for r_1 and r_2 is 0.37, and for r_3 it is 0.31. There is no evidence of rotation, so that the behavior of the grain before twinning on e_3 is unknown.

SPECIMEN 409, GRAIN 6; FIGURE 1 OF PLATE 5, UPPER HALF: Measurement of the *c* axis and a few sharp lamellae e_1 (trending west-northwest, Pl. 5, fig. 1) orients the lattice. A swarm of northwest-trending lamellae have somewhat anomalous orientation and are interpreted as remnant twin lamellae e_2, internally rotated through a few degrees to their present position L_7, during translation gliding on r_1 and r_3, the latter predominating (Fig. 17B). A few prominent northeast-trending lamellae have the dark appearance, somewhat undulating outlines, and striated boundary surfaces characteristic of L_3 lamellae. However, they depart by 30° from the theoretical orientation L_3 and are designated L_3'. Since L_3', r_1, and r_2 are cozonal, the present position of L_3' could be the result of gliding on either r_1 or r_2; but for the given direction of compression, the clockwise sense of rotation eliminates r_2 and is consistent only with r_1 as the active glide system. To account for L_3 a choice must be made between e_1 and e_2 as planes of initial complete twinning. Since e_2 is represented by a swarm of remnant lamellae, L_7, it is the more likely alternative. Two stages of deformation thus are deduced for grain 6. (*Cf.* Fig. 17B.)

(1) Complete twinning on e_2 of a grain whose *c* axis initially was *c'*. In this initial lattice, e_2 is the only *e* plane on which the sense of shear permits twin gliding; S_O on e_2 = 0.44.

(2) Simultaneous gliding on $r_1(S_O = 0.32)$ and $r_3(S_O = 0.38)$. Since the glide direction g_3 of the r_3 system is parallel to L_3, the observed clockwise rotation of L_3 to L_3' must be due solely to gliding on r_1. The total strain resulting from e_2 twinning followed by r_1 gliding (*see* Table 5) is computed as 0.49. This is a minimum value and does not include strain due to gliding on r_3, which is recorded only by lamellae L_7.

SPECIMEN 409, GRAIN 22; FIGURE 3 OF PLATE 5: The lattice is oriented by measurement of the *c* axis and a few sharp e_1 lamellae of late origin. Most conspicuous in Figure 3 of Plate 5 are a few diagonal L_3 lamellae. These are inclined to the plane of the section at only 38° and hence appear as broad bands striated parallel to their intersection with e_1 and e_2. There is nothing to indicate microscopically whether e_1 or e_2 was the plane upon which the original lattice was completely twinned. However the sense of shear on e_1 is inconsistent with twin gliding under given stress conditions. L_3 are therefore interpreted as e_1 lamellae of the original lattice, internally rotated to $\{11\bar{2}0\}$ during complete twinning on e_2. (*Cf.* Fig. 17C.) Of the three *e* planes of the original lattice (e_1', e_2, and e_3', Fig. 17C), only e_2 is appropriately oriented

for twin gliding (S_O = 0.35; sense of shear, +). Also conspicuous in the photograph are subhorizontal lamellae (L_1, Fig. 17C). These are e lamellae internally rotated during gliding on one of the three r systems. Since L_3 has remained unaffected by rotation, the possibility of gliding on r_1 and r_2 is eliminated. The active glide system must have been r_3. This is cozonal with L_1 and e_1, so that the identity of L_1 as internally rotated e_1 lamellae is established. The computed total strain is 43 per cent.

The shear s on r_3 can be calculated independently from rotation of L_3 to L_3' and of e_2 to L_1. The two values differ slightly, so that the total strain is estimated alternatively as 40 per cent and 44 per cent (Table 5). Grain 11 shows effects of external rotation in that the crystallographic orientation of one end differs from that of the rest of the grain. From measurements of the optic axis (c'') and one other plane (r_1'') in the end portion, the axis of external rotation is determined graphically (Turner, Griggs, and Heard, 1954, p. 905) as E. This is close to E', the theoretical axis of external rotation for kink banding, and 42° distant from E'', the axis that would be required for rotation of the glide plane r_2 toward the normal to the axis of compression.

TABLE 5.—DATA ON OBSERVED INTERNAL ROTATION AND CALCULATED STRAIN FOR INDIVIDUAL GRAINS

Specimen	Grain	Rotated lamella	Glide system	χ_0	λ_0	α	β	γ	So	s	$\frac{l_0}{l_1'}$	$\frac{l_1'}{l_1}$	$\frac{l_0}{l_1}$	ϵ
409	6	e_1' to L_3	e_2	40°	47°	...	..	...	0.44	0.69	1.36			
		L_3 to L_3'	r_1	20°	20°	52°	82°	51°	0.32	0.8		1.44	1.96	49%
409	22	e_1' to L_3	e_2	44°	60°	...	...	...	0.35	0.69	1.28			
		e_1 to L_1	r_3	59°	71°	33°	71°	90°	0.29	1.2		1.37	1.75	43%
409	11	e_1' to L_2	e_2	54°	62°	...	...	...	0.38	0.69	1.28			
		L_3 to L_3'	r_2	44°	52°	52°	74°	51°	0.43	0.62		1.30	1.66	40%
		e_2 to L_1	r_2	44°	52°	42°	71°	90°	0.43	0.77		1.38	1.77	44%
											$\frac{l_1'}{l_0}$	$\frac{l_1}{l_1}$	$\frac{l_1}{l_0}$	ϵ
459	113	e_2 to L_1'	r_2	23°	60°	17°	71°	90°	0.20	2.93	1.82			
		L_1' to L_1	r_3	45°	74°	52°	60°	56°	0.19	0.30		1.24	2.26	126%
		e_2 to L_1''	r_3	45°	74°	37°	71°	90°	0.19	0.98	1.37			
		L_1'' to L_1	r_2	23°	60°	23°	47°	80°	0.20	1.28		1.33	1.82	82%
459	205	e_2' to L_2	e_1	45°	45°	...	...	...	0.5	0.69	1.37			
		e_1 to L_1	r_1	27°	27°	43°	71°	90°	0.41	0.73		1.33	1.82	82%
		L_3 to L_3'	r_1	27°	27°	52°	69°	51°	0.41	1.15		1.53	2.10	110%
		L_3 to L_3''	r_1	27°	27°	52°	75°	51°	0.41	1.30		1.61	2.21	121%

SPECIMEN 409, GRAIN 11; FIGURE 2 OF PLATE 5, UPPER HALF: The orientation is determined by the c axis and a few sharp west-northwest-trending e_1 lamellae. The two dark nearly vertical bands are L_3, internally rotated to L_3' during translation gliding on r_2. The clockwise sense of rotation eliminates r_1 as a possible glide system. (*Cf.* Fig. 17D.) There is also a swarm of dark nearly horizontal lamellae, L_1, cozonal with e_2 and the active glide plane r_2, and therefore identified as internally rotated e_2 lamellae. These have been inherited from earlier complete twinning on e_2 of a lattice whose c axis is designated c' in Figure 17D. Note that in this initial lattice only e_2 is suitably stressed for twin gliding (S_O = 0.38, sense of shear, +).

SPECIMEN 459, GRAIN 113: The orientation of the grain is established by measurement of the c axis, well-defined r_3 cleavage, and lamellae e_1 and e_2. A third set of lamellae L_1 has a highly anomalous orientation (Fig. 17E) for which two alternative explanations are possible. These lamellae could be either e_2 or e_3, internally rotated to L_1 by gliding on r_2 (sense of shear counterclockwise) and on r_3 (sense of shear clockwise). For these two systems S_O is almost the same

(0.20) and is notably higher than S_O for r_1 (0.04). To compute the strain, deformation is considered to occur in two stages: e_2 is rotated to L_1' during gliding on r_2, and from L_1' to L_1 during gliding on r_3. The alternative interpretation involves rotation of e_3 to L_1'' during gliding on r_3, and thence to L_1 during gliding on r_2. The strains so computed are 126 per cent and 82 per cent respectively. The grain lies near the boundary of the necked region (*cf.* Pl. 3B) where the strain is distinctly less than the maximum value of 118 per cent as measured at the middle of the neck. Lamellae e_1 afford evidence supporting the second alternative. Although these lamellae have the dark slightly undulating appearance of early structures that have survived deformation, their orientation has not been affected by internal rotation. This is readily understood if the shear on r_2 and on r_3 is almost the same, as required by the second alternative, for then the rotational influences of r_2 and r_3 on e_1 would be equal in magnitude but opposite in sense.

SPECIMEN 459, GRAIN 205: This is typical of those few grains in specimen 459 that have dark L_3 lamellae indicating a completely twinned condition. The crystallographic orientation is given by the c axis and a few sharp lamellae e_1 and e_3 (Fig. 17F). Two sets of internally rotated L_3 lamellae designated L_3' and L_3'' are present. Both have been rotated counterclockwise from the ideal L_3 orientation. Each is cozonal with L_3 and with r_1. Moreover, of the three r glide systems, r_1 has the highest value of S_O (0.41, compared with 0.04 for r_2 and 0.08 for r_3) and is the only one so oriented that it induces counterclockwise rotation of the two sets of L_3 lamellae. The glide system active in the completely twinned lattice can only have been r_1. Accordingly a set of lamellae L_1, almost normal to c, are interpreted as e_1 lamellae internally rotated during r_1 gliding. Where there are two sets of L_3 lamellae, as in the present instance, the plane of complete twinning can be determined uniquely as that e plane which is inclined at 67° to both L_3 planes. This is e_1. In grain 205 there are three independent sets of data on internal rotation, from which the shear on r_1, and hence the strain, may be computed. These give the total strain (*cf.* Table 5) as 82 per cent, 110 per cent, and 121 per cent respectively. The discrepancy is mainly due to variation in lattice orientation within the grain and lack of precision in locating twice-rotated lamellae such as L_3' in highly deformed grains. The grain is situated near grain 113 in an area where the strain in the whole specimen is somewhat less than the maximum value of 118 per cent.

SPECIMEN 443, GRAIN 39: This is the only recorded instance of a grain that has probably been twinned twice to completion. The orientation of the crystal is established by the c axis and several rational e lamellae and r cleavages. It contains a few lamellae which from their dark, heavily striated appearance and sinuous outlines are clearly internally rotated e structures but nevertheless almost coincide with e of the lattice (Fig. 18). A crystal with optic axis c is completely twinned on e_1 to give a new lattice with optic axis c'; at the same time, lamellae e_2 and e_3 of the original lattice are internally rotated to L_3 and L_3' (= $\{11\bar{2}0\}$). A second complete twinning on e_2' now gives a lattice whose optic axis is c''. At the same time L_3 is internally rotated to coincide with e_1'' of the final lattice. L_3' intersects the twin plane e_2' in the glide direction g_2' and is not rotated. It remains L_3' (= $\{11\bar{2}0\}$) in the final lattice. In grain 39 only one set of rotated lamellae approximately coinciding with e_1 is present, and a unique sequence of twinning therefore cannot be reconstructed.

Concluding Statement

A general hypothesis of homogeneous deformation, closely following Handin and Griggs' modification of Taylor's hypothesis, has been adopted to explain deformation of marble at 300°–500°. Strain is assumed to be approximately the same in every grain and is due to twin gliding on $\{01\bar{1}2\} = e$ and translation gliding in the opposite sense on $\{10\bar{1}1\} = r$. Reorienting of grains is the result partly of twinning and partly of external rotation of the grain in the sense opposite to that of internal twin or translation gliding. On the above hypothesis, behavior of individual grains, variously oriented in the stress field, is predicted. These predictions are borne out by petrographic evidence obtained from experimentally deformed marble fabrics:

(1) Preferred orientation of the calcite grains agrees strikingly with predicted patterns.

(2) The observed incidence of L_3 lamellae (certain evidence of complete *e* twinning) demonstrates perfect correlation between observed and predicted abundance of completely twinned grains.

(3) In specimens where completely twinned grains are rare, the orientation of grains showing partial twinning approximates the stable orientation predicted by hypothesis.

(4) Behavior of individual grains, as reconstructed from observed internal rotation of early *e* lamellae, agrees with predicted behavior. It comprises simple *r* translation followed by duplex *r* translation to a point where *e* twinning begins, or complete *e* twinning followed by *r* translation. The calculated values of S_O and the sense of shear on the active glide systems invariably agree with predicted requirements.

(5) The strain in individual grains, computed from measured angles of internal rotation of *e* lamellae, closely approximates the strain recorded for the specimen as a whole—as is required by the hypothesis of homogeneous deformation.

Effects presumed to indicate the beginning of recrystallization were reported at 300° C: decrease in grain size, disappearance of marginal distortion, and the apparent development of intergranular slip surfaces. These effects were not more prominent at 400° C and 500° C. A new effect was noted, however, which might represent incipient general recrystallization: Small lobes and lensoid streaks were found in which the *c* axis was closely parallel to the axis of compression or normal to the axis of extension, regardless of the orientation of the host crystal (Fig. 19; Pl. 5, fig. 4).

Geological Applications

Microscopically measured effects of internal rotation in mineral grains of deformed rocks constitute data from which, under specially favorable circumstances, it should be possible to determine strain. Such strain would be post-crystalline, in that it would necessarily post-date the last phase of metamorphic recrystallization. It would be computed for some constant direction or directions in the rock fabric; for example, percentage shortening parallel to the *c* axis, or percentage elongation parallel to the *b* axis, of a monoclinic fabric.

The special conditions necessary for estimation of natural strain in mineral grains are as follows:

(1) The gliding mechanism must be known.

(2) Lamellae of regular crystallographic orientation, such as those commonly resulting from twinning or exsolution, must be present before deformation.

(3) Such lamellae must be so oriented with respect to the glide system that they can be internally rotated by gliding. Lamellae which are parallel to the glide plane or to the glide direction are excluded from this category.

The only common rock-forming minerals now known to satisfy these requirements are calcite and dolomite. In calcite early $\{01\bar{1}2\}$ twin la-

---

Figure 17.—Projections Illustrating Behavior of Individual Grains as Deduced from Internal Rotation of *e* Lamellae

Equal-area projections, lower hemisphere, on plane of thin section. Marginal arrows indicate axis of compression or of extension. g_1, g_2, g_3 are glide directions in r_1, r_2, and r_3 respectively. L_1, L_3, L_4', etc., are poles of rotated lamellae. Paths of internal rotation are shown by full arcs (with arrows), connected by broken arcs to the active glide plane.

A. Specimen 409, grain 23. Circled points indicate planes and directions in the measured crystal; crosses indicate planes and points in lattice formed by twinning on e_3. r_1 and r_2, common to the two lattices are shown as full arcs.

B. Specimen 409, grain 6. Circled points belong to measured lattice. Crosses belong to original lattice before twinning on e_2. Sense of twin gliding on e_2 shown at center.

C. Specimen 409, grain 22. Circled points belong to measured lattice. Crosses belong to original lattice before twinning on e_2.

D. Specimen 409, grain 11. Circled points belong to measured lattice. Crosses belong to original lattice before twinning on e_2. Orientation of *c* in end portion of grain = c''; $c'' \rightarrow c$ = external rotation about E.

E. Specimen 459, grain 113. Two alternative interpretations of L_4 are shown: e_2 to L_1' to L_4; e_3 to L_1'' to L_4. Both involve gliding on r_2 and r_3.

F. Specimen 459, grain 205. Circled points belong to measured lattice. Crosses belong to original lattice before twinning on e_1. Sense of subsequent gliding on r_1 is shown at center.

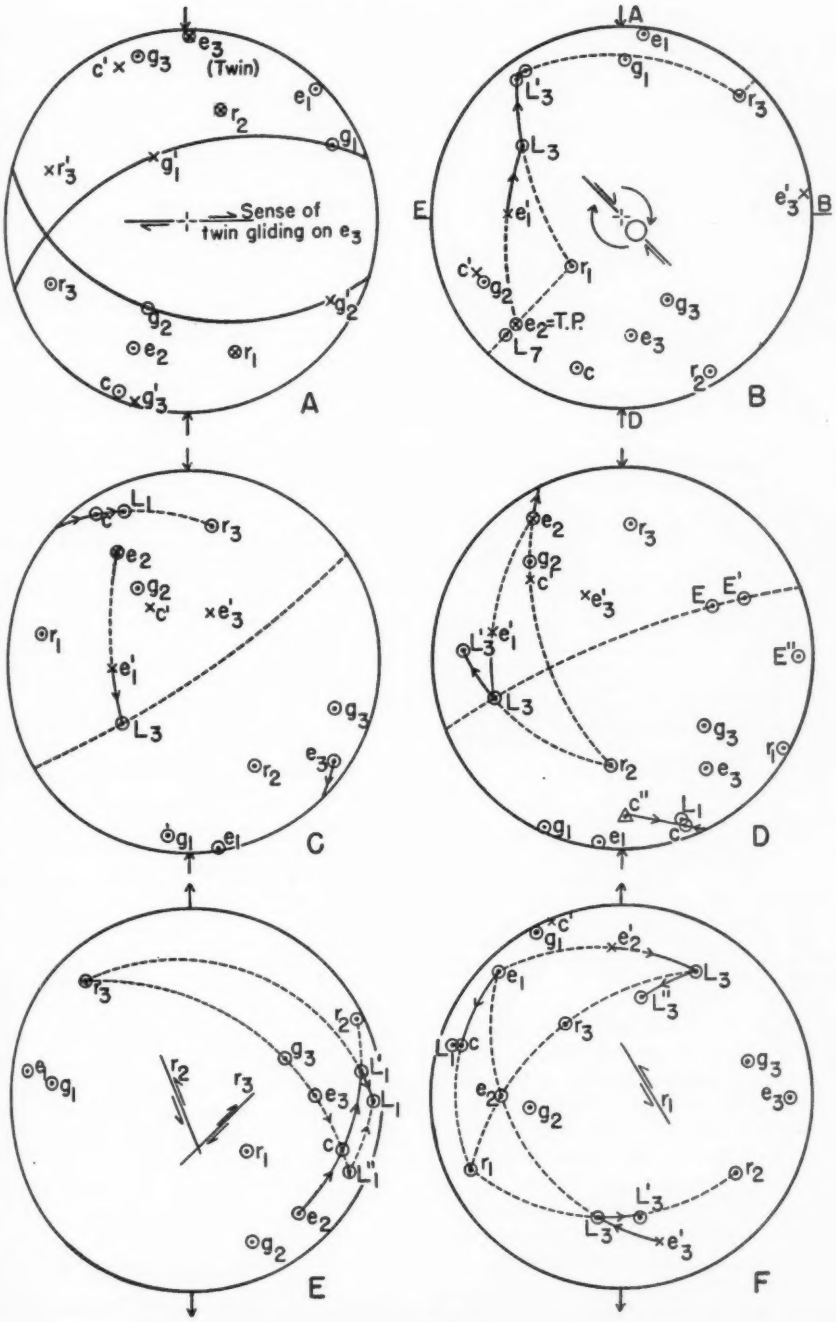

FIGURE 17 A–F

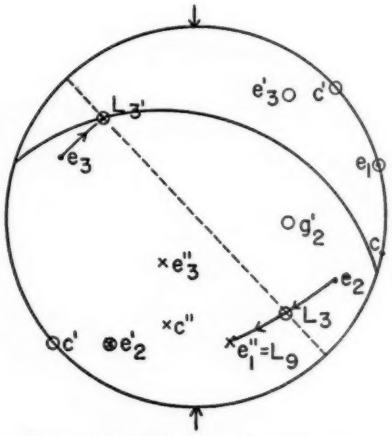

FIGURE 18.—PROJECTION ILLUSTRATING REPEATED COMPLETE TWINNING OF CALCITE

Solid points—initial lattice; open circles—second lattice resulting from complete twinning on e_1; crosses—final lattice resulting from complete twinning of second lattice on e'_2. Broken and solid arcs are {0001} of second and final lattices respectively.

FIGURE 19.—POSSIBLE LOCAL RECRYSTALLIZATION EFFECTS

Specimen 409. Tracing of Grain 10, (Pl. 5, fig. 4). Areas shown in solid black have *c* axis parallel to axis of compression (vertical) and may have formed by local recrystallization within a grain (stippled) of different orientation.

mellae and $\{10\bar{1}1\}$ cleavage cracks may be internally rotated during twin gliding on $\{01\bar{1}2\}$ or translation gliding on $\{10\bar{1}1\}$ at 150°–500° C and confining pressures of 5000 atmospheres. In dolomite deformed at 20°–400° C and confining pressures of 3000–5000 atmospheres, early $\{02\bar{2}1\}$ lamellae and $\{10\bar{1}1\}$ cleavage cracks may be internally rotated by translation gliding on {0001} parallel to an *a* axis (Turner *et al.*, 1954; Higgs and Handin, 1954).

Even in marble and dolomite rock, however, internal rotation of early lamellae has seldom been recorded. This is partly due to lack of precise measurements of lamella orientations, but mainly due to the apparent ease with which calcite and dolomite recrystallize during metamorphism. Within our experience most lamellae, even where they occur in obviously deformed grains, are rationally oriented with respect to the crystal lattice and must have originated after deformation. Known exceptions are rotated lamellae in large relict grains in mylonites (*e.g.* Weiss, 1954, p. 21–23, Pl. 5a). In general, carbonate mylonites and phyllonites should provide interesting material for estimating extent and homogeneity of natural strain. This has not yet been attempted.

Dynamic interpretation of minor *e* twinning in calcite of some marbles has been found to give consistent results (*e.g.* McIntyre and Turner, 1953, p. 231, 235, 239). This is limited, however, to late minor strain postdating the main deformation responsible for existing preferred orientation of calcite grains in the same rocks. Active glide systems responsible for major strain, deduced from measured internal rotation of lamellae, may ultimately prove amenable to dynamic interpretation along similar lines.

There is a definite resemblance between a natural marble fabric and a fabric produced by experimental deformation. The fabric resulting from compression of Yule marble normal to the initial foliation is characterized by elongation of grains normal to the compression axis, a *c*-axis ring maximum around the compression axis (Fig. 9A) and a concentration of *e* twin lamellae normal to the compression axis (Fig. 9B). Sander has recorded similar patterns of preferred orientation of *c* axes and *e* lamellae with reference to the normal to the foliation plane of naturally deformed marble (*e.g.* Sander, 1950, D 61, 60, p. 349, 366). The resemblance may be fortuitous. Presence of internally rotated *e* lamellae in a few grains could provide critical evidence concerning whether or not plastic strain induced by compression normal to the foliation was responsible for the natural preferred-orientation pattern.

REFERENCES CITED

Barrett, C. S., 1952, Structure of metals: N. Y., McGraw-Hill Book Co.

Barrett, C. S., and Levenson, L. H., 1940, The structure of aluminum after compression: Am. Inst. Min. and Metall. Engineers Trans., v. 137, p. 112–126

Beck, P. A., 1954, Annealing of cold worked metals: Philos. Mag. Supp. (Adv. in Physics), v. 3, p. 245–324

Borg, I., and Turner, F. J., 1953, Deformation of Yule marble: Part VI: Geol. Soc. America Bull., v. 64, p. 1343–1352

Calnan, E. A., and Clews, C. J. B., 1950, Deformation textures in face-centered cubic metals: Philos. Mag., v. 41, p. 1085–1100

Cox, H. L., and Sopwith, D. G., 1937, The effect of orientation on stresses in single crystals and of random orientation on strength of polycrystalline aggregates: Phys. Soc. London Proc., v. 49, p. 134–151

Griggs, D. T., and Miller, W. B., 1951, Deformation of Yule marble: Part I: Geol. Soc. America Bull., v. 62, p. 853–862

Griggs, D. T., Turner, F. J., Borg, I., and Sosoka, J., 1953, Deformation of Yule marble: Part V: Geol. Soc. America Bull., v. 64, p. 1327–1342

Handin, J. W., and Fairbairn, H. W., 1955, Experimental Deformation of Hasmark Dolomite: Geol. Soc. America Bull., v. 66, p. 1257–1274

Handin, J. W., and Griggs, D. T., 1951, Deformation of Yule marble: Part II: Geol. Soc. America Bull., v. 62, p. 863–886

Higgs, D. V., and Handin, J., 1954, Experimental deformation of dolomite single crystals: Geol. Soc. America Bull., v. 65, p. 1263

McIntyre, D. B., and Turner, F. J., 1953, Petrofabric analysis of marbles from Mid-Strathspey and Strathavon: Geol. Mag., v. 90, p. 225–240

Robertson, E. C., 1955, Experimental study of the strength of rocks: Geol. Soc. America Bull., v. 66, p. 1275–1314

Sander, B., 1950, Einführung in die Gefügekunde der geologischen Körper, II: Vienna, Springer

Schmidt, E., and Boas, W., 1950, Crystal plasticity: London, Hughes, 353 p.

Taylor, G. I., 1938, Plastic strain in metals: Inst. Metals Jour., v. 62, p. 307–324

Turner, F. J., and Ch'ih, C. S., 1951, Deformation of Yule marble, Part III: Geol. Soc. America Bull., v. 62, p. 887–906

Turner, F. J., Griggs, D. T., and Heard, H., 1954, Experimental deformation of calcite crystals: Geol. Soc. America Bull., v. 65, p. 883–934

Turner, F. J., Griggs, D. T., Heard, H., and Weiss, L. W., 1954, Plastic deformation of dolomite rock at 380°C: Am. Jour. Sci., v. 252, p. 477–488

Weiss, L. W., 1954, A study of tectonic style: Univ. Calif. Pub. Geol. Sci., v. 30, p. 1–102

Department of Geology, University of California, Berkeley, California; Institute of Geophysics, University of California, Los Angeles, California; Victoria University College, Wellington, New Zealand; Department of Geology, University of California, Berkeley, California

Manuscript Received by the Secretary of the Society, July 22, 1955

Project Grants 201-37, 245-38, 294-39, 615-53

Assisted by Grants from the Office of Naval Research and the National Science Foundation

Publication No. 70, Institute of Geophysics, University of California, Los Angeles.